



Universitat Autònoma de Barcelona

ADVERTIMENT. L'accés als continguts d'aquesta tesi queda condicionat a l'acceptació de les condicions d'ús establertes per la següent llicència Creative Commons:  http://cat.creativecommons.org/?page_id=184

ADVERTENCIA. El acceso a los contenidos de esta tesis queda condicionado a la aceptación de las condiciones de uso establecidas por la siguiente licencia Creative Commons:  <http://es.creativecommons.org/blog/licencias/>

WARNING. The access to the contents of this doctoral thesis it is limited to the acceptance of the use conditions set by the following Creative Commons license:  <https://creativecommons.org/licenses/?lang=en>



**Universitat Autònoma
de Barcelona**

Departament de Bioquímica, Biologia Molecular i Biomedicina

Unveiling the multifaceted antimicrobial mechanism of action of human host defence RNases

Tesis presentada por **Javier Arranz Trullén** para optar al grado de Doctor en Bioquímica, Biología Molecular y Biomedicina bajo la dirección de la Dra. **Ester Boix Borràs** y el Dr. **David Pulido Gómez**

**Unitat de Biociències del Departament de Bioquímica i Biologia Molecular.
Universitat Autònoma de Barcelona**

Dra. Ester Boix Borràs

Dr. David Pulido Gómez

Javier Arranz Trullén

Campus de Bellaterra, Septiembre 2016



**Universitat Autònoma
de Barcelona**

Biochemistry, Molecular Biology and Biomedicine Department

Unveiling the multifaceted antimicrobial mechanism of action of human host defence RNases

Thesis presented by **Javier Arranz Trullén** to obtain the PhD in Biochemistry,
Molecular Biology and Biomedicine directed by **Dr. Ester Boix Borràs** and **Dr.
David Pulido Gómez**

**Biosciences Unit of the Biochemistry and Molecular Biology Department
Universitat Autònoma de Barcelona**

Dra. Ester Boix Borràs

Dr. David Pulido Gómez

Javier Arranz Trullén

Campus de Bellaterra, September 2016

Content

Summary/Resumen	7
List of publications	11
Abbreviations	13
1. General introduction	17
1.1 Structural variety establishment and classification of antimicrobial peptides ...	17
1.1.1 Short antimicrobial peptides	17
1.1.1.1 α -helical amino acid structures	19
1.1.1.2 β -sheet amino acid structures	21
1.1.1.3 α -helical and β -sheet mixed structures	22
1.1.1.4 Non- $\alpha\beta$ peptides (extended structures)	23
1.1.2 Antimicrobial polypeptides/proteins	24
1.2 Bio-structural features for antimicrobial activity	24
1.2.1 Secondary structure and length	25
1.2.2 Amphipathicity and polar angle	25
1.2.3 Cyclic structures	26
1.2.4 Hydrophobicity	27
1.2.5 Conserved salt bridges	27
1.2.6 Cationicity	28
1.2.7 Antimicrobial activity hallmarks: specific amino acid residues	28
1.3 Modes of action of AMPs	30
1.4 Immune system and AMPs: an immunomodulatory link	34
1.4.1 Neutralization of LPS	34
1.4.2 Chemotaxis activity	35
1.4.3 Epidermal growth factor interactions and wound healing	35
1.4.4 Adaptive immune response cooperation	35
1.5 Human antimicrobial RNases	36
1.5.1 RNase 3/Eosinophil Cationic Protein	38
1.5.2 RNase 6	38
1.5.3 RNase 7	39
1.5.4 N-terminal RNase derived peptides	40
2. Aims of the thesis	45
3. Results	49
<u>Paper I</u> . Insights into the antimicrobial mechanism of action of Human RNase 6: Structural determinants for bacterial cell agglutination and membrane permeation	53

<u>Paper II</u> . The first crystal structure of human RNase 6 reveals a novel substrate binding and cleavage site arrangement	75
<u>Paper III</u> . Exploring the mechanisms of action of human secretory RNase 3 and RNase 7 against <i>Candida albicans</i>	91
<u>Paper IV</u> . Antifungal mechanism of action at the N-terminus domain of the human RNases	109
<u>Paper V</u> . Endogenous host antimicrobial peptides (AMPs) to tackle antimicrobial resistance in tuberculosis	127
<u>Paper VI</u> . Unveiling the mode of action of human antimicrobial RNases against <i>Mycobacterium tuberculosis</i> using a surrogate macrophage infected model	163
4. General discussion and future Outlook	187
4.1 Unveiling the antimicrobial mechanism of action of human RNase 6	187
4.2 Crystal structure of human RNase 6: Structure- functional insights into its nucleotide binding mode	188
4.3 Characterization of the antimicrobial mechanism of RNases and their N-terminal derived peptides using <i>C. albicans</i> , an eucariotic organism	188
4.4 Host immunogenic antimicrobial peptides (AMPs) to tackle antimicrobial resistance in mycobacteria: An integrated surrogate model for screening of AMPs against <i>Mycobacterium tuberculosis</i>	190
5. Conclusions	195
6. References	199
7. Annexes	219
7.1 Supplementary material of <u>Paper I</u>	221
7.2 Supplementary material of <u>Paper II</u>	223
7.3 Supplementary material of <u>Paper III</u>	236
7.4 Supplementary material of <u>Paper VI</u>	244

Summary

My PhD project is integrated into the large-scale study of the structure and function of human antimicrobial ribonucleases. These cationic and low molecular weight proteins are grouped into the ribonuclease A superfamily, considered one of the best characterized enzymes of the twentieth century. The RNase A superfamily is specific for vertebrates and has attracted remarkable interest due to the diversity of displayed biological properties; and represents an excellent example of a multifunctional protein's family. Together with the main enzymatic activity we must highlight other biological properties such as the angiogenic, immunomodulatory and antimicrobial activities. The reported antimicrobial activity of distantly related family members in early vertebrates suggests that the family arose with an ancestral function in host defence. Besides, the expression of several human RNases has been reported to be induced by infection. In particular, the RNases studied in this work, the human RNases 3, 6 and 7, are mainly expressed in eosinophils, monocytes and epithelial cells respectively. These proteins show a high cationicity due to the high proportion of basic residues and a remarkable antimicrobial activity against a wide range of human pathogens.

Our research group has a consolidated experience in the study of the mechanism of action of human ribonucleases and the experimental work presented in this thesis is contributing to this overall research project. The main results achieved by the present PhD study are outlined below:

- The characterization of the antimicrobial mechanism of RNase 6, both in bacteria cell cultures and using membrane models. Results highlight that the antimicrobial and cell agglutinating activities are mainly located at the N-terminus.
- The resolution of the first three-dimensional structure of ribonuclease 6, obtained at 1.72 Å, which has set the structural basis for future functional studies. The kinetic characterization of RNase 6 mutant variants and the prediction of protein- substrate complexes have identified the enzyme nucleotide binding sites.
- The study of the intracellular activity of ribonucleases 3, 6 and 7 and their derived N-terminal peptides against intracellular resident mycobacteria using a macrophage infected model.
- The analysis of the anti-pathogenic mechanism of action of human antimicrobial proteins and peptides in mycobacterial infections and their applied therapies.
- The comparative characterization of the antimicrobial mechanism of action of human RNases and their N-terminal derived peptides towards *Candida albicans*, as an eukaryote pathogen model.

The results presented in this thesis will contribute to the understanding of the role of human RNases in the immune system and provide the structure- function basis to expand

the initial project into the design of novel peptide mimetic therapeutics agents towards the eradication of resistant infectious diseases.

Resumen

Mi proyecto de doctorado se encuentra integrado dentro del estudio a gran escala de la estructura-función de las ribonucleasas antimicrobianas humanas. Estas proteínas catiónicas y de bajo peso molecular son secretadas por la mayoría de los organismos vertebrados agrupándose dentro la superfamilia de la ribonucleasa A, una de las enzimas mejor caracterizadas del siglo XX. De interés remarcable podríamos considerar su amplio abanico de propiedades biológicas, teniendo en cuenta su diverso historial de propiedades biológicas no catalíticas, convirtiéndolas en un buen modelo de proteínas multifunción. Junto a su principal característica como enzima catalizador de ácidos ribonucleicos, es importante destacar también otro tipo de propiedades biológicas no menos esenciales, como su actividad antimicrobiana, que comparten miembros distantes de la familia sugiriendo una función ancestral en el sistema inmune. Además, se ha visto que la expresión de algunas RNAsas humanas puede ser inducida en procesos infecciosos. En particular, las RNAsas estudiadas en este trabajo, las RNAsas humanas 3, 6 y 7, se expresan principalmente en eosinófilos, monocitos y células epiteliales, respectivamente. Estas proteínas muestran una alta cationicidad debido a su alta proporción de residuos básicos y una notable actividad antimicrobiana frente a una amplia gama de patógenos humanos.

Nuestro grupo de investigación posee una larga trayectoria en el estudio del mecanismo de acción de las ribonucleasas humanas y el trabajo teórico-experimental que se presenta en esta tesis ha contribuido a consolidar el actual proyecto de investigación. Los principales avances llevados a cabo por la presente tesis doctoral se enumeran a continuación:

- La caracterización del mecanismo antimicrobiano de la ribonucleasa 6, evaluando sus propiedades microbicidas frente a patógenos y modelos de membrana. Concretamente se ha revelado su actividad aglutinadora además de demostrarse que su actividad antimicrobiana está localizada básicamente en su extremo N-terminal.
- La resolución de la primera estructura tridimensional de la ribonucleasa 6, obtenida a 1.72 Å, que ha permitido asentar las bases estructurales para futuros estudios funcionales. Análisis complementarios sobre su caracterización cinética y predicción de complejos con diferentes ligandos han revelado sitios de unión y de catálisis que posteriormente han sido confirmados mediante mutagénesis dirigida.
- El estudio de la efectiva actividad antipatogena a nivel intracelular que presentan las ribonucleasas 3,6 y 7 así como sus péptidos derivados N-terminales frente a micobacterias en un modelo de macrófagos infectados.

- La expansión del conocimiento sobre las bases antipatogenas de diferentes péptidos y proteínas antimicrobianas que participan en la erradicación de las infecciones por micobacterias, así como las terapias derivadas.
- La caracterización del mecanismo antimicrobiano de los 8 péptidos N-terminales derivados de las ribonucleasas frente a *Candida albicans*, como modelo de patógeno eucariota

Como conclusión, los resultados obtenidos en esta tesis contribuyen a profundizar en la comprensión de las bases moleculares del papel que desempeñan algunas ribonucleasas en el sistema inmune y expandir el proyecto al diseño de agentes terapéuticos basados en péptidos antimicrobianos con el objetivo de erradicar enfermedades infecciosas causadas por patógenos resistentes.

List of publications

The present thesis is based on the work contained in the list of articles below:

- Paper I. **Arranz-Trullén J**, Pulido D, Prats-Ejarque G, Velázquez D, Torrent M, Moussaoui M, Boix E. Insights into the Antimicrobial Mechanism of Action of Human RNase6: Structural Determinants for Bacterial Cell Agglutination and Membrane Permeation. *Int J Mol Sci.* 2016 Apr 13;17(4). pii: E552. doi: 10.3390
- Paper II. Prats-Ejarque G, **Arranz-Trullén J**, Blanco JA, Pulido D, Nogués MV, Moussaoui M, Boix E. The first crystal structure of human RNase 6 reveals a novel substrate-binding and cleavage site arrangement. *Biochem J.* 2016 Jun 1;473(11):1523-36. doi: 10.1042
- Paper III: Salazar V, **Arranz-Trullén J**, Navarro S, Blanco JA, Sánchez D, Moussaoui M, Boix E. Exploring the mechanisms of action of human secretory RNase 3 and RNase 7 against *Candida albicans*. *MicrobiologyOpen*, 2016 Jun 8 DOI: 10.1002/mbo3.373
- Paper IV: **Arranz-Trullén J**, Salazar VA, Torrent M, Andreu D, Pulido D and Boix E.. Antifungal mechanism of action at the N-terminus domain of the human RNases. (*manuscript in preparation*)
- Paper V: **Arranz-Trullén J**, Pulido D, Bhakta S, Boix E. Endogenous host antimicrobial peptides (AMPs) to tackle antimicrobial resistance in tuberculosis (TB). (*manuscript in preparation*)
- Paper VI: **Arranz-Trullén J**, Lu L, Pulido D, Bhakta S, Boix E. Unveiling the mode of action of human antimicrobial RNases against *Mycobacterium tuberculosis* using a surrogate macrophage infected model. (*manuscript in preparation*)

Abbreviations

Å Ångström

ANG Human angiogenin

APD antimicrobial peptide database

AMP antimicrobial protein/peptide

CD circular dichroism

CP cecropin

DA Dalton

DC dendritic cell

DCD dermcidin

ECP eosinophil cationic protein

EDN eosinophil-derived neurotoxin

EGFR Epithelial growth factor

EDGP eosinophil-derived granule protein

EGF epidermal growth factor

EPX eosinophil peroxidase

HBDs Human β -defensins

hCAP human cationic antimicrobial peptide

HNP Human neutrophil peptide

hRNase Human ribonuclease

LF lactoferrin

LPS lipopolysaccharide

LTA lipoteichoic acid

LUV large unilamellar vesicle

MBP major basic protein

MAC minimum agglutinary concentration

MIC minimum inhibitory concentration

MW molecular weight

NMR nuclear magnetic resonance

PAMPs pathogen associated molecular patterns

PGN peptidoglycan

pI isoelectric point

RNA ribonucleic acid

SEM scanning electron microscopy

TA teichoic acid

TEM transmission electron microscopy

TNF tumour necrosis factor

TLR toll-like receptor

1. GENERAL INTRODUCTION

1. General introduction

In the last decades, more than 7000 naturally occurring peptides have been identified as essential components of human homeostasis, performing specialized functions such as growth factors, hormones, neurotransmitters or defence molecules^{1,2,3}. Antimicrobial peptides (AMPs) are usually produced in different types of organisms, including bacteria, fungi, insects, plants and vertebrates, where most of them exert a defensive role (figure 1)^{4,5}. Unlike proteins, peptides retain no defined consensus amino acid sequence affiliated with biological function. Notwithstanding, traditional antimicrobial peptides sustain some standard features, they are short (lengths ranging from 15 to 50 amino acid residues), amphipathic and mainly cationic. AMPs are capable of killing a wide spectrum of invading microbes in a stoichiometric way⁶. In humans, they are an essential component of the innate immune system and confer protection against numerous pathogens⁷. As effector molecules, they can also elegantly modulate the immune system to promote other physiological functions⁸. The first antimicrobial peptides were isolated and classified a few decades ago. Since then, thousands of them, including antimicrobial long polypeptides and low molecular weight proteins, have been described by many authors and listed in different AMP databases according to different criteria⁹. We could therefore consider that AMPs originated and gradually evolved from elderly defence proteins^{10,11}.

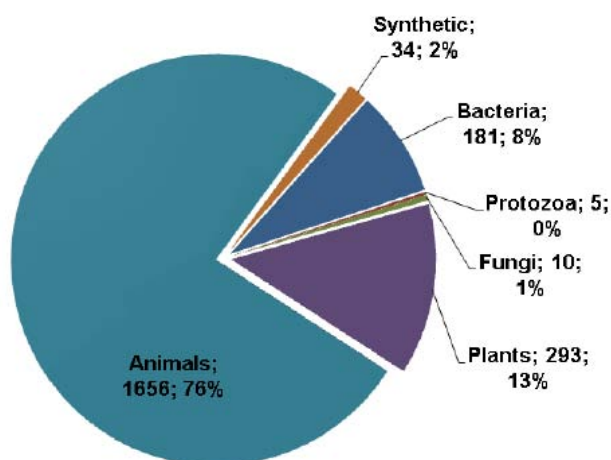


Figure 1. Sources of antimicrobial peptides in the antimicrobial peptide database in March 2013⁵.

1.1 Structural diversity and classification of antimicrobial peptides

1.1.1 Short antimicrobial peptides

A continuously growing number of AMPs are discovered and annotated every year (figure 2). However, the classification of AMPs is a complex issue and has not yet been standardized. During the last years, several databases have been built in order to facilitate the management of information and its analysis¹². The classification of peptides is still

controversial; however, there are currently several approaches for classifying AMPs based on different standards.

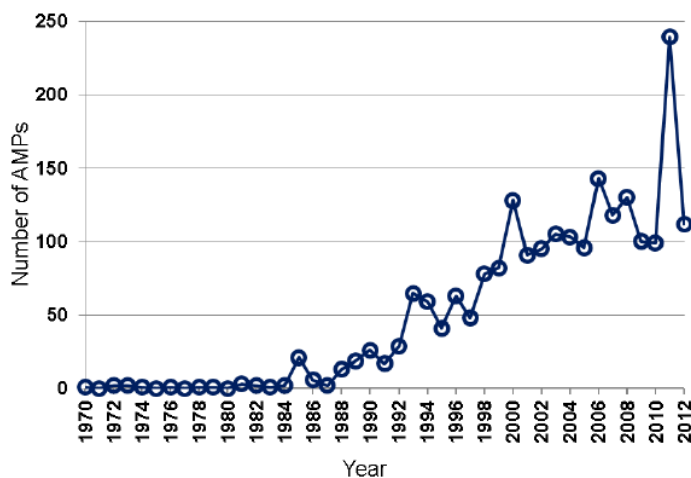


Figure 2. Antimicrobial peptides discovered each year from 1970 to 2012. Data were obtained from the antimicrobial peptide database (<http://aps.unmc.edu/AP>)⁹.

In the present work, the AMP classification method is based on the structural classification system of the antimicrobial peptide database (APD), which contains natural AMPs with known amino acid sequence, demonstrated antimicrobial activity and less than 100 amino acid residues. However, the database has recently been extended to 200 amino acids so that several antimicrobial proteins could also be registered¹³. Following all these criteria, the ADP database supplies a nicely characterized set of peptides and is a well-recognized within the AMP research community. AMPs may be classified based on their sources or biological functions, taking into account their antibacterial, antifungal, antiviral, anticancer, wound healing or immune modulation activities¹⁴. On the other hand, despite the low percentage of AMPs (13%) with known 3D structure, mainly determined by nuclear magnetic resonance in solution (NMR) and to a lesser extent by X-ray diffraction, the three-dimensional structure is, so far, one of the most widely used methods for the classification of AMPs. Currently, due to the small number of AMPs with determined three-dimensional structure, another classification method has been introduced based on peptide bonding patterns, a property which turns out to be independent of the structure, peptide source or activity. This methodology comes from the study of the connection mode of the polypeptide chain and differentiates 5 classes of AMPs¹⁵. However, here we have preferred to use the three-dimensional structure as an established accepted method. Though AMPs were usually classified into α -helical, β -sheet, and extended structures^{14,16} a later classification method¹² proposed to classify AMPs into four families: α , β , $\alpha\beta$, and non- $\alpha\beta$, based on the types of secondary structures¹⁵. The peptides belonging to the α family have predominantly a structure based on alpha helix (figure 3A). Conversely, β family peptides are characterized

by having a majority of beta sheet structure (figure 3B). The $\alpha\beta$ family includes peptides having both secondary structures in a similar proportion (figure 3C) whereas peptides that are included in the non- $\alpha\beta$ family have lost the presence of either of these two secondary structures (figure 3D).

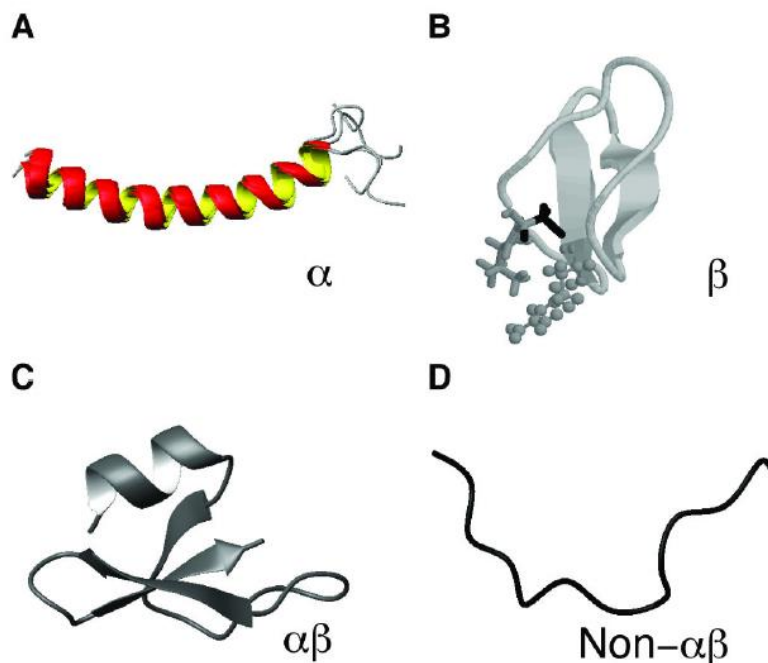


Figure 3. 3D structure antimicrobial peptide classification into four families. (A) α -helical structure of human cathelicidin LL-37 (PDB entry: 2K6O); (B) the β -sheet structure of the plant phy3 domain (PDB entry: 1JNU); (C) the $\alpha\beta$ structure of human β -defensin-1 (HBD-1) (PDB entry: 1IJV); and (D) the non- $\alpha\beta$ structure of cattle indolicidin (PDB entry: 1G89). Taken from ¹⁵.

1.1.1.1 α -helical amino acid structures

This is the most abundant type of peptide, with almost 350 being reported in the APD and isolated from many organisms from different phylogenetic kingdoms. Short α -helical peptides are usually cationic, not exceeding 50 residues in length and stabilized by non-covalent linkages. Among the predominant members of this family we find cathelicidins, cecropin, dermicidin and magainin. Alpha-helical peptide model is shown in figure 4.

Cathelicidins are antimicrobial peptides grouped in a representative host defence peptide family and are mostly expressed in leukocytes and epithelial cells of mammals in response to different pathogens, contributing to their elimination^{17,18}. Human cationic antimicrobial peptide-18 (hCAP-18/LL-37) is nowadays the leading characterized human cathelicidin, which could stage a therapeutic role against viral or bacterial infections as well as other severe diseases like cancer^{19,20}.

Cecropin was the first insect AMP isolated from the bacteria-challenged *Hyalophora cecropia* pupa²¹. In the last decades, another cecropin-like peptides have also been discovered. These peptides consisting in 30-40 amino acid in length are among the most potent induced peptides to counteract invading microbes. A large number of cecropin-like peptides were isolated from a large number of different organisms, including mammals^{22,23}. Cecropin P1 (CP1), a mammalian homolog isolated from nematodes found in the stomachs of pigs, has been reported to be active against Gram-negative bacteria and circular dichroism (CD) results have recently shown that CP1 is able to form a well-defined α -helical structure in the presence of LPS²⁴.

Dermcidin (DCD) is a 110-amino acid precursor peptide with alpha constitutively helix structure secreted into the sweat, where it undergoes proteolytic processing to yield several truncated peptides differing in charge and length, which has been shown to be active against numerous bacterial species by the formation of oligomeric complexes in the plasmatic membrane that subsequently cause their permeabilization^{25,26}. The detection of dermcidin-derived antimicrobial peptides in eccrine sweat demonstrated that sweat actively participates in the constitutive innate immune defence of human skin against infection. In the meantime, a number of studies proved the importance of dermcidin and others derived peptides such as DCD-1L, in skin host defence²⁷. Several reports also state that peptides processed from the dermcidin precursor protein exhibit a range of other biological functions in neuronal and cancer cells²⁸.

Magainins and dermaseptins are two types of cationic, amphipathic α -helical peptides that have been isolated from the skin extracts of frogs *Xenopus laevis* and *Phyllomedusa sauvagei* respectively. Magainins, also called glycine serine peptides consist in 23 amino acid long peptides belonging to a wide family of amphibian α -helical antimicrobial peptides which are active against a broad spectrum of microbes and have also been explored for their contraceptive effects and wound healing^{29,30,31}. Magainin 2 is among the best-studied cationic antimicrobial peptides and binds preferentially to negatively charged membranes and apparently cause their disruption by the formation of transmembrane pores, whose detailed structure is still unclear³². Dermaseptins are 28-34 amino acid length peptides with a conserved Trp residue at position 3, a consensus motif in the middle region of the sequence and a positive charge due to the presence of many Lys residues^{33,34}. Several dermaseptins and their analogues show an inhibitory effect against a broad spectrum of microbial cells^{35,36}.

Interestingly, in order to make more effective and improve the antimicrobial ability of AMPs against bacterial species, novel synthetic hybrids were rationally designed from LL-37, cecropin A and magainin II. AMPs were selected based on their α -helical secondary structure and their fragments were analyzed and combined *in silico* to determine which hybrid peptides would form the best amphipathic cationic α -helices³⁷.

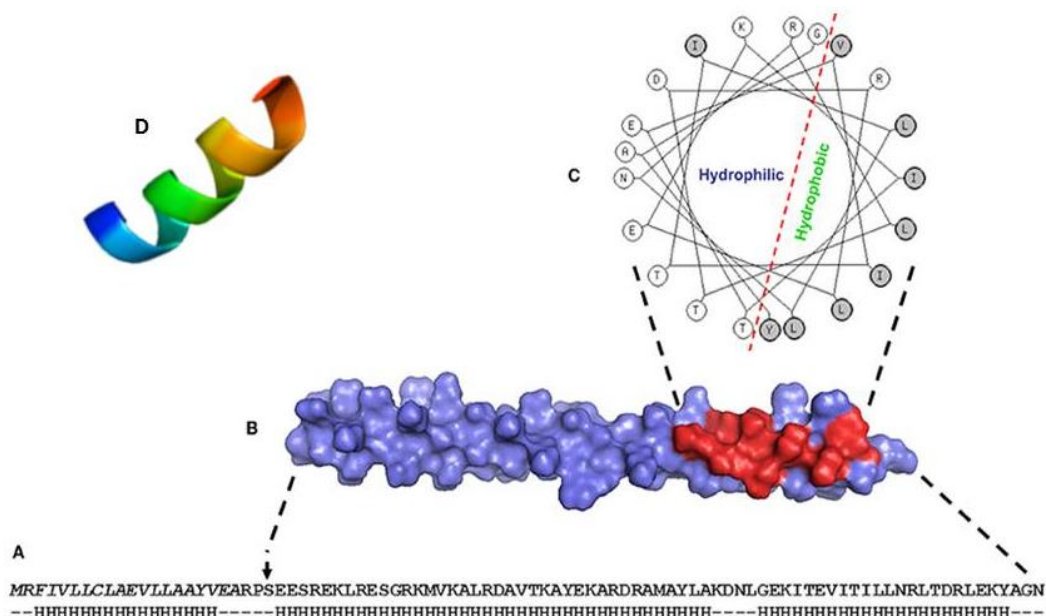


Figure 4. FhHDM-1 is a 8 kDa protein secreted by the trematode *Fasciola hepatica* which is grouped in the cathelicidin family as it has a high propensity to adopt α -helical secondary structure. Similarly to hCAP18, the secreted FhHDM-1 undergoes cleavage by an endogenous protease to release a C-terminal fragment. The 34-residue C-terminal peptide of FhHDM-1 contains a 21-residue amphipathic helix which exhibits a marked structural parallel with the bioactive human LL-37 peptide and is important for its antimicrobial activity and other biological activities. (A) Primary amino acid sequence of the archetypal HDM secreted by *Fasciola hepatica*, FhHDM-1. The N-terminal signal peptide is shown in italics and the predicted secondary structure (predominantly alpha helix) is shown below. (B) Model structure of FhHDM-1 with the residues forming the hydrophobic face of the molecule shown in red. (C) Helical wheel analysis shows that the C-terminal region of FhHDM-1 forms a distinct amphipathic helix. (D) 3D structural representation of LL37. Taken from ³⁸.

1.1.1.2 β -sheet amino acid structures

Peptides and proteins in the β family are composed of mainly β -strands. The beta sheet is the second common type of secondary structure in proteins. A β -sheet is formed by a variable number of beta strands laterally interconnected via hydrogen bonds and normally stabilized by disulphide bonds, giving place to a twisted and pleated sheet. β -branched and aromatic amino acids are usually found in the middle of β -sheets while other types of residues (such as Pro) are located in the border, allegedly to prevent a prone aggregation or even amyloid formation³⁹. There are currently 100 entries for members of this family in the APD¹³, among which we could highlight the α -defensins (HNP-1 – 4, HD-5 and 6), which deserve special mention for their broad recognition and published studies in this cluster.

Human defensins are a set of cationic and rich-cysteine peptides directly involved as mediators in innate immune response due to their immunomodulatory and microbicidal

properties, constituting the major group of AMPs in the mammalian pulmonary host defence system^{40,41,42}. Defensins are grouped into three subfamilies: α - and β -defensins (figure 5), that present a triple-stranded antiparallel β -sheet conformation stabilized by three disulphide bonds, and θ -defensins that are cyclic peptides consisting of a pair of antiparallel β -sheets linked by three disulphide bridges, that provide an extremely stable structure^{43,44}. Within this family are other no less important peptides such as lactoferricin^{45,46}, hepcidin^{47,48}, gomesin⁴⁹, protegrin⁵⁰, tachyplesin⁵¹ among others.

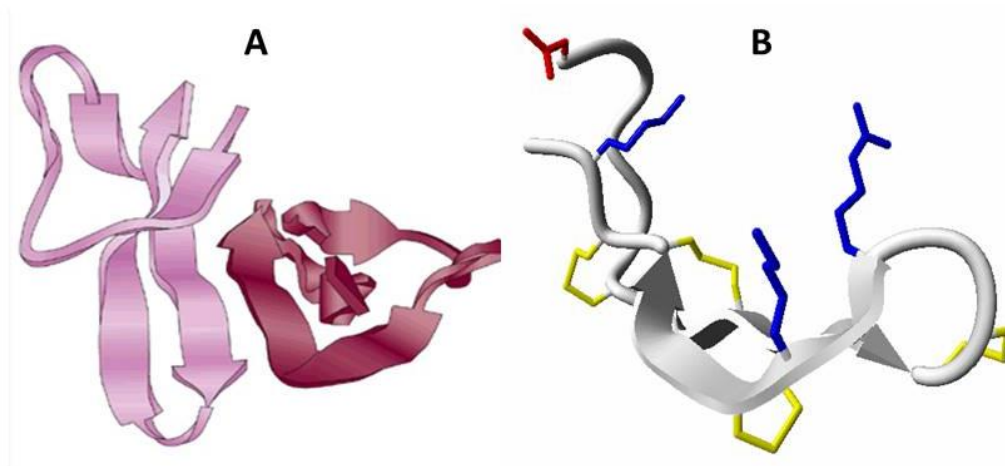


Figure 5. Cartoon structures of representative members of α -defensin and lactoferricin families. (A) Human neutrophil peptide 3 (HNP3, α -defensin) forms a β -sheet-rich dimer. (B) Overview of the structure of hepcidin. β - sheets are shown as grey arrows, cysteines are yellow, positive residues, arginine and lysine, are blue and the negative residue aspartic acid is red (PDB entry: 1m4f). Taken from ^{52,53}.

1.1.1.3 α -helical and β -sheet mixed structures

Peptides within this group are characterized by having both α -helices and β -sheet structures in a balanced percentage. $\alpha\beta$ family is a large group, but ranked third when compared to the aforementioned groups, with nearly 100 peptides listed in the APD. Examples within this group are peptides like drosomycin, an inducible antifungal peptide of 44 residues initially isolated from bacteria-challenged *Drosophila melanogaster*^{54,55}; heliomicin, similar to plant defensin RsAFP2 and active against *C. albicans* and *P. pastoris*⁵⁶; thrombocidins, a bactericidal 68 residue peptide isolated from human blood platelets⁵⁷. Moreover, it is in this section where the antimicrobial ribonucleases can be included as they have a secondary structure based on α -helices and β -sheets (figure 6)⁵⁸.

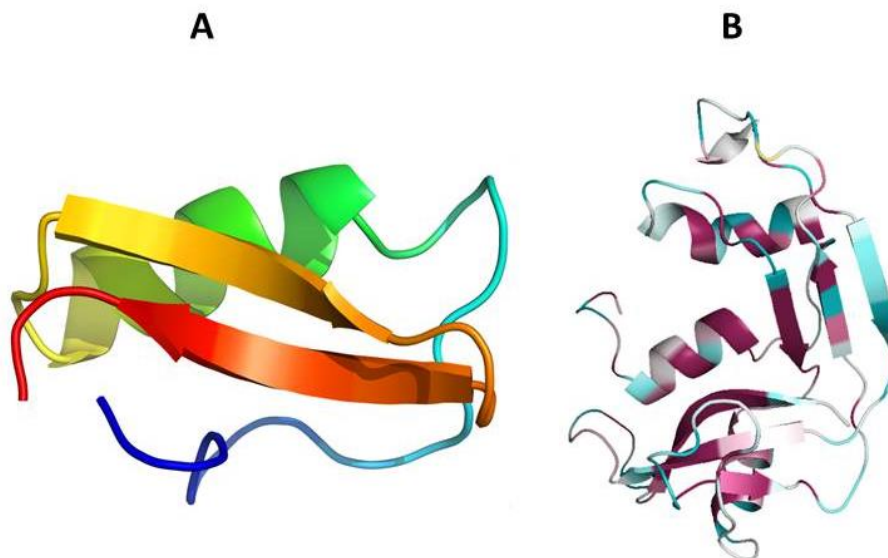


Figure 6. 3D structures of representative members of $\alpha\beta$ family. (A) Drosomycin (PDB entry: 1myn). (B) RNase 3 (PDB entry: 4X08).

1.1.1.4 Non- $\alpha\beta$ peptides

Within this family are grouped those peptides that have an ambiguous secondary structure and whose classification is not straightforward. In this cluster, the peptides are ascribed because of their lack of secondary structural motifs. We are mainly talking about extended linear structures as well as peptides with a predominance of any specific amino acid in their sequence. Titrpticin and indolicidin are 13 amino acid tryptophan-rich peptides derived from porcine precursor protein and bovine neutrophils respectively which have shown both bactericidal and antifungal activities^{59,60} (figure 7). Pyrrocoricin and drosocin are proline-rich bactericidal peptide isolated from the European fire bug *Pyrrhocoris apterus* and *drosophila melanogaster*^{61,62}. Other important peptides belonging to that group are nisin A (non- $\alpha\beta$), a bacteriocin that has been successfully approved as an antimicrobial with commercial relevance in over 50 countries worldwide since its discovery back in 1927⁶³, and histatins, a histidine-rich antimicrobial family of peptides^{63,64}.

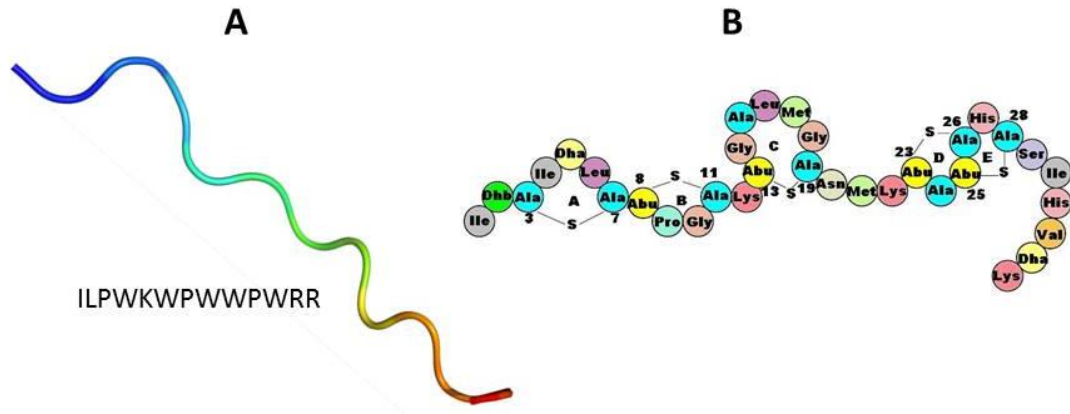


Figure 7. Two representative peptides of the non- $\alpha\beta$ family. A) Indolicidin and B) Nisin A

1.1.2 Antimicrobial polypeptides/proteins

Equally to short peptides, numerous polypeptide structures exert a significant antimicrobial activity against a wide range of pathogens and therefore play a multifunctional role in the host innate defence^{65,66,17}. Lactoferrin, azurocidin and neutrophil elastase are some examples of antimicrobial proteins in mammals besides RNases, to which the present work is focused and therefore is the object of a deeper study later. Lactoferrin (LF) is a multifunctional iron binding glycoprotein which is present in most body fluids and in some human organs, it has a molecular weight of 80 kDa and belongs to the transferrin family which is essential for iron homeostasis regulation⁴⁵. Currently, multiple LF activities apart from iron binding and traffic are evidenced. LF displays important mechanisms involved in host defence and has powerful antibacterial, antiparasitic, antifungal and antiviral effects^{46,67}. The azurocidin, as a leukocyte polymorphonuclear granule protein, is a cationic antimicrobial protein of 37 kD, also called CAP37 or Heparin-Binding protein, due to its high affinity for heparin^{68,69,70}. Shortly after its discovery it was found that the azurocidin, like other antimicrobial proteins, not only displays an antipathogenic mechanism but is also capable of exerting a mediating role in the modulation of host defence system^{71,72}. Neutrophil elastase (NE), also known as elastase 2, is a 29 kD protein, expressed rapidly during myeloid development and secreted by neutrophil during episodes of inflammation or infection. Moreover, NE belongs to the serine protease family⁷³. Interestingly, it has been shown that this protein is able to develop a bactericidal role within phagolysosomes of human neutrophils^{74,75}.

1.2 Bio-structural features for antimicrobial activity

The physical and structural characteristics of any molecule play a key role in the interpretation of their biological activities. Thus, knowledge of those common properties possessed by the AMPs is a breakthrough in the understanding of their antimicrobial

activities. Many studies had led to reveal the main elements that provide these features and therefore placed the AMPs as an essential part of the innate immune system. Nowadays, there is a huge variety of antimicrobial sequences that have promoted a widespread structural diversity. Notwithstanding, the preservation of different structural motifs highlights certain antimicrobial capabilities against different pathogens or targets. Many comparative and alteration sequence analysis have been used to reveal these properties. Secondary structure, hydrophobicity, cationicity and amphipathicity are the most important determinants, although not the only ones, that confer these antimicrobial traits.

1.2.1 Secondary structure and length

Structural information has been an essential tool to know directly the importance of protein folding as well as the secondary structure in antimicrobial activity. Circular dichroism spectroscopy, X-ray crystallography and nuclear magnetic resonance spectroscopy (NMR) have been the most commonly used techniques that have allowed us to decipher the 3D-structure of most of the AMPs. The main structural motifs present in AMPs are the amphipathic alpha helix and beta sheet, nevertheless, some AMPs exist as unstructured or extended forms and only acquire a defined secondary structure in the presence of membranes or phospholipid vesicles^{76,77}. Usually, the existence of alpha helix structures in AMPs facilitates the interaction, destabilization and lysis of cell membranes⁷⁸. Thus, those amino acids that are likely to form this type of secondary structure have been studied to potentially design synthetic AMPs⁷⁹. On the other hand, the length of the polypeptide chain in AMPs is a greatly variable factor and could affect to a greater or lesser degree the antimicrobial capacity. There is much controversy around this topic, and there is still no definite length sequence that has to be taken into account when designing new AMPs.

1.2.2 Amphipathicity and polar angle

The amphipathicity of a peptide structure indicates the quantity and the polarization of hydrophobic and hydrophilic domains. In general terms, the AMPs show a balanced distribution of hydrophobic and hydrophilic residues and frequently possess a net positive charge. The sum of hydrophobicity together with the cationic charge favours the formation of amphipathic structures. One of the most used methods to quantify the amphipathicity is the hydrophobic moment, which is often considered to be related to the peptide antimicrobial activity.^{80,81} Although this property has a direct action on the antimicrobial activity because it drives the mechanism of interaction with the membrane of the pathogen, there is some controversy regarding the relationship between the amphipathic and anti-pathogenic activity as numerous studies have demonstrated that the increase of the amphipathicity promotes the antimicrobial capacity but equally the haemolytic

activity^{82,83,84}. The polar angle is another property mostly present in the alpha helix structures which is intrinsically linked with the hydrophobic moment and amphipathicity. The polar angle is defined as the relative angular ratio between nonpolar and polar residue faces of an amphipathic helix structure (figure 8). An hypothetical alpha helix structure composed equally by a hydrophobic facet and a hydrophilic facet would have a polar angle of 180° (a). Less segregation between domains or an overabundance of hydrophobic residues would cause the appearance of lower polar angle. Studies with synthetic peptides and natural occurring peptides that present a lower polar angle and therefore a greater proportion of hydrophobicity have reported a greater translocation and permeabilization membrane capacity. In contrast, the pores formed by such peptides are more unstable than those formed by peptides with a higher polar angle⁸⁵.

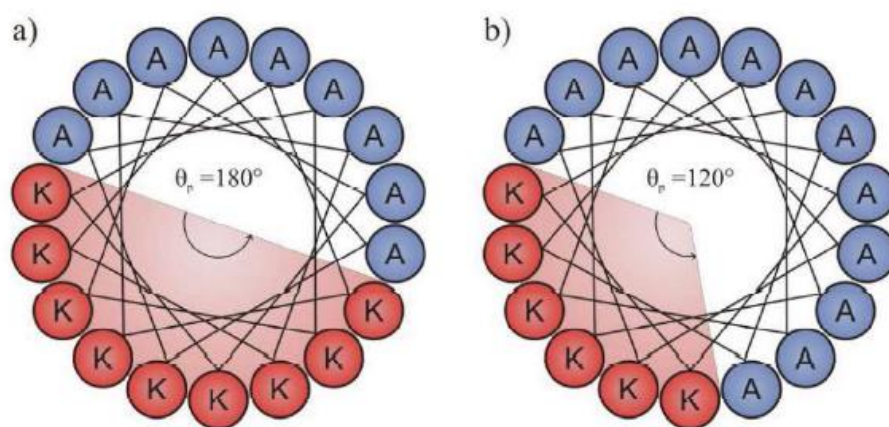


Figure 8. Helical wheel diagram showing two hypothetical amphipathic peptides with different polar angle. Charged hydrophilic residues are red and hydrophobic residues are blue. **a)** One side of the helix has hydrophilic residues and the other hydrophobic. This gives a polar angle of 180° . **b)** One third of the helix is hydrophilic and the two thirds hydrophobic, giving a polar angle of 120° . Taken from⁸⁶.

1.2.3 Cyclic structures

Taking into account the heterogeneity of structures that AMPs can adopt, it is also noteworthy to mention the peptides ability to generate cyclic structures, such as the tachylepsins or protegrins ones. Cyclic AMPs have shown to be effective against several bacterial strains and have also been studied in order to clarify the elements that exert this anti-pathogenic ability⁸⁷. There are several studies showing an increased yield of antimicrobial capacity to the detriment of the haemolytic activity of cyclic peptides as compared with linear analogues⁸⁸. On the other hand, in relation to its mechanism of action, it has been found that such peptides would not only act at the membrane level but also would be able to internalize and carry out their performance on intracellular targets⁸⁹. Moreover, because of the importance of the amphipathicity in terms of antimicrobial

activity, these cyclic peptides would promote an increase in both the structure stability and amphipathicity, and further studies are underway to strengthen these properties⁹⁰.

1.2.4 Hydrophobicity

Peptide hydrophobicity is considered an essential structural feature and is correlated to the functional activity of an AMP. It could be defined as the percentage of hydrophobic residues found in a peptide structure and is generally around 50% in the case of AMPs (figure 9). It participates in the interaction process between peptides and cell membranes and manages the distribution of the peptide structure when it inserts into the lipid bilayer. Thus, increased hydrophobicity results in a loss of antipathogenic specificity as well as an increase in cytotoxicity towards host cells. On the other hand, a hydrophobicity decline clearly reveals a decrease in terms of antimicrobial activity⁹¹.

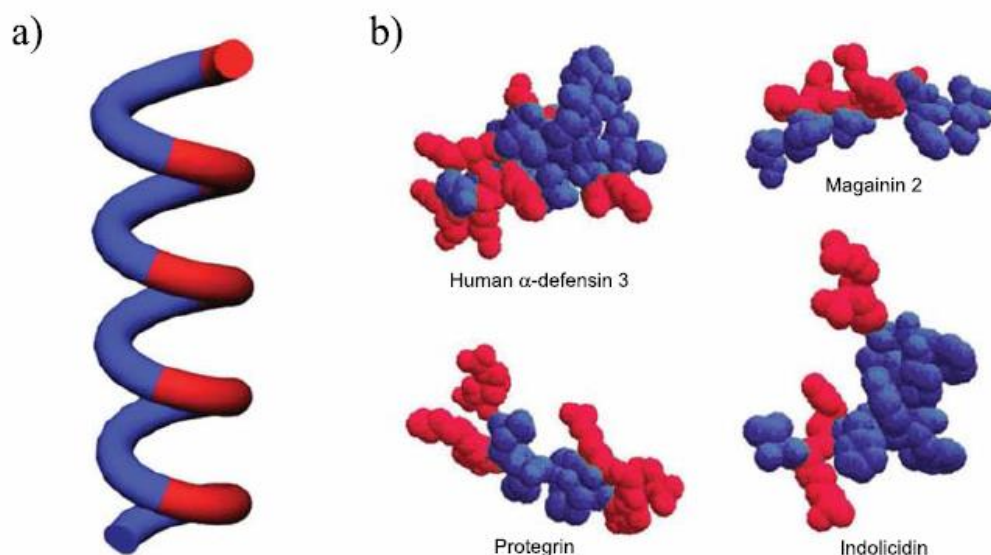


Figure 9. a) Alpha helical representation of an amphipathic structure with charged (red) areas aligning down one side of the helix and hydrophobic residues (blue) down the other side. b) Clustering of cationic and hydrophobic residues of several AMPs of different structural classes. Taken from⁸⁶.

1.2.5 Conserved salt bridges

Salt bridges are within a broad category of noncovalent interactions and they are basically a combination of two non-covalent interactions: a hydrogen bond and an electrostatic interaction. This type of interactions is usually observed in α -helical and β -sheet AMPs structures, favouring the folding and stability. Although salt bridge interactions are weak, the sum of all of them can contribute greatly to the stability of the AMPs secondary structure. Such interactions are usually formed by specific groups of amino acids, the most common would be the anionic carboxylate group in the case of glutamic acid or aspartic acid, the cationic ammonium group in the case of lysine or guanidine group in the case of

arginine^{92,93}. Though such interactions do not directly affect the antimicrobial capacity, they contribute in the pairing of disulfide bridges and therefore in its activity as well as in its proteolytic stability^{94,95}.

1.2.6 Cationicity

One of the most strongly conserved features of AMPs is its cationic nature. This cationicity is given by the number of positively charged residues found in the peptide sequence⁹. Amino acids such as lysine, arginine and histidine contribute to the final net charge of the AMP, ranging in most cases from +2 to +10. The value assigned to this property is attributed to the importance of the electrostatic mechanism of interaction between the negatively charged bacterial membrane and cell wall components (such as phospholipids, lipopolysaccharides, peptidoglycans, teichoic acids...) and positively charged peptide structures. One can speak of a direct correlation between the net charge of a peptide and its effectiveness, but this correlation is lost above a certain cationicity threshold, leading to a decrease of the antimicrobial capacity and an increase of the haemolytic propensity⁹⁶. Furthermore, it has been found that the replacement of this series of positively charged amino acids causes a decrease in both the interaction and the antipathogenic capacity of AMPs⁹⁷.

1.2.7 Antimicrobial activity hallmarks: specific amino acid residues

Although AMPs share structural patterns that confer them their functional characteristics, their amino acid sequence differs greatly, showing a clear absence of common sequence motifs. Each of the amino acids along with all the others residues that make up a sequence are responsible for the characteristics that are finally granted to the polypeptide. Thus, within this section we would like to highlight the great structural and functional value possessed by some amino acids in the AMPs.

Tryptophan (Trp, W)

Apart from the classical amino and carboxylic groups present in all amino acids, tryptophan consists also in a side chain indole. It is an essential amino acid in humans and is classified as a non-polar, aromatic residue. Indole group is responsible for maintaining the potential of hydrogen bonds and participates in other physicochemical characteristics⁹⁸. Some molecular dynamics studies have revealed that tryptophan residues are likely to enter and interact with lipid membranes^{99,100}. Dynamic light scattering, scanning and transmission electron microscopy studies have shown that tryptophan residues facilitate both the insertion of AMPs in the membrane as its disruption^{101,102}. Antimicrobial effectiveness of tryptophan residues has been widely demonstrated by substitutions of one or more residues, which

significantly improve activity against numerous Gram-negative and Gram-positive bacterial strains^{103,104}. In conclusion, Trp residues have a singular predilection for the interface of the lipid bilayers and thus allow insertion of tryptophan rich AMPs into the cell membrane.

Proline (Pro, P)

Classified as nonpolar, aliphatic and non-essential amino acid in humans; proline consists on a ring structure (pyrrolidine) with a secondary amine and its alpha-amino group is attached directly to the side chain, which gives a high stiffness. Proline-rich AMPs are a type of cationic peptides that display a significant antimicrobial activity and tend to adopt helix-based structures. They show an intracellular mechanism of action by pre cytoplasmic translocation in contrast with other AMPs which tend to act at membrane level^{105,106,107}. Some representative members of this group are peptides such as Bac, PR-39, apidaecin or drosocin. Proline-rich peptides have well-recognized properties (antibacterial potency, solubility and low cytotoxicity) and because of this, they have been studied in recent years with the aim of designing synthetic analogues that promote improvement of traditional therapeutic antimicrobial agents¹⁰⁸.

Cysteine (Cys, C)

Cysteine is a semi-essential amino acid with a large reactive capacity and is equipped with a thiol group, which presents a high susceptibility to be oxidized and form a disulfide bridge with another nearby cysteine residue. Disulfide bridges play a significant structural role in numerous AMPs since they increase the stability of their secondary and tertiary structures and prevent their denaturation¹⁰⁹. Some studies have demonstrated that the elimination of this type of intramolecular interactions has a negative impact on the antimicrobial activity in most cases^{110,111}. Polyphemusin 1 and pig protegrin are some of the best known cysteine rich peptides and loss of the ability to kill bacteria occurs when some of their cysteine residues are removed^{112,113,114}.

Lysine (Lys, K) and arginine (Arg, R)

Lysine and arginine are classified as positively charged and aliphatic amino acids. Basically, the main difference lies in their side chains, lysine has a lysyl group while arginine has a side chain of a 3-carbon aliphatic straight chain capped by a complex guanidinium. Both amino acids have a basic character so they are able to direct the interactions that occur between the negatively charged bacterial membranes and AMPs^{115,116}. During the last decades, numerous studies have been conducted in order to understand the properties that offer these amino acids to AMPs, in terms of functionality. Thus, different peptidomimetics have been synthesized with a variable degree of cationicity thanks to the inclusion of these residues in the amino acid sequence¹¹⁷. It has been shown that substitution of arginine for lysine generates slight changes in antimicrobial activity but a significant decrease in haemolytic activity¹¹⁸. Besides facilitating the initial interaction with the membrane

surfaces, it has been found that poly arginine and lysine sequences can be translocated more easily than other homopolymers and moreover, intracellularly, arginine-rich peptides have higher affinity for DNA than lysine-rich peptides¹¹⁹. Supporting that, arginine-rich cell-penetrating peptides have been broadly used on intracellular delivery of bioactive molecules¹²⁰. On the other hand, the rich sequences arginine and lysine have been widely identified in histones, proteins that besides contributing to packaging and structuring of DNA have shown antimicrobial activity generally by an intracellular mechanism, joining fragments of bacterial DNA^{121,122}.

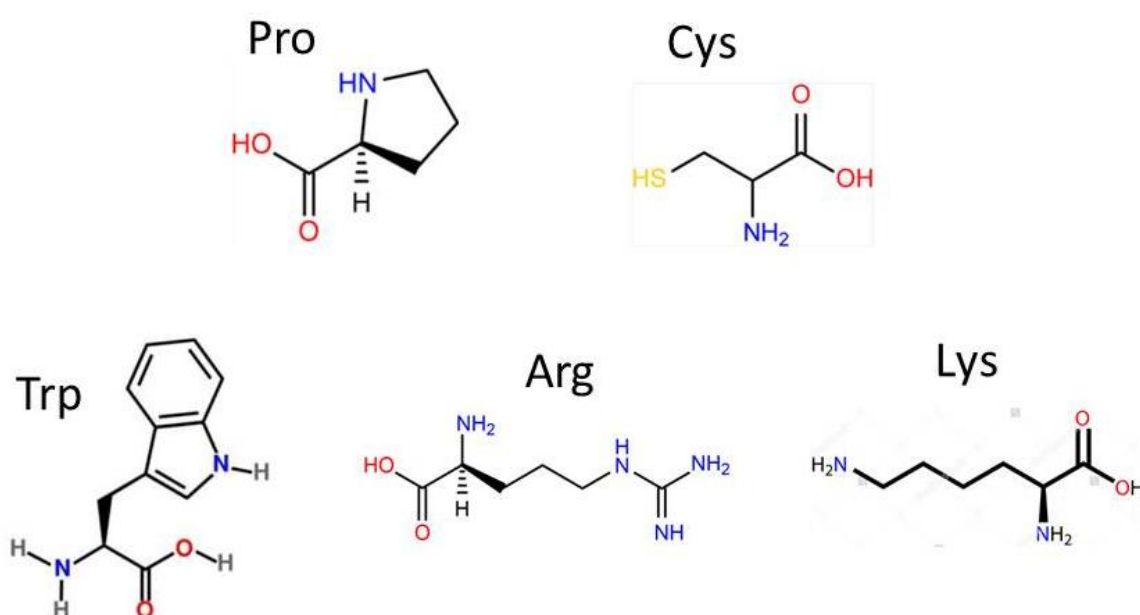


Figure 10. Amino structures with a prominent value of functionality in AMPs

1.3 Modes of action of antimicrobial peptides

Before considering AMPs as therapeutic antimicrobial agents it is important to know and understand their biological properties and mode of action. The mechanism of action of AMPs has been extensively investigated using different experimental techniques, from models with artificial membranes or large unilamellar vesicles (LUVs) to microbial cells, through the use of sensitive markers to detect changes in transmembrane potential and peptide fluorescent labels¹²³. As already mentioned previously, the natural base of the interaction between the AMPs and the pathogen membranes lies in the electrostatic interaction that occurs between the peptide charged hydrophobic faces and the large fraction of microbial membrane anionic compounds. This mechanism would be inefficient in the case of eukaryotic cells because of the high degree of selectivity by AMPs. Microbial cell

membranes have a high anionic lipid content such as phosphatidylglycerol while eukaryotic cell membranes are intensely populated by phosphocholines and cholesterol, this would explain the wide preference possessed by AMPs for bacterial membranes^{124,125,126}.

Thanks to the large number of published studies, many mechanisms of action have been reported and classified in two groups based on their molecular targets: membrane targeting and cell-penetrating peptides¹⁵. Since there is a diverse range regarding models for the mechanism of antimicrobial action and some of them are specific to particular AMPs, it is necessary to understand the consecutive steps that occur in the microbial membrane that precede its destabilization and permeabilization. In general, α -helical AMPs remain unstructured in an aqueous environment (fig. 11a) and during the initial interaction with the pathogen membrane. Following, AMPs undergo a series of transitions acquiring the classical secondary structures at the membrane surface (fig. 11b)^{127,128}. Unlike the latter, β -sheet AMPs are more stable and more structured in solution, mainly thanks to the disulfide bridges, so they do not suffer these transient structural changes. After the AMPs have managed to bind to its target, a basal concentration of peptides to trigger the following steps is needed (fig. 11c)¹²⁹. AMPs accumulate at the membrane environment and acquire the ability to self-associate and penetrate into the lipid bilayer. It is here where they exert their antimicrobial effect from a variety of mechanisms, which will depend on the ability of the peptide to self-assembly as well as the composition of the microbial membrane¹³⁰. After having reached a local threshold concentration of AMPs in the membrane surface, many peptides undergo a series of restructuring and are capable of forming, by multimerization, more complex structures/oligomers which promotes membrane alterations such as pore formation, lipid bilayer curvature and scaffold destabilization, micellization, etc. This translates into a general disruption of the bilayer by loss of membrane potential and increased permeabilization affecting cellular metabolism and killing^{131,132}. The probability of peptides for the formation of these oligomeric structures directly depends on the composition of the microbial membrane as well as the amino acid composition of the peptide while the success of the peptide complex formed will lie in the ability of these structures to reorient the hydrophilic and hydrophobic domains into the membrane core.

Despite the large number of studies, the specific mechanism of action of AMPs is not fully understood. However, as a result of this extensive knowledge a large variety of molecular models have emerged in order to explain the mechanism of action of AMPs¹⁵. The barrel-stave/toroidal pore models and the carpet-like mechanisms have been some of the best known alternative mechanisms that have been used to stage in detail the membrane permeation by α -helical peptides. Barrel-stave model was one of the first models postulated and describes a situation in which once the peptides are attached to the membrane, they would be able to align parallel to each other and perpendicular to the membrane surface getting a circular ultrastructure that would act as a pore or channel. Thus, the peptide hydrophobic domains would interact with membrane lipids while the hydrophilic areas form the lumen of the pore (fig. 11d). Ceratotoxin and alamethicin are examples of AMPs which

use a barrel-stave mechanism to disrupt membranes^{133,134}. Interestingly, it has been shown that the barrel-stave size distribution (number of peptides in the pore) is directly influenced by the composition of the lipid bilayer¹³⁵. Another type of membrane permeation model would be driven by a toroidal pore or wormhole mechanism. Although this model is similar to the barrel-stave structure, the difference is that the peptides interact with the phospholipid head groups and are not in contact with the hydrophobic core of the membrane¹³⁶. In this case, the stability is not as strong as in the barrel-stave model and therefore its half-life is shorter (fig. 3e). Magainins, melitin and protegrins cause transmembrane pores that conform to the toroidal model^{137,138}.

Notwithstanding, not all AMPs mandatorily act via pore formation since there are other modes of action that do not involve specific membrane permeation. This would be the case of carpet-like mechanism, in which after the electrostatic and parallel initial binding of the peptides with the membrane targets, AMPs entirely cover the membrane surface forming a “peptide carpet” and achieve disaggregation of the lipid bilayer into small micelles as a detergent-like process (fig. 11f-g)¹³⁹. AMPs such as cecropins and indolicin destabilize microbial cell walls following a carpet-like mode¹⁴⁰.

Since cell homeostasis and communication machinery are essential for the bacterial pathogenesis, some experimental procedures have been assessed to reveal the likely participation of AMPs on cell wall proteins. Thus, AMPs cell surface interaction has been also identified as an alternative ion exchange interference mechanism, able to inhibit microbial growth¹⁴¹. Some membrane protein complex are responsible for maintaining ionic gradients as well as the production of energy used in the ion exchange to maintain proper pH and prevent cell acidification¹⁴². It has been previously reported that many plasma protein activities can be inhibited by an indirect ionic binding with AMPs¹⁴³.

Irrespective of the cell membrane targeting mechanisms, which they appear to be one of the essential and successful modes of action to eliminate pathogens; there is increasing evidence of cell-penetrating peptides, which have also been associated with inhibition of microbial intracellular targets through their translocation across the membrane without disrupting it. Buforin and indolicin are able to cross the cell membrane and bind to DNA and RNA, inhibiting replication and transcription and thus speeding up the process of cell death^{144,145}. Furthermore, it has recently reported a type of synthetic peptides capable to internalize and bind unprotected genomic DNA, inhibiting DNA-dependent processes and leading to bacterial killing¹⁴⁶. Interestingly, it has been recently reported that some AMPs with an intracellular mode of action can be efficient vehicles for antibacterial peptide nucleic acid targeting essential fatty acid biosynthesis gene expression¹⁴⁷.

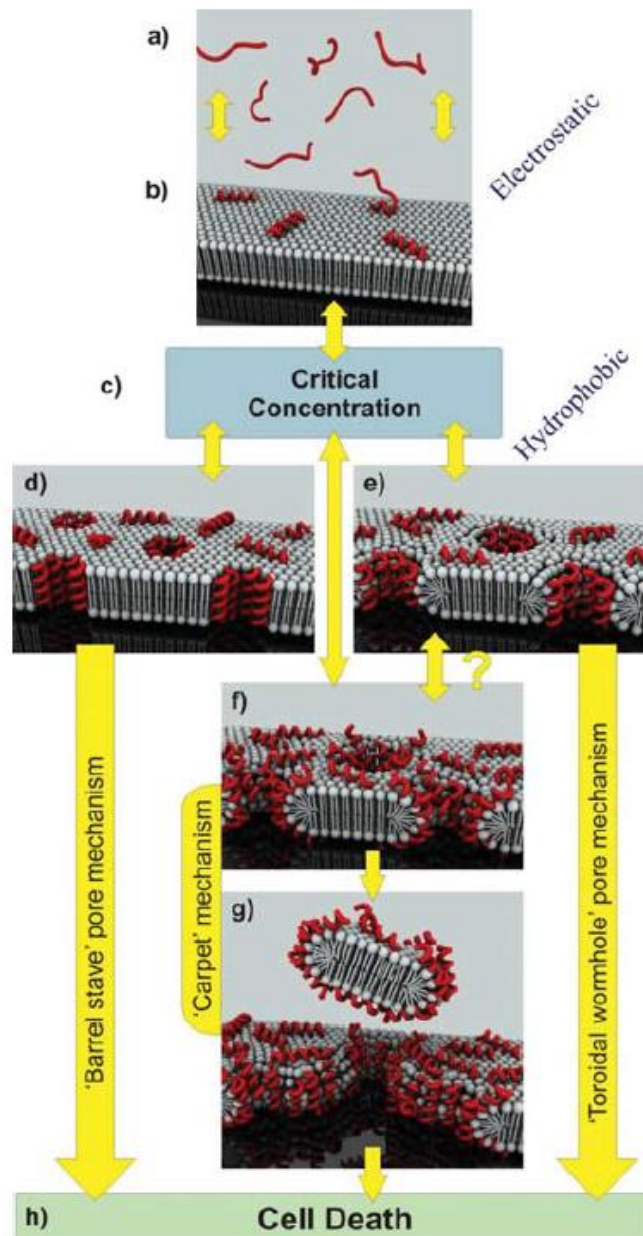


Figure 11. Schematic of the main classical models depicting the mechanisms of helical AMPs action. (a) peptides are unstructured in solution; (b) initial binding to membrane interface mediated by the electrostatic interaction with structural changes in peptides; (c) once the membrane-bound peptides reach a critical concentration, they proceed through a stochastic cooperative transition in a multistep process, destabilizing the membrane via either forming (d) barrel stave pore; (e) toroidal pore or (f) a carpet-like complex with extensive surface coverage (g) resulting in membrane disintegration. (e-f) The formation of toroidal pores can also proceed through a carpet-like process once a critical concentration of extensive surface coverage is reached (h) The overall outcome of these membrane-destabilizing processes is leading to cell death. Taken from⁸⁶.

1.4 Immune system and AMPs: an immunomodulatory link

AMPs are present in myeloid and epithelial cells and are both inducible and constitutively expressed by innate immune response. They are considered as multifunctional participants in the host defence system against microbes. There have been many studies that have highlighted AMPs as a kind of natural antibiotics and have demonstrated that in addition to their antimicrobial traits, they have an important immunomodulatory function and are able to establish a link between innate and adaptive immunity⁸.

1.4.1 Neutralization of LPS

The final outcome in case of serious infections is sepsis (blood poisoning), a health condition characterized by the appearance of a systemic inflammation that threatens the patient's life¹⁴⁸. One of the most frequent problems in intensive care units is the worsening of patients due to the administration of drugs that although they have antimicrobial properties, on the other hand, they facilitate the release of endotoxins into the bloodstream. Thus, the capacity of neutralizing endotoxin by AMPs as antibacterial drugs appears promising¹⁴⁹. The AMP cationic and amphipathic character is responsible for blocking the anionic glycolipids as a first step in the activation of immune cells¹⁵⁰. Numerous investigations have postulated that AMPs are capable of preventing pro-inflammatory responses induced by lipopolysaccharides, suppress the expression of genes induced by endotoxins and encourage the expression of anti-inflammatory genes in macrophages¹⁵¹. Cathelicidins and polymyxin can prevent LPS binding to LPS binding proteins and also inhibit the production of TNF α in bacteria challenged macrophages¹⁵⁰. A scheme of LPS neutralization is depicted in figure 12.

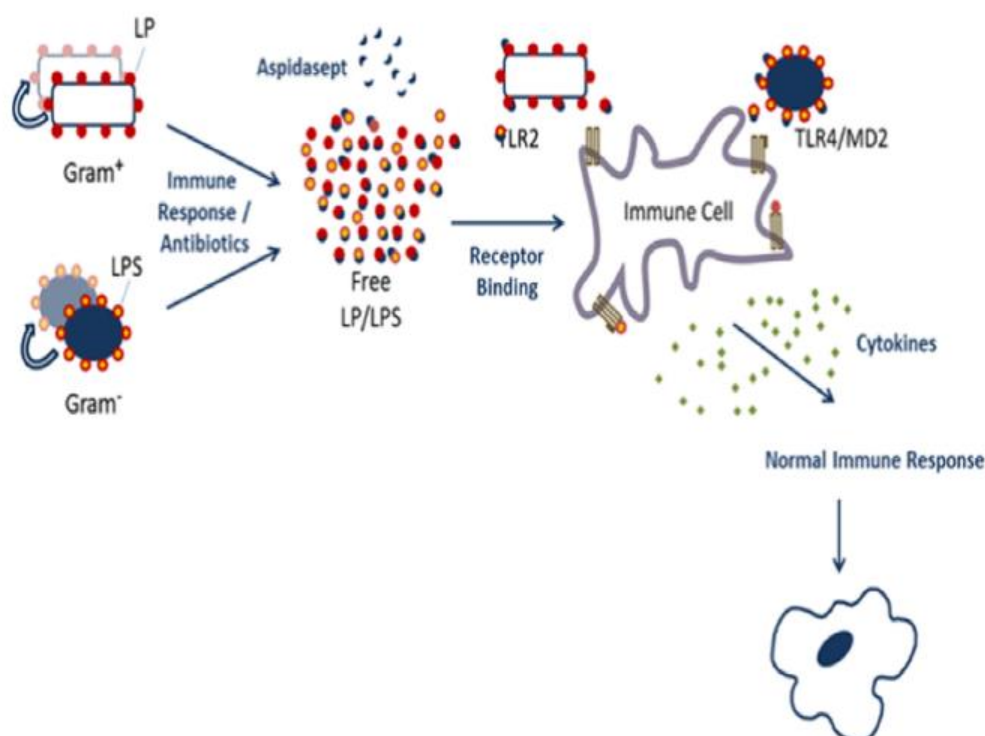


Figure 12. Schematics of the inactivation of bacterial toxins LPS and lipoprotein (LP) by the LPS neutralizing peptide Aspidasept®. The peptide binds to LPS, induces aggregation and converts the LPS aggregate into an inactive multilamellar form. In this form, the toxins cannot interact with serum compounds and cell receptors such as lipopolysaccharide-binding protein (LBP), CD14, and the TLR4/MD-2 system. Taken from¹⁵².

1.4.2 Chemotaxis activity

Defined as the ability of a uni or multicellular organism to move in response to a chemical stimulus, the chemoattraction was one of the first non-microbicidal properties attributed to AMPs. Many studies have shown that AMPs are capable to chemoattract multitude of cells that are part of the immune system such as monocytes, T cells, dendritic cells and neutrophils^{153,154}. It has been shown that human neutrophil defensins are able to produce an chemoattractive effect on both T and dendritic cells, and this process is toxin-sensitive, suggesting that a G protein-coupled receptor is responsible¹⁵⁵. The specificity of AMPs for certain receptors is also important because it determines the outcome of immunomodulation. LL-37 also plays an important immunoregulatory role, it is able to recruit a large number of immune cells and promote the secretion of some cytokines^{156,157}. Thus we could say that the AMPs can also lead chemotaxis in an indirect way since they achieve to induce the expression of a variety of cytokines, increasing and prolonging this phenomenon⁴⁰. Thereby, the AMPs can promote an early stage response to bacterial invasion, which would induce the leukocytes migration to fight infection and subsequently would facilitate an inflammatory regulation, modulating the immune response.

1.4.3 Epidermal growth factor interactions and wound healing

Since neutrophils are the largest producers of LL-37, it is considered that the release of LL-37 in epithelial tissues may contribute to cell signalling. In fact, it has been shown that this signalling pathway may be accomplished by epidermal growth factor receptor (EGFR) transactivation¹⁵⁸. On the other hand, LL-37 would also be able to activate keratinocyte migration and cell proliferation through the EGFR¹⁵⁹. Furthermore, LL-37 has been shown to promote *in vivo* wound healing with other AMPs, acting together with the aim of improving migration and epithelial cell proliferation^{160,161,162}. Accordingly, the cooperative activation of AMPs will strengthen the antimicrobial role of keratinocytes in a synergistic manner on inflammation and cell damage scenarios.

1.4.4 Adaptive immune response cooperation

There have been many studies to elucidate the possible modulator role of AMPs on the adaptive immune system. Some studies/laboratories have found a better immune response to various antigens and an increase in immunoglobulin levels due to the use of AMPs as adjuvants, reinforcing the involvement of AMPs in antibody production and T cell-dependent cellular immunity^{163,164}. The maturation of some immune cells through induction

by co-stimulatory molecules enhances antigen presentation as well as a reinforcement of cell activation, as it has been reported with defensins¹⁶⁵. The results suggest a hypothetical modulatory activity on lymphocytes by AMPs by the regulation of the expression of cytokines. In addition, an elegant study validated the effectiveness of a DNA-vaccine strategy showing how DNA immunization using constructs encoding beta defensins or cytokines displayed an improved humoral immunity against lymphoma¹⁶⁶. Moreover, α -defensins and LL-37 are able to modulate both dendritic and lymphocyte cells, thus improving the production of cytokines and increasing the immune strength^{167,168}. All these findings support that some AMPs such as defensins and other chemoattractant molecules have a key role in both innate and adaptive immunity and therefore a growing interest in their use as immunotherapeutic candidates is anticipated in the near future.

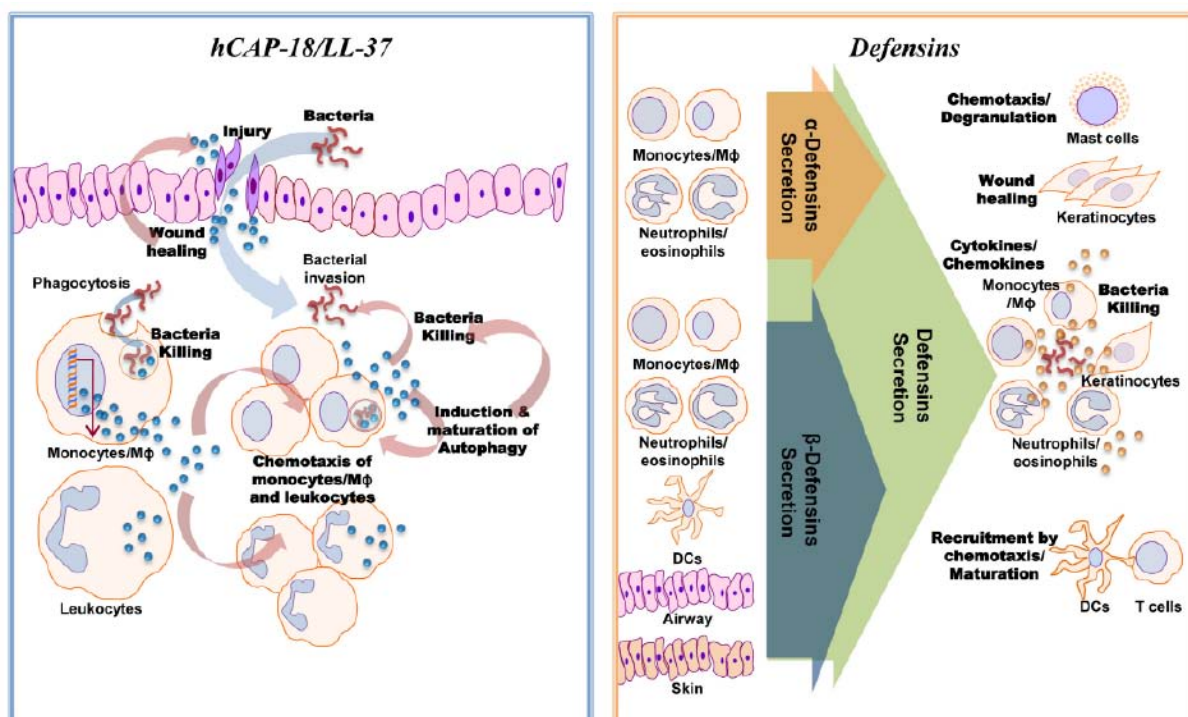


Figure 13. A schematic diagram for the role of AMPs such as cathelicidins and defensins in host immune system. Taken from ¹⁶⁹.

1.5 Human antimicrobial RNases

Human antimicrobial ribonucleases comprise a set of cationic and low molecular weight (12-16 kDa) proteins with multifaceted properties. They belong to the vertebrate-secreted ribonuclease A superfamily, a cluster of proteins whose name comes from the first ribonuclease discovered, the bovine pancreatic ribonuclease (RNase A), probably one of the best characterized enzyme¹⁷⁰. Its abundance, small size and high stability put the ribonuclease A in the spotlight during the 20th century and boasts three Nobel awards for its research¹⁷¹. The eight functional members belonging to the human breed are known as “canonical RNases” ¹⁷² (figure 14). It is worth noting the low sequence similarity between

some members despite belonging to the same family; however, they all share a common overall three-dimensional structure and a unique disulfide bridge pattern that facilitates a proper folding. Furthermore, they are able to degrade RNA substrates by a tryad of equivalent residues that form the catalytic centre, consisting of two histidines and one lysine. Moreover, it should be noted that in addition to their catalytic activity other biological properties were reported for some members. Among these, the antimicrobial activity as well as the ability to modulate the host immune system deserves a special mention, pointing to a possible evolution from an ancestral host-defence function^{173,174,175}. In this thesis we have worked mainly with human RNase 3, 6 and 7, three of the superfamily members that have demonstrated a wide antimicrobial activity and are addressed in more detail in the following sections.

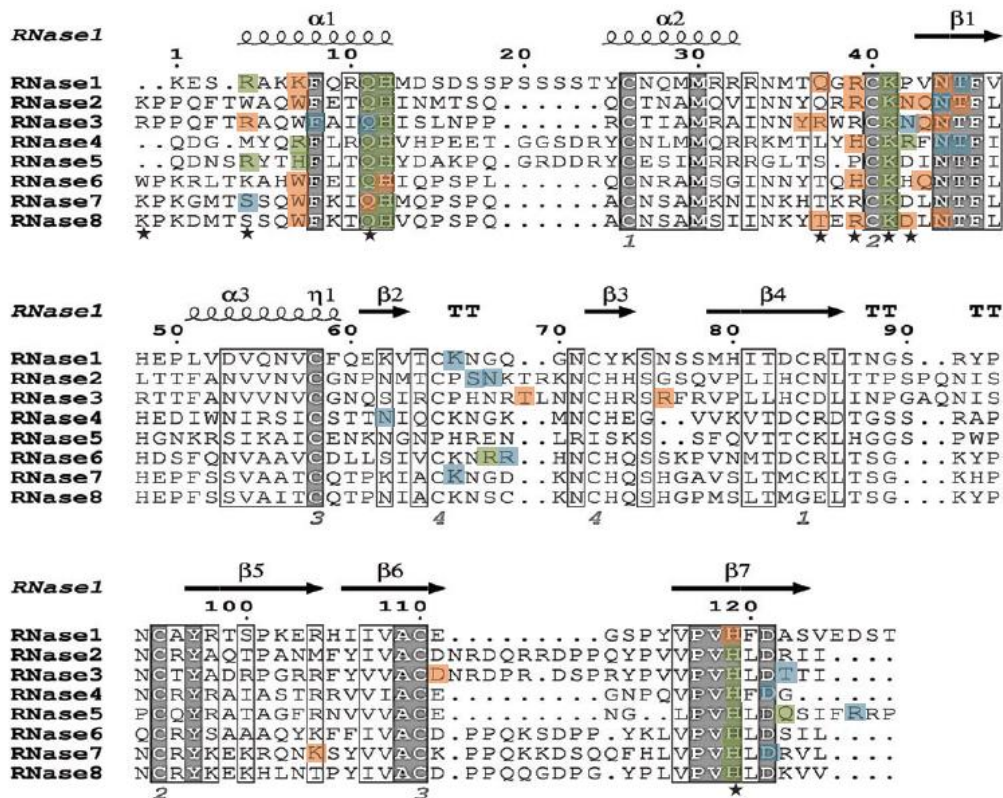


Figure 14. Sequence alignment of the human RNases belonging to the vertebrate-secreted RNase A family. Conserved amino acids in all sequences are boxed in grey. The specific side chain-interacting residues identified in docking analysis are highlighted by coloured boxes: residues interacting with nucleotide probes are in blue, residues interacting with heparin probes are in orange and common residues are in green. Residues that interact with sulphate anions in ECP crystal complex structure (4A20.pdb) are labelled with black stars at the bottom. The alignment was performed using *Clustal W*, and the picture was drawn using the ESPript program (<http://esript.ibcp.fr/ESPript/>). Taken from¹⁷⁶.

1.5.1 RNase 3 / Eosinophil Cationic Protein (ECP)

Multitude of clinical and experimental data have shown the role of eosinophils in the pathogenesis of many diseases and syndromes as well as their immunomodulatory character in the host defence system and maintenance of physiological homeostasis in different tissues^{177,178}. These immune white blood cells are equipped with a series of cationic proteins stored in their secondary granules which can be selectively secreted. Some of these eosinophil-derived granule proteins (EDGPs)¹⁷⁹ are responsible for contributing to the functionality of eosinophils in inflammation of the respiratory tract, tissue damage and anti-pathogenic capacity¹⁸⁰. This group of proteins includes major basic protein-1 and -2 (MBP-1, MBP-2), eosinophil peroxidase (EPX/EPO), eosinophil cationic protein (ECP) and eosinophil-derived neurotoxin (EDN). Following, we will focus on the characteristics of the RNase 3/ECP due to its central role in the present PhD experimental work¹⁸¹.

Human RNase 3 is a small cationic protein of 133 amino acids located in the matrix of the secondary granules of human eosinophils. Its cationicity is generated due to the high proportion of basic residues in their sequence, highlighting the presence of 19 arginine residues, which confer an unusual high isoelectric point (10.8). As other RNase A family members, its structure responds to an $\alpha\beta$ conformation (3 α -helices and six β -sheet) stabilized by four disulphide bridges¹⁸² (figure 15). As an eosinophil granule protein, ECP is able to combine cytotoxic and antipathogenic capabilities with immunomodulatory features that address a wide range of situations that could jeopardize the integrity of the human body. Antimicrobial activity against bacteria and parasite infections^{183,184}, antitumoral¹⁸⁵, antiviral¹⁸⁶, neurotoxic and cytotoxic activities¹⁸⁷ are some of the ECP properties that have been reported.

Evidence is accumulating that RNase 3 participates in host responses and is active against both Gram-negative and Gram-positive bacteria through cell wall and cytoplasmic membrane mechanism of action¹⁸⁸. Interestingly, unlike EDN, ECP ribonuclease activity seems to be not directly implicated in its mode of action¹⁸⁶. On the other hand, a novel bacterial agglutinating process has been proposed for ECP by Torrent *et al.*¹⁸⁹. The agglutination activity seems to be driven by an amyloid-like aggregation of the protein at the bacterial surface and what is more, this agglutination activity can be abolished by a single point mutation (I13A). Peculiarly, both cell wall disruption and bacterial agglutination processes have been located at its N-terminal 45 first residues¹²³.

1.5.2 RNase 6

The discovery of human RNase 6 was an unexpected outcome while trying to track the evolution of the ribonuclease gene family. Rosenberg *et al.*¹⁹⁰ isolated the cDNA encoding this human protein. RNase 6 maintains the classic features of the RNase A superfamily, with a molecular weight of 14.7 KDa, a high overall 3D structural similarity (Figure 15), an elevated isoelectric point (9,49) the presence of the canonical cysteines and the

conservation of the catalytic triad, with a catalytic activity ~30 fold higher than ECP. Subsequently, the detection of its mRNA in both peripheral blood neutrophils and monocytes suggested a human host defence role. Interestingly, chromosomal mapping and divergent evolution studies of several RNase 6 orthologous genes have shown that RNase 6 is a stable lineage in contrast to those determined for primate orthologous of two closely related RNases (EDN and ECP)¹⁹¹. On the other hand, it has been found that this rate of evolution is much higher in rodents than in primates, suggesting that the gene of RNase 6 has been exposed to selective pressure that could explain the high degree of divergence between human and mouse¹⁹². It was not until relatively recently when it has been shown by Becknell *et al*¹⁹³ that RNase 6 is expressed in host innate cell types and has a potential antimicrobial function in the human and murine urinary tract, indicating that its mRNA and protein levels are upregulated during infection. Recently, our group has been pioneer to report its first three-dimensional structure and characterize the mechanism of action of this antimicrobial human ribonuclease¹⁹⁴. The complete structural and kinetic characterization, as well as the elucidation of its powerful antipathogenic activity, has helped to lay the foundations of its functionality, allowing us to identify the key regions that provide its peculiarities. Even though RNase 6 is a restrained catalyst compared to RNase A, it contains unique structure characteristics that facilitate its ability to degrade polymeric substrates. Moreover, the discovery of its three-dimensional structure in line with enzymatic assays have revealed the existence of an alternative catalytic site¹⁹⁴. On the other hand, RNase 6 was found active against Gram-negative and Gram-positive species and a membrane model was used to characterize its mode of action. RNase 6 is able to specifically aggregate Gram-negative bacteria, being Trp1 and Ile13 essential residues for this phenomenon. In addition, as previously described for other antimicrobial RNases, RNase 6 antimicrobial activity is mostly retained at its N-terminus¹⁹⁵.

1.5.3 RNase 7

Tracking human skin for endogenous antimicrobial proteins that could explain the resistance to skin infections, Harder and Schroder isolated from the stratum corneum skin a novel 14.5-KDa epithelial-secreted ribonuclease, which was named RNase 7¹⁹⁶. This skin-derived protein displays broad spectrum antimicrobial activity against many pathogenic microbes such as Gram-positive, Gram-negative bacteria, the yeast *C. albicans* and *Pichia pastoris*, and the dermatophyte *Trichophyton rubrum*^{196,197,198}. RNase 7 is mostly expressed in keratinocytes although its mRNA has been also detected in various epithelial tissues such as both the respiratory and genitourinary tracts¹⁹⁹. Being a small and cationic protein it responds to the typical $\alpha\beta$ RNase A family conformation (figure 15) and displays the ability to degrade many RNA substrates (around 50-fold greater than RNase 3)²⁰⁰. However, as it has also been seen for other RNase A family members, this catalytic activity has not been correlated with its antipathogenic ability^{186,201,197}. RNase 7 structural analysis revealed different surface clusters of cationic residues critical for bactericidal activity²⁰¹ and Wang *et al.*²⁰² have recently shown that the N-terminal region is an essential domain for microbicidal

activity against uropathogens. Furthermore, the RNase 7 chemically synthesized N-terminal peptide has been shown to retain the antimicrobial activity and its mechanism of action is similar to that of the whole protein¹²³.

Several studies conducted by our research group have contributed to partially characterize the mechanism of action of RNase 7. It has been demonstrated that RNase 7 is able to compromise the integrity of the bacterial structure through electrostatically driven modes of action, inducing local membrane destabilization previous to bacterial aggregation^{203,204}. Cell wall compound interaction studies have confirmed a high affinity for LPS and PGN at Gram-negative and Gram-positive surfaces respectively, with the subsequent membrane permeation and release of bacterial cell content. All together, these findings indicate that the RNase 7's ability to destabilize the cell membrane would be the main antibacterial mechanism, leaving aside possible intracellular targets, which up to date have not been identified, corroborating the absence of ribonuclease activity as a complementary antimicrobial mechanism²⁰⁵.

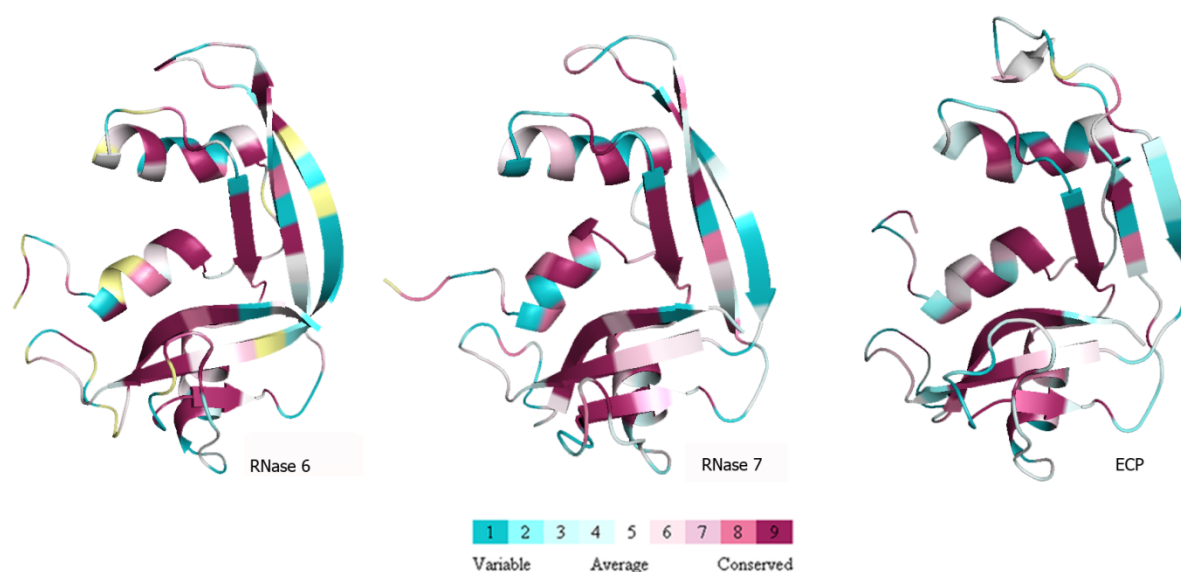


Figure 15. RNase 6 (PDB 4X09;¹⁹⁴), RNase 7 (PDB 2HKY;²⁰¹) and RNase 3/ECP (PDB 4A2O;²⁰⁶) three-dimensional structure surface representations using the CONSURF web server²⁰⁷ featuring the relationships among the evolutionary conservation of amino acid positions in the RNase A family. The three-dimensional structure shows residues coloured by their conservation score using the color-coding bar at the image bottom.

1.5.4 N-terminal RNase derived peptides

Like many other AMPs obtained by proteolysis from host defence proteins and subsequently delivered *in vivo* as active protein fragments²⁰⁸, RNases have been considered as direct participants in antimicrobial processes, as potential source of antimicrobial peptides^{174,209}.

The proteins would exhibit a warehouse role of active AMPs^{210,211,212}. Actually, there are a numerous examples of antimicrobial proteins such as cathelicidins and lactoferrin which are activated *in situ* via specific proteolysis^{213,214} resulting in natural occurring bactericidal peptides, LL-37 and lactoferricin respectively. Interestingly, Zanfardino *et al.* observed that fully denatured Zebra Fish-RNase-3 conserves its bactericidal activity and what is more, it can release an AMP when it is cleaved *in vivo* by a bacterial protease²¹⁵. In this context, our research group described for the first time the existence of a functional antimicrobial domain located at the N-terminus of the RNase 3^{216,217,211}. It has also been shown that this domain can be subdivided into two active regions, residues 24 to 45 are critical for the antimicrobial activity while residues 8-16 would be responsible for the aggregation and membrane destabilization processes²⁰⁹. Encouraged by these results and the fact that many RNases manifest antimicrobial properties, regardless of their ribonuclease activity, Torrent *et al.*¹²³ put in line these findings for the rest of the human RNase A family members, to analyse if the N-terminal antimicrobial domain could have been preserved and/or refined along evolution. The results revealed that the antimicrobial activity is highly retained at the N-terminal region and that the mechanism of action of this domain is similar to the parental protein. In addition to this, computational analyses have suggested that the refinement of this N-terminal domain could have been the result of an evolutionary mechanism to provide a host defence function¹²³. Due to the interest of many pharmaceutical companies for the development of new molecules against resistant strains or the treatment of immune disorders, antimicrobial RNases and their derived N-terminal peptides would offer suitable templates on which to work for the development of novel and broad-spectrum antibiotics.

2. AIMS OF THE THESIS

2. Aims of the thesis

The overall purpose of the present thesis is to deepen the characterization of the mechanism of action of human antimicrobial RNases, focused in underlying their structural determinants and multi-faceted roles requested for displaying their antimicrobial features. Concretely, the particular aims of this work were:

Chapter I:

- To characterize the structural determinants of the mechanism of action of human RNase 6 for bactericidal action

Chapter II:

- To solve the crystal structure of RNase 6 and determine the substrate binding and cleavage site arrangement.

Chapter III:

- To understand the dual mode of action of human RNases 3 and 7 using an eukaryotic pathogen model: *Candida albicans*.

Chapter IV:

- To characterize the antifungal mechanism of action at the N-terminal domain of the human RNases

Chapter V:

- To extend the knowledge of endogenous antimicrobial protein and peptides to counteract antimicrobial resistance in mycobacterial infections

Chapter VI:

- To determine the antimicrobial mechanism of action of human RNases against mycobacteria in a macrophage infected model

3. RESULTS

3. Results

1. Javier Arranz-Trullén, David Pulido, Guillem Prats-Ejarque, Diego Velázquez, Marc Torrent, Mohamed Moussaoui, and Ester Boix, "Insights into the Antimicrobial Mechanism of Action of Human RNase6: Structural Determinants for Bacterial Cell Agglutination and Membrane Permeation", *Int. J. Mol. Sci.*, vol. 17, no. 4, p. 552, Apr. 2016.
2. Guillem Prats-Ejarque, Javier Arranz-Trullen, Jose Antonio Blanco, David Pulido, Maria Victoria Nogues, Mohamed Moussaoui, and Ester Boix, "The first crystal structure of human RNase6 reveals a novel substrate binding and cleavage site arrangement," *Biochem. J.*, no. 2016, 2016.
3. Vivian A. Salazar, Javier Arranz-Trullén, Susanna Navarro, Jose A. Blanco, Daniel Sánchez, Mohammed Moussaoui and Ester Boix, "Exploring the mechanisms of action of human secretory RNase 3 and RNase 7 against *Candida albicans*", *Microbiologyopen* 2016 Jun 8. doi: 10.1002/mbo3.373
4. Javier Arranz-Trullen, Vivian Salazar, David Púlido, David Andreu, Marc Torrent and Ester Boix, "Antifungal mechanism of action at the N-terminus of the human RNases", (*manuscript in preparation*).
5. Javier Arranz-Trullen, David Pulido, Sanjib Bhakta and Ester Boix, "Endogenous host antimicrobial peptides (AMPs) to tackle antimicrobial resistance in tuberculosis (TB)" (*manuscript in preparation*).
6. Javier Arranz-Trullen, Lu Lu, David Pulido, Sanjib Bhakta and Ester Boix, "Unveiling the mode of action of human antimicrobial RNases against *Mycobacterium tuberculosis* using a surrogate infected model macrophage infected model" (*manuscript in preparation*).

PAPER I



Article

Insights into the Antimicrobial Mechanism of Action of Human RNase6: Structural Determinants for Bacterial Cell Agglutination and Membrane Permeation

David Pulido ^{*,†,‡}, Javier Arranz-Trullén [†], Guillem Prats-Ejarque, Diego Velázquez, Marc Torrent [§], Mohammed Moussaoui and Ester Boix ^{*}

Department of Biochemistry and Molecular Biology, Faculty of Biosciences, Universitat Autònoma de Barcelona, E-08193 Cerdanyola del Vallès, Spain; javier.arranz@e-campus.uab.cat (J.A.-T.); guillem.prats.ejarque@uab.cat (G.P.-E.); diego.velazquez@uab.cat (D.V.); marc.torrent@vhir.org (M.T.); mohammed.moussaoui@uab.cat (M.M.)

* Correspondence: d.pulido-gomez@imperial.ac.uk or david.pulido@e-campus.uab.cat (D.P.); ester.boix@uab.cat (E.B.); Tel.: +44-27-594-7915 (D.P.); +34-93-581-4147 (E.B.)

† These authors contributed equally to this work.

‡ Present address: Department of Life Sciences, Imperial College London, South Kensington Campus London, SW7 2AZ London, UK.

§ Present address: Microbiology Department, Hospital del Valle Hebron, 08035 Barcelona, Spain.

Academic Editor: Constantinos Stathopoulos

Received: 31 January 2016; Accepted: 5 April 2016; Published: 13 April 2016

Abstract: Human Ribonuclease 6 is a secreted protein belonging to the ribonuclease A (RNaseA) superfamily, a vertebrate specific family suggested to arise with an ancestral host defense role. Tissue distribution analysis revealed its expression in innate cell types, showing abundance in monocytes and neutrophils. Recent evidence of induction of the protein expression by bacterial infection suggested an antipathogen function *in vivo*. In our laboratory, the antimicrobial properties of the protein have been evaluated against Gram-negative and Gram-positive species and its mechanism of action was characterized using a membrane model. Interestingly, our results indicate that RNase6, as previously reported for RNase3, is able to specifically agglutinate Gram-negative bacteria as a main trait of its antimicrobial activity. Moreover, a side by side comparative analysis with the RN6(1–45) derived peptide highlights that the antimicrobial activity is mostly retained at the protein N-terminus. Further work by site directed mutagenesis and structural analysis has identified two residues involved in the protein antimicrobial action (Trp1 and Ile13) that are essential for the cell agglutination properties. This is the first structure-functional characterization of RNase6 antimicrobial properties, supporting its contribution to the infection focus clearance.

Keywords: RNases; host defence; antimicrobial peptides; cell agglutination; infectious diseases

1. Introduction

The RNaseA superfamily is a vertebrate-specific gene family that comprises a wide set of secreted ribonucleases displaying a variety of biological properties [1,2]. In particular, distant related members were reported to share innate immunity properties, suggesting that the vertebrate RNases have evolved as a host-defense family [3–5]. Eight functional members are found in humans, known as the “canonical RNases” (Figure 1), sharing a common structural fold and catalytic triad [6]. Within the family, we can differentiate three main phylogenetic lineages (RNase5, RNases2/3 and RNases6–8) related to host defense [7–10]. The eosinophil ribonucleases, EDN (eosinophil derived neurotoxin, RNase2) and ECP (eosinophil cationic protein, RNase3), are two secretory ribonucleases stored in

the secondary granules of eosinophils and released at the focus of infection [11,12]. *RNase2* and *3* genes have diverged after gene duplication, accumulating rapidly non-silent mutations through positive selection pressure [13,14]. *RNase2* acts as a potent modulator of the immune host system, and additionally displays a high antiviral activity against rhinovirus, adenovirus and syncytial respiratory virus in a *RNase* catalytic activity dependent manner [15–17]. *RNase3* possesses a highly antimicrobial activity against bacteria [11,18–21], and many parasites, such as helminths and protozoa [22]. By contrast, the antimicrobial properties of *RNase3* are not dependent on the ribonuclease activity of the protein [18,23]. On the other hand, *RNase7* is another *RNase* secreted by a variety of epithelial tissues [24] and displaying a high antimicrobial activity against a wide range of bacteria, regarded as a major contributor to the skin barrier protection [25–28]. In turn, *RNase6* has been related with the host immune system protection, being expressed in neutrophils and monocytes and displaying a high antimicrobial activity [29]. Recently, it has been reported that *RNase6* and *RNase7* play an important role in bacterial clearance at the urinary tract [30]. Nonetheless, our understanding of the antimicrobial mechanism of action of the *RNase6* is still poor.

Although the secreted vertebrate *RNases* share an overall globular three-dimensional prototypical scaffold, a catalytic triad and a particular disulfide pattern, their amino acid sequence identity ranges from 30% to 70%. Notwithstanding, despite the low sequence conservation among some *RNases* homologues, conserved structural features at the N-terminal region correlated to their host-defense properties [3]. Comprehensively, some human *RNases* are endowed with the features present on antimicrobial proteins and peptides (AMPs), sharing a marked cationicity that facilitates the electrostatic interaction with the negatively charged bacterial surfaces, abundance of hydrophobic residues, and the presence of dynamic amphipathic modules that can adopt secondary structures upon interaction with the bacterial envelopes [7,31]. Amidst the antimicrobial human *RNases*, despite their importance in the innate immune system, some members are poorly characterized and their antimicrobial features are yet to be described [17,28,30,32]. That is the case of the human *RNase6*, which is a small cationic protein mainly expressed in neutrophils and monocytes [29]. Interestingly, human *RNase6* has been recently described as a key player in the protection of the urinary tract [30]. In spite of these encouraging findings, little is known about the antimicrobial mechanism of action of this *RNase* during infection.

In this work, we have characterized the antimicrobial mechanism of action of the human *RNase 6* at both cell wall and membrane levels by describing its bactericidal effect against Gram-positive and -negative bacteria using a wide range of biophysical and microscopy approaches. Our results highlight that the antimicrobial properties of the protein are comparable to its *RNase3* homolog and correlate to the bacterial cell damage and agglutination activities. Additionally, the bactericidal membrane leakage and bacterial agglutination properties of the protein are largely retained at its N-terminal domain.

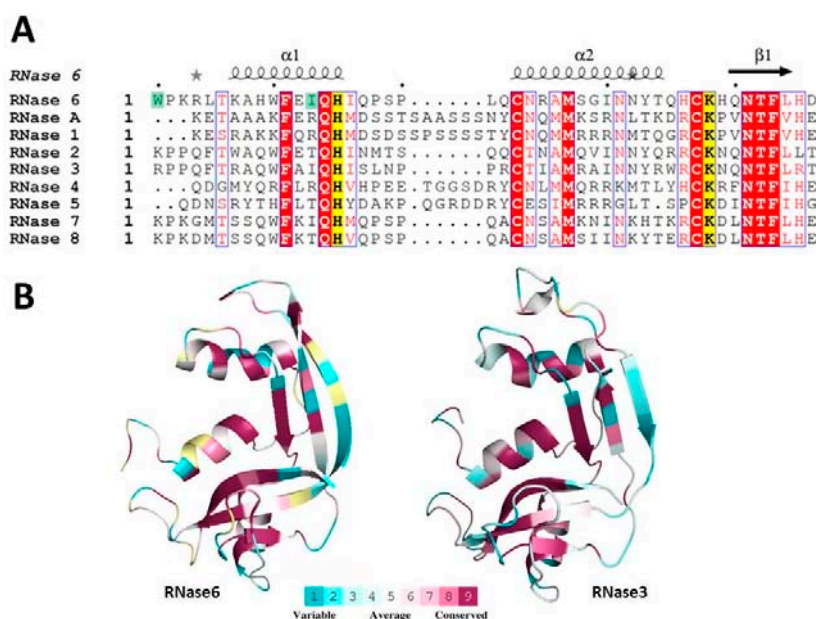


Figure 1. (A) Structure-based sequence of the eight canonical human RNases N-terminal domain together with RNaseA. The active site residues are highlighted in yellow. RNase6 tested mutations related to antimicrobial activity are labeled in green. The alignment was performed using *ClustalW*, and the picture was drawn using *ESPrpt* [33]. Labels are as follows: red box, white character for strict identity; red character for similarity in a group and character with blue frame for similarity across groups (red box, white character: strict identity; red character: similarity in a group; red character with blue frame: similarity across groups; yellow box, black character: catalyst residue); (B) RNase6 (PDB 4X09; [34]) and RNase3 (PDB 4A2O; [35]) three-dimensional structure surface representations using the CONSURF web server ([36]) featuring the relationships among the evolutionary conservation of amino acid positions in the RNaseA family. The three-dimensional structure shows residues colored by their conservation score using the color-coding bar at the image bottom.

2. Results

In order to evaluate the antimicrobial mechanism of action of RNase6, we used different experimental approaches that combined the analysis of the protein activity in synthetic lipid bilayers with its action on bacteria cultures. The antimicrobial properties of the protein and its N-terminus derived peptide were evaluated against Gram-positive and Gram-negative species. Additionally, we have also evaluated the protein affinity for bacterial cell wall lipopolysaccharides (LPS). Finally, N-terminus mutant variants were designed and their bactericidal activity and cell agglutinating properties were compared to the wild-type protein. All the results have been compared to the previously characterized human RNase3, taken as a positive control [21]. On the other hand, the family reference protein (RNaseA) did not display any of the tested antimicrobial and membrane damage activities at the same assayed conditions [37–40].

2.1. Membrane and Cell Wall Interaction

Our first approach to define the antimicrobial mechanism of action of the human RNase6 and its derived N-terminal peptide RN6(1–45) was performed by the characterization of the interaction at the membrane and cell wall levels.

By monitoring the intrinsic tryptophan fluorescence signal of the proteins and peptide upon incubation with phospholipid vesicles and LPS micelles, we were able to record the blue-shift in the tryptophan spectra, that this residue experiences when is embedded in a hydrophobic microenvironment. Thus, in order to assess the protein ability to interact with phospholipid bilayers we registered the intrinsic tryptophan fluorescence signal and the λ_{max} shift in presence of charged (1,2-

dioleoyl-sn-glycero-3-phosphoglycerol (DOPG)), neutral (1,2-dioleoyl-sn-glycero-3-phosphocholine (DOPC)) and mixed (DOPC/DOPG) liposomes (Table 1). The recorded spectrum for both RNases and the RNase6 derived N-terminal peptide showed no significant blue-shift upon incubation with non-charged large unilamellar vesicles (LUV). On the other hand, significant λ_{\max} shift towards the blue was experienced when incubated with both charged and mixed LUV. In addition, the two proteins and the assayed peptide also underwent a blue-shift in their emission spectra in the presence of LPS micelles, thereby indicating their ability to interact with the negatively charged bacterial cell membrane and envelope components.

Table 1. Tryptophan fluorescence in the presence of lipid vesicles and LPS micelles for RNase3, RNase6 and RN6(1–45).

Protein/Peptide	λ_{\max} for Fluorescence Emission (nm)				
	Buffer	DOPC ^a	DOPG ^a	DOPC:DOPG(3:2) ^a	LPS ^a
RNase3	343	-	3	3	4
RNase6	345	-	2	6	4
RN6(1–45)	343	-	8	9	3

^a The shift in the maximum emission wavelength compared with the reference value for buffer sample is indicated.

To further characterize the interaction of RNase3, RNase6 and RN6(1–45) with the bacterial cell wall we performed a fluorimetric assay using the BODIPY[®] cadaverine (BC) probe. Lipopolysaccharide binding affinity was determined as a result of the competitive displacement of BC, which mimics the lipid A portion of the LPS. The binding affinities of RNase3, RNase6 and its N-terminal derived peptide RN6(1–45) for the LPS molecule as a function of the protein concentration were tested. Their 50% effective dose (ED₅₀) values, defined as the concentration for which half BC displacement occurs, and the total BC displacement (shown as a percentage) are displayed in Table 2. Both RNases and the derived peptide displayed a high affinity with the negatively charged LPS molecule, being able to totally displace the BC molecule at a micromolar range.

Table 2. LPS-binding affinity of RNase3, RNase6 and RN6(1–45).

Protein/Peptide	LPS Binding	
	ED ₅₀ (μM) ^a	Max (%) [*]
RNase3	2.54 ± 0.14	100
RNase6	2.83 ± 0.22	76
RN6(1–45)	5.31 ± 1.41	27

^a ED₅₀ values are given as mean ± standard error of the mean (SEM); * 100% refers to a total displacement, whereas 0% corresponds to no displacement of the fluorescent dye, indicating no affinity for LPS.

After defining the interaction at the cell wall and membrane levels; we further characterized the proteins and peptide ability of causing membrane disruption and cell agglutination. Therefore, LUV containing the fluorescent probe 8-aminonaphthalene-1,3,6-trisulfonic acid/p-xylenebipyridinium bromide (ANTS/DPX) were incubated with RNase3, RNase6 and RN6(1–45) and membrane disruption was recorded as a function of the fluorescence increment. Both human RNases were able to totally disrupt the ANTS/DPX LUVs at micro molar concentrations (Table 3). However, the N-terminal derived peptide RN6(1–45) was able to produce the same effect at 2.5-fold more concentration than its parental protein.

Table 3. Liposome leakage activity of RNase3, RNase6 and RN6(1–45).

Protein/Peptide	Liposome Leakage (μM)	
	ED ₅₀ (μM) ^a	Max (%) [*]
RNase3	0.7 \pm 0.1	100
RNase6	1.5 \pm 0.5	100
RN6(1–45)	4.0 \pm 0.5	100

^a ED₅₀ values are given as mean \pm SEM; ^{*} 100% refers to the total leakage of liposome content. The ANTS/DPX liposome leakage fluorescence assay was performed using DOPC/DOPG vesicles as described in the methodology.

Additionally, dynamic light scattering (DLS) allowed us to investigate the physical changes of the LUV population upon interaction with RNase3, RNase6 and RN6(1–45). LUVs of DOPC, DOPG and mixture of DOPC/DOPG, with a vesicle diameter size of 100 nm, were prepared. RNase3, RNase6 and RN6(1–45) promoted the agglutination of charged LUVs in a short time course of 15 min (Figure 2). However, RNase6 and its N-terminal derived peptide were not able to agglutinate neutral LUVs, as previously observed by RNase3 [39].

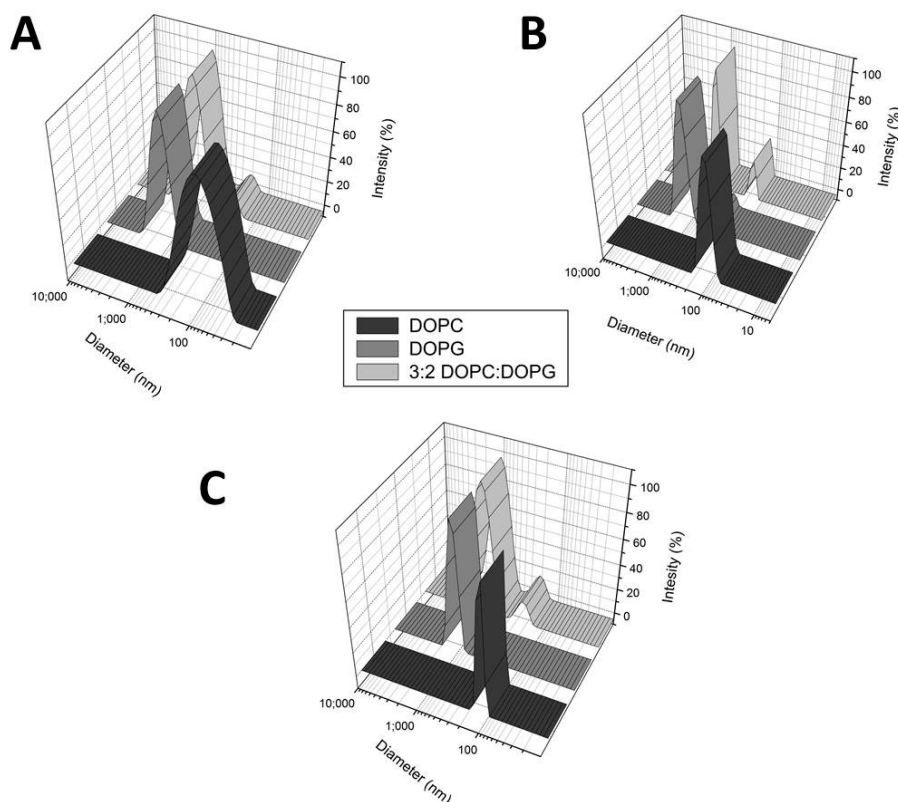


Figure 2. Liposome agglutination activity assayed by DLS. Plots show diameter size (nm) versus intensity of scattered light for DOPG, DOPC or DOPC:DOPG (3:2) in the presence of: (A) RNase3; (B) RNase6; and (C) RN6(1–45). Protein/peptide were added at 5 μM and mean diameter size of liposome population was registered after 15 min.

2.2. Bactericidal Activity

The promising preliminary results on model membranes encouraged us to further investigate the protein and peptide mechanism of action at the bacterial cell level. Based on our previous characterization work on the antimicrobial activity of RNase3 [38], we analyzed here the human RNase6 and its derived N-terminal peptide cytotoxic mechanism on Gram-negative and Gram-positive bacteria.

To assess the antimicrobial activity of the human RNase3, RNase6 and its derived N-terminal peptide RN6(1–45) we determined their minimal bactericidal concentration (MBC) against three representative Gram-negative and Gram-positive species (Table 4). Complementarily, assessment of the protein and peptide antimicrobial activities was also performed by evaluating the reduction of bacterial cell viability using the *BacTiter-Glo* kit assay, which estimates the number of viable cells by quantification of ATP levels (Table S1). Additionally, RNase3, RNase6 and its derived N-terminal peptide RN6(1–45) were able to totally inhibit bacterial growth at low micro molar concentration (Table S2). Both human RNases displayed a high antimicrobial activity in a sub micro molar range against all tested Gram-positive and Gram-negative species. Remarkably, the N-terminal derived peptide RN6(1–45) was able to perform the same cytotoxic effect than its parental protein.

To characterize the cell selectivity of both human RNases and the N-terminal derived peptide, their hemolytic activity was tested on sheep RBCs, the concentration required to cause 50% hemolysis is reported as HC₅₀ (Table 4). The HC₅₀ values obtained for RNase3, RNase6 and RN6(1–45) showed that no hemolytic activity is present under the maximum concentration tested (20 μM), being at least 20- to 100-fold higher than the determined MBC values.

Table 4. Minimal bactericidal concentration (MBC₁₀₀) and hemolytic activity (HC₅₀) of RNase3, RNase6 and RN6(1–45).

Protein/Peptide	MBC ₁₀₀ (μM) ^a						HC ₅₀ (μM) [*]
	<i>E. coli</i>	<i>P. aeruginosa</i>	<i>A. baumannii</i>	<i>S. aureus</i>	<i>M. luteus</i>	<i>E. faecium</i>	
RNase3	0.35 ± 0.02	0.20 ± 0.01	0.40 ± 0.03	0.40 ± 0.03	0.65 ± 0.08	0.90 ± 0.14	>20
RNase6	0.90 ± 0.14	0.90 ± 0.14	0.65 ± 0.08	1.87 ± 0.56	1.35 ± 0.23	1.35 ± 0.23	>20
RN6(1–45)	1.35 ± 0.23	0.40 ± 0.03	0.65 ± 0.08	1.87 ± 0.56	1.35 ± 0.23	1.35 ± 0.23	>20

^a The MBC₁₀₀ was calculated as described in Materials and Methods by colony forming units (CFU) counting on plated Petri dishes. All values are averaged from three replicates of two independent experiments. Values are given as mean ± SEM; ^{*} Hemolytic activity was assayed on sheep red blood cells.

Further investigations on the bactericidal properties of the human RNase6 and its derived peptide were compared by assaying the membrane depolarization activity against two bacterial model species (*E. coli* and *S. aureus*). As previously described [37], RNase3 is able to interact with the Gram-negative and Gram-positive bacterial envelope, and can perturb the cell cytoplasmic membrane, producing half of the total membrane depolarization at concentrations below 1 μM (Table 5). It is worth noticing that comparable results were recorded for RNase6. In contrast, the antimicrobial peptide RN6(1–45) showed a slight decrement for its ability to depolarize bacterial membranes when compared to its parental protein.

Table 5. Depolarization activity on *E. coli* and *S. aureus* cells determined for RNase3, RNase6 and RN6(1–45).

Protein/Peptide	Depolarization (μM)			
	<i>E. coli</i>		<i>S. aureus</i>	
	ED ₅₀	Depol _{max} [*]	ED ₅₀	Depol _{max} [*]
RNase3	0.5 ± 0.1	100.5 ± 3.8	0.7 ± 0.2	100.5 ± 6.7
RNase6	0.6 ± 0.1	64.1 ± 4.2	0.9 ± 0.1	71.7 ± 1.5
RN6(1–45)	1.1 ± 0.3	69.7 ± 5.3	1.2 ± 0.2	76.2 ± 5.6

^{*} Maximum fluorescence value reached at the final incubation time with 5 μM of the proteins and peptides. Membrane depolarization was performed using the membrane potential-sensitive DiSC3(5) fluorescent probe as described in the Methodology. Values are given as mean ± SEM.

In order to analyze the bactericidal kinetics of the two RNases and the RNase6 derived peptide we used the Live/Dead bacterial viability kit. The bacterial population viability was followed by the differential fluorescent staining of Syto 9 and propidium iodide (PI). Syto 9 can cross intact cell

membranes, whereas PI stains damaged membrane dead cells. Therefore, the bacterial killing process was monitored as function of time (Table 6). Human RNase6 and its derived N-terminal peptide RN6(1–45) displayed similar bactericidal kinetics producing half of its total cytotoxic effect after several minutes of incubation. Comparable results were also obtained for RNase3.

Additionally, further inspection of the bactericidal action at the Gram-positive and -negative cell envelope, was applied by electron microscopy. *E. coli* and *S. aureus* were examined by transmission electron microscopy (TEM) after 4 h of incubation with 5 μ M of RNase3, RNase6 and the RN6(1–45) peptide (Figure 3). In accordance with the results presented above, both antimicrobial RNases and the N-terminal peptide showed a potent bactericidal effect against both *E. coli* and *S. aureus*. Both Gram-positive and -negative cells presented a complete disruption of the cell integrity, bacterial swelling, intracellular material spillage, bacterial cell wall layer detachment, and alteration of the cell morphology.

Table 6. Bactericidal kinetics on *E. coli* and *S. aureus* cells determined by the Live/Dead assay for RNase3, RNase6 and RN6(1–45).

Protein/Peptide	Bacterial Viability Assay			
	<i>E. coli</i>		<i>S. aureus</i>	
	t_{50} (min) *	Viability (%) *	t_{50} (min) *	Viability (%) *
RNase3	10.6 \pm 0.1	4.2 \pm 0.3	7.1 \pm 0.1	9.3 \pm 0.2
RNase6	15.4 \pm 0.1	8.8 \pm 0.1	18.0 \pm 0.4	12.9 \pm 0.8
RN6(1–45)	13.1 \pm 0.1	5.2 \pm 0.1	5.5 \pm 0.1	5.8 \pm 0.2

* Viability percentage and half time were determined with the Live/Dead kit after 4 h of incubation of mid-log-phase-grown *E. coli* and *S. aureus* cultures with 5 μ M of protein and peptides. The percentage of viability (%) and half time of viability (t_{50}) after incubation with the proteins are shown. The percentage of live bacteria was represented as a function of time, and t_{50} values were calculated by fitting the data to a simple exponential decay function with Origin 7.0. Values are given as mean \pm SEM.

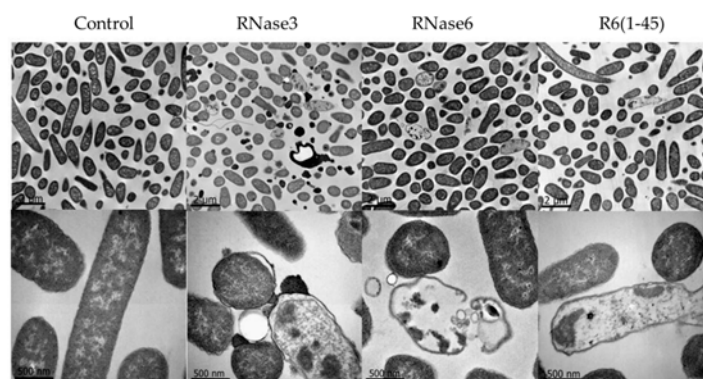


Figure 3. Transmission electron microscopy (TEM) micrographs for *E. coli* cultures incubated in the absence and presence of RNase3, RNase6 and RN6(1–45). Two magnifications (**upper** and **lower** panels) are shown for each condition to visualize the extent of bacteria aggregates and cell morphology. Scale bars correspond to 2 μ m and 500 nm, respectively.

A distinctive feature of the RNase3 mechanism of action is the ability to promote bacterial agglutination of Gram-negative bacteria cells [41,42]. In order to assess whether RNase6 and its derived N-terminal peptide also shared this particular property, their minimal agglutination concentration (MAC) were determined (Table 7). Strikingly, the MAC values obtained showed a potent agglutinating activity for RNase6, which presented the same value as RNase3. Importantly, the N-terminal peptide RN6(1–45) retained significant agglutinating activity, being also able to promote bacterial agglutination at a micro molar range.

Table 7. MAC and bacterial agglutination percentage of RNase3, RNase6 and RN6(1–45) for *E. coli* cell cultures.

Protein/Peptide	MAC (μM) ^a	Agglutination Activity (%) [*]
RNase3	0.20 ± 0.05	60.35 ± 0.50
RNase6	0.20 ± 0.05	80.64 ± 0.50
RN6(1–45)	5 ± 0.50	66.22 ± 0.50

^a *E. coli* cells were treated with increasing protein or peptide concentrations (from 0.01 to 20 μM); ^{*} Agglutination activity percentage registered by incubation of bacteria culture with 5 μM protein concentration for 4 h were calculated by Fluorescence-Activated Cell Sorting (FACS) as described in the Methodology. Values are given as mean \pm SEM.

Henceforth, scanning electron microscopy (SEM) was applied in order to visualize cell population behavior and damage. SEM micrographs revealed tight densely populated bacterial aggregates after incubation with both antimicrobial RNases and the N-terminal derived peptide (Figure 4). In addition, cells were conspicuously damaged displaying a prominent loss of membrane integrity showing frequent blebs and loss of the baton-shaped cell morphology.

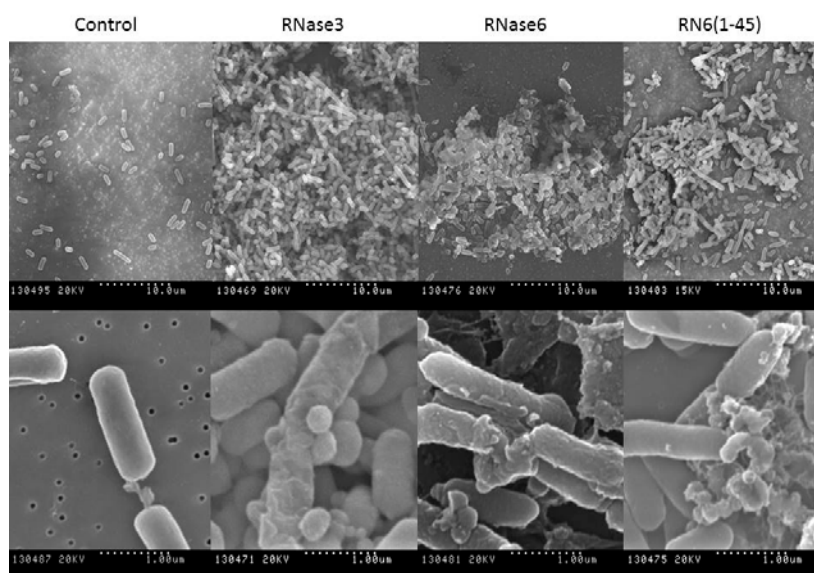


Figure 4. SEM micrographs for *E. coli* cultures incubated in the absence and presence of RNase3, RNase6 and RN6(1–45). Two magnifications (**upper** and **lower** panels) are shown for each condition to visualize the extent of bacteria aggregates and cell morphology. The magnification scale is indicated at the bottom of each micrograph.

Finally, the agglutinating activity of the antimicrobial RNase6 and its derived N-terminal peptide was quantified by FACS (Figure 5 and Table 7). Comparable results were obtained by both RNase3 and 6, which, after 4h incubation, were able to induce the agglutination of most of the bacterial population. Interestingly, the antimicrobial peptide RN6(1–45) displayed a high agglutinating activity promoting a bacterial agglutination activity similar to its parental protein.

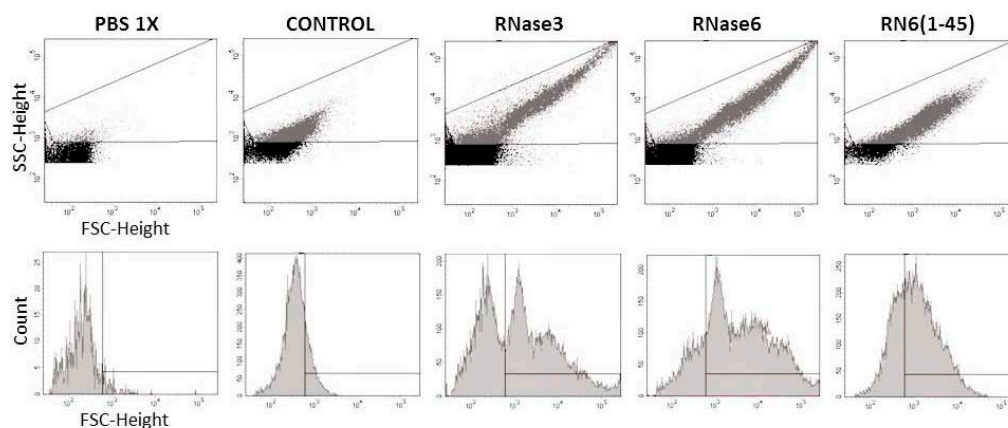


Figure 5. Bacterial agglutination measured by FACS. *E. coli* cultures were incubated in the absence and presence of RNase3, RNase6 and RN6(1–45) at a final concentration of 5 μ M for 4 h. Low-angle forward scattering (FSC-H) is represented on the x -axis and the side scattering (SSC-H) on the y -axis to analyze the size and complexity of the cell cultures. Plots show density of cell population distribution. Buffer background is shown in black and cell population in grey.

2.3. Mutant Design and Characterization

A closer look of the N-terminal region of RNase6 with the prediction software *Aggrescan3D* showed that RNase6 presented an aggregation prone region at the first 16 residues, as reported for RNase3 [3,40]. In order to confirm the presence of the spotted aggregation prone patch, we generated two RNase6 mutants targeting two key residues at the identified region: Trp1 and Ile13 (Figure 1 and Figure S1). In fact, mutation of residue 13 in both RNases sequences reduced the protein aggregation A3D score value, defined as a global indicator of the aggregation propensity/solubility of a protein structure. Interestingly, when we analyzed the A3D aggregation profiles we observed that while the I13A mutation in RNase3 caused a slight reduction ($\approx 20\%$) of the value, the same mutation in the case of RNase6 abolished completely the aggregation propensity score (Figure S1). Structural comparison of the aggregation regions corroborated that mutation of Ile13 decreased the aggregative capacity of both proteins, being much more pronounced for RNase6 (Figure S1). On the other hand, the Trp1 is fully exposed at the protein surface and may perform an equivalent role to Trp35 in RNase3. Indeed, RNase 3-W35A mutant was found defective in its membrane interaction, lipid vesicle lysis, agglutination and bactericidal activities [38,43–45]. Additionally, an active site mutant (H15A) was used as a control reference, where the substitution of the His15 catalytic residue drastically impaired the protein enzymatic activity [34].

Results confirmed the involvement of both Trp1 and Ile13 residues in RNase6 antimicrobial action. In particular, both residues were critical for the protein cell agglutination activity (Table 8). Besides, the results also demonstrated that the hydrophobic patch at the N-terminal region of the protein is also related to the interaction with bacterial cell wall components. LPS binding assays for the two RNase6 mutants showed a decrease in their interaction affinities (Table 8). Moreover, both mutants displayed a poor antimicrobial activity against *E. coli* and *S. aureus* (Table 8). On the other hand, the tested active site mutant (H15A) retained its antimicrobial activity for both studied Gram-negative and Gram-positive species (Table S3).

Table 8. MBC, MAC and LPS Binding activities of RNase3, RNase6 and RNase6 mutants.

Protein/Peptide	MBC ₁₀₀ (μ M) ^a		MAC (μ M)		LPS Binding Assay	
	<i>E. coli</i>	<i>S. aureus</i>	<i>E. coli</i>	<i>S. aureus</i>	ED ₅₀ (μ M)	Max (%) [*]
RNase3	0.35 \pm 0.01	0.40 \pm 0.10	0.22 \pm 0.01	>5	2.54 \pm 0.16	99.89 \pm 4.20
RNase6	0.90 \pm 0.14	1.87 \pm 0.56	0.22 \pm 0.01	>5	2.63 \pm 0.23	75.89 \pm 4.41
RNase6-W1A	1.87 \pm 0.56	3.75 \pm 0.78	>5	>5	3.37 \pm 0.34	38.55 \pm 2.32
RNase6-I13A	3.75 \pm 0.78	>5	>5	>5	4.60 \pm 0.43	27.43 \pm 1.22

^a The MBC₁₀₀ was calculated as described in Materials and Methods. MBC₁₀₀ values were calculated by CFU counting on plated Petri dishes. All values are averaged from three replicates of two independent experiments; ^{*} 100% refers to a total displacement, whereas 0% stands for no displacement of the dye, indicating no binding. Values are given as mean \pm SEM.

3. Discussion

Antimicrobial RNases are small cationic proteins that belong to the vertebrate-specific RNaseA superfamily [46]. In this study, we have thoroughly characterized the antimicrobial mechanism of action of the human RNase6 and compared it along with the most studied human antimicrobial RNase, RNase3 [12,21]. The present results highlight that RNase6 also displays a high antimicrobial activity showing MBC values at sub micro molar for all tested Gram-positive and -negative bacterial species (Table 4). Kinetic viability assays showed that the antibacterial activity occurs in a matter of few minutes incubation time (Table 6). Furthermore, the results obtained by the fluorimetric DiSC3(5) assay showed that RNase6 displays a high membrane depolarization activity (Table 5) indicating that one of the main bactericidal route for these proteins takes place at the membrane level, as previously reported for RNase3. Applying rational mutation at the RNase scaffold and peptide synthesis approaches we have previously unveiled the main structural determinants for the antimicrobial action of human RNase3 [37,38,41,44,45,47,48]. Specifically, we demonstrated that the entirety of the RNase3 protein was not required for the antimicrobial action [38,44]. By applying prediction software for protein antimicrobial regions (AMPA) and by experimental proteolysis mapping, we located the key RNase3 antimicrobial region at the N-terminus [47,49]. Interestingly, a screening of RNase7 fragments also confirmed that the C-terminus was not able to reproduce the protein properties [27]. In fact, recent comparative results suggested that evolution has selected the N-terminal region of the vertebrate ribonucleases to encode the required structural determinants for antimicrobial action [3]. In the present study, we have characterized the N-terminal region of RNase6. The corresponding RN6(1–45) peptide displays almost the same antimicrobial activity than the whole protein; showing a fast and high bactericidal effect mediated by the destabilization of the bacterial membranes. On the other hand, the RNase6 also showed very low cytotoxicity levels against mammalian cells (Table 4). The results suggest that evolution has promoted the antimicrobial properties of RNases with a high selectivity towards pathogen cells.

Moreover, both RNase3 and 6 present the main common features of cationic antimicrobial peptides, presenting a positive net charge that would enable them to interact with the negatively charged bacterial cell envelopes, together with a high percentage of hydrophobic residues that could mediate the interaction with the membrane lipid bilayer [7]. Previous structural characterization of RNase3 confirmed its mechanism of action in a membrane model system [39,43]. In tune with these facts, internal fluorescence tryptophan spectra of the RNase6 showed how the protein is able to interact with negatively charged membranes, as visualized by the blue-shift of the fluorescent emission wavelength (Table 1). Additionally, the structural determinants required for membrane interaction were retained by the N-terminal region, as a significant blue-shift was also registered for the RNase6 derived peptide. On the other hand, the results indicated that RNase6 is able to interact with the negatively charged LPS molecules of the Gram-negative surface (Table 2), serving as the first point of anchor to exert the membranolytic activity. Also, the ANTS/DPX fluorescence assay showed that RNase6 is able to destabilize lipid bilayers very efficiently, presenting a high membrane lysis at low micro molar

concentrations (Table 3). Our previous work identified a key antimicrobial region for RNase3 (residues 24 to 45) essential for membrane leakage, depolarization and LPS binding [47]. Moreover, recent comparative analysis of human RNases N-terminus peptides confirmed their structuration, adopting a secondary helical conformation, in the presence of sodium dodecyl sulfate (SDS) and LPS micelles [3]. Interestingly, we have proven here that the N-terminal region of the homologue RNase6 is also able to reproduce the membrane destabilization properties of the whole protein. Nonetheless, significant differences between the two proteins were observed regarding the LPS binding activity; where the RNase6 N-terminal region shows reduced LPS binding. Differences at the predicted protein LPS binding residues may account for this data [3,42].

Another important feature for RNase3 antimicrobial activity is the ability to agglutinate Gram-negative bacterial cells in a LPS binding dependent manner [42]. We previously demonstrated that RNase3 upon interaction with the negatively charged surfaces of the bacteria underwent conformational changes that triggered the amyloid-like self-aggregation of the protein ensuing in bacterial agglutination and eventual cell death [19,40]. Antimicrobial peptides endowed with a cell agglutinating activity would prevent dissemination of the infectious focus and facilitate the infection clearance by the host innate cells [19,50]. Interestingly, RNase6 is also able to aggregate both lipid vesicles and Gram-negative bacteria in a micro molar range. Electron micrographs not only showed the evident cell damage that RNase6 antimicrobial action produces but they also revealed densely packed bacterial aggregates, as observed for RNase3 [37]. Quantification of the agglutinating activity of the RNase6 by FACS showed that the totality of the bacterial population is agglutinated at 5 μ M protein concentration (Figure 5). Again, the N-terminal region of RNase6 retained the agglutinating properties of the whole protein (Table 7). To confirm this hypothesis, two point mutants were designed at the spotted aggregation propensity region (W1A and I13A). The results confirmed that substitution of both hydrophobic residues reduced considerably the bacterial agglutination activity and antimicrobial action (Table 8). Significant reduction of the protein LPS interaction was also obtained for both mutant variants (Table 8). Interestingly, Trp1 is unique to RNase6 lineage and is conserved in all the sequenced Old World primate genes [51–53]. On the other hand, previous studies from our laboratory highlighted the involvement of Ile13 in the RNase3 agglutination properties [40,45]. Moreover, the residue is present in the three main antimicrobial RNases within the family (Figure 1). Comparison of the 8 N-terminal peptides from the human canonical RNases confirmed the direct correlation between the hydrophobic patch and the protein agglutination and bactericidal properties [3]. Besides, no reduction of the RNase6 antimicrobial activity was observed for the H15A active site mutant (Table S3). Therefore, our present results are confirming that residues Trp1 and Ile13 play a crucial role in RNase6 bacterial cell surface interaction, membrane disruption and bacterial agglutination.

4. Materials and Methods

4.1. Materials and Strains

DOPC and DOPG were from Avanti Polar Lipids (Alabaster, AL, USA). ANTS, DPX and BC were purchased from Invitrogen (Carlsbad, CA, USA). LPS from *E. coli* serotype 0111:B4 were purchased from Sigma-Aldrich (St. Louis, MO, USA). PD-10 desalting columns with Sephadex G-25 were from GE Healthcare (Waukesha, WI, USA). RNase6(1–45) peptide was purchased from Genecust (Dudelange, Luxembourg). Strains used were *Escherichia coli* (BL21; Novagen, Madison, WI, USA), *Staphylococcus aureus* (ATCC 502A; Manassas, VA, USA), *Acinetobacter baumannii* (ATCC 15308; Manassas, VA, USA), *Pseudomonas aeruginosa* (ATCC 47085; Manassas, VA, USA), *Micrococcus luteus* (ATCC 7468; Manassas, VA, USA) and *Enterococcus faecium* (ATCC 19434; Manassas, VA, USA).

4.2. Protein Expression and Purification

Wild-type RNase3 was obtained from a synthetic gene [54]. Human RNase6 was obtained from DNA 2.0 (Menlo Park, CA, USA). Both genes were subsequently cloned into pET11c vectors.

Mutations into the *RNase6* gene were introduced using the Quick change™ site-directed mutagenesis kit (Santa Clara, CA, USA) following the manufacturers procedure. *E. coli* BL21(DE3) (Novagen, Madison, WI, USA) competent cells were transformed with the pET11c/*RNase6* and *RNase3* plasmids. The expression protocol was optimized in Terrific broth (TB). For high yield expression, bacteria were grown in TB, containing 400 µg/mL ampicillin. Recombinant *RNase6* was expressed in *E. coli* BL21(DE3) (Novagen, Madison, WI, USA) cells after induction with 1 mM IPTG (St. Louis, MO, USA), added when the culture showed an OD₆₀₀ of 0.6. The cell pellet was collected after 4 h of culture at 37 °C. Cells were resuspended in 10 mM Tris-HCl, 2 mM EDTA, pH 8, and sonicated at 50 watts for 10 min with 30-s cycles. After centrifugation at 15,000× *g* for 30 min, the pellet fraction containing inclusion bodies was processed as follows: the pellet fraction was washed with 50 mM Tris-HCl, 2 mM EDTA, 0.3 M NaCl, pH 8, and after centrifugation at 20,000× *g* for 30 min, the pellet was dissolved in 12 mL of 6 M guanidine HCl, 0.1 M Tris-acetate, 2 mM EDTA, pH 8.5, containing 80 mM GSH (St. Louis, MO, USA), and incubated under nitrogen for 2 h at room temperature. The protein was then refolded by a rapid 100-fold dilution into 0.1 M Tris-HCl, pH 7.5, containing 0.5 M L-arginine, and GSSG (St. Louis, MO, USA) was added to obtain a GSH/GSSG ratio of 4. Dilution in the refolding buffer was adjusted to obtain a final protein concentration of 30–150 µg/mL. The protein was incubated in refolding buffer for 48–72 h at 4 °C. The folded protein was then concentrated, dialyzed against 0.015 M Tris-HCl, pH 7, and purified by cation exchange chromatography on a Resource S column equilibrated with the same buffer. ECP was eluted with a linear NaCl gradient from 0 to 2 M in 0.015 M Tris-HCl, pH 7 buffer. Further purification was achieved by a second reverse phase chromatography on a Vydac C4 column (Grace-Alltech, Bannockburn, IL, USA). The homogeneity of the purified proteins was checked by 15% SDS-PAGE and Coomassie Blue staining and by N-terminal sequencing.

4.3. Minimal Bactericidal Concentration (MBC)

Antimicrobial activity was expressed as the MBC₁₀₀, defined as the lowest protein concentration that completely kills a microbial population. The MBC of each protein/peptide was determined from two independent experiments performed in triplicate for each concentration. Bacteria cells were incubated at 37 °C overnight in LB broth and diluted to give approximately 5 × 10⁵ CFU (colony forming units)/mL. The bacterial suspension was incubated in LB with peptides at various concentrations (0.1–20 µM) at 37 °C for 4 h. Samples were plated on to Petri dishes and incubated at 37 °C overnight.

4.4. Bacterial Viability Assays

Kinetics of bacterial survival were determined using the Live/Dead bacterial viability kit (Molecular Probes, Invitrogen) in accordance with the manufacturer's instructions. Bacterial strains were grown at 37 °C to an optical density (OD₆₀₀) of 0.2, centrifuged at 5000× *g* for 5 min, and stained in a 0.85% NaCl solution. Fluorescence intensity was continuously measured after protein or peptide addition (10 µM) using a Cary Eclipse spectrofluorimeter (Varian Inc., Palo Alto, CA, USA). To calculate bacterial viability, the signal in the range of 510 to 540 nm was integrated to obtain the Syto 9 signal (live bacteria) and that in the range of 620 to 650 nm was integrated to obtain the propidium iodide (PI) signal (dead bacteria). The percentage of live bacteria was represented as a function of time, and t₅₀ values were calculated by fitting the data to a simple exponential decay function with Origin 7.0 (OriginLab Corporation; Northampton, MA, USA).

Alternatively, bacterial viability was assayed using the *BacTiter-Glo* microbial cell viability kit (Promega; Fitchburg, WI, USA) that estimates the number of viable cells by ATP quantification using a fluorescence assay. Briefly, proteins and peptides were dissolved in 10 mM sodium phosphate buffer, 0.1 M NaCl (pH 7.4), serially diluted from 20 to 0.1 µM, and tested against the bacterial species (OD₆₀₀ ~ 0.2) for 4 h of incubation time. Fifty microliters of culture were mixed with 50 µL of *BacTiter-Glo* reagent in a microtiter plate according to the manufacturer's instructions and incubated at room temperature for 15 min. Luminescence were read on a Victor3 plate reader (Perkin-Elmer,

Waltham, MA, USA) with a 3-s integration time. Fifty percent effective dose concentrations (ED_{50}) were calculated by fitting the data to a dose–response curve with Origin 7.0.

4.5. Bacterial Cell Membrane Depolarization Assay

Membrane depolarization was performed using the membrane potential-sensitive DiSC3(5) fluorescent probe as described previously [41,55]. After interaction with intact cytoplasmic membrane, the fluorescent probe DiSC3(5) was quenched. After incubation with the antimicrobial protein or peptide, the membrane depolarization was induced the probe was released to the medium, ensuing in an increase of fluorescence that can be quantified and monitored as a function of time. Bacterial cultures were grown at 37 °C to an OD_{600} of 0.2, centrifuged at $5.000 \times g$ for 7 min, washed with 5 mM HEPES-KOH, 20 mM glucose (pH 7.2), and resuspended in 5 mM HEPES-KOH 20 mM glucose 100 mM KCl (pH 7.2) to an OD_{600} of 0.05. DiSC3(5) was added to a final concentration of 0.4 μ M, and changes in the fluorescence were continuously recorded after the addition of protein (from 0.01 to 20 μ M) in a Victor3 plate reader. Effective dose values (ED_{50}) were estimated from nonlinear regression analysis.

4.6. Minimal Agglutination Activity (MAC)

Bacterial cells were grown at 37 °C to an OD_{600} of 0.2, centrifuged at $5000 \times g$ for 2 min. One hundred microliters of the bacterial suspension was treated with increasing protein or peptide concentrations (from 0.01 to 20 μ M) and incubated at 37 °C for 1 h. The aggregation behavior was observed by visual inspection, and the agglutinating activity is expressed as the minimum agglutinating concentration of the sample tested, as previously described [42].

4.7. Fluorescence Activated Cell-Sorting (FACS)

Bacterial cells were grown at 37 °C to mid-exponential phase (OD_{600} of 0.6), centrifuged at $5000 \times g$ for 2 min, resuspended in 10 mM sodium phosphate buffer and 100 mM NaCl (pH 7.4) to give a final OD_{600} of 0.2 and pre-incubated for 20 min. A 500- μ L aliquot of the bacterial suspension was incubated with 5 μ M protein/peptide for 4 h. After incubation, 25,000 cells were subjected to FACS analysis using a FACS Calibur cytometer (BD Biosciences; Franklin Lakes, NJ, USA) and a dot-plot was generated by representing the low-angle forward scattering (FSC-H) in the x -axis and the side scattering (SSC-H) in the y -axis to analyze the size and complexity of the cell cultures.

4.8. Scanning Electron Microscopy (SEM)

Scanning electron microscopy (SEM) samples were prepared as previously described [56]. Bacterial culture of *S. aureus* and *E. coli* were grown at 37 °C to mid-exponential phase (OD_{600} of 0.2) and incubated with proteins or peptide (5 μ M) at 37 °C. Sample aliquots (500 μ L) were taken after up to 4 h of incubation and prepared for SEM analysis as previously described [41]. The micrographs were viewed at a 15-kV accelerating voltage on a Hitachi S-570 scanning electron microscope (Hitachi, Ltd.; Chiyoda, Tokio, Japan), and a secondary electron image of the cells for topography contrast was collected at several magnifications.

4.9. Transmission Electron Microscopy

Transmission electron microscopy (TEM) samples were prepared as previously described [56]. *E. coli* and *S. aureus* cultures were grown to an OD_{600} of 0.2 and incubated at 37 °C with 5 μ M proteins or peptides for 4 h. After treatment, bacterial pellets were prefixed with 2.5% glutaraldehyde and 2% paraformaldehyde in 0.1 M cacodylate buffer at pH 7.4 for 2 h at 4 °C and postfixed in 1% osmium tetroxide buffered in 0.1 M cacodylate at pH 7.4 for 2 h at 4 °C. The samples were dehydrated in acetone (50%, 70%, 90%, 95%, and 100%). The cells were immersed in Epon resin, and ultrathin sections were examined in a JEOL JEM 2011 instrument (JEOL, Ltd., Tokyo, Japan).

4.10. Hemolytic Activity

Fresh sheep RBCs (red blood cells) (Oxoid Inc.; Nepean, ON, Canada) were washed three times with PBS (35 mM phosphate buffer and 0.15 M NaCl (pH 7.4)) by centrifugation for 5 min at $3000\times g$ and resuspended in PBS at 2×10^7 cells/mL. RBCs were incubated with protein/peptide at 37°C for 4 h and centrifuged at $13,000\times g$ for 5 min. The supernatant was separated from the pellet and its absorbance measured at 570 nm. The 100% hemolysis was defined as the absorbance obtained by sonicating RBCs for 10 s. HC_{50} was calculated by fitting the data to a sigmoidal function with Origin 7.0.

4.11. Liposome Preparation

Large Unilamellar Vesicles (LUVs) containing DOPC, DOPG or DOPC/DOPG (3:2 molar ratio) of a defined size were obtained from a vacuum drying lipid chloroform solution by extrusion through 100 nm polycarbonate membranes. The lipid suspension was frozen and thawed ten times before extrusion. A 1 mM stock solution of liposome suspension was prepared in 10 mM sodium phosphate, 100 mM NaCl, pH 7.4.

4.12. Intrinsic Tryptophan Fluorescence Analysis

Tryptophan fluorescence emission spectra were recorded using a 280 nm excitation wavelength. Slits were set at 2 nm for excitation and 5–10 nm for emission. Emission spectra were recorded from 300–400 nm at a scan rate of 60 nm/min in a 10 mm \times 10 mm cuvette, with stirring immediately after sample mixing. Protein/peptide spectra at 0.5 μM in 10 mM Hepes buffer, pH 7.4, were obtained at 37°C in the absence or presence of 200 μM liposome suspension or 100 μM LPS micelles. Fluorescence measurements were performed on a Cary Eclipse spectrofluorimeter (Agilent Technologies, Bath, UK). Spectra in the presence of liposomes or LPS were corrected for light scattering by subtracting the corresponding background. For each condition three spectra was averaged. The maximum of the fluorescence spectra was calculated fitting the data to a log-normal distribution function with Origin 7.0.

4.13. Liposome Leakage

The ANTS/DPX liposome leakage fluorescence assay was performed as previously described [43]. Briefly, a unique population of LUVs DOPC/DOPG (3:2) was prepared to encapsulate a solution containing 12.5 mM ANTS, 45 mM DPX, 20 mM NaCl, and 10 mM Tris/HCl, pH 7.5. The ANTS/DPX liposome stock suspension was diluted to 30 μM and incubated at 37°C with protein/peptide, serially diluted from 20 to 0.1 μM in a microtiter plate. Fluorescence measurements were performed on a Victor3 plate reader (PerkinElmer, Waltham, MA, USA). ED_{50} values were calculated by fitting the data to a dose–response curve with Origin 7.0.

4.14. Liposome Aggregation

Liposome aggregation was assessed by Dynamic Light Scattering (DLS). A unique population of LUVs DOPC, DOPG or DOPC/DOPG was incubated at 37°C with 5 μM of each protein/peptide for 15 min. Particle size distribution was measured with a Zetasizer Nano ZS (Malvern Instruments Ltd., Worcestershire, UK). Polydispersity of LUV population was also analyzed. Size radius was plotted *versus* protein concentration.

4.15. LPS Binding Fluorimetric Assay

Protein binding to LPS was assessed using the fluorescent probe BODIPY[®] cadaverine (BC) (St. Louis, MO, USA). BC binds strongly to native LPSs, specifically recognizing the lipid A portion. When a protein that interacts with LPSs is added, the BC is displaced from the complex, and its fluorescence is increased. LPS-binding assays were carried out in 10 mM Hepes buffer at pH 7.2.

The displacement assay was performed by a microtiter plate containing a stirred mixture of either LPS (10 µg/mL) and BC (10 µM). Proteins and peptide were serially diluted from 20 to 0.1 µM. Fluorescence measurements were performed on a Victor3 plate reader (PerkinElmer, Waltham, MA, USA).

4.16. Aggrescan3D Analysis

Aggregation propensity of RNase6 was calculated by Aggrescan3D server [57]. The A3D value was calculated for each protein residue as described. The analysis was performed with the dynamic mode enabled and the distance of aggregation analysis was defined to 10 Å.

4.17. Minimal Inhibitory Concentration (MIC)

Minimal inhibitory concentration expressed as MIC₁₀₀, defined as the lowest protein concentration that completely inhibits microbial growth. The MIC of each protein/peptide was determined from two independent experiments performed in duplicate for each concentration. Bacteria cells were incubated at 37 °C overnight in LB broth and diluted to give approximately 5 × 10⁵ CFU (colony forming units)/mL. The bacterial suspension was incubated in LB with peptides at serially diluted concentrations (0.1–20 µM) at 37 °C for 20 h. Bacterial growth inhibition was determined by measuring the optical density (OD) of the samples at a wavelength of 570 nm.

5. Conclusions

In this work, we have characterized for the first time the bactericidal properties of the human RNase6. Our data suggest that the antimicrobial mechanism of action encompasses two steps: the protein firstly interacts with the negatively charged envelopes of the bacterial cell, promptly followed by a combination of membrane destabilization and bacterial agglutination. Furthermore, the N-terminal domain of the protein was proven to retain the antimicrobial properties of the whole protein; encouraging us to use the scaffold of the human RNase6 for the future development of new peptide based antimicrobial agents.

Supplementary Materials: Supplementary materials can be found at <http://www.mdpi.com/1422-0067/17/4/552/s1>.

Acknowledgments: The authors wish to thank all the staff at the *Servei de Microscopia* of the Universitat Autònoma de Barcelona (UAB) where transmission and scanning electron microscopy were performed; and also to the *Laboratori d'Anàlisi i Fotodocumentació* (UAB) where spectrofluorescence assays were performed. Experimental work was supported by the *Ministerio de Economía y Competitividad* (grant BFU2012-38695) and *Generalitat de Catalunya* (grant 2014-SGR-728) and co-financed by FEDER funds. Javier Arranz-Trullén is a recipient of a personal investigador en formació (PIF) predoctoral fellowship (Universitat Autònoma de Barcelona).

Author Contributions: David Pulido and Ester Boix conceived and designed the experimental work; David Pulido, Javier Arranz-Trullén, Guillem Prats-Ejarque and Diego Velázquez performed the experiments; Marc Torrent, Mohammed Moussaoui, David Pulido, Javier Arranz-Trullén and Ester Boix analyzed the data; David Pulido and Ester Boix drafted the paper; Mohammed Moussaoui, David Pulido and Ester Boix revised the final manuscript.

Conflicts of Interest: There are no conflicts of interest to declare.

Abbreviations

ANTS	8-aminonaphthalene-1,3,6-trisulfonic acid
BC	BODIPY [®] cadaverine
CFU	colony forming units
DLS	dynamic light scattering
DOPC	1,2-dioleoyl-sn-glycero-3-phosphocholine
DOPG	1,2-dioleoyl-sn-glycero-3-phosphoglycerol
DPX	<i>p</i> -xylenebispyridinium bromide
ED ₅₀	50% effective dose
FACS	fluorescent activated cell-sorting
HC	hemolytic activity
LB	Luria-Bertani media
LPS	lipopolysaccharide
LUV	large unilamellar vesicle
MAC	minimal agglutination concentration
MIC	minimal inhibitory concentration
PBS	phosphate buffer saline
RBC	red blood cell
RNase	Ribonuclease
SDS	sodium dodecyl sulfate
SEM	scanning electron microscopy
TB	terrific broth media
TEM	transmission electron microscopy

References

- Beintema, J.J.; Kleineidam, R.G. The ribonuclease a superfamily: General discussion. *Cell. Mol. Life Sci.* **1998**, *54*, 825–832. [[CrossRef](#)] [[PubMed](#)]
- Goo, S.M.; Cho, S. The expansion and functional diversification of the mammalian ribonuclease a superfamily epitomizes the efficiency of multigene families at generating biological novelty. *Genome Biol. Evol.* **2013**, *5*, 2124–2140. [[CrossRef](#)] [[PubMed](#)]
- Torrent, M.; Pulido, D.; Valle, J.; Nogues, M.V.; Andreu, D.; Boix, E. Ribonucleases as a host-defence family: Evidence of evolutionarily conserved antimicrobial activity at the N-terminus. *Biochem. J.* **2013**, *456*, 99–108. [[CrossRef](#)] [[PubMed](#)]
- Cho, S.; Beintema, J.J.; Zhang, J. The ribonuclease a superfamily of mammals and birds: Identifying new members and tracing evolutionary histories. *Genomics* **2005**, *85*, 208–220. [[CrossRef](#)] [[PubMed](#)]
- Pizzo, E.; Merlino, A.; Turano, M.; Russo Krauss, I.; Coscia, F.; Zanfardino, A.; Varcamonti, M.; Furia, A.; Giancola, C.; Mazzarella, L.; *et al.* A new RNase sheds light on the RNase/angiogenin subfamily from zebrafish. *Biochem. J.* **2011**, *433*, 345–355. [[CrossRef](#)] [[PubMed](#)]
- Sorrentino, S. The eight human “Canonical” Ribonucleases: Molecular diversity, catalytic properties, and special biological actions of the enzyme proteins. *FEBS Lett.* **2010**, *584*, 2194–2200. [[CrossRef](#)] [[PubMed](#)]
- Boix, E.; Nogues, M.V. Mammalian antimicrobial proteins and peptides: Overview on the RNase a superfamily members involved in innate host defence. *Mol. Biosyst.* **2007**, *3*, 317–335. [[CrossRef](#)] [[PubMed](#)]
- Pizzo, E.; D’Alessio, G. The success of the RNase scaffold in the advance of biosciences and in evolution. *Gene* **2007**, *406*, 8–12. [[CrossRef](#)] [[PubMed](#)]
- Rosenberg, H.F. RNase a ribonucleases and host defense: An evolving story. *J. Leukoc. Biol.* **2008**, *83*, 1079–1087. [[CrossRef](#)] [[PubMed](#)]
- Gupta, S.K.; Haigh, B.J.; Griffin, F.J.; Wheeler, T.T. The mammalian secreted RNases: Mechanisms of action in host defence. *Innate Immun.* **2013**, *19*, 86–97. [[CrossRef](#)] [[PubMed](#)]
- Malik, A.; Batra, J.K. Antimicrobial activity of human eosinophil granule proteins: Involvement in host defence against pathogens. *Crit. Rev. Microbiol.* **2012**, *38*, 168–181. [[CrossRef](#)] [[PubMed](#)]

12. Acharya, K.R.; Ackerman, S.J. Eosinophil granule proteins: Form and function. *J. Biol. Chem.* **2014**, *289*, 17406–17415. [[CrossRef](#)] [[PubMed](#)]
13. Zhang, J.; Rosenberg, H.F.; Nei, M. Positive darwinian selection after gene duplication in primate ribonuclease genes. *Proc. Natl. Acad. Sci. USA* **1998**, *95*, 3708–3713. [[CrossRef](#)] [[PubMed](#)]
14. Rosenberg, H.F.; Dyer, K.D.; Tiffany, H.L.; Gonzalez, M. Rapid evolution of a unique family of primate ribonuclease genes. *Nat. Genet.* **1995**, *10*, 219–223. [[CrossRef](#)] [[PubMed](#)]
15. Domachowske, J.B.; Dyer, K.D.; Bonville, C.A.; Rosenberg, H.F. Recombinant human eosinophil-derived neurotoxin/RNase 2 functions as an effective antiviral agent against respiratory syncytial virus. *J. Infect. Dis.* **1998**, *177*, 1458–1464. [[CrossRef](#)] [[PubMed](#)]
16. Rosenberg, H.F. Eosinophil-derived neurotoxin/RNase2: Connecting the past, the present and the future. *Curr. Pharm. Biotechnol.* **2008**, *9*, 135–140. [[CrossRef](#)] [[PubMed](#)]
17. Rosenberg, H.F. Eosinophil-derived neurotoxin (EDN/RNase2) and the mouse eosinophil-associated RNases (mEars): Expanding roles in promoting host defense. *Int. J. Mol. Sci.* **2015**, *16*, 15442–15455. [[CrossRef](#)] [[PubMed](#)]
18. Carreras, E.; Boix, E.; Rosenberg, H.F.; Cuchillo, C.M.; Nogues, M.V. Both aromatic and cationic residues contribute to the membrane-lytic and bactericidal activity of eosinophil cationic protein. *Biochemistry* **2003**, *42*, 6636–6644. [[CrossRef](#)] [[PubMed](#)]
19. Torrent, M.; Pulido, D.; Nogues, M.V.; Boix, E. Exploring new biological functions of amyloids: Bacteria cell agglutination mediated by host protein aggregation. *PLoS Pathog.* **2012**, *8*, e1003005. [[CrossRef](#)] [[PubMed](#)]
20. Lien, P.C.; Kuo, P.H.; Chen, C.J.; Chang, H.H.; Fang, S.L.; Wu, W.S.; Lai, Y.K.; Pai, T.W.; Chang, M.D. *In silico* prediction and *in vitro* characterization of multifunctional human RNase3. *Biomed Res. Int.* **2013**, *2013*, 170398. [[CrossRef](#)] [[PubMed](#)]
21. Boix, E.; Salazar, V.A.; Torrent, M.; Pulido, D.; Nogues, M.V.; Moussaoui, M. Structural determinants of the eosinophil cationic protein antimicrobial activity. *Biol. Chem.* **2012**, *393*, 801–815. [[CrossRef](#)] [[PubMed](#)]
22. Singh, A.; Batra, J.K. Role of unique basic residues in cytotoxic, antibacterial and antiparasitic activities of human eosinophil cationic protein. *Biol. Chem.* **2011**, *392*, 337–346. [[CrossRef](#)] [[PubMed](#)]
23. Rosenberg, H.F. Recombinant human eosinophil cationic protein. Ribonuclease activity is not essential for cytotoxicity. *J. Biol. Chem.* **1995**, *270*, 7876–7881. [[CrossRef](#)] [[PubMed](#)]
24. Spencer, J.D.; Schwaderer, A.L.; Dirosario, J.D.; McHugh, K.M.; McGillivray, G.; Justice, S.S.; Carpenter, A.R.; Baker, P.B.; Harder, J.; Hains, D.S. Ribonuclease 7 is a potent antimicrobial peptide within the human urinary tract. *Kidney Int.* **2011**, *80*, 174–180. [[CrossRef](#)] [[PubMed](#)]
25. Harder, J.; Schroder, J.M. RNase7, a novel innate immune defense antimicrobial protein of healthy human skin. *J. Biol. Chem.* **2002**, *277*, 46779–46784. [[CrossRef](#)] [[PubMed](#)]
26. Ryu, S.; Song, P.I.; Seo, C.H.; Cheong, H.; Park, Y. Colonization and infection of the skin by *S. Aureus*: Immune system evasion and the response to cationic antimicrobial peptides. *Int. J. Mol. Sci.* **2014**, *15*, 8753–8772. [[CrossRef](#)] [[PubMed](#)]
27. Wang, H.; Schwaderer, A.L.; Kline, J.; Spencer, J.D.; Kline, D.; Hains, D.S. Contribution of structural domains to the activity of ribonuclease 7 against uropathogenic bacteria. *Antimicrob. Agents Chemother.* **2013**, *57*, 766–774. [[CrossRef](#)] [[PubMed](#)]
28. Spencer, J.D.; Schwaderer, A.L.; Wang, H.; Bartz, J.; Kline, J.; Eichler, T.; DeSouza, K.R.; Sims-Lucas, S.; Baker, P.; Hains, D.S. Ribonuclease 7, an antimicrobial peptide upregulated during infection, contributes to microbial defense of the human urinary tract. *Kidney Int.* **2013**, *83*, 615–625. [[CrossRef](#)] [[PubMed](#)]
29. Rosenberg, H.F.; Dyer, K.D. Molecular cloning and characterization of a novel human ribonuclease (RNase k6): Increasing diversity in the enlarging ribonuclease gene family. *Nucleic Acids Res.* **1996**, *24*, 3507–3513. [[CrossRef](#)] [[PubMed](#)]
30. Becknell, B.; Eichler, T.E.; Beceiro, S.; Li, B.; Easterling, R.S.; Carpenter, A.R.; James, C.L.; McHugh, K.M.; Hains, D.S.; Partida-Sanchez, S.; *et al.* Ribonucleases 6 and 7 have antimicrobial function in the human and murine urinary tract. *Kidney Int.* **2014**, *87*, 151–161. [[CrossRef](#)] [[PubMed](#)]
31. Boix, E.; Torrent, M.; Sanchez, D.; Nogues, M.V. The antipathogen activities of eosinophil cationic protein. *Curr. Pharm. Biotechnol.* **2008**, *9*, 141–152. [[CrossRef](#)] [[PubMed](#)]
32. Amatngalim, G.D.; van Wijck, Y.; de Mooij-Eijk, Y.; Verhoosel, R.M.; Harder, J.; Lekkerkerker, A.N.; Janssen, R.A.; Hiemstra, P.S. Basal cells contribute to innate immunity of the airway epithelium through production of the antimicrobial protein RNase 7. *J. Immunol.* **2015**, *194*, 3340–3350. [[CrossRef](#)] [[PubMed](#)]

33. Robert, X.; Gouet, P. Deciphering key features in protein structures with the new endscript server. *Nucleic Acids Res.* **2014**, *42*, W320–W324. [[CrossRef](#)] [[PubMed](#)]
34. Prats-Ejarque, G.; Arranz-Trullen, J.; Blanco, J.A.; Pulido, D.; Nogues, M.V.; Moussaoui, M.; Boix, E. The first crystal structure of human rnase6 reveals a novel substrate binding and cleavage site arrangement. *Biochem. J.* **2016**. [[CrossRef](#)] [[PubMed](#)]
35. Boix, E.; Pulido, D.; Moussaoui, M.; Nogues, M.V.; Russi, S. The sulfate-binding site structure of the human eosinophil cationic protein as revealed by a new crystal form. *J. Struct. Biol.* **2012**, *179*, 1–9. [[CrossRef](#)] [[PubMed](#)]
36. Ashkenazy, H.; Erez, E.; Martz, E.; Pupko, T.; Ben-Tal, N. ConSurf 2010: Calculating evolutionary conservation in sequence and structure of proteins and nucleic acids. *Nucleic Acids Res.* **2010**, *38*, W529–W533. [[CrossRef](#)] [[PubMed](#)]
37. Torrent, M.; Navarro, S.; Moussaoui, M.; Nogues, M.V.; Boix, E. Eosinophil cationic protein high-affinity binding to bacteria-wall lipopolysaccharides and peptidoglycans. *Biochemistry* **2008**, *47*, 3544–3555. [[CrossRef](#)] [[PubMed](#)]
38. Torrent, M.; de la Torre, B.G.; Nogues, V.M.; Andreu, D.; Boix, E. Bactericidal and membrane disruption activities of the eosinophil cationic protein are largely retained in an N-terminal fragment. *Biochem. J.* **2009**, *421*, 425–434. [[CrossRef](#)] [[PubMed](#)]
39. Torrent, M.; Sanchez, D.; Buzon, V.; Nogues, M.V.; Cladera, J.; Boix, E. Comparison of the membrane interaction mechanism of two antimicrobial RNases: RNase3/ECP and RNase7. *Biochim. Biophys. Acta* **2009**, *1788*, 1116–1125. [[CrossRef](#)] [[PubMed](#)]
40. Torrent, M.; Odorizzi, F.; Nogues, M.V.; Boix, E. Eosinophil cationic protein aggregation: Identification of an N-terminus amyloid prone region. *Biomacromolecules* **2010**, *11*, 1983–1990. [[CrossRef](#)] [[PubMed](#)]
41. Torrent, M.; Badia, M.; Moussaoui, M.; Sanchez, D.; Nogues, M.V.; Boix, E. Comparison of human RNase3 and RNase7 bactericidal action at the Gram-negative and Gram-positive bacterial cell wall. *FEBS J.* **2010**, *277*, 1713–1725. [[CrossRef](#)] [[PubMed](#)]
42. Pulido, D.; Moussaoui, M.; Andreu, D.; Nogues, M.V.; Torrent, M.; Boix, E. Antimicrobial action and cell agglutination by the eosinophil cationic protein are modulated by the cell wall lipopolysaccharide structure. *Antimicrob. Agents Chemother.* **2012**, *56*, 2378–2385. [[CrossRef](#)] [[PubMed](#)]
43. Torrent, M.; Cuyas, E.; Carreras, E.; Navarro, S.; Lopez, O.; de la Maza, A.; Nogues, M.V.; Reshetnyak, Y.K.; Boix, E. Topography studies on the membrane interaction mechanism of the eosinophil cationic protein. *Biochemistry* **2007**, *46*, 720–733. [[CrossRef](#)] [[PubMed](#)]
44. Torrent, M.; Pulido, D.; de la Torre, B.G.; Garcia-Mayoral, M.F.; Nogues, M.V.; Bruix, M.; Andreu, D.; Boix, E. Refining the eosinophil cationic protein antibacterial pharmacophore by rational structure minimization. *J. Med. Chem.* **2011**, *54*, 5237–5244. [[CrossRef](#)] [[PubMed](#)]
45. Pulido, D.; Moussaoui, M.; Nogues, M.V.; Torrent, M.; Boix, E. Towards the rational design of antimicrobial proteins: Single point mutations can switch on bactericidal and agglutinating activities on the RNase a superfamily lineage. *FEBS J.* **2013**, *280*, 5841–5852. [[CrossRef](#)] [[PubMed](#)]
46. Cuchillo, C.M.; Nogues, M.V.; Raines, R.T. Bovine pancreatic ribonuclease: Fifty years of the first enzymatic reaction mechanism. *Biochemistry* **2011**, *50*, 7835–7841. [[CrossRef](#)] [[PubMed](#)]
47. Torrent, M.; di Tommaso, P.; Pulido, D.; Nogues, M.V.; Notredame, C.; Boix, E.; Andreu, D. AMPA: An automated web server for prediction of protein antimicrobial regions. *Bioinformatics* **2011**, *28*, 130–131. [[CrossRef](#)] [[PubMed](#)]
48. Torrent, M.; Nogues, M.V.; Boix, E. Eosinophil cationic protein (ECP) can bind heparin and other glycosaminoglycans through its RNase active site. *J. Mol. Recognit.* **2010**, *24*, 90–100. [[CrossRef](#)] [[PubMed](#)]
49. Sanchez, D.; Moussaoui, M.; Carreras, E.; Torrent, M.; Nogues, V.; Boix, E. Mapping the eosinophil cationic protein antimicrobial activity by chemical and enzymatic cleavage. *Biochimie* **2011**, *93*, 331–338. [[CrossRef](#)] [[PubMed](#)]
50. Gorr, S.U.; Sotsky, J.B.; Shelar, A.P.; Demuth, D.R. Design of bacteria-agglutinating peptides derived from parotid secretory protein, a member of the bactericidal/permeability increasing-like protein family. *Peptides* **2008**, *29*, 2118–2127. [[CrossRef](#)] [[PubMed](#)]
51. Beintema, J.J. Introduction: The ribonuclease a superfamily. *Cell. Mol. Life Sci.* **1998**, *54*, 763–765. [[CrossRef](#)] [[PubMed](#)]

52. Deming, M.S.; Dyer, K.D.; Bankier, A.T.; Piper, M.B.; Dear, P.H.; Rosenberg, H.F. Ribonuclease k6: Chromosomal mapping and divergent rates of evolution within the RNase a gene superfamily. *Genome Res.* **1998**, *8*, 599–607. [[PubMed](#)]
53. Dyer, K.D.; Rosenberg, H.F. The RNase A superfamily: Generation of diversity and innate host defense. *Mol. Divers.* **2006**, *10*, 585–597. [[CrossRef](#)] [[PubMed](#)]
54. Boix, E.; Nikolovski, Z.; Moiseyev, G.P.; Rosenberg, H.F.; Cuchillo, C.M.; Nogues, M.V. Kinetic and product distribution analysis of human eosinophil cationic protein indicates a subsite arrangement that favors exonuclease-type activity. *J. Biol. Chem.* **1999**, *274*, 15605–15614. [[CrossRef](#)] [[PubMed](#)]
55. Yang, S.T.; Lee, J.Y.; Kim, H.J.; Eu, Y.J.; Shin, S.Y.; Hahm, K.S.; Kim, J.I. Contribution of a central proline in model amphipathic alpha-helical peptides to self-association, interaction with phospholipids, and antimicrobial mode of action. *FEBS J.* **2006**, *273*, 4040–4054. [[CrossRef](#)] [[PubMed](#)]
56. Pulido, D.; Torrent, M.; Andreu, D.; Nogues, M.V.; Boix, E. Two human host defense ribonucleases against mycobacteria, the eosinophil cationic protein (RNase3) and RNase7. *Antimicrob. Agents Chemother.* **2013**, *57*, 3797–3805. [[CrossRef](#)] [[PubMed](#)]
57. Zambrano, R.; Jamroz, M.; Szczasiuk, A.; Pujols, J.; Kmiecik, S.; Ventura, S. AGGRESCAN3D (A3D): Server for prediction of aggregation properties of protein structures. *Nucleic Acids Res.* **2015**, *43*, W306–W313. [[CrossRef](#)] [[PubMed](#)]



© 2016 by the authors; licensee MDPI, Basel, Switzerland. This article is an open access article distributed under the terms and conditions of the Creative Commons Attribution (CC-BY) license (<http://creativecommons.org/licenses/by/4.0/>).

PAPER II

The first crystal structure of human RNase 6 reveals a novel substrate-binding and cleavage site arrangement

Guillem Prats-Ejarque*, Javier Arranz-Trullén*, Jose A. Blanco*, David Pulido*¹, M. Victòria Nogués*, Mohammed Moussaoui* and Ester Boix*²

*Department of Biochemistry and Molecular Biology, Faculty of Biosciences, Universitat Autònoma de Barcelona, E-08193 Cerdanyola del Vallès, Spain

Human RNase 6 is a cationic secreted protein that belongs to the RNase A superfamily. Its expression is induced in neutrophils and monocytes upon bacterial infection, suggesting a role in host defence. We present here the crystal structure of RNase 6 obtained at 1.72 Å (1 Å = 0.1 nm) resolution, which is the first report for the protein 3D structure and thereby setting the basis for functional studies. The structure shows an overall kidney-shaped globular fold shared with the other known family members. Three sulfate anions bound to RNase 6 were found, interacting with residues at the main active site (His¹⁵, His¹²² and Gln¹⁴) and cationic surface-exposed residues (His³⁶, His³⁹, Arg⁶⁶ and His⁶⁷). Kinetic characterization, together with prediction of protein–nucleotide complexes by molecular dynamics, was

applied to analyse the RNase 6 substrate nitrogenous base and phosphate selectivity. Our results reveal that, although RNase 6 is a moderate catalyst in comparison with the pancreatic RNase type, its structure includes lineage-specific features that facilitate its activity towards polymeric nucleotide substrates. In particular, enzyme interactions at the substrate 5' end can provide an endonuclease-type cleavage pattern. Interestingly, the RNase 6 crystal structure revealed a novel secondary active site conformed by the His³⁶–His³⁹ dyad that facilitates the polynucleotide substrate catalysis.

Key words: kinetic characterization, molecular dynamics, protein crystallography, RNase A superfamily, RNase k6, sulfate anion.

INTRODUCTION

Human RNase 6 is a protein belonging to the bovine pancreatic ribonuclease A (RNase A) superfamily, a vertebrate-specific family comprising small secretory proteins, sharing a common overall 3D structure and displaying a variety of properties. Together with the first ascribed function of pancreatic RNases to digest RNA, several family members were reported to be involved in innate immunity, showing toxicity towards a wide spectrum of pathogens, from viruses, bacteria, fungi and protozoa to helminth parasites [1–3]. An unusually high evolution rate within the family and the antimicrobial properties of distantly related members suggested a common ancestral innate immunity role [4,5]. In humans, the family includes eight known members, also called the ‘canonical RNases’ (Figure 1A). Despite their low sequence identity, ranging from 30% to 70%, we observe the conservation of the disulfide bonding pattern and the catalytic triad. All members are highly cationic and are localized at the long arm (q) of human chromosome 14 [6,7].

RNase 6, also named RNase k6, was first to be identified during a genomic search for a homologous protein of bovine kidney RNase (RNase k2) and localized on q11 region of chromosome 14 [8,9]. The newly identified human mature protein sequence was found to share 72% identity with its bovine RNase k2 counterpart. Divergence of the kidney RNases in comparison with the prototype reference family pancreatic type RNases supported their involvement in a differentiated biological role. Due to the presence of human RNase 6 in a large variety of tissues and its expression in monocytes and neutrophils, it was proposed that it could play a role in host defence. Indeed, recent studies by Becknell et al. [10] showed the protein expression in macrophages and epithelial cells at the urinary tract in response

to exposure of uropathogenic bacteria. Spencer and co-workers also reported a potent antimicrobial activity *in vitro* against Gram-negative and Gram-positive bacteria for RNase 6, together with its closest homologue, RNase 7, and proposed both proteins as being responsible for the mammalian urinary tract sterility maintenance [11,10]. Experimental evidence was also provided by the reported down-regulation of RNase 6 together with other host innate immunity proteins induced by the human immunodeficiency virus (HIV) [12]. RNase 6 displays 55% amino acid identity with RNase 7, and belongs to the RNase 6, 7 and 8 cluster, sharing with them common structural features (Figure 1A). Interestingly, even though it has been found that eosinophil RNase 2 and RNase 3 gene lineages have undergone one of the highest rates of divergent evolution to produce paralogous genes [13,14], RNase 6 primate gene lineages appear to have evolved in a more conservative mode [9]. On the other hand, a contradictory scenario has been reported in rodents, in which the evolution of RNase 6 presents a substantially higher rate [15]. All in all, a similar tendency towards an isoelectric point increase is shared within the eosinophil lineage.

The RNase A superfamily members share a conserved catalytic mechanism that was thoroughly characterized thanks to the pioneering enzymology studies during the first half of the XX's century [16–18]. RNase A catalyses the cleavage of the 3'5' phosphodiester bond of single polynucleotide substrates, showing selectivity for pyrimidines at the main base subsite (B₁) and a preference for purines at the secondary base site (B₂). Degradation of polynucleotide substrate is also assisted by additional binding sites at both sides of the catalytic centre, referred to as B_n, R_n and p_n for bases, ribose and phosphate binding respectively [19].

Preliminary kinetic characterization of RNase 6 upon its discovery indicated a moderate catalytic efficiency with respect

Abbreviations: C>p, cytidine 2',3'-cyclic phosphate; poly(A), polyadenylic acid; poly(C), polycytidylic acid; poly(U), polyuridylic acid.

¹ Present address: Imperial College London, South Kensington Campus London, London SW7 2AZ, U.K.

² To whom correspondence should be addressed (email Ester.Boix@uab.cat).

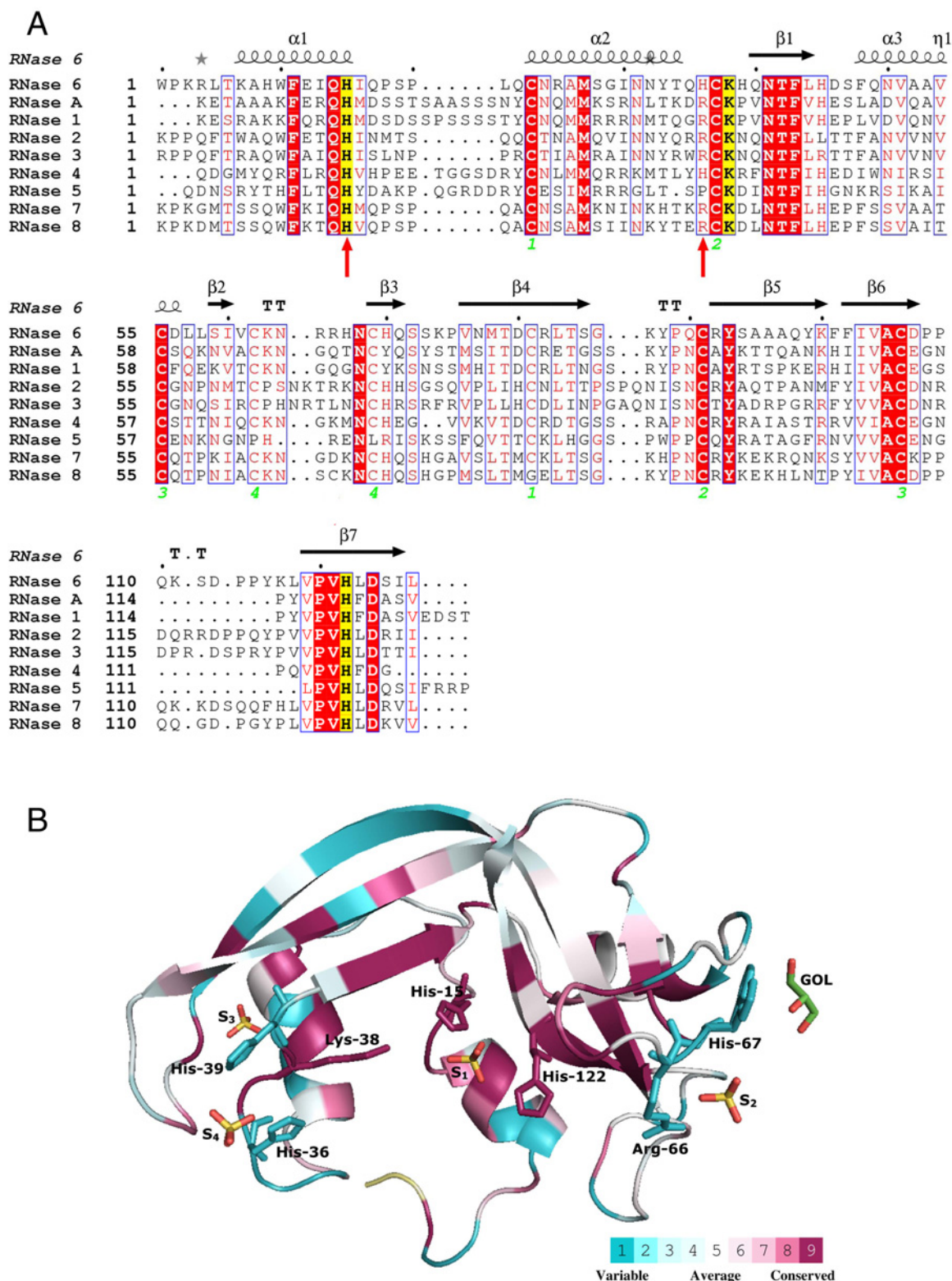


Figure 1 Primary structure of human RNases and 3D structure of RNase 6 coloured by residue conservation score

(A) Structure-based sequence of the eight canonical human RNases together with RNase A. The active sites are highlighted in yellow. The four disulfide bonds are labelled with green numbers. Tested mutations on RNase 6 are indicated with red arrows. The alignment was performed using ClustalW, and drawn using ESPript (<http://esprpt.ibcp.fr/ESPript/>). Labels are as follows: red box, white character for strict identity; red character for similarity in a group and character with a blue frame for similarity across groups. (B) RNase 6 3D structure surface representation using the CONSURF web server (<http://consurf.tau.ac.il/>) featuring the relationships among the evolutionary conservation of amino acid positions within the RNase A family. The 3D structure shows residues coloured by their conservation score using the colour-coding bar at the bottom. Sulfate anions (S1–S4) and the glycerol (GOL) molecule found in the crystal structure are depicted. Conserved residues belonging to the RNase catalytic site and interacting with bound sulfate anions are labelled.

to the family reference member RNase A. Estimation of kinetic parameters using yeast tRNA as a substrate reported approximately a 40-fold reduced catalytic rate in comparison with RNase 2 [8]. Further side-by-side comparison of RNase 6 catalytic efficiency confirmed an overall moderate relative catalytic efficiency, higher than that of RNase 3 but significantly lower than that of RNase 7 [20–22].

In the present paper, we describe the first crystal structure of RNase 6. The protein structural analysis is complemented by its enzymatic characterization to highlight RNase 6's singularity within the RNase A family context.

MATERIALS AND METHODS

Expression and purification of the recombinant proteins

A plasmid containing the gene of recombinant human RNase 6 was transformed in a prokaryote expression system. The cDNA encoding RNase 6 sequence was a gift from Dr Helene Rosenberg (National Institutes of Health, Bethesda, MD, U.S.A.). Mutant variants were constructed using the Quik Change Site-Directed Mutagenesis kit (Stratagene). All constructs were confirmed by DNA sequencing and the purified protein was analysed by MALDI–TOF–MS and N-terminal sequencing.

The genes were subcloned in plasmid pET11c for prokaryote high yield expression. *Escherichia coli* BL21(DE3) competent cells were transformed with the pET11c/RNase 6 plasmid. The expression protocol was optimized from the previously described procedure [20] to optimize the RNase 6 final recovery yield. For high yield expression, bacteria were grown in Terrific broth (TB), containing 400 $\mu\text{g/ml}$ ampicillin. Recombinant protein was expressed after cell induction with 1 mM IPTG added when the culture showed a D_{600} of 0.6. The cell pellet was collected after 4 h of culture at 37 °C. Cells were resuspended in 10 mM Tris/HCl and 2 mM EDTA, pH 8, and sonicated at 50 W for 10 min with 30-s cycles. After centrifugation at 15 000 g for 30 min, the pellet fraction containing inclusion bodies was processed as follows: the pellet fraction was washed with 50 mM Tris/HCl, 2 mM EDTA and 0.3 M NaCl, pH 8, and after centrifugation at 20 000 g for 30 min, the pellet was dissolved in 12 ml of 6 M guanidinium chloride, 0.1 M Tris/acetate and 2 mM EDTA, pH 8.5, containing 80 mM GSH, and incubated under nitrogen for 2 h at room temperature. The protein was then refolded by a rapid 100-fold dilution into 0.1 M Tris/HCl, pH 7.5, containing 0.5 M L-arginine, and GSSG was added to obtain a GSH/GSSG ratio of 4. Dilution in the refolding buffer was adjusted to obtain a final protein concentration of 30–150 $\mu\text{g/ml}$. The protein was incubated in refolding buffer for 48–72 h at 4 °C. The folded protein was then concentrated, buffer-exchanged against 0.015 M Tris/HCl, pH 7, and purified by cation-exchange chromatography on a Resource S column equilibrated with the same buffer. The protein was eluted with a linear NaCl gradient from 0 to 2 M in 0.015 M Tris/HCl, pH 7, buffer. Further purification was achieved by reverse-phase chromatography on a Vydac C_4 column, using an acetonitrile gradient. The homogeneity of the purified proteins was checked by SDS/15% PAGE and Coomassie Blue staining and by N-terminal sequencing. RNase 3 and RNase 7 were expressed as previously described [20,24].

Spectrophotometric kinetic analysis

Polycytidylic acid [poly(C)], polyuridylic acid [poly(U)], polyadenylic acid [poly(A)], poly(A): poly(U), CpA, UpA, UpG and cytidine 2',3'-cyclic phosphate (C>p) (Sigma–Aldrich) were

used as substrates, and the kinetic parameters were determined by a spectrophotometric method as described in [20]. RNase A, used as a control protein, was purchased from Sigma. Assays were carried out in 50 mM sodium acetate and 1 mM EDTA, pH 5.5, at 25 °C, using 1-cm pathlength cells. Substrate concentration was determined spectrophotometrically using the following molar absorption coefficients: $\epsilon_{268} = 8400 \text{ M}^{-1}\cdot\text{cm}^{-1}$ for C>p; $\epsilon_{265} = 21\,000 \text{ M}^{-1}\cdot\text{cm}^{-1}$ for CpA, $\epsilon_{261} = 23\,500 \text{ M}^{-1}\cdot\text{cm}^{-1}$ for UpA, $\epsilon_{261} = 20\,600 \text{ M}^{-1}\cdot\text{cm}^{-1}$ for UpG, $\epsilon_{268} = 6200 \text{ M}^{-1}\cdot\text{cm}^{-1}$ for poly(C), $\epsilon_{260} = 9430 \text{ M}^{-1}\cdot\text{cm}^{-1}$ for poly(U) and $\epsilon_{260} = 4430 \text{ M}^{-1}\cdot\text{cm}^{-1}$ for poly(A):poly(U) for each nucleotide unit. The activity was measured by following the initial reaction velocities using the difference molar absorption coefficients, in relation to cleaved phosphodiester bonds: $\Delta\epsilon_{286} = 1450 \text{ M}^{-1}\cdot\text{cm}^{-1}$ for CpA, $\Delta\epsilon_{286} = 570 \text{ M}^{-1}\cdot\text{cm}^{-1}$ for UpA, $\Delta\epsilon_{280} = 480 \text{ M}^{-1}\cdot\text{cm}^{-1}$ for UpG, $\Delta\epsilon_{250} = 2380 \text{ M}^{-1}\cdot\text{cm}^{-1}$ for poly(C), $\Delta\epsilon_{282} = 829 \text{ M}^{-1}\cdot\text{cm}^{-1}$ for poly(U) and $\Delta\epsilon_{260} = 3400 \text{ M}^{-1}\cdot\text{cm}^{-1}$ for poly(A):poly(U) for transphosphorylation reaction, and $\Delta\epsilon_{286} = 1450 \text{ M}^{-1}\cdot\text{cm}^{-1}$ for C>p hydrolysis reaction [20,25]. Duplicates of seven substrate concentrations (ranging from 0.1 to 2 mM) were tested for each condition. Final enzyme concentrations were selected from 0.1 to 10 μM depending on the RNase activity for each assayed substrate. Kinetic parameters were obtained by the non-linear regression GraFit data analysis program (Erithacus Software). Relative activity of RNase mutants was calculated by comparison of initial velocities (V_0), using a substrate concentration of 0.1 mM for dinucleotides and 0.5 mg/ml for polynucleotides.

Activity staining gel

Zymograms were performed following the method previously described [26]. SDS/15% polyacrylamide gels were cast with 0.3 mg/ml poly(C) (Sigma–Aldrich) and run at a constant current of 40 mA for 1.5 h. Then, the SDS was extracted from the gel with 10 mM Tris/HCl, pH 8, and 10% (v/v) propan-2-ol. The gel was then incubated in the activity buffer (0.1 M Tris/HCl, pH 8) to allow enzymatic digestion of the embedded substrate and then stained with 0.2% (w/v) Toluidine Blue (Merck) in 10 mM Tris/HCl, pH 8, for 10 min. Positive bands appeared white against the blue background. The loading buffer had no 2-mercaptoethanol to facilitate recovery of active enzymes. RNase A (Sigma–Aldrich) was used as a control.

Analysis of polynucleotide cleavage pattern

The characterization of the RNases, substrate cleavage patterns was carried out by studying the digestion product profiles, as previously described [27]. The poly(C) substrate (Sigma–Aldrich) was dissolved at a concentration of 0.5 mg/ml in 10 mM HEPES/KOH at pH 7.5. Then, 50 μl of the poly(C) solution was digested with 10 μl of enzyme solution at 25 °C for 1 h. Enzyme final concentrations were adjusted for each RNase: 50 nM for RNase 6 and RNase 6-H36R and 1.4 μM for RNase 6-H15A and RNase 7-H15A. At different digestion times the products of the reaction were separated by reverse-phase HPLC (Nova Pak C_{18} , Waters) according to the previously described procedure [27,28]. Briefly, the RNase/poly(C) reaction mixtures (50 μl and 15 μl for wild-type and mutant RNase 6 respectively) were injected on to the column equilibrated with solvent A (10% (w/v) ammonium acetate and 1% (v/v) acetonitrile) and the elution was carried out by an initial 10-min wash and 50-min gradient from 100% solvent A to 10% solvent A plus 90% solvent B (10% (w/v) ammonium acetate and 11% (v/v) acetonitrile). Product elution was detected from the absorbance at 260 nm,

and peak identification was performed according to previous characterization of oligocytidylic acids [29].

Protein crystallization

RNase 6 crystals were obtained after high-throughput screening of available commercial kits by the hanging-drop vapour-diffusion methodology at 20 °C. In one of these kits, JCSG-plus™ HT-96 (Molecular Dimensions), RNase 6 at 10 mg/ml was able to crystallize under one condition (0.2 M NaCl, 0.1 M sodium cacodylate, and 2 M (NH₄)₂SO₄, pH 6.5). This condition was optimized to improve the crystal size by the hanging-drop methodology by mixing 1 μl of the protein sample with 1 μl of the crystallization buffer. The best condition resulting from this optimization was 0.05 M NaCl, 0.1 M sodium cacodylate (pH 6.5) and 2 M (NH₄)₂SO₄. Cubic crystals appeared after 10 days of incubation at 20 °C and were soaked in the cryoprotectant solution by adding 15 % glycerol to the crystallization buffer prior to X-ray exposure.

Data collection, processing and protein structure solving

Data were collected at the XALOC BL13 beamline station of ALBA synchrotron (Spain) using a wavelength of 0.9795 Å. Data collection was performed at 100 K using a Pilatus 6M detector (Dectris®), 800 images were taken at $t_{\text{exp}} = 0.2$ s, $\Delta\varphi = 0.2^\circ$. The data obtained were processed with XDS (MPI for Medical Research) [30]. The structure was solved by molecular replacement with Phenix Phaser-MR program using an RNase 6 model constructed upon NMR structure of RNase 7 (PDB ID: 2HKY) [31]. Iterative cycles of refinement and manual building were applied using PHENIX [32] and Coot [33] respectively until no further improvement of R_{free} could be achieved. Finally, the stereochemistry of the structure was validated with SFCHECK [34] and WHAT_CHECK [35]. Table 1 shows the data collection and structure refinement statistics.

Structure modelling

Molecular modelling predictions were carried out using protein–nucleotide docking and molecular dynamics (MD) simulations. Docking simulations were conducted with AutoDock 4.2.6 (Scripps Research Institute) and MD simulations were performed with GROMACS 4.5.5 [36]. RNase A and RNase 6 complexes with dinucleotides (CpA, UpA and UpG) were predicted. The initial RNase A–dinucleotides' positions were determined on the basis of crystallographic data of RNase A bound to d(CpA) [37]. For RNase 6–dinucleotide complexes, the position of the S1 sulfate was taken as reference. Due to the inactive position of His¹²² in the RNase 6 crystal, the position of the histidine was adjusted to the 'active' conformation taking RNase A as a reference (PDB ID: 1RPG).

For MD simulations the force field AMBER99SB-ILDN [38] was used both for protein and RNA components. All of the complexes were centred in a cubic cell with a minimum distance of box to solute of 1.0 nm. The unit cell was filled with transferable intermolecular potential 3P (TIP3P) water [39] in neutral conditions with 150 mM NaCl. Neighbour search was performed using a group cut-off scheme with a cut-off of 1.4 nm for van der Waals interactions and 0.9 nm for the other short-range Lennard–Jones interactions. For long range interactions, smooth particle mesh of Ewald (PME) [40,41] was used with a fourth-order interpolation scheme and 0.16-nm grid spacing for FFT. The bonds were constrained with the P-LINCS algorithm

Table 1 Data collection, processing and structure refinement parameters for the RNase 6 crystal structure (PDB ID: 4X09)

* $R_{\text{merge}} = \sum_{hkl} \sum_{j=1}^N |I_{hkl}(j) - \bar{I}_{hkl}| / \sum_{hkl} \sum_{j=1}^N I_{hkl}(j)$, where N is the redundancy of the data. †Outermost shell is 1.78–1.72 Å. ‡ $R_{\text{crystal}} = \sum_h |F_o - F_c| / \sum_h F_o$, where F_o and F_c are the observed and calculated structure factor amplitudes of reflection h respectively. § R_{free} is equal to R_{crystal} for a randomly selected 5 % subset of reflections not used in the refinement.

Parameter	Value
Data collection	
Space group	$P2_12_12_1$
Unit cell	
a, b, c (Å)	27.73, 38.86, 97.97
α, β, γ (°)	90.0, 90.0, 90.0
Number of molecules in asymmetric unit	1
Resolution (Å)	1.72
Number of total reflections	22981
Number of unique reflections	11717
$R_{\text{merge}}^* \dagger$ (%)	2.8 (23.4)
$I/\sigma I \ddagger$	13.0 (2.4)
Completeness for range† (%)	99.2 (99.0)
Wilson B factor (Å ²)	24.7
Matthews coefficient (Å ³ /Da)	1.80
Solvent content (%)	31.71
Refinement	
Resolution range (Å)	48.98–1.72
$R_{\text{crystal}} \ddagger / R_{\text{free}} \S$ (%)	19.28/22.67
Number of protein atoms	1068
Number of water molecules	124
Number of bound anions	4
RMSD from ideality	
In bond lengths (Å)	0.004
In bond angles (deg)	0.908
Average B factors (Å ²)	
All protein atoms	30.34
Main-chain atoms	27.30
Side-chain atoms	33.23
Sulfate anion atoms	57.60
Glycerol atoms	49.55
Water molecules	40.67

[42], with an integration time step of 2 fs. The energy of the system was minimized using the steepest descent algorithm and equilibrated in two steps. First, an initial constant volume equilibration (NVT) of 100 ps was performed with a temperature of 300 K using a modified Berendsen thermostat. Then, 100 ps of constant pressure equilibration (NPT) was run at 1 bar (100 kPa) with a Parrinello–Rahman barostat [43,44] at 300 K and the same thermostat. Finally, 20 ns production runs were performed under an NPT ensemble without applying restraints. Three independent simulations in periodic boundary conditions were conducted for each complex. The evolution of the average RMSD for all non-hydrogen ligand atoms after least-squares fitting to the original position was calculated.

For prediction of the RNase 6–heptanucleotide complex, the RNase A–d(ATAA) crystal structure was taken as a reference (PDB ID: 1RCN [45]). First, the d(ATAA) co-ordinates were used to build an AUA ribonucleotide. His¹²² of RNase 6 was fixed in the corresponding active conformation. Local search docking with 2000 cycles and 2000 iterations was performed with AutoDock 4.2.6 [46] to adjust the AUA position to RNase 6 active site. Then, three cytidines were added to the 5' end of the tetranucleotide. The sulfate positions of the RNase 6 structures were taken as a reference to place the phosphates corresponding to the extended nucleotide. Then, a steepest descent energy minimization of the complex was performed with GROMACS

4.5.5. MD simulations were also applied using the same protocol described for dinucleotides.

Prediction of pK_a values

Prediction of pK_a values of selected protein residues was performed using the Rosetta online server ROSIE [47]. The estimated pK_a values of selected histidine residues were calculated by using a neighbour sphere of 15 Å and considering the protonation state of ionizable residues. A starting pK_a reference value of 6.3 for each histidine residue was ascribed. The program evaluates all potential conformational rotamers together with the influence of side chain and backbone mobility. RNase A (PDB ID: 7RSA) co-ordinates were used as a reference control. Predicted pK_a values for His¹², His¹⁰⁵ and His¹¹⁹ in RNase A were found in accordance with the previously reported experimental values [48]. His¹⁰⁵ in RNase A and His⁶⁷ in RNase 6 were selected as control solvent-exposed residues, not involved in Coulombic interactions with nearby residues. The RNase A double mutant (RNase A-H7H10) [49] crystal structure (PD ID: 5ET4; Blanco, Salazar, Moussaoui and Boix unpublished results) was also analysed to evaluate the predicted pK_a values for an engineered secondary site located at RNase A secondary phosphate-binding site.

RESULTS

RNase 6 3D structure

RNase 6 crystals diffracted to 1.72 Å. The structure was solved using RNase 7 structure as a model (PDB ID: 2HKY [31]). The crystallographic statistics for the data collection, processing and structure solving are provided in Table 1. Structural data for RNase 6 structure are available in the PDB under the accession number 4X09. The RNase 6 3D structure (Figure 1B) complies with the RNase A superfamily overall conformation, with a kidney-shaped structure formed by seven β -strands and three α -helices cross-linked by four conserved disulfide bonds, as listed in Supplementary Table S1. Loop residues Trp¹-Lys³, Gln¹⁷-Leu²¹, Lys⁶³-Arg⁶⁶, Gly⁸⁶-Gln⁹⁰ and Pro¹⁰⁸-Ser¹¹² are partially disordered. In particular, practically no electron density was visualized for residues Pro², Lys³, Gln¹⁷, Leu²¹, Gly⁸⁶ and Lys⁸⁷ that could not be properly modelled. Alternative side-chain conformations were modelled for some residues (Gln¹⁴, Asn³², Ser⁵⁹, His⁶⁷, Met⁷⁸ and Thr⁷⁹). Specifically, high motion values were observed in loops L1, L2 and L8, where 4% of the residues are disordered, as reported for the RNase 7 structure [31]. Residues involved in crystal packing were analysed by the PISA web server [50]. The intermolecular contacts are listed in Supplementary Table S2. Interactions are found mostly between β 3, β 4, β 5 and β 7 strand residues (Gln⁷¹, Arg⁸², Ala⁹⁷-Tyr⁹⁹, Ser¹²⁵ and Ile¹²⁶) and loop residues. No packing contacts are seen in the environment of the active site, therefore enabling further substrate-binding studies.

An overall comparison of RNase 6 crystal structure with previously solved structures of RNase A superfamily members highlighted some interesting particularities. First, we observed a distinct conformation of the RNase 6 N-terminus, where Trp¹, unique in the RNase A superfamily, folds back towards the protein core. Next, we found several non-conserved histidine residues, unique to RNase 6, that contribute to the protein structure peculiarities. His⁹ was observed to interact with Glu¹² by a salt bridge, which would participate in the stabilization of the first α -helix, as reported in RNase A for the Glu²-Arg¹⁰ salt bridge [51,52]. Unusual rotamer conformations, showing

an unambiguous electron density, were observed for two non-conserved histidines: His³⁶ and His⁶⁷.

RNase 6 sulfate-binding sites

The protein was crystallized in the presence of ammonium sulfate and four sulfate anions were identified in the crystal asymmetric unit (Figure 1B and Supplementary Figure S1). Three of these sulfates corresponded to defined cationic regions exposed at the protein surface and correlate to putative RNA phosphate-binding sites, whereas the fourth sulfate is involved in the crystal packing. Sulfate anion interactions with nearby residues are listed in Supplementary Table S3 and illustrated in Figure 2. Sulfate labelled S1 corresponds to the active site of the enzyme, conserved in all canonical RNases. The presence of either a sulfate or phosphate anion at the enzyme active site was already reported for RNase A [53,54] and other family members: RNase 2-EDN (eosinophil-derived neurotoxin) [55], RNase 3-ECP (eosinophil cationic protein) [56] and RNase 5-angiogenin [57]. On the other hand, the second sulfate (S2) found in the RNase 6 structure binds to a distinct region not reported in any other family members (Arg⁶⁶/His⁶⁷). Comparative studies of our structure with the RNase A-tetranucleotide analogue [45] suggested that this region may represent a distinct phosphate-interaction subsite located at the 5' end of the RNA substrate. In addition, a third sulfate anion was visualized in the RNase 6 structure bound to two histidine residues (His³⁶ and His³⁹), His³⁹ being unique to RNase 6 among all RNase A members. Interestingly, both histidine residues together with a close by lysine residue (Lys⁸⁷) mimic the disposition of a putative RNase active site (Figure 3), as also identified using the PDBeMotif analysis tool available at the PDBe server (<http://www.ebi.ac.uk/pdbe-site/pdbemotif/>).

RNase 6 main active site

The RNase 6 crystal structure illustrates the conservation of the active-site architecture within the RNase A family. Residues His¹⁵, Lys³⁸ and His¹²² (His¹², Lys⁴¹ and His¹¹⁹ RNase A counterparts) build the active-site groove, with His¹²² adopting the so-called 'inactive' orientation [58], a conformation reported to be favoured in acidic and high ionic salt solutions [59]. Comparison of atomic crystal structures for RNase A indicated that His¹¹⁹ can adopt two conformations: A (active) and B (inactive), where the 'active' ring orientation is required for adenine binding at the secondary base B₂ site [37,60]. On the other hand, the active orientation of the RNase A His¹¹⁹ ring was reported to be favoured by the hydrogen bond interaction with the vicinal Asp¹²¹ residue, whose interaction would account for the correct His¹¹⁹ tautomer in catalysis [61]. RNase 6 counterpart (Asp¹²⁴), located in an equivalent conformation, could also perform an equivalent role. However, the inactive His¹²² conformation is fixed in our RNase 6 structure by a hydrogen bond interaction with Lys⁷. Therefore, the close proximity of Lys⁷ might alter significantly the properties of the His¹²² catalytic residue. Likewise, we considered the potential influence of the nearby His³⁶/His³⁹ RNase 6 residues on the other active-site histidine residue (His¹⁵). The presence of cationic residues near to the RNase 6 active site could shape the enzyme's performance, and may account for a reduction in its catalytic efficiency in comparison with RNase A (Table 2 and Supplementary Table S4). Although the RNase 6 structure conserves equivalent positions for some key residues at the active-site environment, such as Gln¹⁴ and Asn⁴¹ (Gln¹¹ and Asn⁴⁴ respectively in RNase A), the close proximity of residues such as Lys⁷, His³⁶ or His³⁹ should not be disregarded.

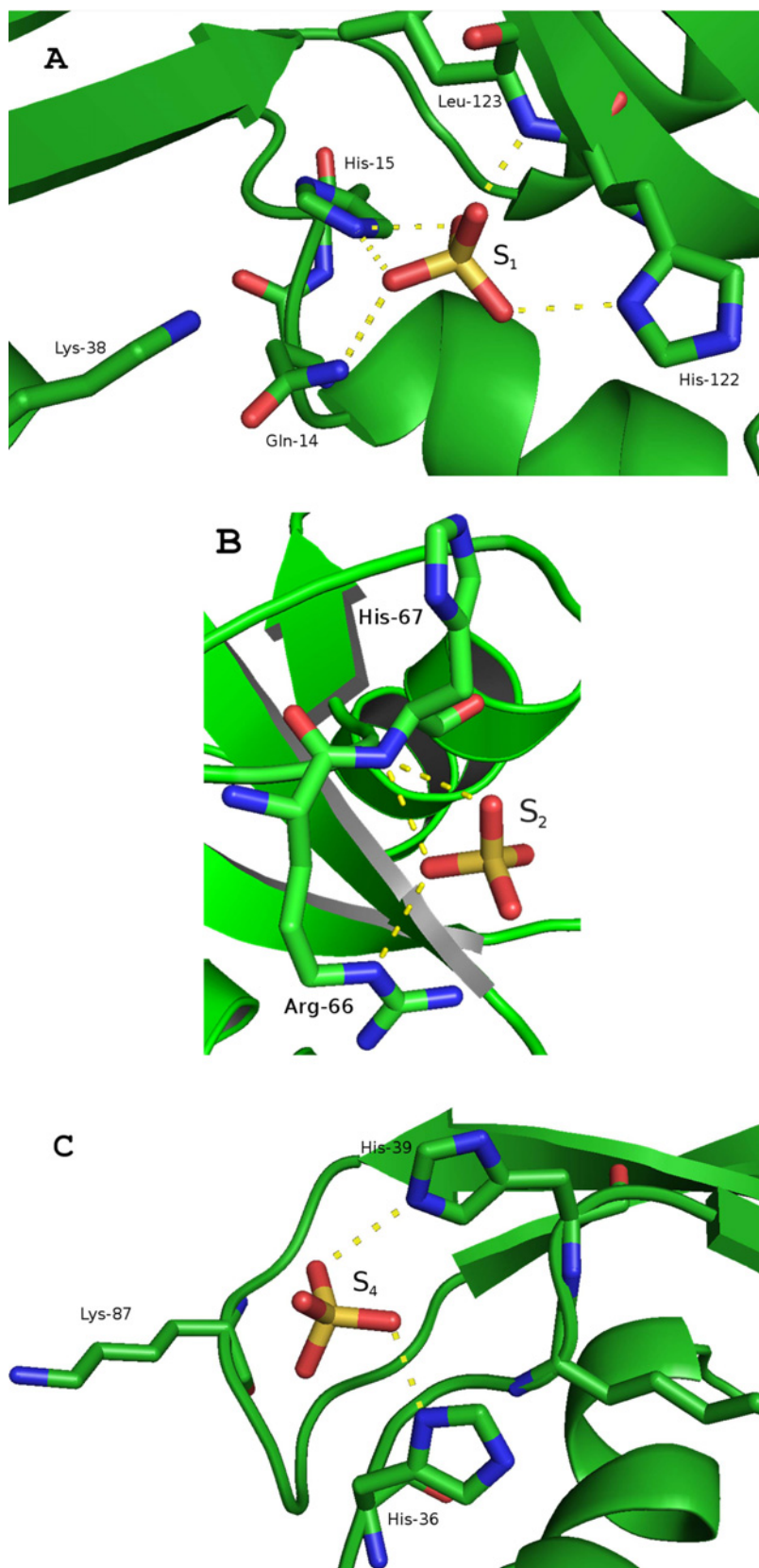


Figure 2 Detail of sulfate binding interactions in the RNase 6 crystal structure

Atoms involved in the protein–anion interactions are listed in Supplementary Table S3. The sulfate involved in the crystal packing (S3) is not shown. The structure was drawn with PyMol 1.7.2 (DeLano Scientific).

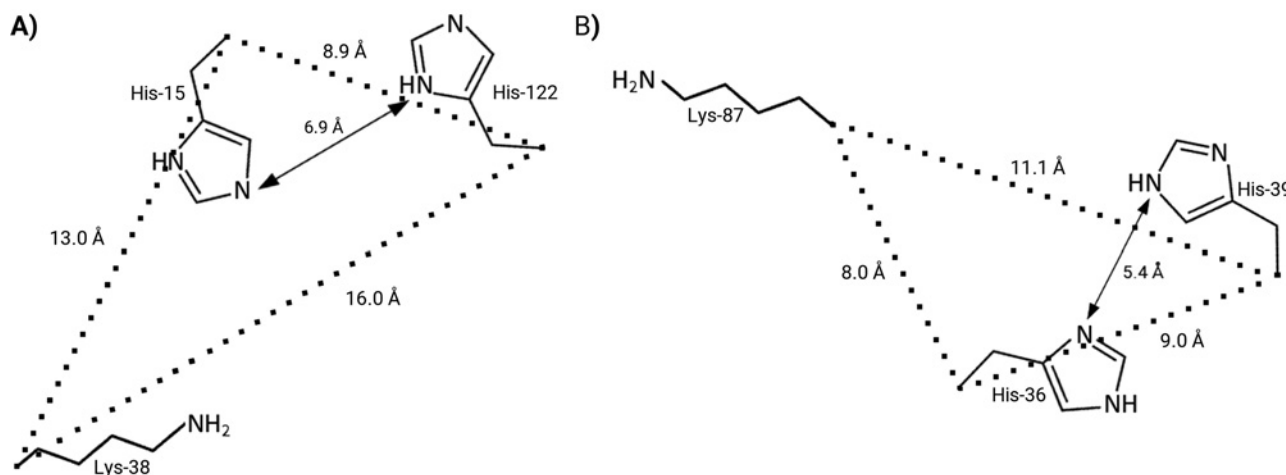


Figure 3 Illustrative scheme of RNase 6 main and putative secondary active sites

Illustrative scheme of the RNase 6 main active site (A) and the putative secondary site (B). CpA atom distances are labelled together with the histidine ND1 to NE2 respective distances. The figure was created with PyMol (DeLano Scientific).

Table 2 Kinetic parameters of RNases for dinucleotide and mononucleotide cyclic phosphate substrates

ND: not detected at the assayed conditions. *All assays were carried out in duplicate by a spectrophotometric assay as described in the Materials and methods section. Kinetic parameters were estimated from non-linear regression data using the GraFit program. †Values shown for RNase A activity are taken from [73–75].

		UpA	UpG	CpA	C>p
RNase 6	K_m (mM)*	2.63 ± 0.3	ND	1.22 ± 0.2	2.06 ± 0.3
	k_{cat} (s^{-1})	12.9 ± 1.1	ND	1.08 ± 0.1	$3.25 \times 10^{-3} \pm 0.06$
	k_{cat}/K_m ($s^{-1} \cdot M^{-1}$)	4.90×10^3	ND	8.85×10^2	1.60
RNase 3	K_m (mM)	2.7 ± 0.66	ND	1.7 ± 0.3	3 ± 0.53
	k_{cat} (s^{-1})	1.22 ± 0.12	ND	0.55 ± 0.06	$3.2 \times 10^{-3} \pm 5.1 \times 10^{-4}$
	k_{cat}/K_m ($s^{-1} \cdot M^{-1}$)	4.47×10^2	ND	3.23×10^2	1.07
RNase A†	K_m (mM)	0.7	2.0	0.5	1.06 ± 0.1
	k_{cat} (s^{-1})	2.69×10^3	1.38×10^2	2.3×10^3	2.28 ± 0.18
	k_{cat}/K_m ($s^{-1} \cdot M^{-1}$)	3.84×10^6	6.9×10^4	4.59×10^6	2.15×10^3

RNase 6 nucleotide-binding sites

The RNase 6 crystal structure was further analysed to elucidate the structural basis for the protein substrate specificity and kinetic properties. Comparison of the RNase 6 structure with RNase A indicated conservation of most residues at the B₁ site. In contrast, non-conserved substitutions were found for Phe¹²⁰ and Ser¹²³ RNase A counterpart residues. Phe¹²⁰ is observed in RNase A to contribute stacking interactions to fix the pyrimidine ring [37]. Nevertheless, a leucine residue in RNase 6, also present in RNase 3, might also contribute to shape the protein base binding hydrophobic cavity. In any case, the presence of Phe¹²⁰ in both RNase A and RNase 4, two very efficient RNase A family members, might also explain their relative higher catalytic activity. On the other hand, B₁ selectivity is considered to be dependent on a Thr–Asp dyad relative position. Thr⁴⁵–Asp⁸³ interactions were attributed in RNase A to shift from cytidine to uridine preference [17]. However, in RNase 6, the presence of Gln⁴⁰, hydrogen-bonded to Asp⁸⁰ (Asp⁸³ counterpart), fixes the latter in a distinct orientation that might interfere in its interaction with Thr⁴² (Thr⁴⁵ counterpart), and modifies the pyrimidine-binding mode. Additionally, RNase A and RNase 4 (an RNase with an unusually strong uridine preference [62]), have an hydrophobic residue at the Gln⁴⁰ position, which was considered to help locating the Thr⁴⁵ residue at the most favoured conformation for uridine base binding

Table 3 Catalytic activity ratio of RNases for the assayed nucleotides

ND: not detected at the assayed conditions. *Data for Poly(U):Poly(A) were taken from [76].

	CpA/UpA	CpA/C>p	Poly(C)/poly(U)	Poly(U)/poly(U):poly(A)
RNase 6	0.18	5.5×10^2	1.02	0.43
RNase 3	0.72	3.0×10^2	1.74	ND
RNase A*	1.20	2.1×10^3	8.14	307

[63]. To note, Gln⁴⁰–Asp⁸⁰ pair is unique to RNase 6 among the eight human canonical RNases (Figure 1). This scenario might explain in RNase 6 the observed increase K_m value for both UpA and CpA with respect to RNase A (Table 2). On the other hand, the orientation of Asp⁸⁰, closer to RNase A counterpart but clearly distinct from RNase 4, may explain RNase 6's moderate preference for uridine at the B₁ site (Table 3). Interestingly, the uridine predilection of RNase 4 would be mostly determined by Arg¹⁰¹ that can directly interact with the uridine carbonyl group and brings Asp⁸⁰ closer to the vicinity of Thr⁴⁵ [64]. Noteworthy, the presence of Arg¹⁰¹ is characteristic of the RNase 4 lineage, whereas RNase A and RNase 6 have a lysine at this position which is pointing in the opposite direction.

Next, we analysed the RNase 6 structure at the secondary base site (B_2). Conservation of Asn⁶⁸ and Asn⁶⁴ (Asn⁷¹ and Asn⁶⁷ in RNase A respectively) is observed. Notwithstanding, the presence of a non-conserved cationic residue at position 66 might alter significantly the region. Additionally, although there is a conservative substitution for Glu¹¹¹ in RNase A (Asp¹⁰⁷ in RNase 6), the distinct loop orientation, due to the presence of a proline residue in RNase 6, modifies considerably the region's putative interactions. Altogether, the B_2 site architecture would provide reduced binding interactions to the purine base, retaining a preference for adenine compared with guanine, as confirmed by our kinetic results (Tables 2 and 3, and Supplementary Table S4) and reported for most of the other tested mammalian RNase A family members [65–67]. Finally, we searched the RNase 6 structure for phosphate-binding sites that could contribute to the recognition of an RNA polymeric substrate, as described for RNase A [19]. Towards this aim, the protein nucleotide-binding mode was further analysed by molecular modelling.

Structure analysis by molecular modelling simulations

MD simulations were performed to predict the overall RNase 6 substrate-binding mode. Three independent runs were carried out for a total of 20 ns. All ligand positions were fully stabilized after a time lapse of 5 ns, showing a final average RMSD ranging from 0.15 to 0.3 nm. First of all, MD simulations were applied to RNase dinucleotide complexes taking as a model reference the RNase A–d(CpA) crystal structure [37]. Results indicated that the CpA and UpA dinucleotides could accommodate in a similar orientation into the RNase 6 catalytic cleft, showing no significant displacement from the original location (Figure 4). A close inspection of predicted RNase 6–dinucleotide interactions corroborated some of the structural features inferred from the crystal structure analysis. Equivalent interactions at the phosphate position suggested a conserved binding mode at the main phosphate-binding site (p_1). Noteworthy, although the starting position of His¹²² in the RNase 6 crystal was found in the inactive conformation, the residue was adjusted to its active orientation before modelling, remaining in the favoured orientation for catalysis after all MD simulations. Interestingly, together with equivalent relative positioning of Gln¹⁴, His¹⁵ and His¹²², the presence in the RNase 6 active-site neighbourhood of Lys⁷ and Trp¹⁰ (Ala⁴ and Lys⁷ in RNase A) would account for significant differences at the p_1 environment.

The binding pattern described for RNase A was also mostly conserved for RNase 6 at the main pyrimidine base site (B_1). Leu¹²³ in RNase 6 was observed to partially supply the Phe¹²⁰-stabilizing role in RNase A, but might induce a minor tilt of the ring plane. Interestingly, together with the conserved bidentate hydrogen bond between Thr⁴² and the pyrimidine base, the close-by Gln⁴⁰ could directly interact with the Asp⁸⁰ and the N3 atom of the pyrimidine base.

On the other hand, the comparison between the secondary base-binding site (B_2) of both RNases showed minor differences in the relative position of the adenine base, but a more pronounced base displacement for the guanine-containing dinucleotides. Equivalent hydrogen bond interactions to adenine were found in RNase 6 for Asn⁶⁴ and Asn⁶⁸ (Asn⁶⁷ and Asn⁷¹ in RNase A), together with base-stacking interactions with His¹²² (His¹¹⁹ in RNase A). However, although the main determinants for adenine binding were conserved, we observed how the presence of Arg⁶⁶, unique to RNase 6, is significantly altering the environment. Indeed, in all of our predicted protein–dinucleotide complexes,

we observed a salt bridge between Arg⁶⁶ and Asp¹⁰⁷, which shifted the aspartate position from the corresponding RNase A anionic residue (Glu¹¹¹).

In particular, a major displacement from the original position was observed for the UpG dinucleotide in complex with both RNases. MD simulations indicated that the guanine base could not properly fit into the B_2 site, promoting non-canonical orientations, where the guanine base was partially displaced. Moreover, in both RNases, the bidentate hydrogen bond to Asn⁶⁸ (Asn⁷¹ in RNase A) was partially lost. Variability among replicates in the dinucleotide positioning reminded the reported productive and non-productive binding mode for the crystallographic complexes of RNase A with 2′/5′-UpG [68]. Additionally, interactions in both RNases between the guanine C2 amino group and the Asp¹⁰⁷ (Glu¹¹¹ in RNase A) residue would fix the base in a less favoured orientation, pushing away the phosphate from the main active site. Nonetheless, the relative UpG displacement from the original position was less pronounced in the predicted RNase A complex, probably due to the contribution of Phe¹²⁰-stacking interactions at B_1 , that provide a better fixation of the pyrimidine base. On its side, the presence in RNase 6 of Lys⁷ close to the active-site environment would favour the displacement of the phosphate towards the p_2 region.

Complementarily, to gain further insight into the protein nucleotide-binding mode we modelled an heptanucleotide complex taking the RNase A–d(ApTpApA) crystal structure [45] as a starting reference model (Figure 5). The oligonucleotide fitted nicely into the enzyme active cleft showing only significant differences from the RNase A-binding mode at the secondary substrate-binding sites. Figure 5 highlights the protein residues at hydrogen bond distance observed in the protein–heptanucleotide complex. Putative RNase 6 substrate-binding sites were ascribed for base and phosphate recognition (Supplementary Table S5). Together with conserved equivalent sites to RNase A, the predicted complex illustrated the presence in RNase 6 structure of unique interacting residues at the RNA 5′ end. A novel specific region at p_{-2} and p_{-3} sites would be conformed by His³⁶, His³⁹ and Lys⁸⁷. In addition, stacking interactions between His³⁶ and the base located at the B_{-2} position were also identified in the model.

Kinetic characterization of RNase 6

Next, we determined the RNase 6 enzymatic activity against a variety of RNA substrates to correlate the protein structure with its enzymatic properties. RNase 6 catalytic efficiency ratio was compared with RNase 3 and RNase A (Supplementary Table S4), as representative family members for low and high catalytic efficiency respectively [18,23,66].

First, kinetic parameters for RNase 6 were calculated for dinucleotide and cyclic mononucleotide substrates (Table 2). Comparison of K_m and k_{cat} values for cyclic mono- and dinucleotides indicated that most of the decrease in the catalytic efficiency of RNase 6 in comparison with RNase A (from 100- to 1000-fold) is due to a reduction in the catalytic constant value. A side-by-side comparison of substrate relative ratio (Table 3) highlighted for RNase 6 a preference for uridine at the B_1 site and selectivity for adenine at B_2 . Additionally, the enzyme activity was assayed against polymeric substrates (Table 3 and Supplementary Table S4). RNase 6 displayed a low catalytic efficiency for polynucleotides in comparison with RNase A (Supplementary Figure S2), showing a similar reduced relative catalytic activity as previously reported for RNase 3 [20]. Interestingly, we observed that RNase 6 had the ability to degrade the double stranded poly(U):poly(A) substrate, a property not shared by RNase 3.

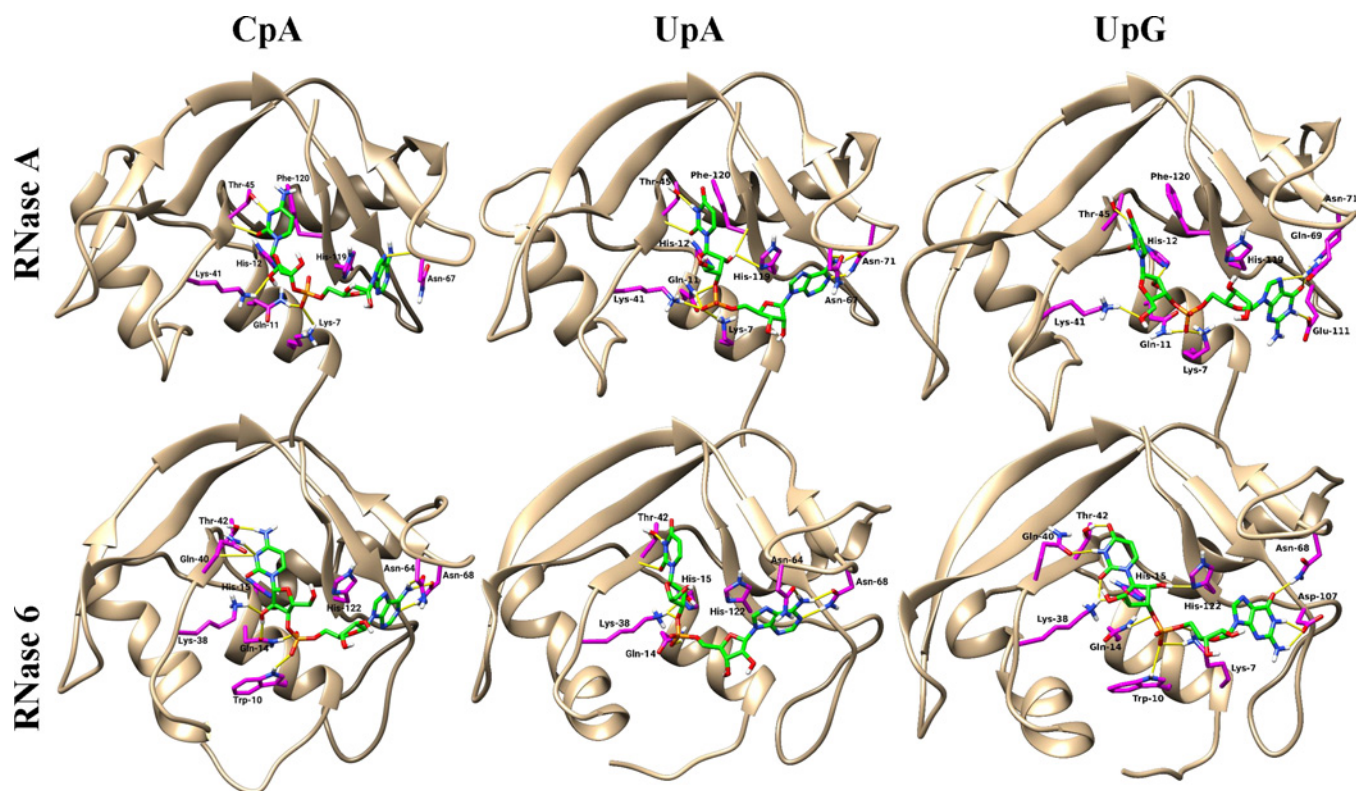


Figure 4 Predicted RNase 6 and RNase A structures in complex with dinucleotides

Predicted structure of RNase 6 and RNase A in complex with CpA, UpA and UpG dinucleotides after MD simulations, as detailed in the Materials and methods section. Nucleotides are coloured green. RNases interacting residues are coloured magenta. Hydrogen bonds are coloured yellow. Structures were drawn with UCSF Chimera 1.10 [77].

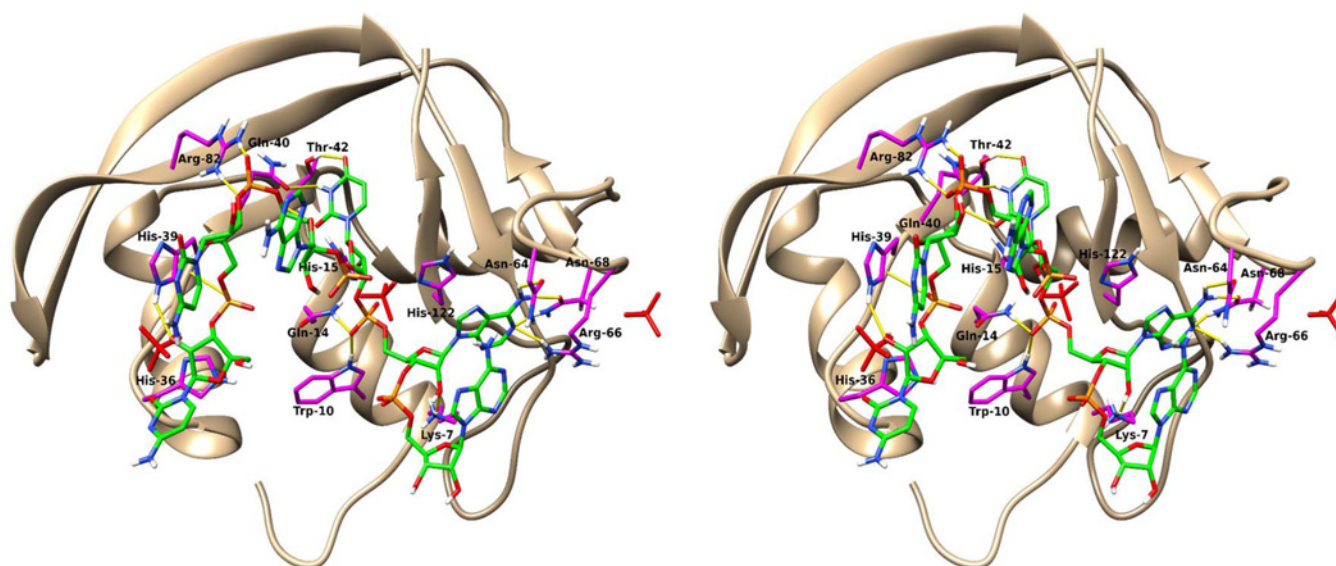


Figure 5 Stereo view of predicted RNase 6 heptanucleotide complex

RNase 6 in complex with CCCAUA heptanucleotide after a MD simulation, as described in the Materials and methods section. The heptanucleotide is coloured green. Interacting residues of RNase 6 are coloured turquoise. Protein-interacting residues and ligand atoms are coloured according to their element. Hydrogen bonds are coloured yellow. Overlapped sulfate ions of the original coordinates of the crystal are coloured magenta. The structures were drawn with UCSF Chimera 1.10 [77].

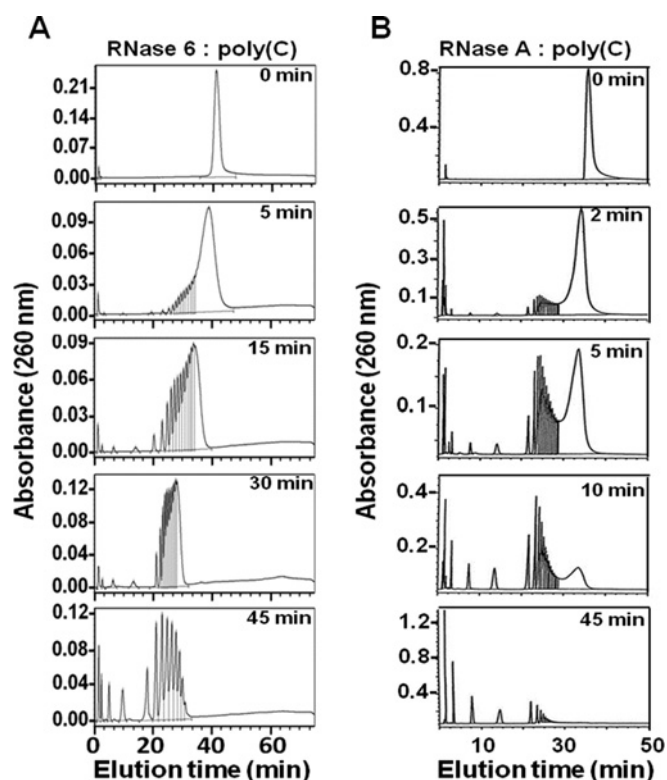


Figure 6 Analysis of polynucleotide cleavage pattern by RNase 6 and RNase A

Poly(C) cleavage pattern obtained by RNase 6 (A) compared with RNase A [27] (B). Chromatography profiles of poly(C) digestion products are shown at selected incubation times corresponding to representative steps of the catalysis process. See the Materials and methods section for substrate digestion conditions.

Complementarily, to evaluate the contribution of the RNase 6-specific subsite arrangement, we analysed the enzyme poly(C) cleavage pattern, as a model of polymeric substrate (Figure 6). The oligonucleotides obtained from the substrate digestion were eluted by reverse-phase chromatography, where the mononucleotide fraction is eluted at the initial conditions and oligonucleotides of increasing size are eluted at increasing retention times. The previously optimized methodology distinguishes between consecutive sizes up to eight or nine nucleotides, whereas the peaks corresponding to higher-molecular-mass components contain more than one oligonucleotide size due to the column discrimination power limitations [29]. Our previous work on RNase A cleavage pattern showed a decrease in the initial poly(C) peak followed by the formation of intermediate oligonucleotides with an average size of around six or seven residues, a pattern that supported the enzyme multisubsite structure providing a characteristic endonuclease-type activity [29]. Noteworthy, RNase 6 displayed a characteristic digestion profile differentiated from that previously obtained for RNase A [27], where there is first the formation of considerably large intermediates which are subsequently digested, giving rise to relatively shorter intermediates. Interestingly, the decrease in the original polynucleotide substrate was enhanced for RNase 6 at short incubation times. On the other hand, the predominance of smaller oligonucleotides did not take place until most of the high-molecular-mass polymeric substrate has been degraded, revealing a singularized cleavage pattern, that could be ascribed to a pronounced endonuclease mechanism.

Table 4 Relative catalytic activities for wild-type RNases 6 and 7 and mutant variants

ND: not detected at the assayed conditions. *Data expressed in percentage of activity in relation to the wild-type protein (%). Mean values were calculated from triplicate assays, showing in all cases a standard error below 10%.

	UpA	CpA	Poly(U)	Poly(U):poly(A)
RNase 6	100	100	100	100
RNase 6-H15A*	13	14	77	63
RNase 6-H36R	94	86	36	40
RNase 6-H15A/H36A	ND	ND	15	5
RNase 7	100	100	100	100
RNase 7-H15A	ND	ND	3	7

Kinetic characterization of RNase 6 mutants

Analysis of the RNase 6 three-dimensional structure and molecular modelling predictions suggested that the enzyme facility to cleave polymeric substrates could be related to the presence of surface-exposed cationic residues that might facilitate the RNA anchorage and degradation. Noteworthy, the presence in RNase 6 of a histidine pair (His³⁶/His³⁹) (Figure 1 and Supplementary Figure S3) that adopts a configuration equivalent to the His¹⁵/His¹²² dyad at the RNase main active site, suggested the existence of a secondary active centre (Figure 3). To evaluate this hypothesis, we designed mutant variants at His¹⁵ and His³⁶. First, the enzyme main active site was removed by His¹⁵ mutation to alanine. His¹⁵ in RNase 6 was selected as the RNase A His¹² counterpart, where the corresponding H12A mutant was reported by Raines and co-workers to totally abolish the RNase A catalytic activity [69]. Additionally, His³⁶ was mutated to arginine to remove the putative secondary catalytic residue while retaining an exposed cationic charge. In addition, most RNase A family members, including RNase 7, the closest RNase 6 homologue, display an arginine residue at an equivalent position (Figure 1 and Supplementary Figure S3). Eventually, a double mutant (His15A/His36A) was engineered to evaluate simultaneously the removal of the main and secondary active sites.

Kinetic characterization of point mutants confirmed the key role of both His¹⁵ and His³⁶ (Table 4). The contribution of His³⁶ was found to be mostly critical for polymeric substrates. On the other hand, we observed how the RNase 6-H15A mutant was retaining a significantly high activity for polymeric substrates (approximately 35–40% relative activity respect to wild-type RNase). Interestingly, for the assayed dinucleotides, a residual relative activity of approximately 15% was observed, which was abolished by the double mutation. Moreover, the RNase 6-H15A activity was further compared with the corresponding RNase 7-H15A mutant (Table 4). The complete abolishment of activity for the RNase 7 active site mutant for dinucleotides, in contrast with RNase 6-H15A, corroborated the hypothesis. On the other hand, a remnant activity for polynucleotides is observed for both the RNase 6 double mutant and the RNase 7-H15A mutant. Likewise, residual catalytic activity for the RNase A-H12K/H119Q mutant was attributed to be solely promoted by the RNA structure distortion induced by the enzyme interaction [49].

Complementarily, the analysis of RNase 6 activity on polymeric substrates was also assayed on an activity staining gel and by the analysis of the polynucleotide digestion products. The side-by-side comparison of the polynucleotide cleavage product profiles obtained by incubation with both RNase 6-H15A and RNase 7-H15A mutants, devoid of the main active-site histidine residue, confirmed the presence in RNase 6 of another cleavage

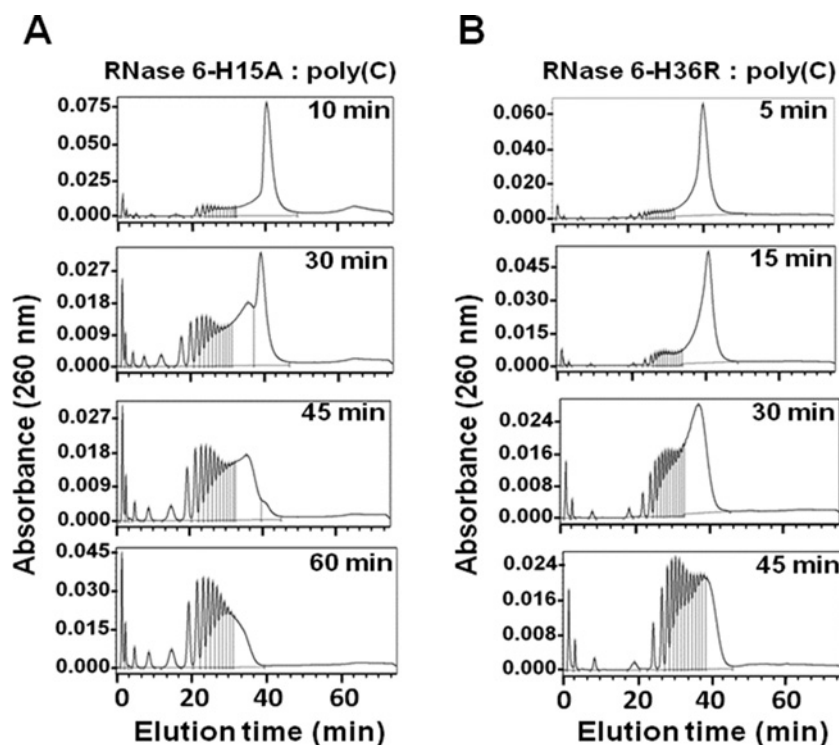


Figure 7 Analysis of polynucleotide cleavage pattern by RNase 6 mutants

Poly(C) cleavage pattern by RNase 6-H15A (A) and RNase 6-H36R (B) mutants. Chromatography profiles of poly(C) digestion products are shown at selected incubation times corresponding to representative steps of the catalysis process.

site. We observed that, using the same assay conditions, a considerable amount of activity is achieved with the RNase 6-H15A mutant, whereas non-significant activity is observed for the corresponding RNase 7-H15A mutant (Supplementary Figure S4). Comparison of both RNases activity on poly(C) together with RNase 6 mutants was also analysed by the zymogram technique (Supplementary Figure S2), where the RNase 6 double mutant displayed no detectable activity at even a 5-fold protein concentration. Interestingly, when comparing the poly(C) digestion pattern along with the His¹⁵ and 36 respective mutants' profiles we observe how both mutants shifted their product elution profile towards a more exonuclease-type pattern, accumulating shorter intermediates than the native enzyme at an earlier stage of the reaction. A similar profile progression was previously reported for RNase 3, described to present a subsites arrangement that would favour an exonuclease cleavage pattern [20].

DISCUSSION

We report in the present paper the first crystal structure RNase 6 in complex with sulfate anions (Table 1). The location of putative phosphate-binding sites was deduced from the position of the sulfate anions in the crystal structure (Figure 2 and Supplementary Table S3). Structural analysis and kinetic characterization were carried out to outline the protein nucleotide-binding sites arrangement. The first sulfate was ascribed to the main RNase A phosphate-binding site, shared with the other RNase A family members [54,55,67]. Two additional sulfate anions were located at the protein-exposed cationic residues (His³⁶/His³⁹ and Arg⁶⁶/His⁶⁷) and would correspond to secondary phosphate-binding sites. In particular, the His³⁶/His³⁹ site is proposed as a novel and unique

site within the RNase A family (Figures 1 and 3). Kinetic studies corroborated the involvement of His³⁶ in enzyme catalysis (Table 4).

The contribution of RNase 6 novel secondary catalytic site in the catalytic mechanism was further analysed by the characterization of the enzyme polynucleotide cleavage pattern (Figure 6). The distribution of substrate digestion products indicated that the breakdown of the polymeric substrate was not a random process. The chromatography profiles revealed the preference of RNase 6 for the binding and cleavage of long RNA strands, where the broken phosphodiester bonds would be located considerably spaced apart from the end of the chain. By comparison with the previously characterized RNase A cleavage pattern [29], we concluded that the RNase 6 activity towards the polymeric substrate was even more endonucleolytic than the previously described for RNase A [19]. On the other hand, we observed how the poly(C) digestion profile underwent a pronounced shift in its cleavage pattern towards an exonuclease-type propensity when the main active-site histidine was mutated (Figure 7).

Complementarily, structural analysis also illustrated a well-defined substrate multisubsite arrangement for RNase 6. Interestingly, the predicted RNase 6 complex with a heptanucleotide by MD (Figure 5) revealed the presence of novel sites at the RNA 5' end that would be ascribed to B₋₂ and p₋₂/p₋₃ sites (Supplementary Table S5).

Interestingly, the RNase 6 structure revealed equivalent histidine ND1 to NE2 atomic distances for His¹⁵/His¹²² and His³⁶/His³⁹, suggesting the presence of a secondary catalytic site. In addition, we observed stacking interactions between the B₋₂ base of the oligonucleotide and His³⁹ in the predicted complex. However, structural analysis identified no additional residues for binding of adjacent bases at both phosphate

sides. Notwithstanding, kinetic data on dinucleotides indicated a reduced efficiency performance for this novel active site. Indeed, the percentage of remnant catalytic activity displayed by the RNase 6-H15A mutant is similar to the activity displayed by a previously engineered RNase A construct with an additional active site created at the p_2 phosphate-binding site position (RNase A-H7H10 variant) [49]. Likewise, a similar scenario might be envisaged for RNase 6 (see Supplementary Table S6 for comparison of estimated pK_a values for both RNase A His⁷/His¹⁰ and RNase 6 His³⁶/His³⁹ pairs). The calculated pK_a values for the corresponding histidine residues exposed at the protein surface indicated that neither of them underwent a significant decrease from the reference value that could provide an efficient base catalyst. Therefore, the predicted pK_a for His³⁶ and His³⁹ could not reproduce properly the efficient RNase A catalytic site [18,48]. And last, but not least, the presence of a third residue that could stabilize the transition state intermediate is not obvious. Interestingly, we find a neighbouring lysine residue (Lys⁸⁷) at the novel site environment that could meet the required RNase active site geometry (see Figure 3 for a schematic illustration). Unfortunately, the Lys⁸⁷ side chain is disordered in the present RNase 6 crystal structure, providing no information on its proper orientation. However, the Lys⁸⁷ side-chain conformation predicted by MD in the RNase 6–heptanucleotide complex did provide interactions with a phosphate located at the p_{-3} site (Supplementary Table S5). Noteworthy, Lys⁸⁷ is found in all primate RNase 6 counterparts, but is absent from the murine sequence [9,15]. Interestingly, even if the RNase A mutant at Lys⁴¹ was shown to drastically reduce the enzyme catalytic efficiency [70], the insertion of a secondary catalytic site for RNase A at the p_2 location conformed by only a histidine dyad was also able to provide approximately 10–15 % of remnant activity in the absence of the main active site [49]. Likewise, the proposed novel RNase 6 secondary site would behave as a poor catalyst. In any case, the present kinetic data indicate that the presence of an anchoring site at the 36–39 region enhances significantly the enzyme catalysis of polymeric substrates. Interestingly, Sorrentino and co-workers' analysis of the enzymatic properties of RNase A family members suggested that the presence of a cationic cluster at that region, combined with an anionic residue at RNase A residue at the 83 position (Asp⁸⁰ in RNase 6), correlated to the facility to destabilize dsRNA, exposing single-stranded stretches to the enzyme for cleavage [65,71,72]. Interestingly, RNase 6 shows a particular overabundance of histidine residues at its polypeptide sequence, in comparison with the other family homologues. As previously mentioned, most of these histidine residues are unique to the RNase 6 lineage (Figure 1B) [9,15]. In particular, we observed two cationic clusters (His³⁶/His³⁹) and (Arg⁶⁶/His⁶⁷) fully conserved among the more evolved primate members. To note, whereas His³⁶ and His⁶⁷ are found in all known primate primary structures, His³⁹ and Arg⁶⁶ are only present in the more evolved primates. Overall, evolutionary pressure would have drifted RNase 6 towards a slightly more cationic primary structure with an overabundance of histidine residues, providing a novel secondary active site. Future research should explore the ultimate implications in the protein's physiological function.

Conclusions

The RNase 6 first crystal structure has provided us the opportunity to explore its structure–function relationship. By combining structural analysis together with molecular modelling and kinetic characterization, we were able to spot key regions contributing to the enzyme's substrate specificity and catalytic properties.

Results highlighted the RNase 6 multisubsite arrangement for substrate binding and the contribution of a secondary catalytic site that facilitates the cleavage of polynucleotide substrates. Further work is needed to fully characterize RNase 6's enzymatic properties towards the understanding of its specific mechanism of action.

AUTHOR CONTRIBUTION

Ester Boix and Mohammed Moussaoui conceived and designed the experimental work. Guillem Prats-Ejarque, Javier Arranz-Trullen, Jose Blanco, Mohammed Moussaoui and David Pulido performed the experiments. Guillem Prats-Ejarque, Mohammed Moussaoui, David Pulido, Victòria Nogués and Ester Boix analysed the data. Guillem Prats-Ejarque, Javier Arranz-Trullen and Ester Boix drafted the paper. Victòria Nogués, Mohammed Moussaoui, Guillem Prats-Ejarque and Ester Boix revised the final paper.

ACKNOWLEDGEMENTS

We thank all of the staff at the beamline BL13 (XALOC) at the ALBA Synchrotron Light Facility (Cerdanyola del Vallès, Spain) for their support during data collection. Heartfelt thanks go to Jordi Joanhuix and Fernando Gil for all of the help provided.

FUNDING

This work was supported by the Ministerio de Economía y Competitividad cofinanced by FEDER funds [grant numbers BFU2012-38695 and BES-2010-036238 (predoctoral fellowship to J.A.B.)]; the Generalitat de Catalunya [grant number 2014-SGR-728]; and the Universitat Autònoma de Barcelona [grant number 406-02-02/2013 (predoctoral fellowship to J.A.)].

REFERENCES

- Boix, E. and Nogués, M.V. (2007) Mammalian antimicrobial proteins and peptides: overview on the RNase A superfamily members involved in innate host defence. *Mol. Biosyst.* **3**, 317–335 [CrossRef](#) [PubMed](#)
- Rosenberg, H.F. (2008) RNase A ribonucleases and host defense: an evolving story. *J. Leukoc. Biol.* **83**, 1079–1087 [CrossRef](#) [PubMed](#)
- Gupta, S.K., Haigh, B.J., Griffin, F.J. and Wheeler, T.T. (2012) The mammalian secreted RNases: mechanisms of action in host defence. *Innate Immun.* **19**, 86–97 [CrossRef](#) [PubMed](#)
- Zhang, J. and Rosenberg, H.F. (2002) Complementary advantageous substitutions in the evolution of an antiviral RNase of higher primates. *Proc. Natl. Acad. Sci. U.S.A.* **99**, 5486–5491 [CrossRef](#) [PubMed](#)
- Pizzo, E. and D'Alessio, G. (2007) The success of the RNase scaffold in the advance of biosciences and in evolution. *Gene* **406**, 8–12 [CrossRef](#) [PubMed](#)
- Hamann, K.J., Ten, R.M., Loegering, D.A., Jenkins, R.B., Heise, M.T., Schad, C.R., Pease, L.R., Gleich, G.J. and Barker, R.L. (1990) Structure and chromosome localization of the human eosinophil-derived neurotoxin and eosinophil cationic protein genes: evidence for intronless coding sequences in the ribonuclease gene superfamily. *Genomics* **7**, 535–546 [CrossRef](#) [PubMed](#)
- Zhang, J., Dyer, K.D. and Rosenberg, H.F. (2002) RNase 8, a novel RNase A superfamily ribonuclease expressed uniquely in placenta. *Nucleic Acids Res.* **30**, 1169–1175 [CrossRef](#) [PubMed](#)
- Rosenberg, H.F. and Dyer, K.D. (1996) Molecular cloning and characterization of a novel human ribonuclease (RNase k6): increasing diversity in the enlarging ribonuclease gene family. *Nucleic Acids Res.* **24**, 3507–3513 [CrossRef](#) [PubMed](#)
- Deming, M.S., Dyer, K.D., Bankier, A.T., Piper, M.B., Dear, P.H. and Rosenberg, H.F. (1998) Ribonuclease k6: chromosomal mapping and divergent rates of evolution within the RNase A gene superfamily. *Genome Res.* **8**, 599–607 [PubMed](#)
- Becknell, B., Eichler, T.E., Beceiro, S., Li, B., Easterling, R.S., Carpenter, A.R., James, C.L., McHugh, K.M., Hains, D.S., Partida-Sanchez, S. and Spencer, J.D. (2015) Ribonucleases 6 and 7 have antimicrobial function in the human and murine urinary tract. *Kidney Int.* **87**, 151–161 [CrossRef](#) [PubMed](#)
- Spencer, J.D., Schwaderer, A.L., Wang, H., Bartz, J., Kline, J., Eichler, T., DeSouza, K.R., Sims-Lucas, S., Baker, P. and Hains, D.S. (2013) Ribonuclease 7, an antimicrobial peptide upregulated during infection, contributes to microbial defense of the human urinary tract. *Kidney Int.* **83**, 615–625 [CrossRef](#) [PubMed](#)

- 12 Jellic, K., Cimbri, R., Nawaz, F., Huang, D.W., Zheng, X., Yang, J., Lempicki, R.A., Pascuccio, M., Van Ryk, D., Schwing, C. et al. (2013) The HIV-1 envelope protein gp120 impairs B cell proliferation by inducing TGF- β 1 production and FCRL4 expression. *Nat. Immunol.* **14**, 1256–1265 [CrossRef](#) [PubMed](#)
- 13 Zhang, J., Dyer, K.D. and Rosenberg, H.F. (2000) Evolution of the rodent eosinophil-associated RNase gene family by rapid gene sorting and positive selection. *Proc. Natl. Acad. Sci. U.S.A.* **97**, 4701–4706 [CrossRef](#) [PubMed](#)
- 14 McDevitt, A.L., Deming, M.S., Rosenberg, H.F. and Dyer, K.D. (2001) Gene structure and enzymatic activity of mouse eosinophil-associated ribonuclease 2. *Gene* **267**, 23–30 [CrossRef](#) [PubMed](#)
- 15 Dyer, K.D., Rosenberg, H.F. and Zhang, J. (2004) Isolation, characterization, and evolutionary divergence of mouse RNase 6: evidence for unusual evolution in rodents. *J. Mol. Evol.* **59**, 657–665 [CrossRef](#) [PubMed](#)
- 16 Richards, F.M. and Wyckoff, H.W. (1971) Bovine pancreatic ribonuclease. *Enzymes IV* 647–806 [CrossRef](#)
- 17 Raines, R.T. (1998) Ribonuclease A. *Chem. Rev.* **98**, 1045–1065 [CrossRef](#) [PubMed](#)
- 18 Cuchillo, C.M., Nogués, M.V. and Raines, R.T. (2011) Bovine pancreatic ribonuclease: fifty years of the first enzymatic reaction mechanism. *Biochemistry* **50**, 7835–7841 [CrossRef](#) [PubMed](#)
- 19 Nogués, M.V., Moussaoui, M., Boix, E., Vilanova, M., Ribó, M. and Cuchillo, C.M. (1998) The contribution of noncatalytic phosphate-binding subsites to the mechanism of bovine pancreatic ribonuclease A. *Cell. Mol. Life Sci.* **54**, 766–774 [CrossRef](#) [PubMed](#)
- 20 Boix, E., Nikolovski, Z., Moiseyev, G., Rosenberg, H.F., Cuchillo, C.M. and Nogués, M.V. (1999) Kinetic and product distribution analysis of human eosinophil cationic protein indicates a subsite arrangement that favors exonuclease-type activity. *J. Biol. Chem.* **274**, 15605–15614 [CrossRef](#) [PubMed](#)
- 21 Rosenberg, H.F. (1995) Recombinant human eosinophil cationic protein. Ribonuclease activity is not essential for cytotoxicity. *J. Biol. Chem.* **270**, 7876–7881 [CrossRef](#) [PubMed](#)
- 22 Harder, J. and Schroder, J.-M. (2002) RNase 7, a novel innate immune defense antimicrobial protein of healthy human skin. *J. Biol. Chem.* **277**, 46779–46784 [CrossRef](#) [PubMed](#)
- 23 Boix, E., Salazar, V.A., Torrent, M., Pulido, D., Nogués, M.V. and Moussaoui, M. (2012) Structural determinants of the eosinophil cationic protein antimicrobial activity. *Biol. Chem.* **393**, 801–815 [CrossRef](#) [PubMed](#)
- 24 Torrent, M., Sanchez, D., Buzon, V., Nogués, M.V., Cladera, J. and Boix, E. (2009) Comparison of the membrane interaction mechanism of two antimicrobial RNases: RNase 3/ECP and RNase 7. *Biochim. Biophys. Acta* **1788**, 1116–1125 [CrossRef](#) [PubMed](#)
- 25 Libonati, M. and Sorrentino, S. (2001) Degradation of double-stranded RNA by mammalian pancreatic-type ribonucleases. *Methods Enzymol.* **341**, 234–248 [CrossRef](#) [PubMed](#)
- 26 Bravo, J., Fernández, E., Ribó, M., Dellorens, R. and Cuchillo, C.M. (1994) A versatile negative-staining ribonuclease zymogram. *Anal. Biochem.* **219**, 82–86 [CrossRef](#) [PubMed](#)
- 27 Moussaoui, M., Guasch, A., Boix, E., Cuchillo, C.M. and Nogués, M.V. (1996) The role of non-catalytic binding subsites in the endonuclease activity of bovine pancreatic ribonuclease A. *J. Biol. Chem.* **271**, 4687–4692 [CrossRef](#) [PubMed](#)
- 28 Nogués, M.V. and Cuchillo, C.M. (2001) Analysis by HPLC of distributive activities and the synthetic (back) reaction of pancreatic-type ribonucleases. *Methods Mol. Biol.* **160**, 15–24 [PubMed](#)
- 29 Cuchillo, C.M., Moussaoui, M., Barman, T., Travers, F. and Nogués, M.V. (2002) The exo- or endonucleolytic preference of bovine pancreatic ribonuclease A depends on its subsites structure and on the substrate size. *Protein Sci.* **11**, 117–128 [CrossRef](#) [PubMed](#)
- 30 Kabsch, W. (2010) XDS. *Acta Crystallogr. D Biol. Crystallogr.* **66**, 125–132 [CrossRef](#) [PubMed](#)
- 31 Huang, Y.C., Lin, Y.M., Chang, T.W., Wu, S.H., Lee, Y.S., Chang, M.D., Chen, C., Wu, S.J. and Liao, Y.D. (2007) The flexible and clustered lysine residues of human ribonuclease 7 are critical for membrane permeability and antimicrobial activity. *J. Biol. Chem.* **282**, 4626–4633 [CrossRef](#) [PubMed](#)
- 32 Adams, P.D., Afonine, P.V., Bunkoczi, G., Chen, V.B., Davis, I.W., Echols, N., Headd, J.J., Hung, L.-W., Kapral, G.J., Grosse-Kunstleve, R.W. et al. (2010) PHENIX: a comprehensive Python-based system for macromolecular structure solution. *Acta Crystallogr. D Biol. Crystallogr.* **66**, 213–221 [CrossRef](#) [PubMed](#)
- 33 Emsley, P. and Cowtan, K. (2004) Coot: model-building tools for molecular graphics. *Acta Crystallogr. D Biol. Crystallogr.* **60**, 2126–2132 [CrossRef](#) [PubMed](#)
- 34 Vaguine, A.A., Richelle, J. and Wodak, S.J. (1999) SFCHECK: a unified set of procedures for evaluating the quality of macromolecular structure-factor data and their agreement with the atomic model. *Acta Crystallogr. D Biol. Crystallogr.* **55**, 191–205 [CrossRef](#) [PubMed](#)
- 35 Hoof, R.W., Vriend, G., Sander, C. and Abola, E.E. (1996) Errors in protein structures. *Nature* **23**, 381
- 36 Pronk, S., Páll, S., Schulz, R., Larsson, P., Bjelkmar, P., Apostolov, R., Shirts, M.R., Smith, J.C., Kasson, P.M., Van Der Spoel, D. et al. (2013) GROMACS 4.5: a high-throughput and highly parallel open source molecular simulation toolkit. *Bioinformatics* **29**, 845–854 [CrossRef](#) [PubMed](#)
- 37 Zegers, I., Maes, D., Poortmans, F., Palmer, R. and Wyns, L. (1994) The structures of RNase A complexed with 3' -CMP and d(CpA): active site conformation and conserved water molecules. *Protein Sci.* **3**, 2322–2339 [CrossRef](#) [PubMed](#)
- 38 Lindorff-Larsen, K., Piana, S., Palmo, K., Maragakis, P., Klepeis, J.L., Dror, R.O. and Shaw, D.E. (2010) Improved side-chain torsion potentials for the Amber ff99SB protein force field. *Proteins* **78**, 1950–1958 [PubMed](#)
- 39 Jorgensen, W.L., Chandrasekhar, J., Madura, J.D., Impey, R.W. and Klein, M.L. (1983) Comparison of simple potential functions for simulating liquid water. *J. Chem. Phys.* **79**, 926 [CrossRef](#)
- 40 Darden, T., York, D. and Pedersen, L. (1993) Particle mesh Ewald: an N-log(N) method for Ewald sums in large systems. *J. Chem. Phys.* **98**, 10089 [CrossRef](#)
- 41 Essmann, U., Perera, L., Berkowitz, M.L., Darden, T., Lee, H. and Pedersen, L.G. (1995) A smooth particle mesh Ewald method. *J. Chem. Phys.* **103**, 8577 [CrossRef](#)
- 42 Hess, B. (2008) P-LINCS: a parallel linear constraint solver for molecular simulation. *J. Chem. Theory Comput.* **4**, 116–122 [CrossRef](#) [PubMed](#)
- 43 Parrinello, M. and Rahman, A. (1981) Polymorphic transitions in single crystals: a new molecular dynamics method. *J. Appl. Phys.* **52**, 7182–7190 [CrossRef](#)
- 44 Nosé, S. and Klein, M.L. (1983) Constant pressure molecular dynamics for molecular systems. *Mol. Phys.* **50**, 1055–1076 [CrossRef](#)
- 45 Fontecilla-Camps, J.C., de Llorens, R., le Du, M.H. and Cuchillo, C.M. (1994) Crystal structure of ribonuclease A.d(ApTpApApG) complex. Direct evidence for extended substrate recognition. *J. Biol. Chem.* **269**, 21526–21531 [PubMed](#)
- 46 Morris, G.M., Huey, R., Lindstrom, W., Sanner, M.F., Belew, R.K., Goodsell, D.S. and Olson, A.J. (2009) AutoDock4 and AutoDockTools4: automated docking with selective receptor flexibility. *J. Comput. Chem.* **30**, 2785–2791 [CrossRef](#) [PubMed](#)
- 47 Kilambi, K.P. and Gray, J.J. (2012) Rapid calculation of protein pKa values using Rosetta. *Biophys. J.* **103**, 587–595 [CrossRef](#) [PubMed](#)
- 48 Fisher, B.M., Schultz, L.W. and Raines, R.T. (1998) Coulombic effects of remote subsites on the active site of ribonuclease A. *Biochemistry* **37**, 17386–17401 [CrossRef](#) [PubMed](#)
- 49 Moussaoui, M., Cuchillo, C.M. and Nogués, M.V. (2007) A phosphate-binding subsite in bovine pancreatic ribonuclease A can be converted into a very efficient catalytic site. *Protein Sci.* **16**, 99–109 [CrossRef](#) [PubMed](#)
- 50 Krissinel, E. and Henrick, K. (2007) Inference of macromolecular assemblies from crystalline state. *J. Mol. Biol.* **372**, 774–797 [CrossRef](#) [PubMed](#)
- 51 Rico, M., Gallego, E., Santoro, J., Bermejo, F.J., Nieto, J.L. and Herranz, J. (1984) On the fundamental role of the Glu 2- ... Arg 10 + salt bridge in the folding of isolated ribonuclease A S-peptide. *Biochem. Biophys. Res. Commun.* **123**, 757–763 [CrossRef](#) [PubMed](#)
- 52 Chatani, E. and Hayashi, R. (2001) Functional and structural roles of constituent amino acid residues of bovine pancreatic ribonuclease A. *J. Biosci. Bioeng.* **92**, 98–107 [CrossRef](#) [PubMed](#)
- 53 Berisio, R., Sica, F., Lamzin, V.S., Wilson, K.S., Zagari, A. and Mazzarella, L. (2002) Atomic resolution structures of ribonuclease A at six pH values. *Acta Crystallogr. D Biol. Crystallogr.* **58**, 441–450 [CrossRef](#) [PubMed](#)
- 54 Fedorov, A.A., Joseph-McCarthy, D., Fedorov, E., Sirakova, D., Graf, I. and Almo, S.C. (1996) Ionic interactions in crystalline bovine pancreatic ribonuclease A. *Biochemistry* **35**, 15962–15979 [CrossRef](#) [PubMed](#)
- 55 Leonidas, D.D., Boix, E., Prill, R., Suzuki, M., Turton, R., Minson, K., Swaminathan, G.J., Youle, R.J. and Acharya, K.R. (2001) Mapping the ribonucleolytic active site of eosinophil-derived neurotoxin (EDN): high resolution crystal structures of EDN complexes with adenylic nucleotide inhibitors. *J. Biol. Chem.* **276**, 15009–15017 [CrossRef](#) [PubMed](#)
- 56 Boix, E., Pulido, D., Moussaoui, M., Nogués, M.V. and Russi, S. (2012) The sulfate-binding site structure of the human eosinophil cationic protein as revealed by a new crystal form. *J. Struct. Biol.* **179**, 1–9 [CrossRef](#) [PubMed](#)
- 57 Holloway, D.E., Chavali, G.B., Hares, M.C., Subramanian, V. and Acharya, K.R. (2005) Structure of murine angiogenin: features of the substrate- and cell-binding regions and prospects for inhibitor-binding studies. *Acta Crystallogr. D Biol. Crystallogr.* **61**, 1568–1578 [CrossRef](#) [PubMed](#)
- 58 Borkakoti, N. (1983) The active site of ribonuclease A from the crystallographic studies of ribonuclease-A-inhibitor complexes. *Eur. J. Biochem.* **132**, 89–94 [CrossRef](#) [PubMed](#)
- 59 Berisio, R., Lamzin, V.S., Sica, F., Wilson, K.S., Zagari, A. and Mazzarella, L. (1999) Protein titration in the crystal state. *J. Mol. Biol.* **292**, 845–854 [CrossRef](#) [PubMed](#)
- 60 deMel, V.S., Martin, P.D., Doscher, M.S. and Edwards, B.F. (1992) Structural changes that accompany the reduced catalytic efficiency of two semisynthetic ribonuclease analogs. *J. Biol. Chem.* **267**, 247–256 [PubMed](#)
- 61 Schultz, L.W., Quirk, D.J. and Raines, R.T. (1998) His...Asp catalytic dyad of ribonuclease A: structure and function of the wild-type, D121N, and D121A enzymes. *Biochemistry* **37**, 8886–8898 [CrossRef](#) [PubMed](#)
- 62 Hofsteenge, J., Vicentini, A. and Zelenko, O. (1998) Ribonuclease 4, an evolutionarily highly conserved member of the superfamily. *Cell. Mol. Life Sci.* **54**, 804–810 [CrossRef](#) [PubMed](#)

- 63 Vicentini, A.M., Kote-Jarai, Z. and Hofsteenge, J. (1996) Structural determinants of the uridine-preferring specificity of RNase PL3. *Biochemistry* **35**, 9128–9132 [CrossRef PubMed](#)
- 64 Terzyan, S.S., Peracaula, R., de Llorens, R., Tsushima, Y., Yamada, H., Seno, M., Gomis-Ruth, F.X. and Coll, M. (1999) The three-dimensional structure of human RNase 4, unliganded and complexed with d(Up), reveals the basis for its uridine selectivity. *J. Mol. Biol.* **285**, 205–214 [CrossRef PubMed](#)
- 65 Sorrentino, S. (1998) Human extracellular ribonucleases: multiplicity, molecular diversity and catalytic properties of the major RNase types. *Cell. Mol. Life Sci.* **54**, 785–794 [CrossRef PubMed](#)
- 66 Sorrentino, S. (2010) The eight human "canonical" ribonucleases: molecular diversity, catalytic properties, and special biological actions of the enzyme proteins. *FEBS Lett.* **584**, 2194–2200 [CrossRef PubMed](#)
- 67 Boix, E., Blanco, J.A., Nogués, M.V. and Moussaoui, M. (2013) Nucleotide binding architecture for secreted cytotoxic endoribonucleases. *Biochimie* **95**, 1087–1097 [CrossRef PubMed](#)
- 68 Vitagliano, L., Merlino, A., Zagari, A. and Mazzarella, L. (2000) Productive and nonproductive binding to ribonuclease A: X-ray structure of two complexes with uridylyl(2',5')guanosine. *Protein Sci.* **9**, 1217–1225 [CrossRef PubMed](#)
- 69 Park, C., Schultz, L.W. and Raines, R.T. (2001) Contribution of the active site histidine residues of ribonuclease A to nucleic acid binding. *Biochemistry* **40**, 4949–4956 [CrossRef PubMed](#)
- 70 Trautwein, K., Holliger, P., Stackhouse, J. and Benner, S.A. (1991) Site-directed mutagenesis of bovine pancreatic ribonuclease: lysine-41 and aspartate-121. *FEBS Lett.* **281**, 275–277 [CrossRef PubMed](#)
- 71 Libonati, M. and Sorrentino, S. (1992) Revisiting the action of bovine ribonuclease A and pancreatic-type ribonucleases on double-stranded RNA. *Mol. Cell. Biochem.* **117**, 139–151 [CrossRef PubMed](#)
- 72 Yakovlev, G., Moiseyev, G.P., Sorrentino, S., De Prisco, R. and Libonati, M. (1997) Single-strand-preferring RNases degrade double-stranded RNAs by destabilizing its secondary structure. *J. Biomol. Struct. Dyn.* **15**, 243–250 [CrossRef PubMed](#)
- 73 Shapiro, R., Fett, J.W., Strydom, D.J. and Vallee, B.L. (1986) Isolation and characterization of a human colon carcinoma-secreted enzyme with pancreatic ribonuclease-like activity. *Biochemistry* **25**, 7255–7264 [CrossRef PubMed](#)
- 74 Follmann, H., Wieker, H.J. and Witzel, H. (1967) On the mechanism of the ribonuclease reaction. 2. The pre-ordering in the substrate as the accelerating factor in dinucleoside phosphates and analogous compounds. *Eur. J. Biochem.* **1**, 243–250 [CrossRef PubMed](#)
- 75 Boix, E., Nogués, M.V., Schein, C.H., Benner, S.A. and Cuchillo, C.M. (1994) Reverse transphosphorylation by ribonuclease A needs an intact p2-binding site. *J. Biol. Chem.* **269**, 2529–2534 [PubMed](#)
- 76 Sorrentino, S. and Glitz, D.G. (1991) Ribonuclease activity and substrate preference of human eosinophil cationic protein (ECP). *FEBS Lett.* **288**, 23–26 [CrossRef PubMed](#)
- 77 Pettersen, E.F., Goddard, T.D., Huang, C.C., Couch, G.S., Greenblatt, D.M., Meng, E.C. and Ferrin, T.E. (2004) UCSF Chimera – a visualization system for exploratory research and analysis. *J. Comput. Chem.* **25**, 1605–1612 [CrossRef PubMed](#)

Received 4 January 2016/23 March 2016; accepted 24 March 2016
Accepted Manuscript online 24 March 2016, doi:10.1042/BCJ20160245

PAPER III

ORIGINAL RESEARCH

Exploring the mechanisms of action of human secretory RNase 3 and RNase 7 against *Candida albicans*

Vivian A. Salazar¹, Javier Arranz-Trullén¹, Susanna Navarro^{1,2}, Jose A. Blanco¹, Daniel Sánchez¹, Mohammed Moussaoui¹ & Ester Boix¹

¹Department of Biochemistry and Molecular Biology, Faculty of Biosciences, Universitat Autònoma de Barcelona, Cerdanyola del Vallès E-08193, Spain

²Institut de Biotecnologia i Biomedicina, Universitat Autònoma de Barcelona, Cerdanyola del Vallès E-08193, Spain

Keywords

Cytotoxicity, host–pathogen interactions, infectious diseases, innate immunity.

Correspondence

Ester Boix, Department of Biochemistry and Molecular Biology, Biosciences Faculty, Universitat Autònoma de Barcelona, Cerdanyola del Vallès 08193, Spain. Tel: +34-93-5814147; Fax: +34-93-5811264; E-mail: ester.boix@uab.cat

Funding Information

Ministerio de Economía y Competitividad and Feder funds (Grant BFU2012-38965) Generalitat de Catalunya Universitat Autònoma de Barcelona

Received: 29 February 2016; Revised: 30 March 2016; Accepted: 4 April 2016

doi: 10.1002/mbo3.373

The three-dimensional crystal structures of RNase 3-H15A was submitted to the Protein Data Bank (PD ID code: 4OWZ).

Introduction

Fungal infections are a threat to hospitalized and immunocompromised patients. *Candida albicans* is a major common fungal pathogen in humans that colonizes the skin and the mucosal surfaces of most healthy individuals. Together with superficial infections, such as oral or vaginal candidiasis, a life-threatening systemic infection can eventually occur (Mayer et al. 2013). *Candida albicans* is the causative agent of most candidiasis, but other emerging species, such as *Candida glabrata* and *Candida krusei*, are also considered to be threats to patient populations. *Candida* infections have increased dramatically over the

Abstract

Human antimicrobial RNases, which belong to the vertebrate RNase A superfamily and are secreted upon infection, display a wide spectrum of antipathogen activities. In this work, we examined the antifungal activity of the eosinophil RNase 3 and the skin-derived RNase 7, two proteins expressed by innate cell types that are directly involved in the host defense against fungal infection. *Candida albicans* has been selected as a suitable working model for testing RNase activities toward a eukaryotic pathogen. We explored the distinct levels of action of both RNases on yeast by combining cell viability and membrane model assays together with protein labeling and confocal microscopy. Site-directed mutagenesis was applied to ablate either the protein active site or the key anchoring region for cell binding. This is the first integrated study that highlights the RNases' dual mechanism of action. Along with an overall membrane-destabilization process, the RNases could internalize and target cellular RNA. The data support the contribution of the enzymatic activity for the antipathogen action of both antimicrobial proteins, which can be envisaged as suitable templates for the development of novel antifungal drugs. We suggest that both human RNases work as multitasking antimicrobial proteins that provide a first line immune barrier.

last two decades. Considering the increase in *Candida* pathogenesis, mostly in immunocompromised patients, but also in healthy individuals, active research has focused on new therapies and treatments. Several factors and activities that contribute to the pathogenic potential of this fungus have been identified. As a first consideration, *Candida albicans* displays a complex cell wall organization that plays a role in maintaining structural integrity and mediating adherence. Its specific composition, which is predominantly composed of carbohydrates (Chitin, β -1,3 glucan, and β -1,6 glucan), offers resistance to host molecular defense and is impermeable to most potential antifungal drugs (Molero et al. 1998; Mayer et al. 2013).

Knowledge of pathogenicity mechanisms, ranging from cell wall complexity to the adhesion and host cell invasion mechanism (Chaffin 2008), is crucial for the rational design of novel antifungal drugs (Molero et al. 1998; Mayer et al. 2013). Antimicrobial peptides (AMPs) and in particular, those secreted by the human skin, our first natural barrier against infections, are regarded as appealing candidates for applied antifungal therapy (den Hertog et al. 2005; Vylkova et al. 2007; Andrès 2012). Indeed, AMPs offer a chemical defense system that protects the skin from potential pathogenic microorganisms threatening to colonize host tissues (Harder and Schroder 2002; Bardan et al. 2004; Gläser et al. 2005). Among skin AMPs, there are peptides with reported antifungal activity, such as cathelicidins (López-García et al. 2005) and defensins (De Smet and Contreras 2005). Both peptides are rapidly released at high local concentrations when needed in response to infection or epidermal injury (Dorschner et al. 2001; Niyonsaba and Ogawa 2005; Sørensen et al. 2006). Moreover, the constant level of some constitutively produced antimicrobial peptides and proteins at skin surfaces suggests that these AMPs have been optimized during evolution to protect the skin surface from infection (Schröder and Harder 2006). In particular, human RNase 7 is one of the main products that is constitutively released by keratinocytes (Schröder and Harder 2006). RNase 7 not only has a well-documented bactericidal activity (Harder and Schroder 2002; Torrent et al. 2010a; Pulido et al. 2013b) but also inhibits the growth of yeast (Harder and Schroder 2002; Huang et al. 2007) and dermatophytes (Fritz et al. 2012).

Interestingly, RNase 7 is a member of the RNase A superfamily (Fig. 1). This family, which includes other secretory RNases with antimicrobial properties (Boix and Nogués 2007), is a protein family that is suggested to have emerged with an ancestral host defense role (Pizzo and D'Alessio 2007; Rosenberg 2008). Antimicrobial RNases are expressed by epithelial tissues and blood cell types, and their expression can be induced by inflammatory agents and bacterial infection (Gupta et al. 2012; Spencer et al. 2013; Amatngalim et al. 2015; Becknell et al. 2015). In particular, RNase 3 and RNase 7 are the main representative members that show a high bactericidal activity (Torrent et al. 2010a, 2012; Pulido et al. 2013b). RNase 7 is expressed in the skin-derived stratum, the gut, and the respiratory and genitourinary tracts (Spencer et al. 2013; Becknell et al. 2015) and is particularly active against both gram-negative and gram-positive species, such as *Enterococcus faecium*, *Pseudomonas aeruginosa*, and *Escherichia coli* (Harder and Schroder 2002; Huang et al. 2007; Torrent et al. 2010a).

On its turn, RNase 3, another of the main antimicrobial RNases within the RNase A superfamily (Fig. 1), also called the Eosinophil Cationic Protein (ECP), is involved

in inflammatory processes mediated by eosinophils and is released by the secondary granules upon infection (Acharya and Ackerman 2014). RNase 3 has also been reported to display high antimicrobial activity against both gram-negative bacteria, such as *E. coli*, *Acinetobacter baumannii*, and *Pseudomonas sp.* (Torrent et al. 2011b), and gram-positive species, such as *Staphylococcus aureus*, *Micrococcus luteus*, and *E. faecium*, (Torrent et al. 2011b) as well as *Mycobacteria* (Pulido et al. 2013b).

In this work, we explored the antifungal properties of both RNase 3 and 7. We used *C. albicans* as a eukaryotic pathogen model, which has proven to be an appropriate first approach to understand the distinct levels of action of antimicrobial RNases.

Experimental Procedures

Protein expression and purification

Recombinant RNase 3 and RNase 7 were expressed in *E. coli* BL21 (DE3) using the pET11c plasmid vector as previously described (Torrent et al. 2009). Protein expression, solubilization from inclusion bodies, refolding, and purification steps were carried out as described (Boix et al. 1999). RNase 3-H15A, RNase 3-W35A, and RNase 7-H15A variants were constructed using the Quick Change Site-Directed Mutagenesis kit (Stratagene, La Jolla, CA). All constructs were confirmed by DNA sequencing and the purified protein was analyzed by MALDI-TOF MS and N-terminal sequencing.

Crystal structure determination

Recombinant protein was purified by cation exchange and reverse phase chromatographies as previously described (Boix et al. 2012a). RNase 3-H15A mutant was crystallized following the conditions for wild-type RNase 3 modified from (Mallorquí-Fernández et al. 2000). Protein sample was lyophilized and resuspended at 12 mg/mL in 20 mmol/L sodium cacodylate pH 5.0 and equilibrated against 7% Jeffamine™ M-600, 0.1 mol/L Na citrate, pH 5.2, 10 mmol/L FeCl₃. One microliter of the sample was mixed with an equal volume of the reservoir solution and set to incubation at 20°C. After 5 to 10 days, crystals appeared and were soaked using 30% methyl pentanediol as cryofreezing agent. Data were captured at 100 K using a $\lambda_{\text{XRD}} = 0.9795 \text{ \AA}$ at the BL13 beamline of the ALBA Synchrotron Light Facility (Spain). XDS (Kabsch, 2010) was used for data processing. Scaling was performed with SCALA and molecular replacement with PHASER (McCoy et al., 2007) using as a model the RNase 7 NMR structure (PDB coordinate file 2HKY (Huang et al. 2007)). Iterative cycles of refinement and manual structure fitting were performed with PHENIX

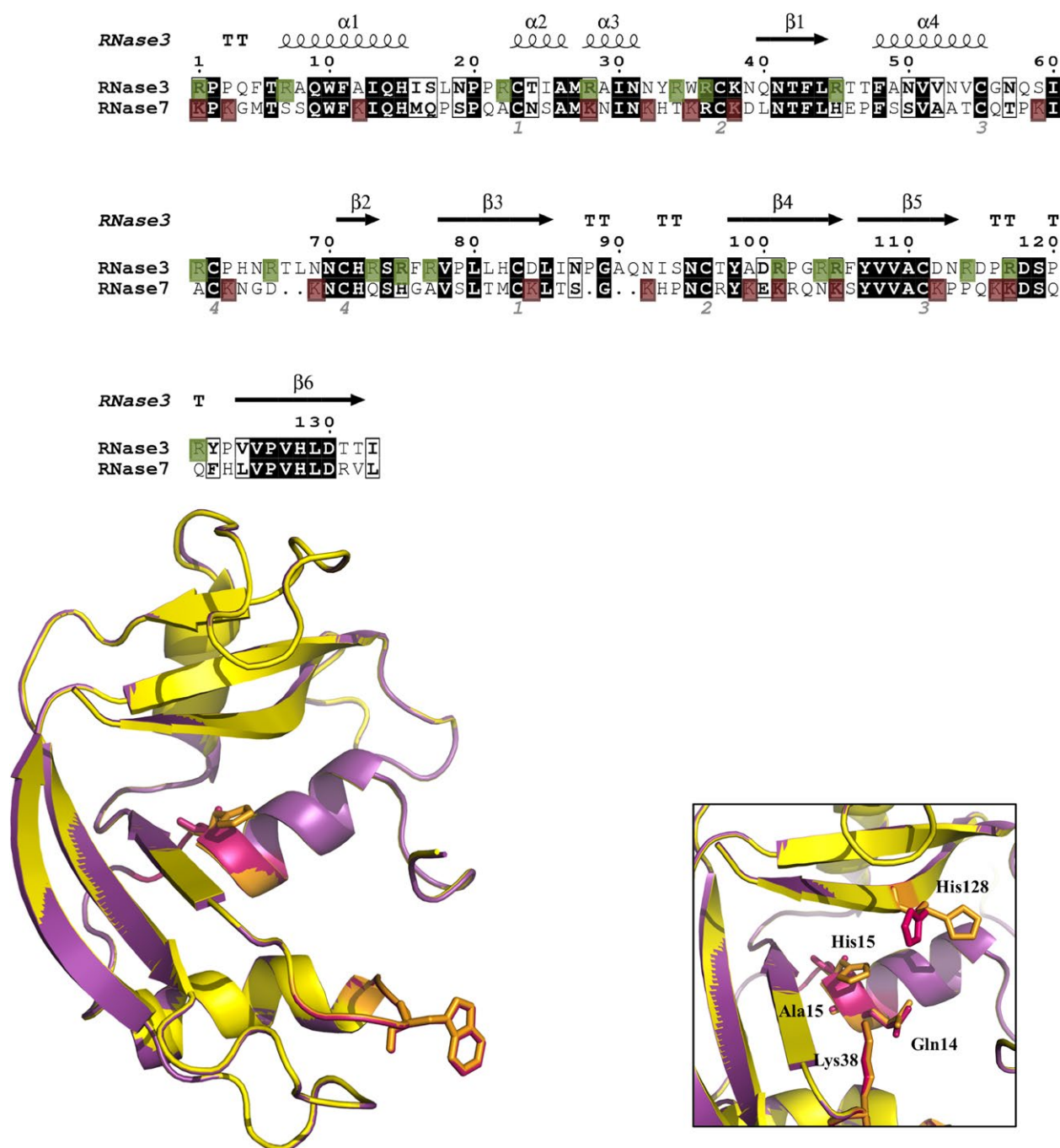


Figure 1. (A) Sequence alignment of RNase 3 and RNase 7. Primary sequences (UniProt codes: P12724 and Q9H1E1) were used, respectively. RNase 3 three-dimensional structure is indicated (PDB ID: 4OXF). Cationic residues are shown in both proteins in green and fuchsia boxes, respectively. The alignment was performed using the ESPript program (<http://esript.ibcp.fr/EsPript/>). (B) Three dimensional representation of crystal structures of wild-type RNase 3 (yellow; PDB ID: 4OXF) and active site mutant RNase 3-H15A (purple; PDB ID: 4OWZ). Mutated residues (His 15 and Trp 35) are depicted in baton sticks. (C) Detail of active centre in both proteins. Picture was drawn with *PyMOL* Molecular Graphics System (Schrödinger, LLC).

(Adams et al., 2010) and COOT (Emsley and Cowtan, 2004) until R_{free} could not be further improved (Brunger, 1992). Finally, the stereochemistry of the structure was validated with SFCHECK (Vaguine et al., 1999). Table S1

shows all the data collection and structure refinement statistics. Solvent accessible surface areas for protein residues were calculated using the *Areaimol* software (The CCP4 suite: programs for protein crystallography, 1994).

Enzymatic activity analysis

The RNases enzymatic activities of RNase 3, RNase 7, and active site mutants were measured spectrophotometrically by registering the degradation of the oligocytidylic acid (Cp)₄C>p at 286 nm in a Cary Eclipse spectrophotometer. The (Cp)₄C>p acid, purified from poly(C), was used as a substrate, as previously described (Boix et al. 1999). Assay conditions were 1 μmol/L protein, 84 μmol/L oligocytidylic acid in 0.2 mol/L NaAcO, pH 5.0, 3 min incubation time, and 25°C. Alternatively, a zymogram analysis was performed using a 15% SDS-PAGE gel containing polyuridylic acid, poly(U), as a substrate according to the method previously described (Bravo et al. 1994).

Model membrane leakage activity

Membrane leakage activity was assessed by ANTS/DPX (8-aminonaphthalene-1,3,6-trisulfonic acid disodium salt/p-xylenebispyridinium bromide) as previously (Torrent et al. 2007). Large unilamellar vesicles of dioleoyl-phosphatidyl choline: dioleoyl-phosphatidyl glycerol (3:2 molar ratio), containing 12.5 mmol/L ANTS and 45 mmol/L DPX in 20 mmol/L NaCl, 10 mmol/L Tris/HCl, pH 7.5, were diluted to 30 μmol/L and incubated at 25°C with the proteins for 45 min. Leakage was monitored as the increase in fluorescence ($\lambda_{\text{excitation}} = 386 \text{ nm}$; $\lambda_{\text{emission}} = 535 \text{ nm}$).

Fluorescent labeling of RNases

RNase 3, RNase 3-H15A, RNase 3-W35A, RNase 7-H15A, and RNase 7 were labeled with Alexa Fluor 488 Labeling kit (Molecular Probes, Invitrogen, Carlsbad, CA), following the manufacturer's instruction as previously described (Torrent et al. 2010a). To 0.5 mL of 2 mg/mL protein solution in phosphate saline buffer (PBS), 50 μL of 1 mol/L sodium bicarbonate, pH 8.3, was added. The protein was incubated for 1 h at room temperature with the reactive dye, with stirring, and the labeled protein was separated from the free dye by PD-10 desalting column.

Candida albicans growth conditions

Candida albicans (ATCC 90028) cells were maintained at -70°C and incubated overnight with agitation at 37°C in Sabouraud Dextrose broth (mycological peptone, glucose, pH 5.6) Fluka-Sigma S3306. Previous to each assay, cells were subcultured for ~2–3 h to yield a midlogarithmic culture.

Minimum fungicidal concentration

Candida albicans ATCC 90028 was cultured overnight in Sabouraud Dextrose broth at 37°C and subcultured the

next day in fresh Sabouraud and grow to an optical density of 0.4 at 600 nm (mid log-phase). Cells were washed twice in nutrient broth or PBS, and diluted to $\sim 2 \times 10^6$ cells/mL. Proteins serially diluted were added to 2×10^5 cells from 20 to 0.1 μmol/L final concentration. *Candida albicans* was incubated at 37°C during 4 h in Sabouraud nutrient broth, PBS or 10 mmol/L sodium phosphate buffer, pH 7.5. Following, the samples were plated onto Sabouraud Petri dishes and incubated at 37°C overnight. Antifungal activity was expressed as the MFC, defined as the lowest protein concentration required for more than 99% of microorganism killing. MFC of each protein was determined from two independent experiments performed in triplicate for each concentration.

Cell viability assay

Antimicrobial activity was also assayed by following the cell viability of *C. albicans*, using the BacTiter-Glo™ Microbial Cell Viability kit (Promega, Madison, WI), which measures the number of viable fungal cells, by ATP quantification. ATP, as an indicator of metabolically active cells, is indirectly measured by a coupled luminescence detection assay. The luminescent signal is proportional to the amount of ATP required for the conversion of luciferin into oxyluciferin in the presence of luciferase.

An overnight culture of *C. albicans* was used to inoculate fresh Sabouraud liquid culture, and logarithmic phase culture was grown to an OD₆₀₀ of 0.2. RNase 3, RNase 7, and mutants were added to 0.1 mL of cell culture at a final concentration from 0.025 to 20 μmol/L. The *C. albicans* viability was followed after 4 h of incubation at 37°C. 50 μL of incubation culture was mixed with 50 μL of BacTiter-Glo™ reagent in a microtiter plate following the manufacturer instructions and incubated at room temperature for 10 min. Luminescence was read on a Victor3 plate reader (PerkinElmer, Waltham, MA) with a 1-s integration time. IC₅₀ values were calculated by fitting the data to a dose–response curve.

Cell survival assay

Candida albicans viability assay was performed using the Live/Dead® microbial viability kit as previously described (Torrent et al. 2010a). *Candida* strain was grown at 37°C to $\sim 5 \times 10^6$ cells/mL, centrifuged at 5000 × g for 5 min and resuspended in a 0.85% NaCl solution, in accordance with the manufacturer instructions. *Candida albicans* cell culture was stained using a SYTO®9/propidium iodide 1:1 mixture. SYTO®9 is a DNA green fluorescent dye that diffuses thorough intact cell membranes and propidium iodide is a DNA red fluorescent dye that can only access the nucleic acids of membrane damaged cells, displacing

the DNA bound SYTO[®]9. The method allows the labeling of intact viable cells and membrane compromised cells, which are labeled in green and red, respectively, referred to as live and dead cells. The viability kinetics was monitored using a Cary Eclipse Spectrofluorimeter (Varian Inc., Palo Alto, CA). Cell viability profiles were registered after adding from 1 to 5 $\mu\text{mol/L}$ of final protein concentration. To calculate the cell viability, the fluorescence in the range of 510–540 nm and 620–650 nm were integrated to obtain the SYTO[®]9 (live cell) and the propidium iodide (dead cell) signals, respectively. Then, the percentage of live bacteria was represented as a function of time.

Cell viability by confocal microscopy

The kinetics of *C. albicans* survival was followed by confocal microscopy for 180 min at 37°C. Experiments were carried out in a plate-coverslide system. Two hundred and fifty microliters of *C. albicans* $\sim 4 \times 10^6$ cells/mL were stained as described below and mixed with the protein at 5 $\mu\text{mol/L}$ final concentration. *Candida albicans* cell cultures were prestained using the SYTO[®]9/propidium iodide 1:1 mixture provided in the Live/Dead[®] staining kit (Molecular Probes, Eugene, OR). Confocal images of the yeast culture were captured using a laser scanning confocal microscope (Leica TCS SP2 AOBS equipped with a HCX PL APO 63, $\times 1.4$ oil immersion objective; Leica Microsystems, Wetzlar, Germany). SYTO[®]9 was excited using a 488 nm argon laser (515–540 nm emission collected) and propidium iodide was excited using a diode pumped solid-state laser at 561 nm (588–715 nm emission collected). To record the time-lapse experiment, Life Data Mode software (Leica) was used, obtaining an image every minute.

Alternatively, labeled protein distribution in cell cultures was followed by confocal microscopy. 300 μL of *Candida albicans* yeast ($\sim 4 \times 10^6$ cell/mL) was incubated with Alexa-labeled proteins at 1 to 5 $\mu\text{mol/L}$ during 1 h in PBS. Previously, cells were washed with PBS and labeled with Hoescht 33342 at 0.5 $\mu\text{g/mL}$ for 10 min before observation of unfixed cells in Leica TCS SP5 AOBS equipped with a PL APO 63 $\times 1.4$ -0.6 CS oil immersion objective (Leica Microsystems, Mannheim, Germany). Fluorochromes were excited by 405 nm (Hoescht 33342) and 488 nm (Alexa Fluor 488 nm) and both emissions collected with a HyD detector. Alexa Fluor 488-labeled proteins were added directly to the cultures and time lapse was recorded at intervals of 30 sec for 1 h.

Cell membrane depolarization assay

Membrane depolarization was assayed by monitoring the DiSC₃(5) fluorescence intensity change in response to changes in transmembrane potential as described previously (Torrent et al. 2008). *Candida albicans* cells were

grown at 37°C to the midexponential phase and resuspended in 5 mmol/L Hepes-KOH, 20 mmol/L glucose and 100 mmol/L KCl at pH 7.2. DiSC₃(5) was added to a final concentration of 0.4 $\mu\text{mol/L}$. Changes in the fluorescence for alteration of the cell plasma membrane potential were continuously monitored at 20°C at an excitation wavelength of 620 nm and an emission wavelength of 670 nm. When the dye uptake was maximal, as indicated by a stable reduction in the fluorescence as a result of quenching of the accumulated dye in the membrane interior, protein in 5 mmol/L Hepes-KOH buffer at pH 7.2 was added at a final protein concentration from 1 to 5 $\mu\text{mol/L}$ and incubated for 50 min. Maximum depolarization was calculated when the fluorescence signal was fully stabilized and the depolarization percentage was calculated taking Triton X-100 at 10% as a positive control. The time required to reach a stabilized maximum fluorescence reading was recorded for each condition, and the time required to achieve half of total membrane depolarization was estimated from the nonlinear regression curve. All conditions were assayed in duplicate.

Cell membrane permeabilization activity

Membrane permeabilization was evaluated by using the Sytox[®] Green uptake assay. Sytox[®] Green is a cationic cyanine dye (≈ 900 Da) that is not membrane permeable. When a cell's plasma membrane integrity is compromised, influx of the dye, and subsequent binding to DNA, causes a large increase in the fluorescence signal. For Sytox[®] Green assays, *Candida albicans* cells were grown to midexponential growth phase at 37°C and then centrifuged, washed, and resuspended in PBS. Cell suspensions in PBS ($\sim 2 \times 10^6$ cells/mL) were incubated with 1 $\mu\text{mol/L}$ Sytox[®] Green for 15 min in the dark prior to the influx assay. At 2 to 4 min after initiating data collection, proteins at 1 and 5 $\mu\text{mol/L}$ final concentration were added to the cell suspension, and the increase in Sytox[®] Green fluorescence was measured (excitation wavelength at 485 nm and emission at 520 nm) for 50 min in a Cary Eclipse spectrofluorimeter. Bacterial cell lysis with 10% Triton X-100 was taken as the maximum fluorescence reference value.

Cell binding assay

Candida albicans cells were cultured overnight in Sabouraud Dextrose broth at 37°C and subcultured the next day in fresh Sabouraud and grow to an optical density of 0.4 at 600 nm (mid log-phase). Cells were washed twice in PBS, and diluted to $\sim 2 \times 10^6$ cells/mL. Cells were incubated in 100 μL of PBS at 37°C with proteins at 1 $\mu\text{mol/L}$ final concentration during different periods of time up to 1 h. Following, the samples were centrifugated at

13000 rpm. The supernatant samples were concentrated using 10 kDa cut-off filters to 20 μ L. The presence of the proteins was checked by 15% SDS-PAGE and Coomassie Blue staining. Reference protein controls were treated following the same protocol in the absence of cells.

Fluorescent-assisted cell sorting (FACS) assay

The evolution of cell population was followed by cell cytometry. *Candida albicans* cells were grown at 37°C to midexponential phase ($\sim 2 \times 10^6$ cells/mL), centrifuged at $5000 \times g$ for 2 min, resuspended in PBS. 500 μ L aliquot of the yeast suspension was incubated with 1 to 5 μ mol/L of Alexa-Fluor-labeled protein for 60 min. After incubation, 25,000 cells were washed three times with PBS buffer and subjected to FACS analysis using a FACSCalibur cytometer (BD Biosciences, Franklin Lakes, NJ) and excitation and emission wavelengths of 488 nm and 515–545 nm, respectively. Internal fluorescence uptake was evaluated at 2, 5, 15, and 60 min in 10,000 cells. Dead cells were stained with PI dye added at a final concentration of 10 μ g/mL.

Cellular RNA degradation

A *C. albicans* cell culture suspension ($\sim 6 \times 10^6$ cells/mL) was incubated in PBS and treated with the proteins at 3 μ mol/L final concentration for 30, 60, and 120 min. After incubation, cells were sedimented and resuspended in lysis buffer, 10% SDS and Phenol:Chloroform: isoamyl alcohol (IAA) and mixed with zirconia beads. RNA isolation was done using the Ribopure Yeast kit (Invitrogen) according to manufacturer's instructions. Samples were analyzed in a high sensitivity nucleic acid microfluidic chip using an *Experion* automated electrophoresis system (Bio-Rad, Madrid, Spain). Cellular RNA populations were quantified by virtual gel densitometry.

Statistical analysis

Results are reported as mean \pm SD. Each mutant was compared with the corresponding wild-type protein. Statistical analysis was performed by the paired Student's t-test using STATA 11 software and IBM SPS 19 software. One-way analysis of variance (ANOVA) was applied. *P* values < 0.05 were considered significant.

Results

Human RNases against *Candida albicans*

The antifungal mechanisms of action of RNase 3 and RNase 7 on *Candida albicans* were characterized through

a variety of methodological approaches. This is the first direct report of the involvement of both enzymatic and membrane damage activities in the RNases' antimicrobial activity. Single-point mutations that ablate either the protein catalytic (H15A) or cell-binding (W35A) activities were designed to evaluate the distinct protein properties.

The protein toxicity on yeast cells was first analyzed by plotting the colony-forming unit (CFU) reduction as a function of the protein concentration. Both RNases showed an effective protein concentration in the low micromolar range (Table 1), achieving minimal fungicidal concentrations (MFC₁₀₀) at approximately 2 to 4 μ mol/L (30–60 μ g/mL), as evaluated in nutrient media (Sabouraud broth) and phosphate saline buffer (PBS) (Table 1). The antifungal activity was also assessed by a cell viability assay based on the quantification of the ATP levels that revealed similar IC₅₀ values for both RNases. The calculated antifungal activity was comparable to the previously reported bactericidal activity (Torrent et al. 2012). Equivalent MFCs were achieved for low and high ionic strength phosphate buffers (Table S2), as previously observed for RNase 3 bactericidal activity (Torrent et al. 2012). However, the addition of increasing amounts of Ca²⁺ or NaCl to the nutrient growth media impaired considerably the RNases fungicidal activity (Table S2), as previously reported for the bactericidal action of RNase 3 (Lehrer et al. 1989) and other AMPs (Krishnakumari et al. 2009). Binding to *Candida* cells was assessed by monitoring the free unbound protein after incubation at sublethal concentrations in PBS for 1 h at 37°C (Fig. S1). No binding was achieved in equivalent assay conditions by the homologous RNase A, used here as a non antimicrobial reference protein.

Table 1. Antifungal activities of RNase 3, RNase 7, and mutant variants on *Candida albicans*.

Protein	MFC ₁₀₀ (μ mol/L)		IC ₅₀ (μ mol/L)
	Sabouraud Broth	PBS	
RNase 7	2.5–5	2.5	1.60 \pm 0.09
RNase 7-H15A	3.5–5	2.5–5	1.93 \pm 0.07*
RNase 3	2.5	2.5	2.50 \pm 0.01
RNase 3-H15A	5–10	5–10	3.45 \pm 0.08**
RNase 3-W35A	>20	>20	9.03 \pm 0.52**

Minimal fungicidal concentration (MFC₁₀₀) values were calculated by CFU counting on plated Petri dishes as described in the methodology. *C. albicans* cultures were treated with the proteins diluted in either the Sabouraud nutrient growth media or in a phosphate saline buffer (PBS). IC₅₀, given as mean \pm SD, were determined using the Bactiter-Glo™ kit as detailed in the Experimental Procedures. Values are averaged from three replicates of two independent experiments. For the comparison of numerical variables between wild-type and mutant, the Student's t-test was used. Values of *P* < 0.05 * and *P* < 0.009 ** are indicated.

Additionally, RNase 3 and RNase 7 action at the cell plasma membrane was evaluated by assessing their ability to trigger the depolarization and permeabilization of the cell membrane (Table 2). Complementarily, studies of both the kinetics of the depolarization and permeabilization activities of the enzymes were compared. Furthermore, a time course monitoring of the protein toxicity on the yeast cell population was completed using the Live/Dead® staining kit, where a major reduction in the cell survival percentage was shown after 1 h (Fig. S3). Next, we labeled the recombinant proteins with an Alexa Fluor fluorescent marker and tracked the location of the proteins in cell cultures, in which the cell nuclei were stained with Hoechst stain (Fig. S2). The protein distribution was analyzed and it was observed that the protein and cell signals colocalized (Fig. 2). The protein internalization was also visualized at sublethal concentrations and short incubation times after removal of any remaining free protein (Fig. 2D).

A dual mode for RNases antifungal activity

The mechanism of action against *C. albicans* was then analyzed by ablating either the enzymatic activity or cell binding ability of the proteins. To assess the potential contribution of the catalytic activity of the RNases on their antimicrobial action, we prepared mutants of both RNases with defective active sites. The active site mutants were designed by making substitutions at His 15 within the active site catalytic triad (Boix et al. 1999; Huang et al. 2007), where His 15 is the counterpart of His 12 in RNase A (Fig. 1) (Cuchillo et al. 2011). The histidine to alanine substitution almost abolished all of the protein enzymatic activity for both RNases (Table 4) as previously reported by Raines and coworkers for the RNase A-H12A mutant counterpart (Park et al. 2001). Additionally, the overall three-dimensional structure and the active site architecture of the mutant protein were maintained, as

confirmed by solving the RNase 3-H15A mutant X-ray crystal structure (PDB ID: 4OWZ) (Fig. 1 and Table S1). The functional characterization of both active site mutants confirmed that these mutant proteins conserved their membrane lytic activity, showing an equivalent leakage activity on lipid vesicles (Table 4). Furthermore, the potential contribution of the H15 residue on the proteins' affinity for the cell membrane was discarded, being a residue poorly exposed to the protein surface (solvent accessible surface area, SASA, for His 15 ~ 14 Å²; 4A2Y.pdb (Boix et al. 2012a)).

Following, we compared the recombinant variants with ablated active sites with the wild-type proteins in yeast cell cultures (Table 1). The protein activities were evaluated both by comparing the CFU count and assessing the cell viability by monitoring the ATP levels (Table 1). Differences between the cytotoxicities of the wild-type and active site mutants were observed at sublethal concentrations and final incubation times. A kinetic time course of yeast cell viability indicated that the catalytically defective proteins showed a delay in their t_{50} values together with a lower rate of cell death at the final incubation time (Table 3). On the other hand, the active site mutations did not interfere with the protein membrane lysis activity on synthetic lipid vesicles (Table 4). Notably, depolarization time course profiles revealed no major differences between wild-type and active site mutant proteins in comparison with the membrane binding defective mutant (Tables 2 and 3). Additionally, there was no difference in the protein binding to the yeast cells for the H15A variant, as quantified by a fluorescence assisted cell sorting (FACS) assay (Fig. 3). On the other hand, by combining FACS analysis and propidium iodide (PI) staining, we also estimated the live and dead cell subpopulations, confirming that the membranes of the cells were not significantly compromised at the assayed conditions (Figs. 3 and S4).

Table 2. Cell membrane depolarization and permeabilization activities of RNases on *Candida albicans*.

Protein	Max. membrane depolarization (AU) ¹	Membrane depolarization (%) ²	Max. membrane permeabilization (AU) ¹	Membrane permeabilization (%) ²
RNase 7	165.77 ± 1.10	71.67 ± 0.1	134.56 ± 1.95	45.90 ± 0.5
RNase 7-H15A	153.96 ± 1.65*	66.54 ± 0.9	93.05 ± 1.24*	31.52 ± 0.3
RNase 3	80.07 ± 0.90	34.62 ± 0.08	104.93 ± 2.80	35.55 ± 0.4
RNase 3-H15A	67.27 ± 1.13*	29.08 ± 1.0	61.32 ± 0.63**	20.77 ± 0.2
RNase 3-W35A	28.42 ± 0.42**	12.28 ± 0.7	24.84 ± 0.25**	8.46 ± 0.6

Maximum membrane depolarization and permeabilization activities were determined at 1 μmol/L final protein concentration at final incubation time using the DiSC₃(5) probe and Sytox® Green, respectively, as described in Experimental Procedures. All values, given as mean ± SD, are averaged from three replicates of two independent experiments.

¹Arbitrary fluorescence unit (AU) values are indicated for maximum membrane depolarization and permeabilization.

²The calculated percentages refer to the maximum values achieved at final incubation time, referred to the positive control (10% of Triton X-100).

The *P* value were calculated using as reference each wild-type activity (*corresponds to *P* < 0.05 and ** to *P* < 0.009).

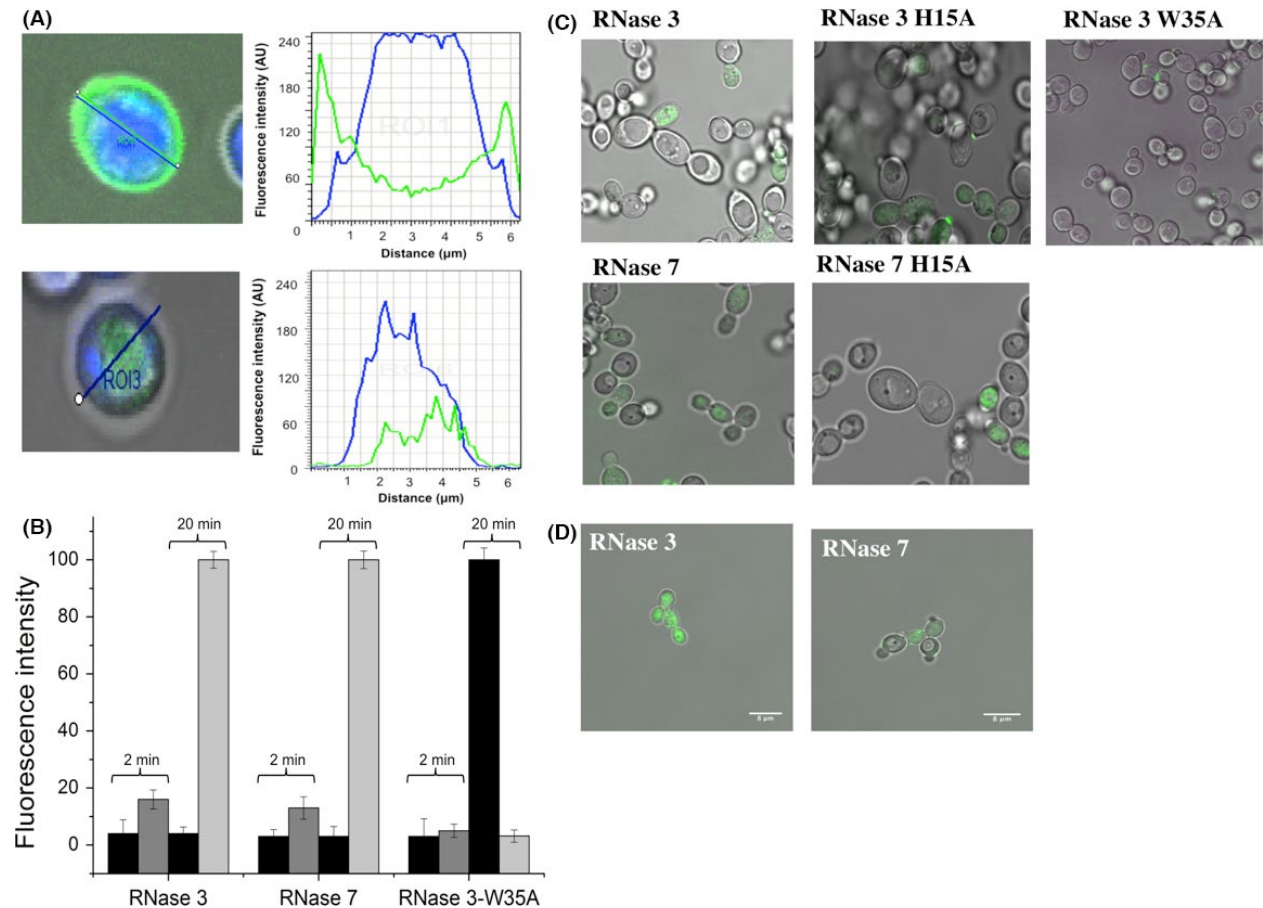


Figure 2. Confocal microscopy analysis of *Candida albicans* cell culture ($\sim 3 \times 10^6$ cells/mL) incubated with 1 $\mu\text{mol/L}$ of RNase 3, RNase 7 and mutants labeled with Alexa Fluor 488 (green). (A and B) Cells were stained with Hoescht 33342 dye (blue) following the assay incubation conditions detailed in the Experimental Procedures section. Fluorescence and differential interference contrast (DIC) merge images were taken. Analysis was made at 2 and 20 min after protein addition at 1 $\mu\text{mol/L}$ final concentration. After protein addition, the evolution of the fluorescence signals was analyzed by confocal microscopy. A total of 20 cells were analyzed by regions of interest (ROIs) using the Leica TCS software. Yeast size mean was adjusted according to Hoescht-labeled distribution and disc image. The cell mean size was around 4.5 μm and a distance between 4.5 and 8 μm was ascribed to the cell environment. (A) Profiles of fluorescence intensity for Alexa Fluor 488-labeled protein (green) and *C. albicans* cells stained with Hoescht 33342 (blue). Examples of fluorescence profiles are shown at 2 min and 20 min for RNase 3. (B) Bar graphs of total internal and external fluorescence intensity values (maximum peak) are shown. Black bar corresponds to outer fluorescence and gray and light gray bar to inner fluorescence at 2 and 20 min, respectively. (C and D) Confocal microscopy analysis of *Candida* cell culture ($\sim 3 \times 10^6$ cells/mL) incubated with 1 $\mu\text{mol/L}$ of RNase 3, RNase 7 and mutants labeled with alexa fluor 488. Distribution of Alexa Fluor 488-labeled protein in treated *C. albicans* cells visualized by confocal microscopy, (C) Protein localization in yeast cells after 20 min of incubation at 37°C with labeled proteins. (D) Merged images after additional PBS washes to eliminate fluorescence background and free-labeled proteins. The images were taken using a Leica TCS SP5 AOBs microscope.

Lastly, the potential effect of the RNases on the yeast intracellular RNA was assessed. Total cellular RNA was extracted from treated cultures and analyzed by capillary electrophoresis (Fig. 4A). To estimate the relative activity on cellular RNA, the corresponding time course of the decrease in rRNA subunits was evaluated by densitometry as a function of time (Fig. 4B). The results confirmed that there was a drastic reduction in the cellular RNA degradation rate for the active site mutants. All assays were carried out at sublethal conditions, as confirmed by a simultaneous time course monitoring of the cell culture

population by optical density at 600 nm and CFU counting. Moreover, no significant reduction in the cell viability at the assayed conditions was observed by the quantification of the ATP levels during the first 15 min (Fig. S5). We even observed a slight increase in the ATP concentration at the very beginning of the incubation time, which might be attributed to a blockage of the cell protein synthesis machinery, probably induced by the RNase binding to cellular nucleic acids.

Complementarily, we assayed an RNase 3 mutant version (W35A), previously reported as defective in its

Table 3. Comparison of calculated time to achieve 50% activity (t_{50}) for membrane depolarization, membrane permeabilization, and cell survival.

Protein	Membr. depolarization t_{50} (sec)	Membr. permeabilization t_{50} (sec)	Cell survival t_{50} (sec)	Cell survival (%)
RNase 7	261.23	595.53	1397	38.2
RNase 7-H15A	288.53	698.15*	1763*	54.86**
RNase 3	251.36	490.84	2354	56.87
RNase 3-H15A	356.75*	975.5**	2965*	67.89**

All assays were carried out at 1 $\mu\text{mol/L}$ final protein concentration. Depolarization was assayed using DISC3(5) dye, cell leakage by the Sytox Green assay and survival percentage at final incubation time (120 min) was evaluated using the Live/dead® kit. T-student was applied for comparison of numerical variables using as reference each activity corresponding to wild-type protein, where * corresponds to $P < 0.05$ and ** to $P < 0.009$.

Table 4. Relative enzymatic activity was determined by the spectrophotometric method using $(\text{Cp})_4\text{C}>\text{p}$ substrate as described in the Experimental Procedures section.

Protein	RNase activity (%)	LUV leakage ED_{50} ($\mu\text{mol/L}$)
RNase 7	100	1.14 \pm 0.03
RNase 7-H15A	9	1.24 \pm 0.09
RNase 3	100	1.33 \pm 0.71
RNase 3-H15A	0	1.44 \pm 0.14

Leakage of large unilamellar vesicles (LUV) is expressed as 50% effective dose (ED_{50}), given as mean \pm SD, averaged from three replicates of two independent experiments.

protein-membrane interaction without affecting its RNase activity (Carreras et al. 2003; Nikolovski et al. 2006; Torrent et al. 2007). The present results confirm the key role of the surface exposed Trp (Fig. 1B) in the toxicity of the protein to yeast cells. The W35A mutant displays a two to threefold reduction in its fungicidal (Table 1) and membrane destabilizing activities (Table 2). Mostly, the abilities of RNase 3 to cause membrane depolarization and disruption were severely impaired (Table 2). Indeed, by confocal microscopy, we visualized how the labeled W35A mutant does not associate to the yeast cell surface and is not internalized (Figs. 2 and S2). Furthermore, there was no significant rate of intracellular RNA cleavage, which corroborates that the protein has a defective internalization mechanism (Fig. 4).

Discussion

There is an urgent need to develop alternative antibiotics. Exploring the mechanisms of action of our own self-defense machinery is a promising strategy toward the design of new drugs. Human antimicrobial RNases, which are secreted upon infection and display a variety of cytotoxic activities, provide a suitable working model. In particular, several members of the vertebrate RNase A family were previously reported to display toxicity against fungal pathogens, such as RNase 5 (Hooper et al. 2003), RNase 7 (Harder

and Schroder 2002; Huang et al. 2007) or RNase 8 (Rudolph et al. 2006).

In this work, we have selected the two most studied human antimicrobial RNases, the eosinophil RNase 3 and the skin-derived RNase 7, which are upregulated upon infection (Glaser et al. 2009; Mohammed et al. 2011; Boix et al. 2012b; Becknell et al. 2015) and are directly implicated in the host defense against fungal infections (Rothenberg and Hogan 2006; Rosenberg et al. 2013). *Candida albicans* was chosen here because it is a simple eukaryotic pathogen that provides a suitable model to analyze the distinct protein targets at the cellular level. High fungicidal activities were achieved for both RNases, with MFCs on the low micromolar scale (Table 1). Together with the analysis of the RNases' membrane damage, we have followed their cell internalization and enzymatic action. The present results highlight that the RNases have a dual mode of action. Indeed, antimicrobial RNases should be regarded as multifunctional proteins, combining an enzymatic activity and a mechanical action at the membrane level, together with other described immunomodulatory activities (Boix and Nogués 2007; Gupta et al. 2012). Similar examples of multitargeted antimicrobial proteins are available in the literature, combining intracellular targets with a variety of immunomodulating properties (Hancock and Sahl 2006; Peschel and Sahl 2006; Nicolas 2009; Haney and Hancock 2013). Unfortunately, the methodological limitations and the disparity of experimental conditions have mostly delayed the understanding of the mechanism of AMPs (Nicolas 2009; Spindler et al. 2011; Stalmans et al. 2013). It is noteworthy that many proposed roles of AMPs, such as immunomodulation or intracellular targeting, are only observed when working at sublethal assay conditions (Holm et al. 2005; Haney and Hancock 2013).

In this context, the present results once again highlight the key influence of the selection of assay conditions. Our results indicated that the labeled protein readily associated to the yeast cells at short incubation time and was subsequently internalized (Figs. 2 and S2). By tracking the cell population using a cell sorting assay combined

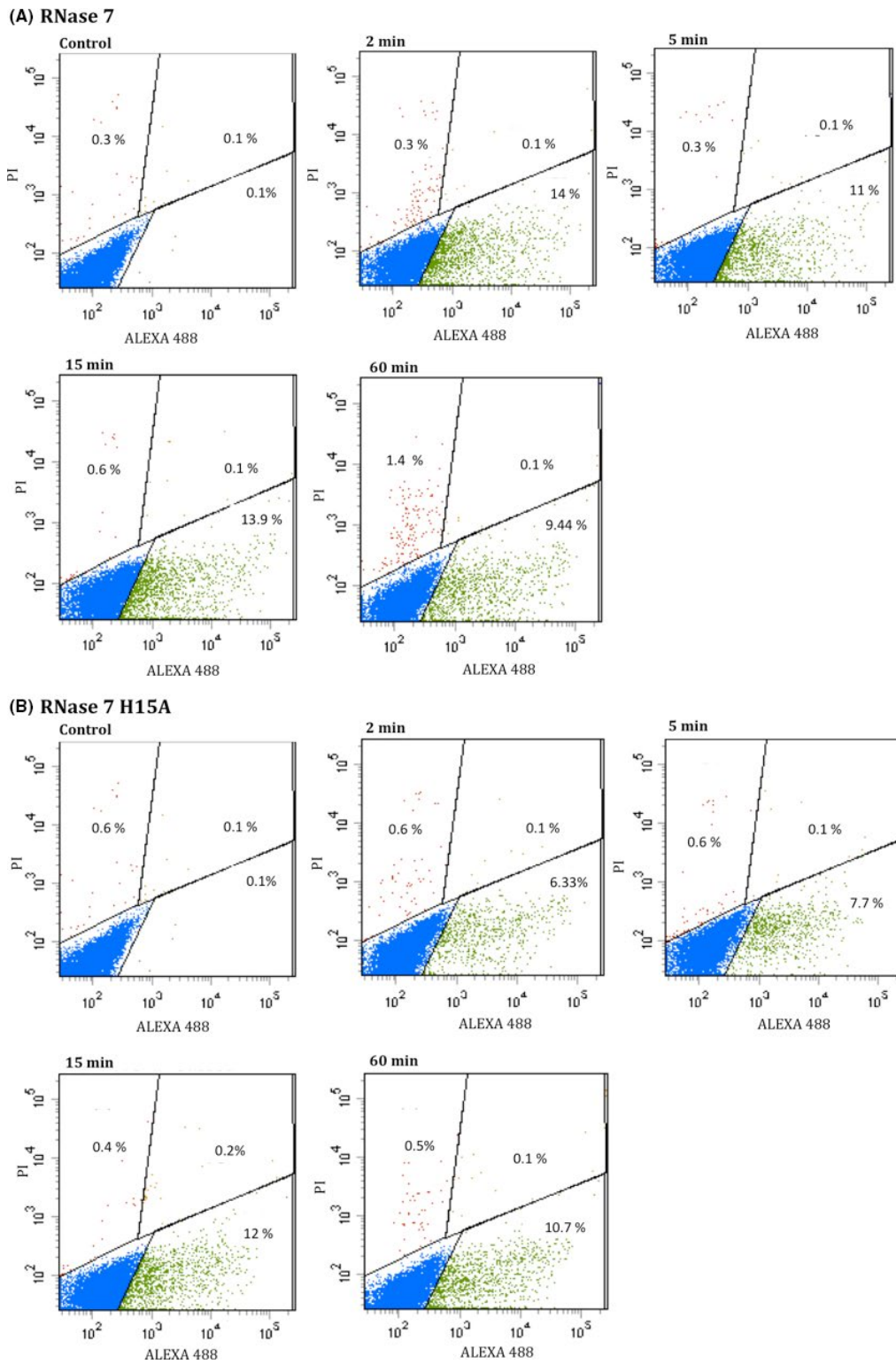


Figure 3. Analysis of *Candida albicans* cell culture (1×10^6 cells/mL) incubated with $1 \mu\text{mol/L}$ of protein by FACS. Cells were gated by Forward scatter (FSC)/Side scatter (SSC). Additionally, the incubation mixture was treated with PI to identify the dead cell population. After addition of RNase 7 (A) and RNase 7-H15A (B) the samples were analyzed using a FACSCalibur cytometer at 2, 5, 15 and 60 min. Dot plot diagrams of Protein Alexa Fluor 488/PI show cell population divided in: free live cells (blue), cells with uptake protein (green), free dead cells (red), and dead cells with protein uptake (orange). Control corresponds to untreated cells.

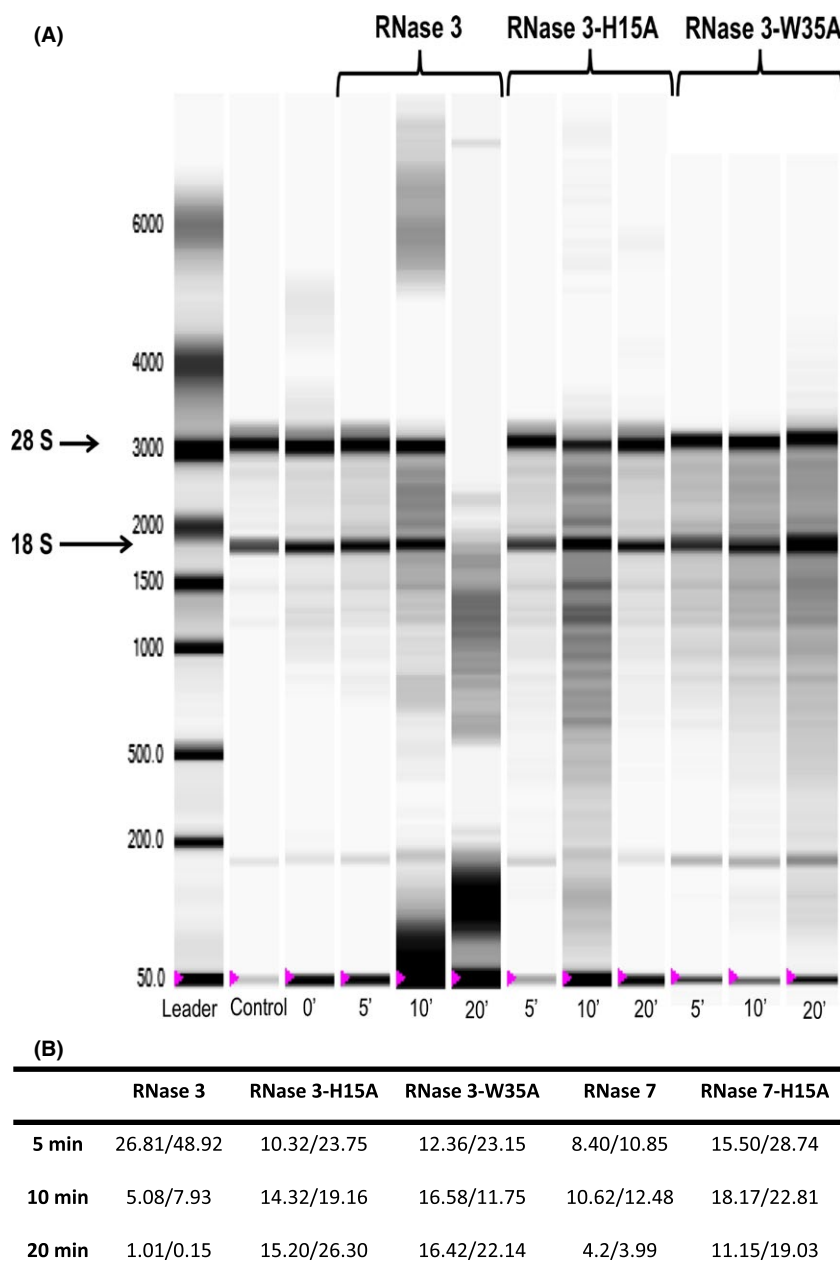


Figure 4. Effect of RNases on *Candida albicans* cellular RNA. 1 mL of yeast cell suspension ($\sim 1 \times 10^7$ cells/mL) was treated with 3 $\mu\text{mol/L}$ of each protein and incubated at different time intervals. Following, total RNA was extracted as described in Experimental Procedures. (A) Samples were analyzed by an *Experion* automated electrophoresis system and RNA was visualized with the *Experion* software. Left lane contains molecular mass markers, where reference base pairs are indicated. Control lane corresponds to cellular RNA from untreated cells. The RNA extraction was made at different time intervals up to 20 min. (B) Peak area corresponding to 18/28s subunits of rRNA of treated cells with wild-type and mutant RNases are shown for each incubation time.

with staining of membrane compromised cells, we confirmed that in the assayed conditions, there was no significant cell death (Figs. 3 and S4). The timing of events illustrated how cell membrane damage is only achieved at longer incubation times or higher protein concentrations. Consequently, previous results obtained at higher

protein concentrations attributed RNase 3 cytotoxicity merely to cell lysis action (Carreras et al. 2003; Torrent et al. 2007; Singh and Batra 2011; Torrent et al., 2010b). Additionally, we cannot discard other complementary processes, such as the RNases' binding to nucleic acids and blockage of the cell protein translation machinery.

Indeed, a previous report on the bactericidal activity of RNase 7 already suggested its putative interaction with cellular nucleic acids (Lin et al. 2010), as reported for other cationic AMPs (Brogden 2005; Nicolas 2009).

Contribution of the RNase catalytic activity to the cytotoxic properties within the RNase A superfamily members remains a matter of controversy. Although we can find some reports on the RNase antimicrobial activity inhibition by either diethyl pyrocarbonate (DEPC) treatment or by the proteinaceous RNase inhibitor (RI) (Abtin et al. 2009), the experimental results should be interpreted with caution. Indeed, the horseshoe-like shaped inhibitor structure can engulf the RNase inside its internal cavity, covering the cationic residues involved in the protein antimicrobial activity, as proposed for the RI interference of RNase 7 binding to LPS (Spencer et al. 2014). Similarly, treatment with DEPC would modify not only the catalytic His but other His residues exposed at the protein surface.

In any case, our results confirmed that not only are RNase 3 and RNase 7 internalized in yeast cells (Fig. 2), they also contribute by their enzymatic activities to the cell killing process. Both RNase H15A variants showed impaired catalytic activity but retained their destabilization action on lipid bilayers (Table 4). Besides, both active site mutants retained their cell binding and internalization abilities (Figs. 2 and 3). On the contrary, the reduction in their fungicidal activity was significant (Table 1) and the cellular RNA degradation rates for the active site mutants were drastically reduced (Fig. 4).

In addition, the RNase 3-W35A defective mutant was used to probe the contribution of the association of the protein to the cell surface. Residue W35 lies at a protein patch involved in interactions with lipid bilayers and extracellular matrix components (García-Mayoral et al. 2010; Torrent et al. 2011a; Lien et al. 2013), proposed to serve as a vehicle for drug delivery (Fang et al. 2013). In particular, the W35 residue was identified to participate in the binding of LPS and glycosaminoglycans (Fan et al. 2008; García-Mayoral et al. 2013; Pulido et al. 2013a). We can hypothesize that equivalent interactions may also contribute to the proteins' association with the *Candida* cell wall, which is predominantly composed of glucan components. Indeed, common binding motifs are found for beta-glucan pattern recognition proteins and other carbohydrate-binding proteins, such as LPS and heparan sulfate. In particular, a shared binding motif for LPS and 1,3-beta-glucans is involved in invertebrate innate immunity (Iwanaga and Lee 2005).

Our studies on *Candida* also highlighted the requirement of the Trp residue for membrane damage, protein internalization, and cellular RNA degradation (Figs. 2, 4 and S2; Table 2). Interestingly, cell internalization is easily

achieved by other members of the vertebrate RNase A family (Haigis and Raines 2003; Benito et al. 2008; Chao and Raines 2011; Sundlass et al. 2013). As an example, the cellular trafficking and ribonucleolytic activities of human RNase 5 are essential for its angiogenic action (Thiyagarajan et al. 2012). The antimicrobial RNases might also be regarded as "cell penetrating proteins." Indeed, the intracellular routing of secretory RNases could promote their physiological role in innate immunity; a process that can be regulated by the presence of the ribonuclease inhibitor (RI), which is ubiquitous in the cytosol of mammalian cells (Lomax et al. 2014). Interestingly, very recent results on the down regulation of RI during uropathogen infections suggests a direct mechanism that facilitates the antimicrobial activity of RNases when required (Spencer et al. 2014).

Understanding the determinants that can assist protein translocation without inducing any cell damage is desired for the design of alternative targeted drugs. Although many cationic and amphipathic AMPs are classified as cationic penetrating peptides (CPPs) (Brogden 2005; Nicolas 2009; Stalmans et al. 2013), most CPP behavior has only been tested against mammalian cells (Last et al. 2013), but few peptides have been described against putative eukaryote pathogens (Do et al. 2014). Thus, the study of CPPs in yeast is an emerging field that offers promising biotechnological applications (Nekhotiaeva et al. 2004; Holm et al. 2005; Mochon and Liu 2008; Marchione et al. 2014).

In conclusion, the observed antimicrobial effective doses for both RNases were found to be in the low micromolar range, which is promising in the design of antifungal agents. Hence, the human RNases secreted from blood and epithelial cells, which combine membrane lytic and enzymatic RNase activities, could work as first line safeguard sentinels. In a wider context, the vertebrate secreted RNases could contribute to the protection of a variety of body fluids, from seminal to placental fluids, tears, or even milk (D'Alessio et al. 1991; Leonardi et al. 1995; Harris et al. 2010). Indeed, a nonspecific RNA degradation activity would represent one of the quickest and most effective ways of targeting pathogen viability. We can speculate that secreted RNases may exert a direct host defense role by the removal of pathogenic RNA, both within infected cells and resident at the extracellular matrix (Gupta et al. 2012). Therefore, as innate immunity effectors, human RNases are proving to be an ideal system for the design of nonantigenic nanodelivery tools to fight invading pathogens. AMPs offer the opportunity of finding new antifungal agents, as few effective antifungal peptides are currently available (Swidergall and Ernst 2014; Tsai et al. 2014). Thus, the study of human antimicrobial RNases provide a promising model for the design of new applied therapies against fungal infections.

Acknowledgments

Spectrofluorescence assays were performed at the *Laboratori d'Anàlisi i Fotodocumentació*, Universitat Autònoma de Barcelona. The work was supported by the *Ministerio de Economía y Competitividad* (BFU2012-38965), co-financed by FEDER funds and by the *Generalitat de Catalunya* (2009SGR-795; 2014SGR-728). VAS was a recipient of a “Francisco José de Caldas” predoctoral fellowship, *Colciencias*. JA was a recipient of a predoctoral fellowship (*Personal Investigador en Formación*, Universitat Autònoma de Barcelona). Diffraction data was collected at BL13 beamline station at ALBA synchrotron with the collaboration of ALBA staff.

Conflict of Interest

All authors declare no conflict of interests.

References

- Abtin, A., L. Eckhart, M. Mildner, M. Ghannadan, J. Harder, J.-M. Schröder, et al. 2009. Degradation by stratum corneum proteases prevents endogenous RNase inhibitor from blocking antimicrobial activities of RNase 5 and RNase 7. *J. Invest. Dermatol.* 129:2193–2201.
- Acharya, K. R., and S. J. Ackerman. 2014. Eosinophil granule proteins: form and function. *J. Biol. Chem.* 289:17406–17415.
- Adams, P. D., P. V. Afonine, G. Bunkoczi, V. B. Chen, I. W. Davis, N. Echols, et al. 2010. PHENIX: a comprehensive Python-based system for macromolecular structure solution. *Acta Crystallogr. D Biol. Crystallogr.* 66:213–221.
- Amatngalim, G. D., Y. van Wijck, Y. de Mooij-Eijk, R. M. Verhoosel, J. Harder, A. N. Lekkerkerker, et al. 2015. Basal cells contribute to innate immunity of the airway epithelium through production of the antimicrobial protein RNase 7. *J. Immunol.* 194:3340–3350.
- Andrés, E. 2012. Cationic antimicrobial peptides in clinical development, with special focus on thanatin and heliomicin. *Eur. J. Clin. Microbiol. Infect. Dis.* 31:881–888.
- Bardan, A., V. Nizet, and R. L. Gallo. 2004. Antimicrobial peptides and the skin. *Expert. Opin. Biol. Ther.* 4:543–549.
- Becknell, B., T. E. Eichler, S. Beceiro, B. Li, R. S. Easterling, A. R. Carpenter, et al. 2015. Ribonucleases 6 and 7 have antimicrobial function in the human and murine urinary tract. *Kidney Int.* 87:151–161.
- Benito, A., M. Vilanova, and M. Ribó. 2008. Intracellular routing of cytotoxic pancreatic-type ribonucleases. *Curr. Pharm. Biotechnol.* 9:169–179.
- Boix, E., and M. V. Nogués. 2007. Mammalian antimicrobial proteins and peptides: overview on the RNase A superfamily members involved in innate host defence. *Mol. Biosyst.* 3:317–335.
- Boix, E., Z. Nikolovski, G. Moiseyev, H. F. Rosenberg, C. M. Cuchillo, and M. V. Nogués. 1999. Kinetic and product distribution analysis of human eosinophil cationic protein indicates a subsite arrangement that favors exonuclease-type activity. *J. Biol. Chem.* 274:15605–15614.
- Boix, E., D. Pulido, M. Moussaoui, M. V. Nogués, and S. Russi. 2012a. The sulfate-binding site structure of the human eosinophil cationic protein as revealed by a new crystal form. *J. Struct. Biol.* 179:1–9.
- Boix, E., V. A. Salazar, M. Torrent, D. Pulido, M. V. Nogués, and M. Moussaoui. 2012b. Structural determinants of the eosinophil cationic protein antimicrobial activity. *Biol. Chem.* 393:801–815.
- Bravo, J., E. Fernández, M. Ribó, R. Dellorens, and C. M. Cuchillo. 1994. A versatile negative-staining ribonuclease zymogram. *Anal. Biochem.* 219:82–86.
- Brogden, K. A. 2005. Antimicrobial peptides: pore formers or metabolic inhibitors in bacteria? *Nat. Rev. Microbiol.* 3:238–250.
- Brünger, A. T. 1992. Free R value: a novel statistical quantity for assessing the accuracy of crystal structures. *Nature* 355:472–475.
- Carreras, E., E. Boix, H. Rosenberg, C. M. Cuchillo, and M. V. Nogués. 2003. Both aromatic and cationic residues contribute to the membrane-lytic and bactericidal activity of eosinophil cationic protein. *Biochemistry* 42:6636–6644.
- Chaffin, W. L. 2008. *Candida albicans* cell wall proteins. *Microbiol. Mol. Biol. Rev.* 72:495–544.
- Chao, T. Y., and R. T. Raines. 2011. Mechanism of ribonuclease a endocytosis: analogies to cell-penetrating peptides. *Biochemistry* 50:8374–8382.
- Collaborative Computational Project, Number 4. 1994. The CCP4 suite: programs for protein crystallography. *Acta Crystallogr. D Biol. Crystallogr.* 50:760–763.
- Cuchillo, C. M., M. V. Nogués, and R. T. Raines. 2011. Bovine pancreatic ribonuclease: fifty years of the first enzymatic reaction mechanism. *Biochemistry* 50:7835–7841.
- D'Alessio, G., A. Di Donato, A. Parente, and R. Piccoli. 1991. Seminal RNase: a unique member of the ribonuclease superfamily. *Trends Biochem. Sci.* 16:104–106.
- De Smet, K., and R. Contreras. 2005. Human antimicrobial peptides: defensins, cathelicidins and histatins. *Biotechnol. Lett.* 27:1337–1347.
- Do, N., G. Weindl, L. Grohmann, M. Salwiczek, B. Kokschi, H. C. Korting, et al. 2014. Cationic membrane-active peptides - anticancer and antifungal activity as well as penetration into human skin. *Exp. Dermatol.* 23:326–331.

- Dorschner, R. A., V. K. Pestonjamas, S. Tamakuwala, T. Ohtake, J. Rudisill, V. Nizet, et al. 2001. Cutaneous injury induces the release of cathelicidin anti-microbial peptides active against group A streptococcus. *J. Invest. Dermatol.* 117:91–97.
- Emsley, P., and K. Cowtan. 2004. Coot: model-building tools for molecular graphics. *Acta Crystallogr. D Biol. Crystallogr.* 60:2126–2132.
- Fan, T., S. Fang, C. Hwang, C. Hsu, X. Lu, S. Hung, et al. 2008. Characterization of molecular interactions between eosinophil cationic protein and heparin. *J. Biol. Chem.* 283:25468–25474.
- Fang, S., T. Fan, H.-W. Fu, C.-J. Chen, C.-S. Hwang, T.-J. Hung, et al. 2013. A novel cell-penetrating peptide derived from human eosinophil cationic protein. *PLoS ONE* 8:e57318.
- Fritz, P., V. Beck-Jendroschek, and J. Brasch. 2012. Inhibition of dermatophytes by the antimicrobial peptides human β -defensin-2, ribonuclease 7 and psoriasis. *Med. Mycol.* 50:579–584.
- García-Mayoral, M. F., M. Moussaoui, B. G. De La Torre, D. Andreu, E. Boix, M. V. Nogués, et al. 2010. NMR structural determinants of eosinophil cationic protein binding to membrane and heparin mimetics. *Biophys. J.* 98:2702–2711.
- García-Mayoral, M. F., Á. Canales, D. Díaz, J. López-Prados, M. Moussaoui, J. L. De Paz, et al. 2013. Insights into the glycosaminoglycan-mediated cytotoxic mechanism of eosinophil cationic protein revealed by NMR. *ACS Chem. Biol.* 8:144–151.
- Glaser, R., F. Navid, W. Schuller, C. Jantschitsch, J. Harder, J. M. Schroder, et al. 2009. UV-B radiation induces the expression of antimicrobial peptides in human keratinocytes in vitro and in vivo. *J. Allergy Clin. Immunol.* 123:1117–1123.
- Gläser, R., J. Harder, H. Lange, J. Bartels, E. Christophers, and J.-M. Schröder. 2005. Antimicrobial psoriasin (S100A7) protects human skin from *Escherichia coli* infection. *Nat. Immunol.* 6:57–64.
- Gupta, S. K., B. J. Haigh, F. J. Griffin, and T. T. Wheeler. 2012. The mammalian secreted RNases: mechanisms of action in host defence. *Innate Immun.* 19:86–97.
- Haigis, M. C., and R. T. Raines. 2003. Secretory ribonucleases are internalized by a dynamin-independent endocytic pathway. *J. Cell Sci.* 116:313–324.
- Hancock, R. E. W., and H.-G. Sahl. 2006. Antimicrobial and host-defense peptides as new anti-infective therapeutic strategies. *Nat. Biotechnol.* 24:1551–1557.
- Haney, E. F., and R. E. W. Hancock. 2013. Peptide design for antimicrobial and immunomodulatory applications. *Biopolymers* 100:572–583.
- Harder, J., and J.-M. Schroder. 2002. RNase 7, a novel innate immune defense antimicrobial protein of healthy human skin. *J. Biol. Chem.* 277:46779–46784.
- Harris, P., K. M. Johannessen, G. Smolenski, M. Callaghan, M. K. Broadhurst, K. Kim, et al. 2010. Characterisation of the anti-microbial activity of bovine milk ribonuclease4 and ribonuclease5 (angiogenin). *Int. Dairy J.* 20:400–407.
- den Hertog, A. L., van Marle J., van Veen H. A., W. Van't Hof, J. G. Bolscher, E. C. Veerman, et al. 2005. Candidacidal effects of two antimicrobial peptides: histatin 5 causes small membrane defects, but LL-37 causes massive disruption of the cell membrane. *Biochem. J.* 388:689–695.
- Holm, T., S. Netzereab, M. Hansen, Ü. Langel, and M. Hällbrink. 2005. Uptake of cell-penetrating peptides in yeasts. *FEBS Lett.* 579:5217–5222.
- Hooper, L. V., T. S. Stappenbeck, C. V. Hong, and J. I. Gordon. 2003. Angiogenins: a new class of microbicidal proteins involved in innate immunity. *Nat. Immunol.* 4:269–273.
- Huang, Y. C., Y. M. Lin, T. W. Chang, S. H. Wu, Y. S. Lee, M. D. Chang, et al. 2007. The flexible and clustered lysine residues of human ribonuclease 7 are critical for membrane permeability and antimicrobial activity. *J. Biol. Chem.* 282:4626–4633.
- Iwanaga, S., and B. L. Lee. 2005. Recent advances in the innate immunity of invertebrate animals. *J. Biochem. Mol. Biol.* 38:128–150.
- Kabsch, W. 2010. XDS. *Acta Crystallogr. D Biol. Crystallogr.* 66:125–132.
- Krishnakumari, V., N. Rangaraj, and R. Nagaraj. 2009. Antifungal activities of human beta-defensins HBD-1 to HBD-3 and their C-terminal analogs Phd1 to Phd3. *Antimicrob. Agents Chemother.* 53:256–260.
- Last, N. B., D. E. Schlamadinger, and A. D. Miranker. 2013. A common landscape for membrane active peptides. *Protein Sci.* 22:870–882.
- Lehrer, R. I., D. Szklarek, A. Barton, T. Ganz, K. J. Hamann, and G. J. Gleich. 1989. Antibacterial properties of eosinophil major basic protein and eosinophil cationic protein. *J. Immunol.* 142:4428–4434.
- Leonardi, A., F. Borghesan, D. Faggian, A. Secchi, and M. Plebani. 1995. Eosinophil cationic protein in tears of normal subjects and patients affected by vernal keratoconjunctivitis. *Allergy* 50:610–613.
- Lien, P. C., P. H. Kuo, C. J. Chen, H. H. Chang, S. L. Fang, W. S. Wu, et al. 2013. In silico prediction and in vitro characterization of multifunctional human RNase3. *Biomed. Res. Int.* 2013:170398.
- Lin, Y. M., S. J. Wu, T. W. Chang, C. F. Wang, C. S. Suen, M. J. Hwang, et al. 2010. Outer membrane protein I of *Pseudomonas aeruginosa* is a target of cationic antimicrobial peptide/protein. *J. Biol. Chem.* 285:8985–8994.
- Lomax, J. E., C. M. Bianchetti, A. Chang, G. N. Phillips, B. G. Fox, and R. T. Raines. 2014. Functional evolution of ribonuclease inhibitor: insights from birds and reptiles. *J. Mol. Biol.* 426:3041–3056.

- López-García, B., P. H. A. Lee, K. Yamasaki, and R. L. Gallo. 2005. Anti-fungal activity of cathelicidins and their potential role in *Candida albicans* skin infection. *J. Invest. Dermatol.* 125:108–115.
- Mallorquí-Fernández, G., J. Pous, R. Peracaula, J. Aymamí, T. Maeda, H. Tada, et al. 2000. Three-dimensional crystal structure of human eosinophil cationic protein (RNase 3) at 1.75 Å resolution. *J. Mol. Biol.* 300:1297–1307.
- Marchione, R., D. Daydé, J. L. Lenormand, and M. Cornet. 2014. ZEBRA cell-penetrating peptide as an efficient delivery system in *Candida albicans*. *Biotechnol. J.* 9:1088–1094.
- Mayer, F. L. L., D. Wilson, and B. Hube. 2013. *Candida albicans* pathogenicity mechanisms. *Virulence* 4:119–128.
- McCoy, A. J., R. W. Grosse-Kunstleve, P. D. Adams, M. D. Winn, L. C. Storoni, and R. J. Read. 2007. Phaser crystallographic software. *J. Appl. Crystallogr.* 40:658–674.
- Mochon, A. B., and H. Liu. 2008. The antimicrobial peptide histatin-5 causes a spatially restricted disruption on the *Candida albicans* surface, allowing rapid entry of the peptide into the cytoplasm. *PLoS Pathog.* 4:e1000190.
- Mohammed, I., A. Yeung, A. Abedin, A. Hopkinson, and H. S. Dua. 2011. Signalling pathways involved in ribonuclease-7 expression. *Cell. Mol. Life Sci.* 68:1941–1952.
- Molero, G., R. Díez-Orejas, F. Navarro-García, L. Monteoliva, J. Pla, C. Gil, et al. 1998. *Candida albicans*: genetics, dimorphism and pathogenicity. *Int. Microbiol.* 1:95–106.
- Nekhotiaeva, N., A. Elmquist, G. K. Rajarao, M. Hällbrink, U. Langel, and L. Good. 2004. Cell entry and antimicrobial properties of eukaryotic cell-penetrating peptides. *FASEB J* 18:394–396.
- Nicolas, P. 2009. Multifunctional host defense peptides: intracellular-targeting antimicrobial peptides. *FEBS J.* 276:6483–6496.
- Nikolovski, Z., V. Buzón, M. Ribó, M. Moussaoui, M. Vilanova, C. M. Cuchillo, et al. 2006. Thermal unfolding of eosinophil cationic protein/ribonuclease 3: a nonreversible process. *Protein Sci.* 15:2816–2827.
- Niyonsaba, F., and H. Ogawa. 2005. Protective roles of the skin against infection: implication of naturally occurring human antimicrobial agents β -defensins, cathelicidin LL-37 and lysozyme. *J. Dermatol. Sci.* 40:157–168.
- Park, C., L. W. Schultz, and R. T. Raines. 2001. Contribution of the active site histidine residues of ribonuclease A to nucleic acid binding. *Biochemistry* 40:4949–4956.
- Peschel, A., and H.-G. Sahl. 2006. The co-evolution of host cationic antimicrobial peptides and microbial resistance. *Nat. Rev. Microbiol.* 4:529–536.
- Pizzo, E., and G. D'Alessio. 2007. The success of the RNase scaffold in the advance of biosciences and in evolution. *Gene* 406:8–12.
- Pulido, D., M. Moussaoui, M. V. Nogués, M. Torrent, and E. Boix. 2013a. Towards the rational design of antimicrobial proteins: single point mutations can switch on bactericidal and agglutinating activities on the RNase A superfamily lineage. *FEBS J.* 280:5841–5852.
- Pulido, D., M. Torrent, D. Andreu, M. V. Nogués, and E. Boix. 2013b. Two human host defense ribonucleases against mycobacteria, the eosinophil cationic protein (RNase 3) and RNase 7. *Antimicrob. Agents Chemother.* 57:3797–3805.
- Rosenberg, H. F. 2008. RNase A ribonucleases and host defense: an evolving story. *J. Leukoc. Biol.* 83:1079–1087.
- Rosenberg, H. F., K. D. Dyer, and P. S. Foster. 2013. Eosinophils: changing perspectives in health and disease. *Nat. Rev. Immunol.* 13:9–22.
- Rothenberg, M. E., and S. P. Hogan. 2006. The eosinophil. *Annu. Rev. Immunol.* 24:147–174.
- Rudolph, B., R. Podschun, H. Sahly, S. Schubert, J. M. Schröder, and J. Harder. 2006. Identification of RNase 8 as a novel human antimicrobial protein. *Antimicrob. Agents Chemother.* 50:3194–3196.
- Schröder, J.-M., and J. Harder. 2006. Antimicrobial peptides in skin disease. *Drug Discov. Today Ther. Strateg.* 3:93–100.
- Singh, A., and J. K. Batra. 2011. Role of unique basic residues in cytotoxic, antibacterial and antiparasitic activities of human eosinophil cationic protein. *Biol. Chem.* 392:337–346.
- Sørensen, O. E., D. R. Thapa, K. M. Roupé, E. V. Valore, U. Sjöbring, A. A. Roberts, et al. 2006. Injury-induced innate immune response in human skin mediated by transactivation of the epidermal growth factor receptor. *J. Clin. Invest.* 116:1878–1885.
- Spencer, J. D., A. L. Schwaderer, H. Wang, J. Bartz, J. Kline, T. Eichler, et al. 2013. Ribonuclease 7, an antimicrobial peptide upregulated during infection, contributes to microbial defense of the human urinary tract. *Kidney Int.* 83:615–625.
- Spencer, J. D., A. L. Schwaderer, T. Eichler, H. Wang, J. Kline, S. S. Justice, et al. 2014. An endogenous ribonuclease inhibitor regulates the antimicrobial activity of ribonuclease 7 in the human urinary tract. *Kidney Int.* 85:1179–1191.
- Spindler, E. C., J. D. F. Hale, T. H. Giddings, R. E. W. Hancock, and R. T. Gill. 2011. Deciphering the mode of action of the synthetic antimicrobial peptide bac8c. *Antimicrob. Agents Chemother.* 55:1706–1716.
- Stalmans, S., E. Wynendaele, N. Bracke, B. Gevaert, M. D'Hondt, K. Peremans, et al. 2013. Chemical-Functional Diversity in Cell-Penetrating Peptides. *PLoS ONE* 8:e71752.
- Sundlass, N. K., C. H. Eller, Q. Cui, and R. T. Raines. 2013. Contribution of electrostatics to the binding of

- pancreatic-type ribonucleases to membranes. *Biochemistry* 52:6304–6312.
- Swidrigall, M., and J. F. Ernst. 2014. Interplay between *Candida albicans* and the antimicrobial peptide army. *Eukaryot. Cell* 13:950–957.
- Thiyagarajan, N., R. Ferguson, V. Subramanian, and R. Acharya. 2012. Structural and molecular insights into the mechanism of action of human angiogenin-ALS variants in neurons. *Nat. Commun.* 3:1114–1121.
- Torrent, M., E. Cuyás, E. Carreras, S. Navarro, O. López, A. de la Maza, et al. 2007. Topography studies on the membrane interaction mechanism of the eosinophil cationic protein. *Biochemistry* 46:720–733.
- Torrent, M., S. Navarro, M. Moussaoui, M. V. Nogués, and E. Boix. 2008. Eosinophil cationic protein high-affinity binding to bacteria-wall lipopolysaccharides and peptidoglycans. *Scan. Electron Microsc.* 47: 3544–3555.
- Torrent, M., D. Sanchez, V. Buzon, M. V. Nogués, J. Cladera, E. Boix, et al. 2009. Comparison of the membrane interaction mechanism of two antimicrobial RNases: RNase 3/ECP and RNase 7. *Biochim. Biophys. Acta* 1788:1116–1125.
- Torrent, M., M. Badia, M. Moussaoui, D. Sanchez, M. V. Nogués, and E. Boix. 2010a. Comparison of human RNase 3 and RNase 7 bactericidal action at the Gram-negative and Gram-positive bacterial cell wall. *FEBS J.* 277:1713–1725.
- Torrent, M., F. Odorizzi, M. V. Nogués, and E. Boix. 2010b. Eosinophil cationic protein aggregation: identification of an N-terminus amyloid prone region. *Biomacromolecules* 11:1983–1990.
- Torrent, M., M. V. Nogués, and E. Boix. 2011a. Eosinophil cationic protein (ECP) can bind heparin and other glycosaminoglycans through its RNase active site. *J. Mol. Recognit.* 24:90–100.
- Torrent, M., D. Pulido, B. G. De La Torre, M. F. García-Mayoral, M. V. Nogués, M. Bruix, et al. 2011b. Refining the eosinophil cationic protein antibacterial pharmacophore by rational structure minimization. *J. Med. Chem.* 54:5237–5244.
- Torrent, M., D. Pulido, M. V. Nogués, and E. Boix. 2012. Exploring New Biological Functions of Amyloids: bacteria Cell Agglutination Mediated by Host Protein Aggregation. *PLoS Pathog.* 8:2012–2014.
- Tsai, P.-W. W., Y.-L. L. Cheng, W.-P. P. Hsieh, and C.-Y. Y. Lan. 2014. Responses of *Candida albicans* to the human antimicrobial peptide LL-37. *J. Microbiol.* 52:581–589.
- Vaguine, A. A., J. Richelle, and S. J. Wodak. 1999. SFCHECK: a unified set of procedures for evaluating the quality of macromolecular structure-factor data and their agreement with the atomic model. *Acta Crystallogr. D Biol. Crystallogr.* 55:191–205.
- Vylkova, S., J. N. Sun, and M. Edgerton. 2007. The role of released ATP in killing *Candida albicans* and other extracellular microbial pathogens by cationic peptides. *Purinergic Signal.* 3:91–97.

Supporting Information

Additional supporting information may be found in the online version of this article:

Table S1. Data collection, processing and structure refinement statistics of RNase 3-H15A crystal structure solving.

Table S2. Effect of NaCl and Ca²⁺ addition on the antifungal activity of RNase 3 and RNase 7.

Figure S1. Binding of RNase 3 and RNase 7 to *Candida* cells.

Figure S2. Effects of RNase 3, RNase 3-H15A and RNase 3-W35A on *C. albicans* visualized by confocal microscopy.

Figure S3. Kinetic profile of *C. albicans* cell survival incubated with RNase 3 and RNase 7.

Figure S4. Analysis of *C. albicans* cell culture incubated with wild-type and mutant RNases by FACS.

Figure S5. Kinetic profile of cellular ATP levels of *C. albicans* incubated with RNase 3 and RNase 3-H15A.

PAPER IV

Antifungal mechanism of action at the N-terminus of the human RNases

Arranz-Trullén J^{1,2}; Salazar VA¹; Torrent M¹; Andreu D³; Pulido D^{1*} and Boix E^{1*}

¹Department of Biochemistry and Molecular Biology, Faculty of Biosciences, Universitat Autònoma de Barcelona, Cerdanyola del Vallès, Spain

²Mycobacteria Research Laboratory, Department of Biological Sciences, ISMB, Birkbeck, University of London, London, UK

³Department of Experimental and Health Sciences, Universitat Pompeu Fabra, Dr. Aiguader 88, 08003 Barcelona, Spain

*corresponding authors: Ester Boix: Ester.Boix@uab.cat;d.pulido-gomez@imperial.ac.uk

Keywords: host-pathogen interaction, antimicrobial peptides, infectious diseases, cytotoxicity, innate immunity

Abstract

As part of the ordinary human microbiome, *Candida albicans* is a polymorphic fungus able to dwell as a permanent but innocuous commensal in most healthy individuals. However, *C. albicans* occasionally can cause infections in a wide range, even reaching compromise the life of the host in the most severe cases such as systemic infections. Moreover, as *C. albicans* can persist in the host and interfere in its homeostatic responses, it is crucial to develop antifungal agents to strengthen the immune system and eradicate the pathogen without harming the host cells. In this context, antimicrobial proteins and peptides secreted by the own host immune cells are promising candidates to design novel drugs. Previous work from our laboratory indicated that several members from the vertebrate specific secretory RNases family were effective in vitro as antifungal agents. The antimicrobial RNases are small and cationic proteins secreted upon infection and endowed with diverse biological properties. Due to their direct and fast antimicrobial action, they can contribute to the host defence response and supply an essential immune barrier. Interestingly, their mechanism of action is mostly unrelated to their RNase enzymatic activity and is mostly retained at the protein N-terminus. In this context, the N-terminal derivative peptides corresponding to the eight human RNases were tested against *C. albicans* with the aim of evaluating their mechanism of action against an eukaryotic pathogen. Results corroborated that the most effective peptides corresponded to the parental proteins with reported bactericidal activity against both Gram negative and Gram positive species. The present results are in agreement with previous antifungal assays, sustaining the candidacidal activity of hRNases and demonstrate that the activity is predominantly preserved at the N-terminal region, setting antimicrobial hRNases as promising templates for the design of novel antibiotics.

Introduction

Candida albicans is one of the most common fungal pathogens. The yeast pathogenicity rate has increased nowadays along with the emergence of drug-resistant strains, urging the need for innovation and development of new effective antifungal agents. Together with the most common candidiasis in skin and mucosal infections, some fungal septic shock cases are also reported in elderly or immunosuppressed patients³. Knowledge about the complexity surrounding the wide variety of mechanisms of pathogenicity is essential for the rational development of novel antifungal agents. Antimicrobial proteins and peptides (AMPs) are considered one of the main ancestral host defence systems. Largely distributed throughout the different organism tissues, AMPs play an essential role as part of the human innate immune system, constantly protecting the body against microbial invasion and diseases^{4,5,6}. Because of their wide distribution, physicochemical features and biological activities that provide a rapid antimicrobial activity against a broad spectrum of microbes, AMPs have recently attracted significant attention as novel antibiotic candidates^{7,8,9}. Furthermore, due to their direct and multifaceted killing mechanism, the use of AMPs as antibiotics should reduce the appearance of resistant pathogens, a scenario that has been favoured by the abuse of conventional antibiotics¹⁰. In the search for novel antifungal agents, our group has recently reported that human antimicrobial RNases, a family of proteins with antipathogenic properties, are effective against the pathogenic yeast *Candida albicans* through a dual mode of action. Interestingly, the fungicidal activity of some hRNases is initiated by the binding to the pathogen cell wall, followed by their translocation and intracellular targeting¹¹. In an effort to improve, optimize and understand the killing mechanism of the N-terminal region of these proteins, which has been shown to be the antimicrobial hub and retain the parental protein antimicrobial activity, we synthesized the eight N-terminal peptides corresponding to the first 45 residues of each of the Ribonuclease A family members². Additionally, peptides corresponding to Arg to Lys and Lys to Arg substitutions for the N-terminal of the two main antimicrobial RNases (RNase 3 and 7 homologues) were synthesized in order to check the contribution of Arg/ Lys enrichment in the peptide antipathogen selectivity. A comparative approach was performed to analyse the fungicidal activity, cytotoxicity, cell wall binding and killing kinetics of hRNase-derived peptides. Previous work on Gram negative and Gram positive bacterial species corroborated that the hRNase-derived peptides retained the high antimicrobial activity of the parental hRNases showing reduced haemolysis². In this study, we demonstrate that hRNases 3, 6 and 7 derived peptides exhibited a prominent antifungal activity. Moreover, none of the hRNase-derived peptides were toxic on cultured mammalian cells. The promising results place hRNase-derived peptides in the spotlight for further therapeutic research, deepening the knowledge on the interplaying among fungal pathogens and innate host response.

Materials and Methods

Peptide synthesis

Peptides were synthesized as previously described². Fmoc-protected amino acids and HBTU [2-(1H-benzotriazol-1-yl)-1,1,3,3-tetramethyluronium hexafluorophosphate] were obtained from Iris Biotech. Fmoc-Rink-amide (MBHA) resin was from Novabiochem. HPLC-grade ACN (acetonitrile) and peptide-synthesis-grade DMF(dimethylformamide), DIEA (N,N-di-isopropylethylamine) and TFA (trifluoroacetic acid) were from Carlo Erba-SDS. Solid-phase peptide synthesis was done by Fmoc-based chemistry on Fmoc-Rink-amide (MBHA) resin (0.1 mmol) in a model 433 synthesizer (Applied

Biosystems) running FastMoc protocols. Couplings used an 8-fold molar excess each of Fmoc-amino acid and HBTU and a 16-fold molar excess of DIEA. Side chains of trifunctional residues were protected with t-butyl (aspartate, glutamate, serine, threonine and tyrosine), t-butyloxycarbonyl (lysine and tryptophan), 2,2,4,6,7- pentamethyldihydrobenzofuran-5-sulfonyl (arginine) and trityl (asparagine, glutamine and histidine) groups. After chain assembly, full deprotection and cleavage were carried out with TFA/water/tri-isopropylsilane (95:2.5:2.5, by vol.) for 90 min at room temperature (25 °C). Peptides were isolated by precipitation with ice-cold diethyl ether and separated by centrifugation (3000 g for 20 min at 4 °C), dissolved in 0.1 M acetic acid, and freeze-dried. Analytical reversed-phase HPLC was performed on a Luna C18 column (4.6 mm × 50 mm, 3 μm; Phenomenex). Linear 5– 60% gradients of solvent B (0.036% TFA in ACN) into solvent A (0.045% TFA in water) were used for elution at a flow rate of 1 ml/min and with UV detection at 220 nm. Preparative HPLC runs were performed on a Luna C18 column (21.2 mm × 250 mm, 10 μm; Phenomenex), using linear gradients of solvent B (0.1% in ACN) into solvent A (0.1%TFA in water), as required, with a flow rate of 25 ml/min. MALDI–TOF mass spectra were recorded in the reflector or linear mode in a Voyager DE-STR workstation (Applied biosystems) using an α-hydroxycinnamic acid matrix. Fractions of adequate (>90%) HPLC homogeneity and with the expected mass were pooled and freeze-dried for subsequent experiments. Recombinant hRNase 3 was expressed and purified as previously described¹¹.

***Candida albicans* growth conditions**

C. albicans (ATCC 90028) cells were maintained at -80°C (15% glycerol) and incubated overnight with agitation at 30°C in Sabouraud Dextrose broth (mycological peptone, glucose, pH 5.6, Fluka- Sigma S3306). Previous to each assay, cells were subcultured for ~ 2-3 h to yield a mid-logarithmic culture.

Minimum fungicidal concentration

C. albicans ATCC 90028 was cultured overnight in Sabouraud Dextrose broth at 30°C and subcultured the next day in fresh Sabouraud and grow to an optical density of 0.4 at 600 nm (mid log-phase). Cells were washed twice in nutrient broth or PBS, and diluted to $\approx 2 \times 10^6$ cells/mL. Peptides serially diluted were added to 2×10^5 cells from 20 to 0.1 μM final concentration. *C. albicans* was incubated at 30°C during 4 hr in Sabouraud nutrient broth, PBS or 10 mM sodium phosphate buffer, pH 7.5. Following, the samples were plated onto Sabouraud Petri dishes and incubated at 30°C overnight. Antifungal activity was expressed as the MFC, defined as the lowest peptide concentration required for more than 99% of microorganism killing. MFC of each protein was determined from two independent experiments performed in triplicate for each concentration.

Minimal agglutination activity (MAC)

C. albicans cells were grown at 30°C to an OD₆₀₀ of 1.0, cells were then diluted to an OD₆₀₀ of 0.1, centrifuged at 5,000 xg for 2 min, and resuspended either in 1X PBS or Sabouraud nutrient broth. An aliquot of 100 μl of the cellular suspension was treated with increasing peptide concentrations (from 0.01 to 20 μM) and incubated at 30°C for 1-4 hr. The aggregation behaviour was observed by visual inspection, and the agglutinating activity is expressed as the minimum agglutinating concentration of the sample tested, as previously described¹².

Cell viability assay

Antimicrobial activity was also assayed by following the cell viability of *C. albicans*, using the BacTiter-Glo™ Microbial Cell Viability kit (Promega), which measures the number of viable fungal cells, by ATP quantification. ATP, as an indicator of metabolically active cells, is indirectly measured by a coupled luminescence detection assay. The luminescent signal is proportional to the amount of ATP required for the conversion of luciferin into oxyluciferin in the presence of luciferase. An overnight culture of *C. albicans* was used to inoculate fresh Sabouraud liquid culture, and logarithmic phase culture was grown to an OD600 of 0.2. hRNase derived N-terminal peptides were added to 0.1 ml of cell culture at a final concentration from 0.025 to 20 µM. The *C. albicans* viability was followed after 4h of incubation at 37°C. 50 µl of incubation culture were mixed with 50 µl of BacTiter-Glo™ reagent in a microtiter plate following the manufacturer instructions and incubated at room temperature for 10 min. Luminescence was read on a Victor3 plate reader (PerkinElmer, Waltham, MA) with a 1-s integration time. IC50 values were calculated by fitting the data to a dose-response curve.

Cell survival assay

C. albicans viability assay was performed using the Live/DeadR microbial viability kit as previously described¹³. *Candida* strain was grown at 37°C to $\sim 5 \times 10^6$ cells/ml, centrifuged at 5000 xg for 5 min and resuspended in a 0.85% NaCl solution, in accordance with the manufacturer instructions. *C. albicans* cell culture was stained using a SYTO®9/propidium iodide 1:1 mixture. SYTO®9 is a DNA green fluorescent dye that diffuses thorough intact cell membranes and propidium iodide is a DNA red fluorescent dye that can only access the nucleic acids of membrane damaged cells, displacing the DNA bound SYTO®9. The method allows the labelling of intact viable cells and membrane compromised cells, which are labelled in green and red respectively, referred to as live and dead cells. The viability kinetics was monitored using a Cary Eclipse Spectrofluorimeter (Varian Inc., Palo Alto, CA, USA). Cell viability profiles were registered after adding from 1 to 5 µM of final peptide concentration. To calculate the cell viability, the fluorescence in the range of 510 - 540 nm and 620 - 650 nm were integrated to obtain the SYTO®9 (live cell) and the propidium iodide (dead cell) signals respectively. Then, the percentage of live bacteria was represented as a function of time.

Cell membrane depolarization assay

Membrane depolarization was assayed by monitoring the DiSC3 fluorescence intensity change in response to changes in transmembrane potential as described previously¹⁴. *Candida albicans* cells were grown at 37°C to the mid-exponential (OD~0.4) and resuspended in 5 mM Hepes-KOH, 20 mM glucose and 100 mM KCl at pH 7.2. DiSC3 was added to a final concentration of 0.4 µM. Changes in the fluorescence for alteration of the cell plasma membrane potential were continuously monitored at 20 °C at an excitation wavelength of 620 nm and an emission wavelength of 670 nm. When the dye uptake was maximal, as indicated by a stable reduction in the fluorescence as a result of quenching of the accumulated dye in the membrane interior, protein in 5 mM Hepes-KOH buffer at pH 7.2 was added at a final peptide concentration from 1 to 5 µM and incubated for 50 min. Maximum depolarization was calculated when the fluorescence signal was fully stabilized and the depolarization percentage was calculated taking Triton X-100 at 10% as a positive control. The time required to reach a stabilized maximum fluorescence reading was recorded for each condition, and

the time required to achieve half of total membrane depolarization was estimated from the nonlinear regression curve. All conditions were assayed in duplicate.

Cell membrane permeabilization activity

Membrane permeabilization was evaluated by using the Sytox® Green uptake assay. Sytox® Green is a cationic cyanine dye (≈ 900 Da) that is not membrane permeable. When cells plasma membrane integrity is compromised, influx of the dye, and subsequent binding to DNA, causes a large increase in the fluorescence signal. For Sytox® Green assays, *Candida albicans* cells were grown to mid-exponential growth phase at 37°C and then centrifuged, washed, and resuspended in PBS. Cell suspensions in PBS ($\sim 2 \times 10^6$ cells/mL) were incubated with 1 $\mu\text{mol/L}$ Sytox® Green for 15 min in the dark prior to the influx assay. At 2 to 4 min after initiating data collection, proteins at 1 and 5 $\mu\text{mol/L}$ final concentration were added to the cell suspension, and the increase in Sytox® Green fluorescence was measured (excitation wavelength at 485 nm and emission at 520 nm) for 50 min in a Cary Eclipse spectrofluorimeter. Bacterial cell lysis with 10% Triton X-100 was taken as the maximum fluorescence reference value.

Cell binding assay

Candida albicans cells were cultured overnight in Sabouraud Dextrose broth at 37°C and subcultured the next day in fresh Sabouraud and grow to an optical density of 0.4 at 600 nm (mid log-phase). Cells were washed twice in PBS, and diluted to $\sim 2 \times 10^6$ cells/mL. Cells and β -1,3-Glucan (0.4mg/mL) (ref. 89862, Sigma) were respectively incubated in 100 μL of PBS at 37°C with hRNase 3 and the N-terminal derived peptide at 1 $\mu\text{mol/L}$ final concentration during different periods of time up to 1 h. Following, the samples were centrifugated at 13000 rpm. The supernatant samples were concentrated using 10 kDa cut-off filters to 20 μL . The presence of the proteins and peptide was checked by 15%-18% SDS-PAGE and Coomassie Blue staining. Reference protein controls were treated following the same protocol in the absence of cells.

Cytotoxicity assay

The assay was performed in 96-well cell culture flat-bottom plates (Costar; Appleton Woods) in triplicate. Proteins or peptides were serially diluted from 50 to 0.1 μM (100 μl) in each well. To each well, 100 μL of diluted RAW 264.7 and THP1 cells (NCTC #91062702) and #88081201 respectively) (5×10^5 cells/mL) was added. After 48 h of incubation, the monocytes were washed twice with 1X PBS, and fresh RPMI-1640 complete medium was added. Plates were then treated with 30 μl of a freshly prepared 0.01% resazurin solution and incubated overnight at 37°C. The following day the change in colour was observed and the fluorescence intensity was measured (λ_{ex} 560 nm, λ_{em} 590 nm, FLUOstar OPTIMA microplate reader; BMG LABTECH GmbH). The 50% growth inhibitory concentration (GIC_{50}) was determined based on a resazurin fluorescence assay.

Results

Peptides design and physicochemical characterization

The hRNase-derived peptides were designed taking as a reference the 1–45 segment in hRNase 3, based on previous work in our laboratory that defined the protein minimal domain retaining full antimicrobial properties^{15,16,2}. Here, the eight N-terminal peptides, comprising equivalent structural regions of the human canonical RNases N-termini [residues 1–45 of hRNases 2, 6, 7 and 8; residues

1–48 of hRNases 1 and 4; and residues 1–47 of RNase 5; Table 1] were selected for synthesis. In all cases, the peptides included the first two α -helices as well as a short first β -strand from the parental protein. As applied previously¹⁷, the two cysteine residues present at the N-terminal region, disulfide-linked to a distant cysteine residue in the native protein, were replaced by isosteric serine residues. Complementarily, Lys/Arg hRNase N-terminal derived peptides were engineered for hRNase 3 and hRNase 7 peptides, that incorporate Arg to Lys substitutions for hRNase 3 and Lys to Arg substitutions for hRNase 7, named as 3K and 7R respectively. The measured molecular weights, antimicrobial effectivity, cytotoxicity and key physicochemical parameters of the peptides are summarized in table 1. It is noteworthy to underline the high pI and the degree of hydrophobicity of these peptides (Table 1), showing values within the standard range of most-known AMPs¹⁸ which are considered essential for their functional activity¹⁹. Table 1 also includes an estimation of the antimicrobial activity of their respective parental hRNases. It is important to note that the effective values for both haemolysis (shown in previous studies²) and cytotoxicity on mammalian cells (Table 1) are only shown at more than 10x the achieved antimicrobial values, indicating a good therapeutic index. Therefore, results would support specificity towards microbial forms, without any compromise to the viability of the host cells.

Table 1 Foremost features of the hRNase-derived peptides

Peptide [†]	Sequence	Hydrophobicity	pI	Protein Antimicrobial activity* [‡]	Citotoxicity (RAW/THP1) (GIC ₅₀ , μ M [§])
RN1	---KESRAKKFQRQHMDSDSSPSSSTYSNQMMRRRNMTQGRSKPVNTFVH	-1.575	11.40	n.r	>50/>50
RN2	KPPQFTWAQWFETQHINMTSQ-----QSTNAMQVINNYQRRSKNQNTFLL	-1.069	10.28	-	>25/>50
RN3	RPPQFTRAQWFATQHISLNPP-----RSTIAMRAINNYRWRSKNQNTFLR	-0.764	11.88	+++ [‡]	>25/>50
RN3K	KPPQFTKAQWFATQHISLNPP-----KSTIAMKAINNYKWKSKNQNTFLK	-0.824	11.02	+++	>25/>50
RN4	--QDGMY-QRFLRQHVHPEET-GGSDRYSNLMMQRRKMTLYHRSKRFNTFIH	-1.228	10.15	n.r	>50/>50
RN5	--QDNSRYTHFLTQHYDAKPQ-GRDDRYSESIMRRRGLTS-PSKDINTFIH	-1.430	9.40	-	>50/>50
RN6	WPKRLTKAHWFETQHIQPSPL-----QSNRAMSGINNYTQHSKHQNTFLH	-1.096	10.45	+++	>25/>50
RN7	KPKGMTSSQWFKIQHMQPSPQ-----ASNSAMKNINKHTKRSKDLNTFLH	-1.209	10.75	+++ [‡]	>25/>50
RN7R	RPRGMTSSQWFRIQHMQPSPQ-----ASNSAMRNINRHTRRSRDLNTFLH	-1.302	12.88	+++	>25/>50
RN8	KPKDMTSSQWFKTQHVQPSPQ-----ASNSAMSIINKYTERSKDLNTFLH	-1.044	9.70	+	>50/>50

*Antimicrobial activity of the parental proteins tested against bacterial strains, obtained from^{2,20}.

[‡] Antifungal activity of parental proteins assayed previously against *C. albicans*¹¹

[†] The N-terminal derived peptides are numbered according to their respective parental proteins, K and R indicate Lys and Arg peptide enrichment.

[§] Taken from³³

Candidacidal activity of hRNases is retained at the N-terminus

Previous work in our laboratory indicated a high candidacidal activity for hRNases 3, 6 and 7¹. Here, we report the antifungal activity of the eight N-terminal peptides corresponding to the eight human canonical RNases. First, the minimum fungicidal concentration (MFC) against infective *Candida albicans* was determined. MFC values are summarized in Table 2. Five peptides (1, 3, 4, 6 and 7) were found active against *C. albicans*, with MFC ranging from 0.6 to 4 μ M, a range close to that observed for the previously tested hRNases¹¹. On the other hand, peptides 2, 5 and 8 were inactive. When these results on *Candida* (Table 1) were compared with the available literature data on the bactericidal activity of hRNases², similar results between the antimicrobial activities of the two sets of data were found. Accordingly, we confirm that the candidacidal activity of hRNases is highly preserved at the N-terminus.

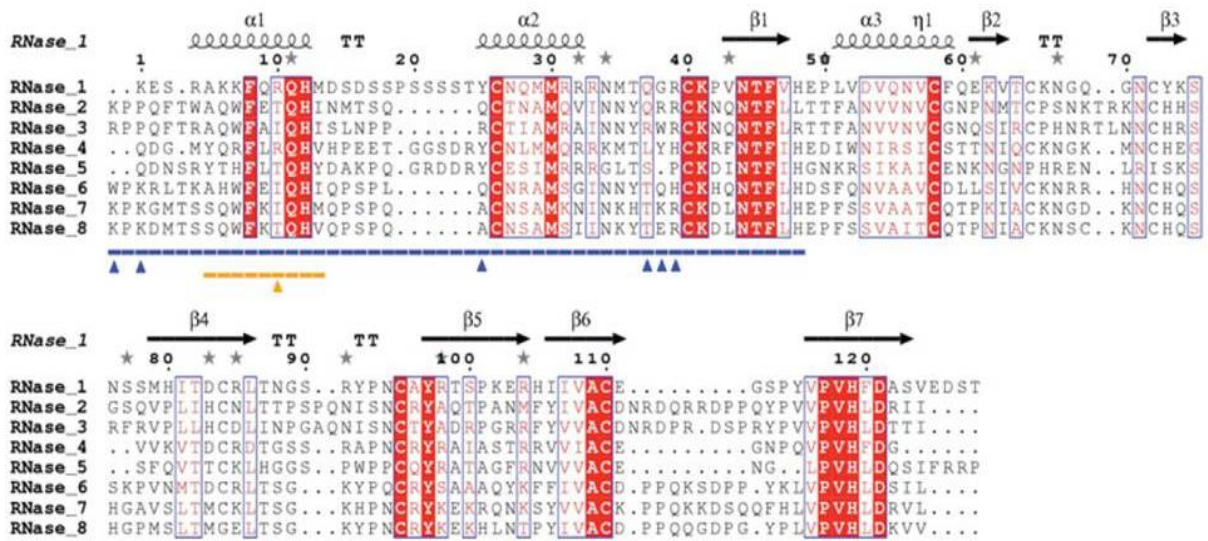


Figure 1. Sequence alignment of hRNases. Conserved regions are boxed; highly conserved amino acids are coloured in white over a red background, whereas moderately conserved amino acids regions are coloured in red. The secondary structure of hRNase 3 is displayed as a reference on top of the alignment. The N-terminal antimicrobial domain is highlighted in blue and the agglutination-promoting region in yellow. Arrows denote key residues in both regions. Taken from ².

Another specific feature of AMPs, already described for hRNase 3 and its N-terminal domain ²¹, is the ability to agglutinate bacteria, a property proposed to facilitate the removal of the infection focus. Supporting this fact, we previously reported that hRNases are able to agglutinate *C. albicans* ¹¹. In order to check whether hRNase-derived peptides also share this property against *C. albicans*, their MAC was determined (Table 2). Surprisingly, all peptides showed aggregation properties at low concentration (< 2 μ M), even in the cases where the parental protein was inactive, suggesting that the required features for the yeast cells is shared by all hRNases N-terminus. In any case, after incubation of *C. albicans* cell cultures with the hRNase-derived peptides, the most significant agglutination was observed for peptide 3, as previously observed in studies with Gram negative bacteria cultures ². Secondarily, peptides 2, 4 and 6 also displayed significant activity. However, when comparing MAC results between *C. albicans* and *E. coli* ² we could only observe a positive agreement for peptides 3 and 6, being the two more agglutinating peptides within the family. Interestingly, data showed best MAC values in the case of *C. albicans*, suggesting that the peptides would have a greater affinity for fungi wall components.

Table 2. Antifungal activities of hcrNases peptides on *Candida albicans*

hcrNase peptide	MFC ₁₀₀ (μM)		IC ₅₀ (μM)	MAC (μM)
	Sabouraud broth	PBS		
RN1	3.75 ± 0.50	3.75 ± 0.30	2.10 ± 0.20	1.80 ± 0.40
RN2	>20	>20	>20	0.40 ± 0.10
RN3	0.62 ± 0.20	0.62 ± 0.10	0.22 ± 0.05	< 0.1
RN3K	4.25 ± 0.30	4.25 ± 0.30	2.08 ± 0.27	< 0.1
RN4	4.00 ± 0.50	3.75 ± 0.20	1.80 ± 0.30	0.40 ± 0.10
RN5	>20	>20	>20	1.80 ± 0.40
RN6	2.00 ± 0.50	1.75 ± 0.30	1.80 ± 0.20	0.40 ± 0.10
RN7	0.93 ± 0.20	0.93 ± 0.10	0.45 ± 0.10	0.90 ± 0.30
RN7R	2.83 ± 0.10	2.83 ± 0.10	1.62 ± 0.32	ND ¹
RN8	>10	>10	>10	0.90 ± 0.20

Minimal fungicidal concentration (MFC₁₀₀) was determined as the lowest concentration of peptide that killed at least 99.9% of the initial inoculum. Values were calculated by CFU counting on plated Petri dishes as described in the methodology. *C. albicans* cultures were treated with the proteins diluted in either the Sabouraud nutrient growth media or in a phosphate saline buffer (PBS). IC₅₀ was determined using the Bactiter-Glo™ kit as detailed in the Experimental Procedures. Values are averaged from three replicates of two independent experiments. Values are given as mean ± SEM.

¹ND: Not detected even at the highest assayed peptide concentration (20μM).

To characterize the cell selectivity of peptides 1-8, both haemolytic activity² and cytotoxicity were tested on sheep RBCs and RAW 264.7/THP1 cell lines respectively. Previous results indicated that active peptides against *Candida albicans* (1, 3-4 and 6-8) showed haemolytic activities between 10 and 20 μM, whereas no haemolysis was detected for peptides 2 and 5)². Potential toxicity to host cells was previously checked through the resazurin fluorescence assay using mice macrophage and human monocyte cell lines. All hRNase-derived peptides showed no toxicity at the maximum tested concentration (25/50 μM for RAW and THP1 cells respectively (see Table 1). The effective fungicidal concentrations were at least two orders of magnitude lower than the haemolytic and cytotoxicity values. Therefore, results would support specificity towards microbial forms, without any compromise to the viability of the host cells, presenting the derivatives peptides as useful candidates for antifungal therapies.

Additionally, RN3K and RN7R peptides were synthesized in order to check whether antifungal effectiveness was altered by the substitution of Lys or Arg residues respectively. There were significant differences in terms of antifungal effectiveness between RN3K and RN7R when compared with their standard non-modified N-terminal derived peptides, which showed lower MFC values. On the other hand, further work would be necessary to confirm the null aggregation capacity of RN7R.

The antifungal mechanism of hcrNase-derived peptides relies on a cell envelope assault

As reported in previous work on antimicrobial hRNases, one of the first steps to counteract the microbe invasion is based on the cell wall binding and membrane destabilization²². In an effort to characterize the antifungal mechanism of hRNase-derived peptides 1-8, we assessed their capacity to depolarize and permeabilize *C. albicans* cytoplasmic membranes. Results showed that overall most of the peptides that were shown to be more active against *C. albicans* stated high membrane permeabilization and depolarization values (Table 3), which are in agreement with previous

depolarization and leakage values in both Gram negative and Gram positive bacteria species². However, permeabilization ability is slightly reduced for hRNase 1, 2 and 4 peptides (Table 3). For a better characterization of the mechanism, we compared the kinetics of the killing process by hCRNase-derived peptides as well as the cell survival rates (Table 4). At a fixed peptide concentration, nearby the estimated MFC values (2 μ M), only the peptides 3, 6 and 7 could reach a significant activity. RN3 showed the best values in terms of cell survival, depolarization and permeabilization, followed by RN7 and RN6.

Table 3. Cell membrane depolarization and permeabilization activities of hCRNases peptides on *Candida albicans*.

hCRNase peptide	Membrane Depolarization		Membrane Permeabilization
	ED ₅₀ (μ M)	Depol _{max} *	Perm. (%) ¹
RN1	4.63 \pm 0.70	65.2 \pm 4.6	8.3 \pm 0.4
RN2	3.63 \pm 1.20	28.6 \pm 5.7	12.4 \pm 0.2
RN3	0.60 \pm 0.40	100 \pm 3.2	73.2 \pm 1.1
RN4	3.58 \pm 1.60	76.2 \pm 4.8	38.7 \pm 0.1
RN5	1.51 \pm 10	39.1 \pm 5.1	21.8 \pm 0.4
RN6	0.62 \pm 0.10	86.2 \pm 5.2	48.4 \pm 0.8
RN7	0.53 \pm 0.18	71.5 \pm 3.7	53.9 \pm 0.5
RN8	0.15 \pm 0.20	36.1 \pm 4.4	11.2 \pm 0.2

*Maximum fluorescence value reached at the final incubation time with 2 μ M of the peptides. Membrane depolarization and permeabilization were performed using the membrane potential-sensitive DiSC3 fluorescent probe and Sytox® Green, respectively, as described in the Methodology. Values are given as mean \pm SEM.

¹The calculated percentages refer to the maximum values achieved at final incubation time, referred to the positive control (10 % of Triton X-100). All values are averaged from three replicates of two independent experiments.

Two main layers can be distinguished in *C. albicans* cell wall; an outer layer composed mainly by glycoproteins and an inner layer in which polysaccharides predominate. These polysaccharides confer stiffness and favour the cell shape. Beta-1,3 glucan, beta-1,6 glucan and chitin are the prevailing polysaccharides, comprising 40%, 20% and 2% of the cell wall dry weight respectively²³.

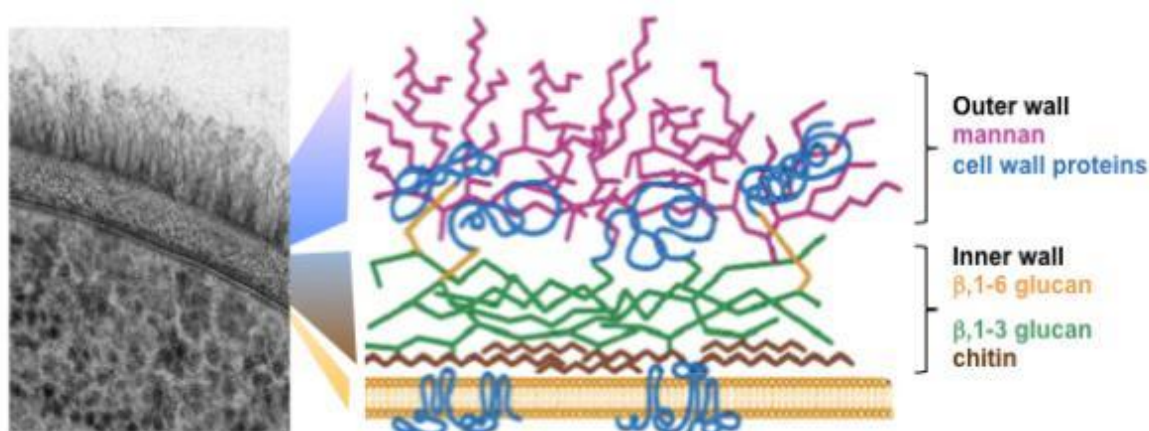


Figure 2. Structure of *Candida albicans* cell wall. Taken from³⁴.

As hRNase 3 was previously proven to bind to different bacterial cell wall components such as lipopolysaccharide (LPS) and peptidoglycans^{13,16}, as well as heterosaccharides present at the eukaryote extracellular matrix^{24,25}, we complementarily assessed the ability of hRNase 3 and its N-terminal derived peptide, selected as the most antimicrobial active member of the family, to bind both *C. albicans* cells and the beta-1,3-Glucan, a major component of the fungi cell wall. Results shown in Figure 3 confirm that hRNase 3, as well as the N-terminal derived peptide, are able to bind to the *C. albicans* cell wall and that the binding percentage increases as a function of the incubation time. On the other hand, hRNase derived N-terminal peptides were previously reported to have the ability to bind anionic liposomes and trigger the vesicles lysis². Moreover, a positive correlation is observed regarding the lytic activity of RNases 3, 4, 6 and 7 both in bacteria, liposomes and *C. albicans*¹, corroborating that these peptides share the characteristic AMPs features, displaying an unspecific antimicrobial activity against both prokaryotic and eukaryotic pathogens.

Table 4. Comparison of calculated time to achieve 50 % activity (t_{50}) for membrane depolarization, membrane permeabilization and cell survival.

hRNase peptide	Membr. depolarization	Membr. permeabilization	Cell survival	Cell survival
	t_{50} (min)		Cell survival (%)	
RN1	16 ± 2.3	28.1 ± 2.5	56.6 ± 2.6	66.6 ± 1.1
RN2	18 ± 3.8	26.6 ± 3.2	44.7 ± 1.3	72.5 ± 0.6
RN3	1.6 ± 0.3	4.2 ± 0.7	14.7 ± 0.7	15.0 ± 1.7
RN4	12 ± 1.7	18.3 ± 2.6	25.2 ± 1.2	65.2 ± 9.7
RN5	19 ± 2.4	34.7 ± 4.2	62.5 ± 2.2	39.5 ± 0.3
RN6	5.6 ± 1.2	8.4 ± 1.8	22.4 ± 1.4	25.7 ± 2.2
RN7	4.2 ± 0.8	6.1 ± 1.5	17.0 ± 0.8	12.0 ± 1.1
RN8	21 ± 3.2	35.0 ± 4.8	50.7 ± 1.7	27.8 ± 1.2

All assays were carried out at 2 μ M final protein concentration. Depolarization was assayed using DISC3 dye, cell leakage by the Sytox[®] Green assay and survival percentage at final incubation time (120 min) was evaluated using the Live/dead[®] kit. 50 % effective time (t_{50}) is given as mean \pm SEM, averaged from three replicates of two independent experiments.

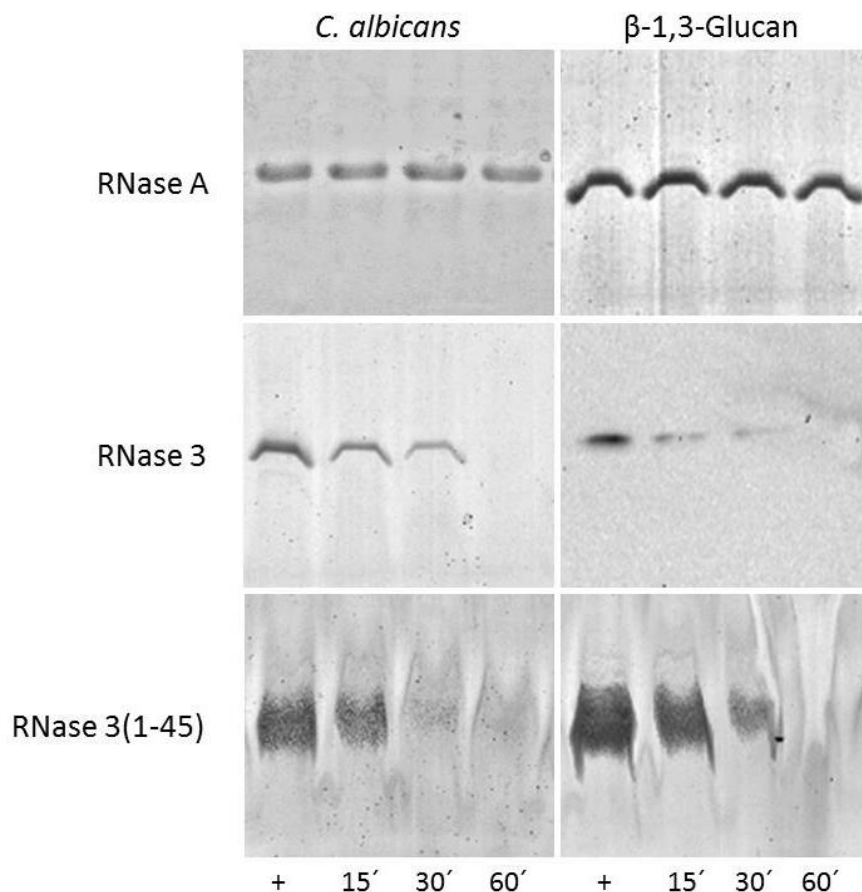


Figure 3. Binding of hRNase 3 peptide to *C. albicans* and β -1,3-Glucans. RNase A was taken as a negative control for cell and β -1,3-Glucan binding, respectively. *C. albicans* cells and β -1,3-Glucan were incubated at different time (15, 30 and 60 min) with the proteins and peptide. The supernatant soluble fraction was collected and applied to the gel as described in the Experimental Procedures. Supernatant represents the soluble fraction, which contains the unbound protein/peptide, while the pellet is the insoluble fraction containing the bound protein or peptide. 15% and 18% SDS-PAGE were respectively used to separate the protein and peptide fractions. Protein and peptide were independently loaded to the gel as positive controls (+).

Discussion

Several members of the RNase A superfamily show antimicrobial features apparently unrelated to their catalytic activity^{16,20}. In an attempt to deepen the understanding of their biological role it has been suggested that RNases might have emerged as a host-defence family in vertebrate evolution^{2,26}. As commented above, previous studies on RNase A family members have revealed that the antimicrobial activity is retained by their N-terminal fragments^{16,2}. The 1-45 segment includes in RNase 3 the first two α -helices as well as a short β -strand from the parental protein, although RMN studies indicate that the peptide in solution adopts a unique extended α helix^{24,15} (Figure 1). Figure 4 illustrates how the helical secondary structure would provide to the final N-terminal peptide a characteristic amphipathic nature. Comparative evolution studies across different lineages of vertebrate RNases suggested that the N-terminal region has retained a host defence role along evolution². Structural comparison of the structure of N-terminal domain of RNase 3 solved by NMR²⁴ and the comparative CD analysis of the eight hRNases peptides indicated that without sharing a high sequence identity all the peptides adopt an equivalent α helical structuration². Noteworthy, as

reported for many other AMPs²⁷, the eight peptides were mostly unstructured when free in an aqueous solution and increased their α -helical content in the presence of a membrane like environment².

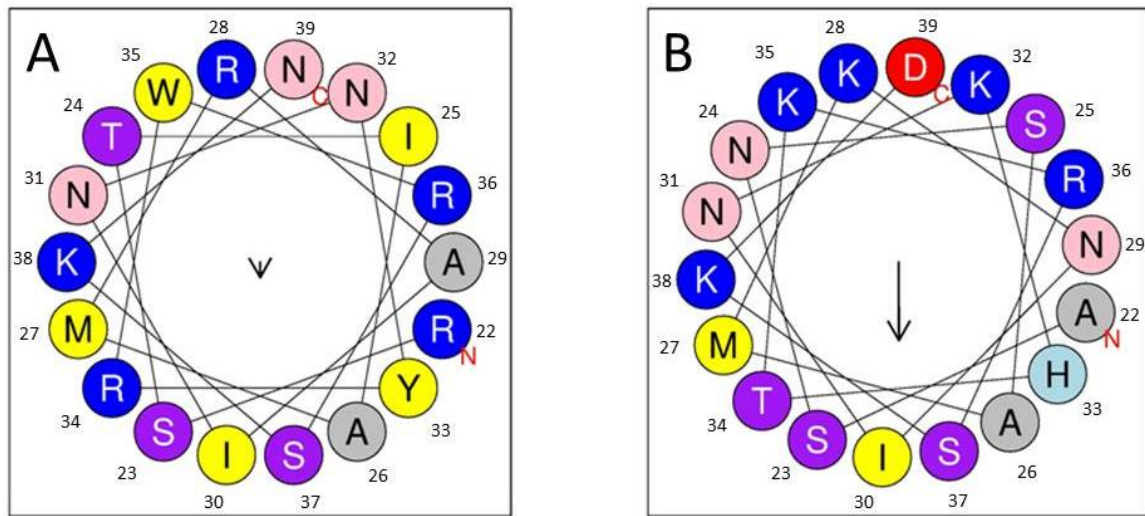


Figure 4. Helical wheels of RNase 3(A) and RNase 7(B) N-termini peptides considering a unique α -helix encompassing residues 22 to 40 as predicted by RMN for RNase 3 (drawn by heliquest²⁸). Cationic residues are highlighted in blue, uncharged residues in grey, polar residues in purple, nonpolar residues in yellow, polar/uncharged residues in pink and anionic residues in red. N- terminal and C-terminal domains are designated with N and C letters respectively. Taken from²⁴

In order to expand the knowledge of the mechanism of action of hRNases against *Candida albicans*, which has been recently observed to take place by a dual mode¹¹, we aimed to thoroughly characterize the antifungal properties of the hRNase derived N-terminal peptides. This comparative study of the N-terminal region of the hRNases against a human eukaryotic pathogen such as *Candida albicans* has allowed us to deepen in the mechanism of action of these proteins and confirm again that the antimicrobial activity of hRNases is preserved at their N-terminal domain. The present results show a high antifungal activity, showing MFC values at sub micro molar range for all tested derivative peptides, with the RNase N-terminal derived peptides 3, 6 and 7 being the most effective ones (Table 1). These results are in agreement with previous studies where the parental proteins were tested against *C. albicans*¹¹ and the derivative peptides assayed against different Gram-negative/Gram-positive bacterial species^{2,15,16,29}. Another specific feature of the N-terminal peptides is the cell agglutinating ability, proposed as a mechanism to contain the pathogens at the infection focus^{25,12}. However, no clear correlation was observed between the present results on *Candida* cells agglutination and previous studies working with bacteria cultures. Whereas in the present results we have seen *Candida* clumping by RNases 2 and 7 N-terminal peptides, previous studies reported the absence of bacterial agglutination for both proteins and their N-terminal peptides^{30,2}. Overall, higher agglutination activities are observed for *Candida* cells. Previous work identified aggregation prone domains at the N-terminus of RNases, showing a correlation between positive agglutination values and the sequences aggregation propensity². Besides, the bacteria cell agglutination was also observed to be enhanced by the LPS interaction¹². We report here evident binding of RNase 3 and its derived peptide for both *Candida* cells and their main cell wall component (figure 3). Further work is to be carried out to evaluate the distinct binding affinities towards other cell wall components. Additionally, due to the overabundance of lysine and arginine residues in hRNase 7 and 3

respectively (figure 1), another objective of this work was to elucidate whether this relative abundance is related to a selectivity towards prokaryotic or eukaryotic pathogens. Towards this goal, hRNase 7 and hRNase 3 N-terminal peptides were synthesized by exchanging the lysines by arginines and backwards respectively. There is evidence in the literature about the importance of some residues that favours endocytosis. It has been suggested that the quantity of Arg and Lys residues as well as their ratio and distribution seem to be essential in some AMPs and cell penetrating peptides (CPPs) for cellular uptake³¹. Interestingly, Arg content in peptides facilitated the mammalian cellular uptake and improved their cytotoxic activity. However, not only the cationic residue composition of peptides was found to be imperative, but also the sequence in addition to peptide conformation have a high impact in the effectiveness of AMPs to cross eukaryotic membranes and target internalized pathogens³². In our case, RNase 3 and 7 analogs were not shown to be more effective than their respective reference peptides. Complementary, recent comparative studies on the eight RNase peptides using an infected macrophage model are showing that the RNase 3, 6 and 7 N-terminal derived peptides are the only ones that effectively reduced the growth of resident micobacteria in an ex vivo macrophage infected model³³. Overall, both depolarization and membrane permeation results observed for the eight parental RNase peptides against *C. albicans* were in agreement with those previously published using different bacterial strains², showing that RN3, 6 and 7 are the most antimicrobially effective.

In conclusion, results obtained here correlated well with those obtained from previous candidacidal assays, suggesting that the antifungal mechanisms are consistently conserved at the N-termini of the antimicrobially active hRNases and designate peptides 3, 6 and 7 as the best candidates to develop antifungal agents.

Acknowledgements

The authors wish to thank the Laboratori d'Anàlisi i Fotodocumentació (UAB), where spectrofluorescence assays were performed. We also would like to thank Javier Valle (UPF) for his contribution in the peptide synthesis. JAT was the recipient of a UAB predoctoral fellowship. Experimental work was supported by the *Ministerio de Economía y Competitividad* (Grants BFU2012-38695 and SAF2015-66007P) co-financed by FEDER funds and *Generalitat de Catalunya* (Grant 2014-SGR-728).

References

1. Salazar, V. A. *et al.* Exploring the mechanisms of action of human secretory RNase 3 and RNase 7 against *Candida albicans*. *Microbiologyopen* (2016). doi:10.1002/mbo3.373
2. Torrent, M. *et al.* Ribonucleases as a host-defence family: evidence of evolutionarily conserved antimicrobial activity at the N-terminus. *Biochem. J.* **456**, 99–108 (2013).
3. Jabra-Rizk, M. A. *et al.* *Candida albicans* Pathogenesis: Fitting Within the ‘Host-Microbe Damage Response Framework’. *Infect. Immun.* (2016). doi:10.1128/IAI.00469-16
4. Zasloff, M. Antimicrobial peptides of multicellular organisms. *Nature* **415**, 389–95 (2002).
5. Zasloff, M. Antimicrobial peptides in health and disease. *N. Engl. J. Med.* **347**, 1199–200 (2002).
6. Gordon, Y. J., Romanowski, E. G. & McDermott, A. M. A review of antimicrobial peptides and

- their therapeutic potential as anti-infective drugs. *Curr. Eye Res.* **30**, 505–15 (2005).
7. Wang, G., Li, X. & Wang, Z. APD2: the updated antimicrobial peptide database and its application in peptide design. *Nucleic Acids Res.* **37**, D933-7 (2009).
 8. Boman, H. G. Antibacterial peptides: basic facts and emerging concepts. *J. Intern. Med.* **254**, 197–215 (2003).
 9. Fosgerau, K. & Hoffmann, T. Peptide therapeutics: Current status and future directions. *Drug Discov. Today* **20**, 122–8 (2014).
 10. Batoni, G., Maisetta, G., Brancatisano, F. L., Esin, S. & Campa, M. Use of antimicrobial peptides against microbial biofilms: advantages and limits. *Curr. Med. Chem.* **18**, 256–79 (2011).
 11. Salazar, V. A. *et al.* Exploring the mechanisms of action of human secretory RNase 3 and RNase 7 against *Candida albicans*. *Microbiologyopen* 1–16 (2016). doi:10.1002/mbo3.373
 12. Pulido, D. *et al.* Antimicrobial action and cell agglutination by the eosinophil cationic protein are modulated by the cell wall lipopolysaccharide structure. *Antimicrob. Agents Chemother.* **56**, 2378–2385 (2012).
 13. Torrent, M. *et al.* Comparison of human RNase 3 and RNase 7 bactericidal action at the Gram-negative and Gram-positive bacterial cell wall. *FEBS J.* **277**, 1713–1725 (2010).
 14. Torrent, M., Navarro, S., Moussaoui, M., Nogués, M. V. & Boix, E. Eosinophil cationic protein high-affinity binding to bacteria-wall lipopolysaccharides and peptidoglycans. *Biochemistry* **47**, 3544–55 (2008).
 15. Torrent, M. *et al.* Refining the eosinophil cationic protein antibacterial pharmacophore by rational structure minimization. *J. Med. Chem.* **54**, 5237–5244 (2011).
 16. Torrent, M., de la Torre, B. G., Nogués, V. M., Andreu, D. & Boix, E. Bactericidal and membrane disruption activities of the eosinophil cationic protein are largely retained in an N-terminal fragment. *Biochem. J.* **421**, 425–434 (2009).
 17. Rosenberg, H. F. Recombinant human eosinophil cationic protein. Ribonuclease activity is not essential for cytotoxicity. *J. Biol. Chem.* **270**, 7876–81 (1995).
 18. Wang, G., Li, X. & Wang, Z. APD3: the antimicrobial peptide database as a tool for research and education. *Nucleic Acids Res.* **44**, (2016).
 19. Yin, L. M., Edwards, M. A., Li, J., Yip, C. M. & Deber, C. M. Roles of hydrophobicity and charge distribution of cationic antimicrobial peptides in peptide-membrane interactions. *J. Biol. Chem.* **287**, 7738–45 (2012).
 20. Boix, E. *et al.* Structural determinants of the eosinophil cationic protein antimicrobial activity. *Biol. Chem.* **393**, 801–15 (2012).
 21. Torrent, M. *et al.* Comparison of the membrane interaction mechanism of two antimicrobial RNases: RNase 3/ECP and RNase 7. *Biochim. Biophys. Acta* **1788**, 1116–25 (2009).
 22. Torrent, M. *et al.* Comparison of the membrane interaction mechanism of two antimicrobial RNases: RNase 3/ECP and RNase 7. *Biochim. Biophys. Acta - Biomembr.* **1788**, 1116–1125 (2009).

23. Gow, N. A. R., van de Veerdonk, F. L., Brown, A. J. P. & Netea, M. G. *Candida albicans* morphogenesis and host defence: discriminating invasion from colonization. *Nat. Rev. Microbiol.* **10**, 112–22 (2012).
24. García-Mayoral, M. F. *et al.* NMR structural determinants of eosinophil cationic protein binding to membrane and heparin mimetics. *Biophys. J.* **98**, 2702–11 (2010).
25. Torrent, M., Pulido, D., Nogués, M. V. & Boix, E. Exploring New Biological Functions of Amyloids: Bacteria Cell Agglutination Mediated by Host Protein Aggregation. *PLoS Pathog.* **8**, (2012).
26. Boix, E. & Nogués, M. V. Mammalian antimicrobial proteins and peptides: overview on the RNase A superfamily members involved in innate host defence. *Mol. Biosyst.* **3**, 317–35 (2007).
27. Nguyen, L. T., Haney, E. F. & Vogel, H. J. The expanding scope of antimicrobial peptide structures and their modes of action. *Trends Biotechnol.* **29**, 464–72 (2011).
28. Gautier, R., Douguet, D., Antonny, B. & Drin, G. HELIQUEST: a web server to screen sequences with specific alpha-helical properties. *Bioinformatics* **24**, 2101–2 (2008).
29. Pulido, D., Torrent, M., Andreu, D., Nogués, M. V. & Boix, E. Two human host defense ribonucleases against mycobacteria, the eosinophil cationic protein (RNase 3) and RNase 7. *Antimicrob. Agents Chemother.* **57**, 3797–805 (2013).
30. Pulido, D., Moussaoui, M., Nogués, M. V., Torrent, M. & Boix, E. Towards the rational design of antimicrobial proteins: single point mutations can switch on bactericidal and agglutinating activities on the RNase A superfamily lineage. *FEBS J.* **280**, 5841–52 (2013).
31. Chao, T.-Y. & Raines, R. T. Mechanism of ribonuclease A endocytosis: analogies to cell-penetrating peptides. *Biochemistry* **50**, 8374–82 (2011).
32. Bahnsen, J. S., Franzyk, H., Sandberg-Schaal, A. & Nielsen, H. M. Antimicrobial and cell-penetrating properties of penetratin analogs: effect of sequence and secondary structure. *Biochim. Biophys. Acta* **1828**, 223–32 (2013).
33. Arranz-Trullén J; Pulido D; Bhakta S and Boix E. Unveiling the mode of action of human antimicrobial RNases against *Mycobacterium tuberculosis* using a surrogate macrophage infected model. *Manuscr. Prep.*
34. Neil A.R. Gow, Frank L. van de Veerdonk, Alistair J.P. Brown, and Mihai G. Netea. *Candida albicans* morphogenesis and host defence: discriminating invasion from colonization. *Nat Rev Microbiol.* 10(2): 112-122 (2011).

PAPER V

Endogenous host antimicrobial peptides (AMPs) to tackle antimicrobial resistance in tuberculosis

Javier Arranz^{1,2}, David Pulido^{1,3}, Sanjib Bhakta² and Ester Boix^{1*}

¹Department of Biochemistry and Molecular Biology, Faculty of Biosciences, Universitat Autònoma de Barcelona, 08193, Cerdanyola del Vallès, Spain

²Mycobacteria Research Laboratory, Institute of Structural and Molecular Biology, Department of Biological Sciences, Birkbeck, University of London, Malet Street, Bloomsbury, London WC1E 7HX, UK³Present address: Imperial College London, South Kensington Campus London, London SW7 2AZ, United Kingdom

*corresponding authors: Ester Boix: Ester.Boix@uab.cat

Keywords: antimicrobial peptides, innate immunity, tuberculosis, infectious diseases, mycobacteria

Tuberculosis, Antimicrobial resistance, Host immune responses, Antimicrobial peptides

List of abbreviations:

AMP (antimicrobial peptide), Ahpc (alkyl hydroperoxide reductase enzyme subunit C TB (tuberculosis), ECP (eosinophil cationic protein), DCs (dendritic cells), HNP (human neutrophil peptides), IFN γ (interferon gamma), LF (lactoferrin), LTBI (latent tuberculosis infection), MDR (multidrug resistance), MsrA (methionine sulfoxide reductase), *Mycobacterium tuberculosis* bacilli (Mtb), NE (neutrophil elastase), NETs (neutrophil extracellular traps), NK (natural killer), NO (nitric oxide), PBMC (peripheral blood nuclear cell, PECs (epithelial cells), PRRs (pattern recognition receptors), RNI (reactive nitrogen intermediates), SAMPs (synthetic antimicrobial peptides), XDR (extensively drug-resistance)

Abstract

Tuberculosis remains nowadays a devastating infectious disease and represents a worldwide global threat. Despite the great effort that has been applied to develop effective antituberculosis drugs, the potentiality of antimicrobial peptides remains unexploited. Although a considerable amount of literature is accessible on the mechanism of action of antimicrobial peptides (AMPs) against a wide diversity of pathogens, research on their activity on mycobacteria is still scarce. In particular, we are urged to combine all available strategies to eradicate intracellular infection resistant forms, such as *Mycobacterium* species. In this context, we should not underestimate the key role of our own host defence peptides. The present review tries to summarize the current knowledge on the AMPs involved in the host immune response against tuberculosis. Particular attention has been paid on the mechanism of action of human host defence peptides and the applied structure based design of alternative therapies.

1.Introduction

Tuberculosis (TB) is currently one of the most devastating infectious diseases having caused around 1.5 million TB deaths, with 9 million new TB cases in 2014 and with approximately a

third of the world's population harbouring its latent form [1]. TB represents a major worldwide threat and is the second leading cause of death from a single infectious microorganism after AIDS. Although the development of the first combined anti-TB drug-therapy dramatically improved the disease prognosis outcome, the current alarming rise in multidrug resistance (MDR) and extensively drug-resistance (XDR) in anti-tubercular chemotherapy is jeopardising our early attempt to control TB and the disease re-emerges as a global health emergency [2][3]. In addition, *Mycobacterium tuberculosis* bacilli (Mtb) as a successful human pathogen, can remain in host cells keeping under control their immune responses using a wide repertoire of escape pathways [4]. Moreover, to complicate matters further, latent Tb infections (LTBI) have become a serious global threat because of their tricky diagnosis, treatment and its ability to revert to active infections on immune-compromise circumstances [5], such as HIV infection and some inflammatory therapies [6]. Therefore, a full-scale comprehension of host immune capability and the mode by which *Mycobacterium tuberculosis* handles/endures the host defences will be needed to cope with the illness [7].

Considering that both innate and adaptive immunity show essential roles against mycobacteria proliferation [8], a multitudinous deployment of distinct alternative immune mechanisms [9][10], should be assembled to tackle TB infection resistance. Despite the initial underestimation of antimicrobial proteins peptides (AMPs) role in the immune system and the difficulties encountered in their attempt to reach the market, nowadays it is firmly established that AMPs are multifunctional molecules with a key role in the mammalian host innate defence. In addition, due to the rapidly spreading drug resistance among XDR-Mtb and TDR- Mtb strains, the use of both natural and synthetic AMPs and their combination with conventional drugs is enabling the creation of a new generation of truly promising antibiotics [1]. As *Mycobacterium tuberculosis* can survive and replicate within macrophages, novel anti-TB agents should be able to internalize inside the host cells to annihilate the mycobacteria without damaging the host. In this review, emphasis is placed on both latent tuberculosis immunity, including mycobacteria evasion mechanisms, and innate host defence machinery. We will focus on AMPs, either exploited naturally by our immune system or artificially synthesized as potential therapeutics to overcome and eradicate the pathogen infection. Finally, we will shortly discuss the advantages, handicaps and obstacles of AMPs confronted by its merchandising and clinical use.

2. Immunology and mycobacterial tolerance insights

Tuberculosis (TB) is an airborne respiratory infection, which is conveyed through mycobacterial aerosolized particles from active focus of the disease (active TB patients) [11]. Peculiarly, *M. tuberculosis* is inhaled into the organism through the respiratory tract reaching the pulmonary epithelium, where the interaction takes place with other cell types: alveolar macrophages, pulmonary epithelial cells (PECs) and dendritic cells (DCs). Alveolar macrophages absorb mycobacteria and frequently kill them but its entire destruction depends on the virulence of the strain and the mycobactericidal capability of the host

phagocytes. Hence, the way the macrophages react against the infection will establish the development and the denouement of the infection. Those tubercular bacilli that escape this incipient destruction can multiply and shatter the macrophage, which triggers the activation of signalling cascades causing the release of factors that foster recruitment of inflammation cells to pulmonary tract [12]. At this point, *Mycobacterium tuberculosis* begins to grow exponentially while macrophages accumulate without causing any tissue damage in the area. A few weeks later acquired immunity triggers the arrival of antigen-specific T lymphocytes that proliferate in the damaged area and help macrophages to kill intracellular mycobacteria. Subsequently, the bacterial logarithmic growth stops due to the formation of areas of necrosis (granulomes) (Figure 1A) and the infection remains latent. At this stage, the disease may be reactivated from granulomatous areas and spread to other areas, being difficult to distinguish from reinfection [12]. This reactivation is usually concomitant with some kind of weakness or suppression of the immune system, explaining the high rate of TB co-incidence with HIV [13].

Evasion, survival and reactivation: how do mycobacteria achieve this?

Mycobacterium tuberculosis has evolved to dwell inside one of the most inhospitable cell types that exist within the human body, the macrophages (Figure 1B). Likely, Mycobacteria thanks to a long-term interaction with macrophages have been able to develop strategies to evade their main immune function, predominantly by blocking phagocytosis and phagosome maturation. How *M. tuberculosis* succeeds is still unknown. However, many mechanisms are known to provide benefits for mycobacteria in its survival within the macrophage [14]. This ability to replicate within host cells differentiate pathogenic from non-pathogenic mycobacteria and the most significant difference that could support this skill is its ability to grow as free amoebae [15]. To date, we can highlight several ways in which mycobacteria can abolish host defence pathways and maintain a latent infection.

- Mycobacterial cell wall and proliferation: a particular hallmark

As a result of the continuous selective pressures exerted by the host immune system on mycobacteria a series of adjustments were developed in order to guarantee their survival. Largely, this adaptation to a hostile environment is enabled by a peculiar heterogeneous proliferation as well as by the production of a complex structure consisting of several cell wall layers. In most bacterial types, cell division takes place following a symmetrical pattern which concludes with the emergence of two daughter cells of equal size [16][17]. Nevertheless, some authors have recently reported that mycobacteria are able to proliferate using a unique division and elongation irregular pattern that determines a mycobacterial heterogeneous subpopulation [18]. Otherwise, the complex network of macromolecules such as peptidoglycan, arabinogalactan and mycolic acids, which are conglomerated by other proteins and polysaccharides, conform the main mycobacterial cell wall scaffold (Figure 1C) and constitute a difficult crossing-barrier for antimicrobial agents [19] (Figure 1D). The high proportion of lipids in the cell wall prevents Gram staining and

determines that mycobacteria can only be stained by acid-fast dyes such as Ziehl-Neelsen stain [20]. Furthermore, it has been found that the characteristics and composition of the cell wall can be modified during infection [21]. Accordingly, the presence of this population of cell resizable mycobacteria of different growth properties and with a miscellaneous cell wall composition could potentially promote the progression and latency of mycobacterial encroachment.

- **Phagosome-lysosomal pathway and autophagy modulation**

Mycobacterium tuberculosis is able to interfere with the phagosomal maturation pathway, which takes place through a series of steps of fusion and fission aimed to transfer the compounds phagocytosed by macrophages to lysosomes [22]. At this stage several mechanisms take place towards the elimination of the pathogens, among them: oxidative environment (production of reactive oxygen and nitrogen species), vacuolar acidification, lytic enzymes activation and changes in ion fluxes (Figure 1D) [23]. *Mycobacterium* is able to interfere not only in the recruitment of vesicular ATPase proton pump but also in the acquisition of markers for the endocytic pathway, like the Ras related protein Rab7, and promotes an increased acidification and a reduction of PIP3 levels in phagosomal membranes [24]. This modulation of phagocytic maturation seems to be carried out by components of the cell membrane. It has been reported that mannosylated lipoarabinomannan contributes to this interference, causing a defective protein recruitment [24]. Many immune factors play an essential role both in transport and blocking mycobacteria. For instance, Interferon gamma (IFN γ) is a macrophage activation cytokine that induces the expression of several genes involved in the transport of intracellular mycobacteria. Together with the upregulated production of related immune response proteins, interferon controls many phagocytic activities of the host response [25]. The production of this soluble cytokine, which is so important in causing the activation of cytokines, is undermined when the mycobacterial infection begins [25].

- **Resistance against reactive nitrogen intermediates (RNI) and nitric oxide (NO)**

The production of NO is another well-known anti-pathogenic mechanism carried out by activated macrophages. In its turn, NO production also generates RNIs by nitric oxide synthase (NOS) [26]. The enzyme is abundant in epithelioid macrophages, multinucleated giant cells, alveolar macrophages, and epithelial cells [27]. This antimicrobial mechanism has proven effective against mycobacterium tuberculosis both *in vitro* [28] and *in vivo* [29]. *M. tuberculosis* has developed several mechanisms to address the evasion of toxicity produced by NO and RNI. Among them we can highlight the expression of alkyl hydroperoxide reductase enzyme subunit C (AhpC), which allows the decomposition of peroxynitrite, an important antibacterial oxidant, thus providing antioxidant protection [30]. Methionine sulfoxide reductase (MsrA) is another protein used by *M. tuberculosis* to reduce peroxynitrite levels and protect itself against oxidative damage from reactive nitrogen intermediates [31].

- **Antigen presentation interference**

Apart from the innate immune evasion mechanisms, there are other mechanisms activated by the dwelling mycobacteria, such as the interference of the MHC antigen presentation process, which plays an essential role during the host defence adaptive immune response. There are different pathways for the presentation of mycobacterial antigens, by which the T cells obtain the necessary information to implement the systemic protection machinery by the release of different killing molecules. In that way, it has been shown that prosperous intracellular *mycobacterium* species have been able to develop subtle mechanisms with the objective of limiting the presentation and the subsequent antigen processing [32]. This is one of the undoubted cases by which *Mycobacterium tuberculosis* uses an inhibition antigen presentation system in order to avoid and manipulate the adaptive immune responses [33]. Interestingly, this interference in the antigen presentation pathway has been shown to be carried out at several levels: 1) inhibition of proteolysis within the phagosome during processing of the antigen [34], 2) inhibition of MHC class II gene expression during its formation [35], 3) assembly and transport prevention of MHC class II to endosomal vesicles during its mobilization [36], inhibition of peptide loading on to MHC class molecules in endosome [36]. In addition, the disruption/modulation of T cell maturation/differentiation together with the secretion of immunological decoy proteins and the induced delay on triggering the adaptive response are some of the most common mechanisms used by Mtb to subvert, disrupt and evade the mycobacterial host immune response [37].

3. Mechanisms of action of AMPs against Mycobacteria

Lack of effective treatments against tubercular epidemics has promoted the search for biomolecules with new-fangled mycobactericidal mechanisms of action in order to intercept this growing health emergency. Despite a low level of sequence identity, AMPs adopt similar structural folds, indicating the existence of parallel mechanisms of antimicrobial action among distant living organisms. One of the main mechanisms by which the AMPs exert their effect is based on their ability to permeate the cell membrane (Figure 1D), either fully disrupting the lipid bilayer or creating transient pores [38]. Numerous AMPs have acquired amphipathic and cationic structures such as short β -sheets and α -helices that allow them to establish electrostatic interactions with bacterial membranes. The first step of AMPs interaction with the pathogen is generally mediated by their positive net charge and amphipathicity. Unlike eukaryotic cells, in which the anionic lipids are predominantly in the inner leaflet of the lipid membrane providing neutral cell surface, prokaryotic cells contain a large amount of negatively charged lipids in both sides, presenting a negatively charged surface [39]. In that way, physicochemical protein/peptide-lipid interactions supply an engaging tool for host immunity [40]. In addition, some AMPs have the ability to translocate across the membrane performing their bactericidal effect intracellularly [41]. Considering the significant variety of AMPs traits, the existence of a unique mycobacterial mechanism is

unlikely. However, we can still outline several AMPs properties that could particularly target some mycobacteria features. The first challenge that antimycobacterial peptides must face is how to overcome the first barrier of the cellular protection, the cell wall, composed mostly by mycolic acids (Figure 1C). Defensins and cathelicidins are an example of multifunctional AMPs that can exert a direct killing mechanism against mycobacteria through membrane disruption. The binding between the mycobacterial anionic surface compounds and the cationic residues of the proteins drive the membrane permeabilization [42]. Moreover, replacement of lysines by arginines in lactoferrins variants enhances their micobactericidal effect against *Mycobacterium avium* [43]. On the other hand, the highly hydrophobic scaffold of the mycobacterial envelope, with an outer membrane glycolipid layer, confers protection against AMPs action. In that way, amino acid sequence edition of template AMPs, such as the increase in the proportion of α -helical structure and peptide hydrophobicity, has being engineered as an alternative to upgrade their mycobactericidal features [44]. Moreover, since cell homeostasis and communication machineries are essential for the mycobacterial pathogenesis, some AMPs are directly targeting cell wall proteins. Thus, AMPs cell surface interaction has been identified as an alternative mechanism of ion exchange interference that can inhibit the mycobacterial growth [45]. The interaction between AMPs and the outer mycobacterial surface proteins can alter the cell pH regulation, blocking key enzymatic functions, and reducing the viability of mycobacterial strains such as *M. bovis* BCG and *M. smegmatis* [46]. ATPases and others plasma membrane proteins have been also identified as pivotal targets in anti-TB drugs development [47]. Although most of the AMPs exert their action on bacterial membranes, some studies have shown that AMPs have multiple targets, including intracellular structural components such as nucleic acids [48]. Representative AMPs of this group are magainin 2 and buforin 2, which effectively can cross the lipid bilayer without causing significant membrane damage and bind to both RNA and DNA [49]. Selective mycobactericidal action has been achieved by synthetic antimicrobial peptides (SAMPs) that can be internalized by mycobacterial cells without causing membrane damage and bind to mycobacterial DNA, inhibiting replication and transcription processes, leading to cell death [50].

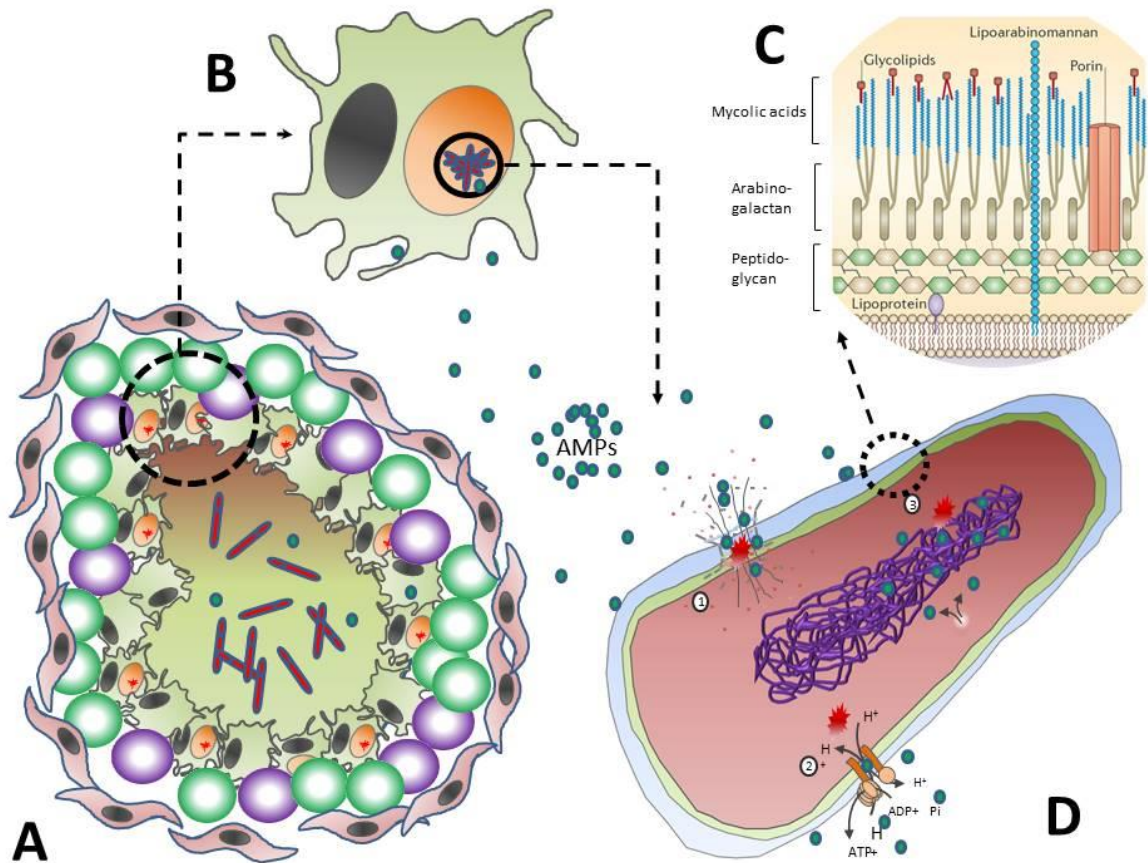


Figure 1. Schematic illustration of AMP mode of action against mycobacteria. A) Following induction of the immune response by mycobacteria, AMPs are directed towards the area of infection where they can be recruited into the necrotic and hypoxic granuloma. B) At the cellular level, the epithelial macrophages are in charge of mycobacteria removal. The destruction of the pathogens takes place inside the phagolysosomes, thanks to the action of lytic enzymes an oxidative environment and the performance of AMPs. C) Mycobacteria cell wall (adapted from [51]). D) Main known mechanisms of action of AMPs against *Mycobacteria*. D₁) Cell wall and plasmatic membrane disruption. D₂) Cell growth inhibition and metabolic stress caused by ion exchange interference on membrane protein complexes. D₃) AMP internalization and subsequent target of mycobacteria macromolecules, such as nucleic acids.

4. AMPs of the human innate immune system: mycobactericidal, immunomodulatory and other related features

When TB becomes active, its severity, location and outcome is highly variable. Mycobacterial bacilli can colonize almost anywhere in the body but often cause an infection in the pulmonary tract. Innate immune response is initiated in most cases in the alveolar spaces, due to the encounter between mycobacteria and macrophages residing therein. Mycobacterial components are identified by several pattern recognition receptors (PRRs) resulting in the activation of signalling pathways and the subsequent leukocyte activation. The foremost innate immunity effector cell types include natural killer (NK) cells, mast cells, eosinophils, basophils, phagocytic cells, neutrophils and dendritic cells (DC), apart from other innate effector mechanisms such as anatomical barriers, inflammatory processes and the complement system.

Notwithstanding, the ultimate denouement of the infection will depend on the host immune response. In order to counter the intrusive pathogen, a large assortment of antimicrobial proteins and peptides are released by innate immune system cells into the affected tissue [52]. AMPs as players of the non-specific immune response, are regarded as one of the oldest protection weaponry used by the immune system (Figure 2) [53]. The use of AMPs arises as a hopeful alternative approach to commercial drugs, providing a broad-spectrum bactericidal action, a natural origin and low predisposition to develop resistance. As mentioned before, one of the biggest challenges in the development of new effective therapies against mycobacteria is the resistance acquired during treatment. This intrinsic resistance is partly due to complexity of their cell wall, composed of a series of glycoconjugates and complex lipids interspersed to form an impermeable barrier to many conventional antimycobacterial antibiotics [54]. A suitable mycobactericidal drug is expected to bind and disrupt the cell membrane as AMPs do. Furthermore, it has been found that the effective dose of anti-mycobacterial drugs could even be halved in combination with AMPs, and these could become more potent in an in vivo environment, as their effects would improve with the interaction of monocytes and T cells [55]. Research on how innate immunity deals mycobacterial infection is still scarce and only few examples of AMPs are currently known. In this section we will focus on the study of the main known human AMPs secreted by innate immunity effector cells to counterbalance mycobacterial infections (Table 1).

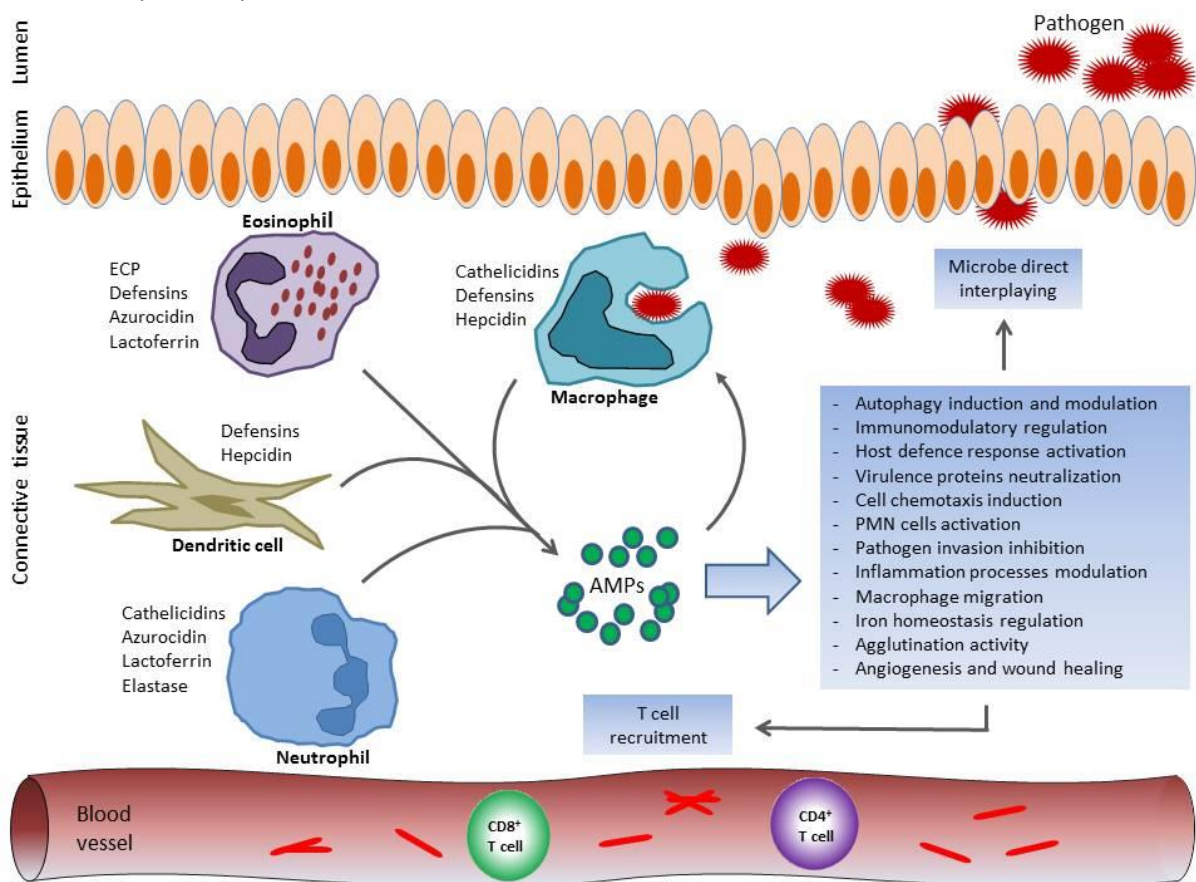


Figure 2. Antimycobacterial features and properties of AMPs expressed in host innate immune cells.

Cathelicidins

Cathelicidins are antimicrobial peptides mostly expressed in leukocytes and epithelial cells of mammals in response to different pathogens, contributing to their eradication [56]. The human cationic antimicrobial peptide-18 (hCAP-18) is nowadays the leading characterized human cathelicidin, which could stage a therapeutic role against microbial infections as well as other major diseases like cancer [57][58]. Human cathelicidin hCAP-18 is essentially conformed by two regions, a highly conserved N-terminal sequence, called cathelin and the bactericidal C-terminal region known as LL-37 [59] (figure 3A). Both regions may be separated by a series of proteolytic processes, leading to the activation of the C-terminal region which encompasses the LL-37 peptide [60]. LL-37 contributes to the recruitment of T-cells to the site of infection [61] and also displays diverse antipathogen and antitumoral activities [62]. On the other hand, accumulating evidence attributed to LL-37 a key role in mycobacterial infection [63]. In particular, a significant overexpression of LL-37 on neutrophils, epithelial cells and alveolar macrophages has been observed during Mtb infection [64]. The infection of mononuclear cells promotes the up-regulation synthesis of LL-37 via vitamin D pathway [65]. Interestingly, studies based on vitamin D deficiency have shown a clear susceptibility to tuberculosis, while supplementation with vitamin D derivatives improved the efficiency to overcome TB [66][67]. Phagosomal pathway is known to be a key defensive procedure to eradicate *M. tuberculosis* and recently studies point to vitamin D3 as an inducer of autophagy in human monocytes as well as an inhibitor of intracellular mycobacterial growth, via up-regulation of autophagy-related genes expression [68]. It has also being reported that the peptide LL-37 is able to cause a decrease in the rate of proliferation of MDR Mtb strains in the pulmonary tract [69] and has an remarkable immunomodulatory effect during *Mycobacterium tuberculosis* infection in macrophages [70]. Jointly, all these experimental evidences highlight cathelicidin LL-37 not only as a forthright antimicrobial peptide but also as a prominent modulator of autophagy during mycobacterial infection [71].

Defensins

Human defensins are a set of cationic and rich-cysteine peptides directly involved as mediators in innate immune response due to their immunomodulatory and microbicidal properties. They constitute one of the major group of AMPs in the mammalian pulmonary host defence system [72]. Additionally, defensins can be induced and activated by proteolysis pathways to acquire their antibacterial activity [73]. Defensins are divided into two subgroups, according to their tertiary structure: alpha and beta – defensins (figure 3B). They show substantial variation in terms of amino acid sequences, probably due to selective pressures that may have promoted its broad spectrum anti-pathogen activity [74]. These peptides are mainly secreted in neutrophils, hence they receive the name of human neutrophil peptides (HNPs). Nevertheless, low levels of expression have been also detected in eosinophils as well as in epithelial cells of the mucosa [75]. Interestingly, high-throughput

gene expression PBMCs profiles analysis from patients with tuberculosis and M. tuberculosis-infected healthy donors, revealed the existence of an overexpression of defensins levels in TB patients [76]. On the other hand, it is reported that although macrophages express small amounts of HNPs, they achieve increased intracellular levels via neutrophil-phagocytosis. Besides, defensins have been observed to colocalize with tuberculosis bacilli in early endosomes, suggesting their contribution in mycobacteria eradication [77]. Moreover, some studies have revealed both membrane and intracellular modes of action, such as DNA binding [78]. Furthermore, it has been found that defensins have a preservative role in human eosinophils. Specifically, eosinophils induce α -defensin in response to *Mycobacterium bovis* infection, contributing to the inhibition of mycobacteria infection [75]. Studies carried out in cells infected with Mtb have elucidated an important expression of intracellular beta-defensins, supporting the antimicrobial role of these peptides to combat tuberculosis infection [79]. Thus, additional studies show that the administration of HNPs maximizes antipathogen capacity of macrophages against various microbes, including Mtb [80][81]. On the other hand, synergism studies between defensins and conventional antituberculosis drugs have shown that these peptides might be administered in conjunction with antitubercular chemotherapy, since this combination reduces the dose of drug administered and also significantly diminishes the bacterial load on vital organs [82]. These findings together with other experimental work with tuberculosis animal models entrench the therapeutic application in favour of defensins [83].

Hepcidin

Hepcidin is a short and highly cationic antimicrobial peptide that was originally detected in serum and urine [84][85] (figure 3C). It is predominantly synthesized in hepatocytes and released from a precursor by proteolysis. Hepcidin expression is induced by infectious or inflammatory processes and plays a prominent role in the iron homeostasis, regulating uptake and mobilization [86][87]. Specifically, Hepcidin would down-regulate the iron transmembrane transport through its union with ferroportin, a transmembrane protein that exports iron to the extracellular space [88]. The reduction in extracellular iron concentrations makes pathogen invasion conditions more hostile, due to iron availability limitation [89][90]. Interestingly, during infection, hepcidin is released into the bloodstream and it is considered to be responsible of the anemia associated with inflammation [91]. In addition, anemia is a common difficulty encountered in TB [92]. Moreover, Lafuse and co-workers demonstrated that mycobacterial infection induced the emergence of high levels of hepcidin in macrophages phagosomes and confirmed the peptide inhibition of *Mycobacterium tuberculosis* growth *in vitro* [93]. Further research confirmed these results and also reported the presence of hepcidin in other innate cell types such as dendritic cells. The peptide expression in non-phagocyte cells suggests an extracellular mycobactericidal activity mediated by iron reduction in both alveolar and interstitial spaces [94]. Particularly, as a result of the action of hepcidin on iron levels, differences in the expression of the peptide could be related to different phenotypes of iron homeostasis in TB patients. A

significant association between serum hepcidin level and the HAMP-582A>G variants in TB patients was envisaged as useful in the diagnosis and prognosis of tuberculosis [95].

Lactoferrin

Lactoferrin (LF) is another AMP related to iron homeostasis regulation. It is a multifunctional iron binding glycoprotein which is present in most human body fluids and several tissues. It has a molecular weight of 80 kDa and belongs to the transferrin family [96]. Recent studies highlight additional activities apart from iron binding and traffic. LF displays important mechanisms involved in host defence and has powerful antibacterial, antiparasitic, antifungal and antiviral effects [97][98]. While the mechanism of LF multifunctionality is still not fully understood, it appears that there is a growing evidence for its multifaceted antibacterial action. LF may exert its bactericidal effect on iron-dependent bacteria by kidnapping this metal and negatively interfering in their metabolism [99]. Another bacterial killing mechanism developed by LF is the use of its proteolytic activity, whereby achieving neutralization of virulence proteins [100]. Previous studies have demonstrated the presence of LF in macrophages and blood cells and its activity against different human pathogens such as *Toxoplasma*, *Plasmodium*, *Leishmania*, *Trypanosoma*, and *Mycobacterium*. In addition, the presence of iron in the protein has been shown to have a determinant role, improving various host defence activities [101]. Moreover, LF immunomodulatory capacity would also contribute to the eradication of TB in many scenarios. Particularly, it has been observed that mice treated with LF manifest an increase in the proportion of IL-12/ IL-10, which results in increased Th1 cells, with a protective role against Mtb [102]. On the other hand TB-antigen presentation to T cells is enhanced [103]. Following, macrophages activated by Mtb would end production of reactive oxygen species and acidification of phagosomes. In addition, other studies have clearly demonstrated the immunomodulatory role of LF, improving BCG-vaccine efficacy when LF is used as adjuvant [104][105][106]. Recently, it has been reported that LF expressed in azurophilic granules of neutrophils is capable of killing *Mycobacterium smegmatis* [107].

Azurocidin

Azurocidin, a leukocyte polymorphonuclear granule protein, is a cationic antimicrobial protein of 37 kD, also called CAP37 or Heparin-Binding protein, due to its high affinity for heparin [108][109][110]. Shortly after its discovery it was found that azurocidin, like other antimicrobial proteins, not only displayed an antipathogenic activity but was also capable of exerting a mediating role in the modulation of the host defence system [111][112]. Azurocidin is stored in secretory granules and is released into the endothelial area by PMN, rapidly reaching the infected or inflammation area [113]. Azurocidin, at the front line of infection, activates monocytes, macrophages and epithelial cells [114][115][116]. Thereby, azurocidin has a wide range antimicrobial activity, working efficiently at acidic pH, a condition promoted in mature phagolysosomes [117]. Interestingly, it has recently been

reported that azurophilic granule proteins are implicated in mycobacterial killing, facilitating the fusion of mycobacteria-containing phagosomes with lysosomes [107].

Neutrophil Elastase

Neutrophil elastase (NE), also known as elastase 2, is a 29 kD protein, belonging to the serine protease family, expressed during myeloid development and secreted by neutrophils during episodes of inflammation or infection[118]. Interestingly, it has been shown that this protein is able to develop a bactericidal role within phagolysosomes of human neutrophils [119][120]. Many studies emphasize NE multifunctionality; as an example, we can highlight the protein breaking of the tight junctions to facilitate the migration of polymorphonuclear cells to the inflammation/infection area and the induction of cell chemotaxis [121]. Complementarily, NE is also reported to annihilate mycobacteria extracellularly but in a rather peculiar way. Neutrophils kill mycobacteria via granule fusion with the phagosome. Often, these granules, transporting antimicrobial proteins such as NE, are released together with chromatin, resulting in the formation of extracellular fibrillar structures that can facilitate bacteria arrest. These neutrophil extracellular traps (NETs) are responsible for the removal of virulence factors and play an important bactericidal role [122]. Interestingly, Belaouaj et al investigated the role of NE in host defence against bacteria by generating knock out (NE^{-/-}) mice, and observed that mice deficient in this serine protease, were more susceptible to bacterial infections [123]. On the other hand, it has been reported that NE conferred a protective effect against *Mycobacterium bovis* in mice pulmonary tract [124].

Antimicrobial RNases

Antimicrobial RNases are small secretory proteins belonging to the RNase A superfamily. They are highly cationic and possess a wide range of antipathogen activities [125]. RNase A family members share an active site architecture that enables them to cleave single stranded RNAs. Besides, the distinct RNases have been shown to be involved in a large number of biological properties, representing an excellent example of multitasking proteins [126]. In particular, some members display host defence related activities, being effective against a wide range of human pathogens, suggesting a non-specific mechanism of action. Besides, the antibacterial activity of distant related RNases suggested that the family might have evolved from a common ancestor with a defined role in host defence [127][128]. Interestingly, some antimicrobial RNases have demonstrated high mycobactericidal activity. RNase 3, also known as the Eosinophil Cationic Protein (ECP), is mainly expressed in the secondary granules of eosinophils during infection and inflammation processes [129][130] and secondarily by activated neutrophils [131]. Complementarily, the signal peptide of the ECP (ECPsp) was found to promote the migration of macrophages via proinflammatory molecules to sites of infection and inflammation [132]. Interestingly, ECP is secreted, together with α -defensin, in response to mycobacteria infection [75]. Although the recruitment of eosinophils and neutrophils in the respiratory tract due to *Mycobacterium tuberculosis* was first regarded as a mere participation in the inflammation of the infected

area [133] further work has shown that both cell types would directly act at the focus of infection [134][135]. It is here, inside the granuloma, a tuberculosis inflammation hallmark, where eosinophils together with neutrophils would release the content of their granules into macrophages [136][137]. Indeed, it has been found that infected macrophages absorb granules of eosinophils and neutrophils along with their antimicrobial proteins [77]. Since it has been shown that eosinophils and neutrophils are effective competitors in mycobacterial infection scenario [138][139] and RNase 3 is one of the main eosinophil secondary granule proteins reported to be secreted by *M. bovis BCG* infection [75], this antimicrobial protein might play a crucial role in the mechanism by which eosinophils eradicate mycobacteria. Additionally, RNase 7, also called the skin derived RNase, is another RNase A superfamily member that is secreted by diverse epithelial tissues that exerts a protective role against a variety of pathogens [140][141][142][143]. Interestingly, it has recently been observed that recombinant RNase 3 and RNase 7 can eradicate mycobacteria *in vitro* [144] and, very recent results indicate that the human RNases 3, 6 and 7 can also inhibit the growth of intracellular dwelling mycobacteria in an ex vivo macrophage infection model [145]. Bearing in mind that RNase 6 expression is induced in macrophages upon bacteria infection [143], one might hypothesize that this antimicrobial protein can play a physiological role against intracellular dwelling mycobacteria.

Synthetic antimicrobial peptides

In the race against TB, novel synthetic AMPs with potent mycobactericidal activities have been developed [146][55][147]. These synthetic analogues are often considered to be the next generation of antibiotics and have attracted the attention of many companies aiming to develop new anti-TB therapies [148]. Particular interest has been drawn by the D-LAK peptides, a family composed by a serial of synthetic AMPs consisting of 25 D-enantiomer amino acid residues in a primary sequence designed to adopt a left-handed α -helix conformation with a charge angle of 120°. Each D-LAK peptide is engineered to contain eight lysine residues with a nominal charge of +9 at neutral pH [149]. These peptides have been designed based on previous studies, where the use of alpha helical AMPs enhanced the antibacterial activity against attenuated Mtb strains and decreases their haemolytic effect [150][151]. Additionally, as other tested alpha helical peptides, the D-LAK based AMPs provide antimycobacterial activity at non-toxic concentrations and can be combined with existing antitubercular drugs, such as isoniazid or rifampicin, to improve TB treatment effectiveness [149][152]. Furthermore, D-LAK peptides can be administered satisfactorily as dry powder by spray against MDR-TB strains [153]. On the other hand, other synthetic AMPs were proven successful, such as synthetic cathelicidin HHC-10, that is able to inhibit the growth of *Mycobacterium bovis BCG* both in vitro and in C57BL/6 model mice [154]. Interestingly, the N terminus derived peptides of RNases 3 and 7 were also found effective against several *Mycobacterium* species [144] (Arranz-Trullén, unpublished results). Indeed, the RNases first 45 amino acids encompasses a highly cationic and amphipathic region that

adopts an extended α -helix in a membrane-like environment [155][156][157] (Figure 3D). Interestingly, the RNases derived peptides include an aggregation prone sequence which promotes Gram Negative bacteria agglutination[158] and would also mediate the particular high mycobacterial cell aggregation activity[144][145] observed for the RN3 and RN6 peptides, a property that might enhance the microbial clearance at the infectious focus[158].

Table 1

AMPs involved in Immune Host Defence against Mycobacteria

AMP	Cellular type/source	Main reported mechanism of action	Immunomodulatory and other host defence properties	References
Cathelicidins	Neutrophils, monocytes/macrophages,	Cellular lysis	Cytokine modulation	[63]
	keratinocytes, lymphocytes,		Autophagy regulation Angiogenesis promotion and wound healing Recruitment of T-cells to the site of infection	[64][65] [68]
	epithelial cells and broncho-alveolar lavage fluids		NETs promotion	[62][159][160] [161]
Defensins	Monocytes/Macrophages, Eosinophils, DCs, T-cells, PBMCs, airway epithelial cells	Action at membrane level and intracellular targets (DNA)	Immunomodulatory effects	[76]
			Preservative effects against mycobacteria in eosinophils Cytokine Activation	[77][75][79][80] [75]
				[162] [78]
Hepcidin	Hepatocytes, macrophages, dendritic cells	Pathogen invasion inhibition	Inflammation induction	[86][87][88]
		Iron homeostatic regulation		[163][89][91] [93][94]
Lactoferrin	PMNs cells Expressed in various organs (mammary gland, uterus, kidney brain)	Iron kidnapping Permeabilization of cytoplasmic membrane Neutralization of virulence proteins by protease activity	Th1 cells activation via interleukin promotion	[96]
			BCG-vaccine efficacy enhancement	[97][98] [107]
				[102][103]
				[104][105][106] [100]
Azurocidin	Secretory vesicles and primary granules of polymorphonuclear	Cell wall binding and leakage	Monocytes, macrophages and epithelial cells activation	[164][165][166] [111][112]

	leukocytes (PMN)		Heparin binding activity Phagosome-Lysosome fusion promotion	[108][109][110] [107]
Neutrophil elastase	Neutrophil azurophilic granules	Membrane level disruption Serine protease activity	PMNs migration Cell chemotaxis induction NETs formation	[118][121] [119][120] [124],[122]
RNase 3 (Eosinophil cationic protein)	Matrix of eosinophil large specific granules and minoritary in neutrophils	Cell wall and membrane disruption Cell agglutination	Migration of leucocytes via proinflammatory molecules to sites of infection and inflammation Potential RNA degradation	[129][130] [131][167][168] [136][137][75] [144][132][145]

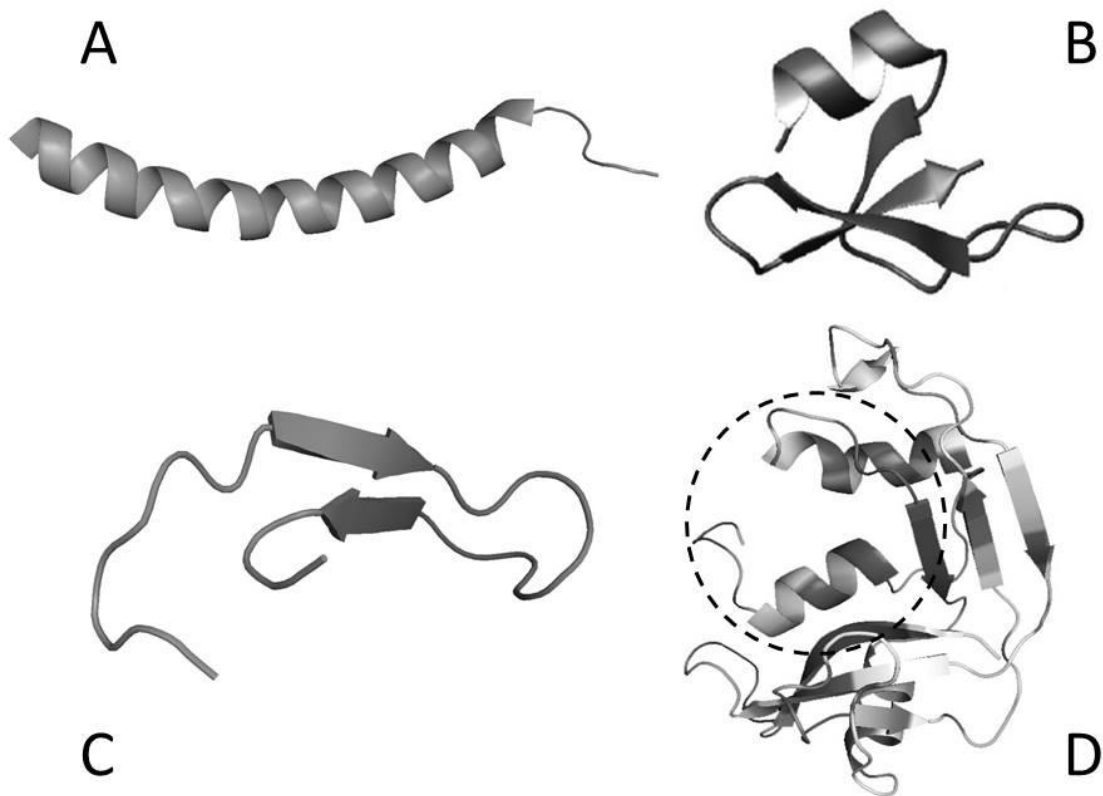


Figure 3. 3D Graphical illustration of representative AMPs with reported antimycobacterial properties. (A) human cathelicidin LL-37 (PDB entry: 2K6O); (B) human β -defensin-1 (HBD-1) (PDB entry: 1IJV); (C) Hepcidin (PDB entry: 1M4F) and (D) RNase 3/ECP (PDB entry: 4A2O) (the region comprising the active N-terminal derived peptide is indicated in the dashed circle).

5. Conclusions: current position and future outlook

In recent years, thousands of antimicrobial peptides have been identified from natural sources and these are often an essential component of the non-specific host defence response [169][170][171]. On the other hand, despite the existence of a wide range of antibiotics and their great success since their entry into the worldwide trade, an increasing demand of new drugs to tackle the multidrug-resistance mycobacteria strains is currently emerging into the global market [1]. The antimicrobial proteins and peptides (AMPs), given their direct bacilli killing mechanism and attractive intracellular pharmacological potential, promise a valuable pattern model for novel therapeutic agents against mycobacterial infections. Despite their appealing properties, AMPs-based therapies are encountering difficulties to enter into the pharmaceutical industry. Although the synthesis high cost is one of the main drawbacks that peptide manufacturing faces, some companies are already managing commercial-scale peptide production platforms [172]. Additionally, a transition is taking place towards the production of smaller analogue molecules cheaper than their natural counterparts [173]. Novel design strategies of AMPs are focused on reducing their toxicity towards eukaryotic cells while increasing their selectivity towards prokaryotic targets [174]. Another major drawback of AMPs therapy is their susceptibility to proteolytic cleavage once administered into the systemic circulation. Remarkably, it has been found that several species of pathogens are able to induce the proteolytic inactivation of AMPs [175]. To counteract this inconvenient several strategies have been developed such as conjugation with fatty acids, acylation or encapsulation within biodegradable particles or liposomes. The latter option has even demonstrated to improve the stability and distribution of the drug towards the site of action [176][177][178][179]. In addition, the antimicrobial activity of some peptides appears to be decimated in physiological saline and serum conditions [180], while others, like LL-37, may undergo the opposite effect and are favoured by the host immune system [181]. Besides, AMPs tend to have a short half-life, are prone to aggregate and show occasionally poor solubility [182]. However, there are currently different strategies and predictive software to prevent aggregation and improve physicochemical properties. Complementarily, cleavage protection can be enhanced through secondary structure stabilization [183]. Furthermore, recent studies on mycobacterial infection reveal how some species such as *Mycobacterium tuberculosis* are capable of inhibiting the release of mature active AMPs by blocking the host protein processing of the precursor form [171]. Thus the administration of supplementary AMPs or an immunomodulatory hormonal induction would be necessary to achieve an effective eradication of the pathogen [184]. Notwithstanding, peptide based therapy to treat infectious diseases is recently experiencing a resurgence [185][186]. Since AMPs, as mere components of the immune system, promote the direct killing of mycobacteria and often have immunomodulatory effects, their clinical application as alternative therapeutic agents against human tuberculosis should be evaluated in deep. Their non-specific mechanisms of action and substantial capacity over conventional antibiotics to neutralize sepsis or endotoxemia, seem to have triggered an intense search by the pharmaceutical industry.

Moreover, the effectiveness of BCG vaccine is highly variable (0-80%) and the emergence of novel XDR and MDR Tb strains is a major challenge to face. In this context, and considering the current anti-tuberculosis drug weaknesses, AMPs represent a stately alternative therapy. We are convinced that the future development of peptide-based therapy will continue to address all the above mentioned weaknesses. One could anticipate that an extensive structure base approach could culminate with the future design and production of multifunctional drugs specifically tailored to tackle resistant mycobacterial infections.

References

- [1] A. Zumla, A. George, V. Sharma, R. H. N. Herbert, A. Oxley, and M. Oliver, "The WHO 2014 global tuberculosis report--further to go.," *Lancet. Glob. Heal.*, vol. 3, no. 1, pp. e10-2, Jan. 2015.
- [2] E. M. Zager and R. McNerney, "Multidrug-resistant tuberculosis.," *BMC Infect. Dis.*, vol. 8, p. 10, Jan. 2008.
- [3] C. Dye, "Doomsday postponed? Preventing and reversing epidemics of drug-resistant tuberculosis.," *Nat. Rev. Microbiol.*, vol. 7, no. 1, pp. 81-7, Jan. 2009.
- [4] A. Gupta, A. Kaul, A. G. Tsolaki, U. Kishore, and S. Bhakta, "Mycobacterium tuberculosis: immune evasion, latency and reactivation.," *Immunobiology*, vol. 217, no. 3, pp. 363-74, Mar. 2012.
- [5] A. Maitra, C. A. Danquah, F. Scotti, T. K. Howard, T. K. Kamil, and S. Bhakta, "Tackling tuberculosis: Insights from an international TB Summit in London," *Virulence*, vol. 6, no. 6, pp. 561-572, Jul. 2015.
- [6] J. Keane, S. Gershon, R. P. Wise, E. Mirabile-Levens, J. Kasznica, W. D. Schwieterman, J. N. Siegel, and M. M. Braun, "Tuberculosis associated with infliximab, a tumor necrosis factor alpha-neutralizing agent.," *N. Engl. J. Med.*, vol. 345, no. 15, pp. 1098-104, Oct. 2001.
- [7] K. Dheda, C. E. Barry, and G. Maartens, "Tuberculosis.," *Lancet (London, England)*, Sep. 2015.
- [8] J. L. Flynn and J. Chan, "Immunology of tuberculosis.," *Annu. Rev. Immunol.*, vol. 19, pp. 93-129, Jan. 2001.
- [9] P. T. Liu and R. L. Modlin, "Human macrophage host defense against Mycobacterium tuberculosis.," *Curr. Opin. Immunol.*, vol. 20, no. 4, pp. 371-6, Aug. 2008.
- [10] Y. Li, Y. Wang, and X. Liu, "The Role of Airway Epithelial Cells in Response to Mycobacteria Infection," *Clin. Dev. Immunol.*, vol. 2012, pp. 1-11, Jan. 2012.
- [11] A. M. Dannenberg, "Perspectives on clinical and preclinical testing of new tuberculosis vaccines.," *Clin. Microbiol. Rev.*, vol. 23, no. 4, pp. 781-94, Oct. 2010.
- [12] R. van Crevel, T. H. M. Ottenhoff, and J. W. M. van der Meer, "Innate immunity to

- Mycobacterium tuberculosis.," *Clin. Microbiol. Rev.*, vol. 15, no. 2, pp. 294–309, Apr. 2002.
- [13] Y. Shen, L. Shen, P. Sehgal, D. Huang, L. Qiu, G. Du, N. L. Letvin, and Z. W. Chen, "Clinical Latency and Reactivation of AIDS-Related Mycobacterial Infections," *J. Virol.*, vol. 78, no. 24, pp. 14023–14032, Nov. 2004.
- [14] S. Falkow, "Is persistent bacterial infection good for your health?," *Cell*, vol. 124, no. 4, pp. 699–702, Feb. 2006.
- [15] M. Hagedorn, K. H. Rohde, D. G. Russell, and T. Soldati, "Infection by Tubercular Mycobacteria Is Spread by Nonlytic Ejection from Their Amoeba Hosts," *Science (80-.)*, vol. 323, no. 5922, pp. 1729–1733, Mar. 2009.
- [16] A. Typas, M. Banzhaf, C. A. Gross, and W. Vollmer, "From the regulation of peptidoglycan synthesis to bacterial growth and morphology.," *Nat. Rev. Microbiol.*, vol. 10, no. 2, pp. 123–36, Feb. 2012.
- [17] C. Tropini, T. K. Lee, J. Hsin, S. M. Desmarais, T. Ursell, R. D. Monds, and K. C. Huang, "Principles of bacterial cell-size determination revealed by cell-wall synthesis perturbations.," *Cell Rep.*, vol. 9, no. 4, pp. 1520–7, Nov. 2014.
- [18] B. Singh, R. G. Nitharwal, M. Ramesh, B. M. F. Pettersson, L. A. Kirsebom, and S. Dasgupta, "Asymmetric growth and division in Mycobacterium spp.: compensatory mechanisms for non-medial septa.," *Mol. Microbiol.*, vol. 88, no. 1, pp. 64–76, Apr. 2013.
- [19] R. Bansal-Mutalik and H. Nikaido, "Mycobacterial outer membrane is a lipid bilayer and the inner membrane is unusually rich in diacyl phosphatidylinositol dimannosides.," *Proc. Natl. Acad. Sci. U. S. A.*, vol. 111, no. 13, pp. 4958–63, Apr. 2014.
- [20] R. Vasanthakumari, K. Jagannath, and S. Rajasekaran, "A cold staining method for acid-fast bacilli.," *Bull. World Health Organ.*, vol. 64, no. 5, pp. 741–3, 1986.
- [21] S. Bhamidi, L. Shi, D. Chatterjee, J. T. Belisle, D. C. Crick, and M. R. McNeil, "A bioanalytical method to determine the cell wall composition of Mycobacterium tuberculosis grown in vivo.," *Anal. Biochem.*, vol. 421, no. 1, pp. 240–9, Feb. 2012.
- [22] K. Rohde, R. M. Yates, G. E. Purdy, and D. G. Russell, "Mycobacterium tuberculosis and the environment within the phagosome.," *Immunol. Rev.*, vol. 219, pp. 37–54, Oct. 2007.
- [23] T. Soldati and O. Neyrolles, "Mycobacteria and the Intraphagosomal Environment: Take It With a Pinch of Salt(s)!", *Traffic*, vol. 13, no. 8, pp. 1042–1052, Aug. 2012.
- [24] I. Vergne, "Mycobacterium tuberculosis Phagosome Maturation Arrest: Mycobacterial Phosphatidylinositol Analog Phosphatidylinositol Mannoside Stimulates Early Endosomal Fusion," *Mol. Biol. Cell*, vol. 15, no. 2, pp. 751–760, Dec. 2003.

- [25] B.-H. Kim, A. R. Shenoy, P. Kumar, R. Das, S. Tiwari, and J. D. MacMicking, "A family of IFN- γ -inducible 65-kD GTPases protects against bacterial infection.," *Science*, vol. 332, no. 6030, pp. 717–21, May 2011.
- [26] J. MacMicking, Q. W. Xie, and C. Nathan, "Nitric oxide and macrophage function.," *Annu. Rev. Immunol.*, vol. 15, pp. 323–50, Jan. 1997.
- [27] H.-S. Choi, P. R. Rai, H. W. Chu, C. Cool, and E. D. Chan, "Analysis of nitric oxide synthase and nitrotyrosine expression in human pulmonary tuberculosis.," *Am. J. Respir. Crit. Care Med.*, vol. 166, no. 2, pp. 178–86, Jul. 2002.
- [28] J. Chan, Y. Xing, R. S. Magliozzo, and B. R. Bloom, "Killing of virulent *Mycobacterium tuberculosis* by reactive nitrogen intermediates produced by activated murine macrophages.," *J. Exp. Med.*, vol. 175, no. 4, pp. 1111–22, Apr. 1992.
- [29] J. Chan, K. Tanaka, D. Carroll, J. Flynn, and B. R. Bloom, "Effects of nitric oxide synthase inhibitors on murine infection with *Mycobacterium tuberculosis*.," *Infect. Immun.*, vol. 63, no. 2, pp. 736–40, Feb. 1995.
- [30] J. Chan and J. Flynn, "The immunological aspects of latency in tuberculosis.," *Clin. Immunol.*, vol. 110, no. 1, pp. 2–12, Jan. 2004.
- [31] G. S. John, N. Brot, J. Ruan, H. Erdjument-Bromage, P. Tempst, H. Weissbach, and C. Nathan, "Peptide methionine sulfoxide reductase from *Escherichia coli* and *Mycobacterium tuberculosis* protects bacteria against oxidative damage from reactive nitrogen intermediates," *Proc. Natl. Acad. Sci.*, vol. 98, no. 17, pp. 9901–9906, Jul. 2001.
- [32] C. V Harding, L. Ramachandra, and M. J. Wick, "Interaction of bacteria with antigen presenting cells: influences on antigen presentation and antibacterial immunity.," *Curr. Opin. Immunol.*, vol. 15, no. 1, pp. 112–9, Feb. 2003.
- [33] R. S. Flannagan, G. Cosío, and S. Grinstein, "Antimicrobial mechanisms of phagocytes and bacterial evasion strategies.," *Nat. Rev. Microbiol.*, vol. 7, no. 5, pp. 355–66, May 2009.
- [34] C. Moreno, A. Mehlert, and J. Lamb, "The inhibitory effects of mycobacterial lipoarabinomannan and polysaccharides upon polyclonal and monoclonal human T cell proliferation.," *Clin. Exp. Immunol.*, vol. 74, no. 2, pp. 206–10, Nov. 1988.
- [35] E. H. Noss, R. K. Pai, T. J. Sellati, J. D. Radolf, J. Belisle, D. T. Golenbock, W. H. Boom, and C. V Harding, "Toll-like receptor 2-dependent inhibition of macrophage class II MHC expression and antigen processing by 19-kDa lipoprotein of *Mycobacterium tuberculosis*.," *J. Immunol.*, vol. 167, no. 2, pp. 910–8, Jul. 2001.
- [36] Z. Hmama, R. Gabathuler, W. A. Jefferies, G. de Jong, and N. E. Reiner, "Attenuation of HLA-DR expression by mononuclear phagocytes infected with *Mycobacterium tuberculosis* is related to intracellular sequestration of immature class II

- heterodimers.," *J. Immunol.*, vol. 161, no. 9, pp. 4882–93, Nov. 1998.
- [37] M. F. Goldberg, N. K. Saini, and S. A. Porcelli, "Evasion of Innate and Adaptive Immunity by *Mycobacterium tuberculosis*," *Microbiol. Spectr.*, vol. 2, no. 5, Oct. 2014.
- [38] W. C. Wimley, "Describing the mechanism of antimicrobial peptide action with the interfacial activity model.," *ACS Chem. Biol.*, vol. 5, no. 10, pp. 905–17, Oct. 2010.
- [39] K. Matsuzaki, "Why and how are peptide-lipid interactions utilized for self-defense? Magainins and tachyplesins as archetypes.," *Biochim. Biophys. Acta*, vol. 1462, no. 1–2, pp. 1–10, Dec. 1999.
- [40] M. Rahnamaeian, "Antimicrobial peptides: modes of mechanism, modulation of defense responses.," *Plant Signal. Behav.*, vol. 6, no. 9, pp. 1325–32, Sep. 2011.
- [41] M. Zasloff, "Antimicrobial peptides of multicellular organisms.," *Nature*, vol. 415, no. 6870, pp. 389–95, Jan. 2002.
- [42] P. M??ndez-Samperio, "The human cathelicidin hCAP18/LL-37: A multifunctional peptide involved in mycobacterial infections," *Peptides*, vol. 31, no. 9, pp. 1791–1798, 2010.
- [43] T. Silva, B. Magalhães, S. Maia, P. Gomes, K. Nazmi, J. G. M. Bolscher, P. N. Rodrigues, M. Bastos, and M. S. Gomes, "Killing of *Mycobacterium avium* by lactoferricin peptides: Improved activity of arginine- and d-Amino-Acid-containing molecules," *Antimicrob. Agents Chemother.*, vol. 58, no. 6, pp. 3461–3467, 2014.
- [44] J. S. Khara, F. K. Lim, Y. Wang, X.-Y. Ke, Z. X. Voo, Y. Y. Yang, R. Lakshminarayanan, and P. L. R. Ee, "Designing α -helical peptides with enhanced synergism and selectivity against *Mycobacterium smegmatis*: Discerning the role of hydrophobicity and helicity.," *Acta Biomater.*, vol. 28, pp. 99–108, Dec. 2015.
- [45] S. Sharma, I. Verma, and G. K. Khuller, "Biochemical interaction of human neutrophil peptide-1 with *Mycobacterium tuberculosis* H37Ra.," *Arch. Microbiol.*, vol. 171, no. 5, pp. 338–42, Apr. 1999.
- [46] M. Rao, T. L. Streur, F. E. Aldwell, and G. M. Cook, "Intracellular pH regulation by *Mycobacterium smegmatis* and *Mycobacterium bovis* BCG.," *Microbiology*, vol. 147, no. Pt 4, pp. 1017–24, Apr. 2001.
- [47] P. Santos, A. Gordillo, L. Osses, L. M. Salazar, and C. Y. Soto, "Effect of antimicrobial peptides on ATPase activity and proton pumping in plasma membrane vesicles obtained from mycobacteria," *Peptides*, vol. 36, no. 1, pp. 121–128, 2012.
- [48] R. E. Hancock and M. G. Scott, "The role of antimicrobial peptides in animal defenses.," *Proc. Natl. Acad. Sci. U. S. A.*, vol. 97, no. 16, pp. 8856–61, 2000.
- [49] K. Takeshima, A. Chikushi, K.-K. Lee, S. Yonehara, and K. Matsuzaki, "Translocation of analogues of the antimicrobial peptides magainin and buforin across human cell membranes.," *J. Biol. Chem.*, vol. 278, no. 2, pp. 1310–5, Jan. 2003.

- [50] A. Sharma, A. A. runrao Pohane, S. Bansal, A. Bajaj, V. Jain, and A. Srivastava, "Cell penetrating synthetic antimicrobial peptides (SAMPs) exhibiting potent and selective killing of mycobacterium by targeting its DNA," *Chemistry*, vol. 21, no. 9, pp. 3540–3545, 2015.
- [51] L. Brown, J. M. Wolf, R. Prados-Rosales, and A. Casadevall, "Through the wall: extracellular vesicles in Gram-positive bacteria, mycobacteria and fungi.," *Nat. Rev. Microbiol.*, vol. 13, no. 10, pp. 620–30, Oct. 2015.
- [52] D.-M. Shin and E.-K. Jo, "Antimicrobial Peptides in Innate Immunity against Mycobacteria," *Immune Netw.*, vol. 11, no. 5, p. 245, Oct. 2011.
- [53] S. A. Baltzer and M. H. Brown, "Antimicrobial peptides: promising alternatives to conventional antibiotics.," *J. Mol. Microbiol. Biotechnol.*, vol. 20, no. 4, pp. 228–35, Jan. 2011.
- [54] A. K. Mishra, N. N. Driessen, B. J. Appelmelk, and G. S. Besra, "Lipoarabinomannan and related glycoconjugates: structure, biogenesis and role in Mycobacterium tuberculosis physiology and host–pathogen interaction," *FEMS Microbiol. Rev.*, vol. 35, no. 6, pp. 1126–1157, Nov. 2011.
- [55] P. Méndez-Samperio, "Role of antimicrobial peptides in host defense against mycobacterial infections.," *Peptides*, vol. 29, no. 10, pp. 1836–41, Oct. 2008.
- [56] M. Zanetti, "The role of cathelicidins in the innate host defenses of mammals.," *Curr. Issues Mol. Biol.*, vol. 7, no. 2, pp. 179–96, Jul. 2005.
- [57] R. J. Fahy and M. D. Wewers, "Pulmonary defense and the human cathelicidin hCAP-18/LL-37.," *Immunol. Res.*, vol. 31, no. 2, pp. 75–89, Jan. 2005.
- [58] K. Bandurska, A. Berdowska, R. Barczyńska-Felusiak, and P. Krupa, "Unique features of human cathelicidin LL-37.," *Biofactors*, vol. 41, no. 5, pp. 289–300, Sep. 2015.
- [59] M. Zanetti, R. Gennaro, and D. Romeo, "Cathelicidins: a novel protein family with a common proregion and a variable C-terminal antimicrobial domain.," *FEBS Lett.*, vol. 374, no. 1, pp. 1–5, Oct. 1995.
- [60] O. E. Sørensen, P. Follin, A. H. Johnsen, J. Calafat, G. S. Tjabringa, P. S. Hiemstra, and N. Borregaard, "Human cathelicidin, hCAP-18, is processed to the antimicrobial peptide LL-37 by extracellular cleavage with proteinase 3.," *Blood*, vol. 97, no. 12, pp. 3951–9, Jun. 2001.
- [61] De Yang, Q. Chen, A. P. Schmidt, G. M. Anderson, J. M. Wang, J. Wooters, J. J. Oppenheim, and O. Chertov, "LL-37, the neutrophil granule- and epithelial cell-derived cathelicidin, utilizes formyl peptide receptor-like 1 (FPRL1) as a receptor to chemoattract human peripheral blood neutrophils, monocytes, and T cells.," *J. Exp. Med.*, vol. 192, no. 7, pp. 1069–74, Oct. 2000.

- [62] Y. Kai-Larsen and B. Agerberth, "The role of the multifunctional peptide LL-37 in host defense.," *Front. Biosci.*, vol. 13, pp. 3760–7, Jan. 2008.
- [63] A. Sonawane, J. C. Santos, B. B. Mishra, P. Jena, C. Progida, O. E. Sorensen, R. Gallo, R. Appelberg, and G. Griffiths, "Cathelicidin is involved in the intracellular killing of mycobacteria in macrophages.," *Cell. Microbiol.*, vol. 13, no. 10, pp. 1601–17, Oct. 2011.
- [64] B. Rivas-Santiago, R. Hernandez-Pando, C. Carranza, E. Juarez, J. L. Contreras, D. Aguilar-Leon, M. Torres, and E. Sada, "Expression of cathelicidin LL-37 during Mycobacterium tuberculosis infection in human alveolar macrophages, monocytes, neutrophils, and epithelial cells.," *Infect. Immun.*, vol. 76, no. 3, pp. 935–41, Mar. 2008.
- [65] P. T. Liu, S. Stenger, D. H. Tang, and R. L. Modlin, "Cutting edge: vitamin D-mediated human antimicrobial activity against Mycobacterium tuberculosis is dependent on the induction of cathelicidin.," *J. Immunol.*, vol. 179, no. 4, pp. 2060–3, Aug. 2007.
- [66] G. R. Campbell and S. A. Spector, "Autophagy induction by vitamin D inhibits both Mycobacterium tuberculosis and human immunodeficiency virus type 1.," *Autophagy*, vol. 8, no. 10, pp. 1523–5, Oct. 2012.
- [67] Z. Hmama, K. Sendide, A. Talal, R. Garcia, K. Dobos, and N. E. Reiner, "Quantitative analysis of phagolysosome fusion in intact cells: inhibition by mycobacterial lipoarabinomannan and rescue by an 1alpha,25-dihydroxyvitamin D3-phosphoinositide 3-kinase pathway.," *J. Cell Sci.*, vol. 117, no. Pt 10, pp. 2131–40, Apr. 2004.
- [68] J.-M. Yuk, D.-M. Shin, H.-M. Lee, C.-S. Yang, H. S. Jin, K.-K. Kim, Z.-W. Lee, S.-H. Lee, J.-M. Kim, and E.-K. Jo, "Vitamin D3 induces autophagy in human monocytes/macrophages via cathelicidin.," *Cell Host Microbe*, vol. 6, no. 3, pp. 231–43, Sep. 2009.
- [69] B. Rivas-Santiago, C. E. Rivas Santiago, J. E. Castañeda-Delgado, J. C. León-Contreras, R. E. W. Hancock, and R. Hernandez-Pando, "Activity of LL-37, CRAMP and antimicrobial peptide-derived compounds E2, E6 and CP26 against Mycobacterium tuberculosis.," *Int. J. Antimicrob. Agents*, vol. 41, no. 2, pp. 143–8, Feb. 2013.
- [70] F. Torres-Juarez, A. Cardenas-Vargas, A. Montoya-Rosales, I. González-Curiel, M. H. Garcia-Hernandez, J. A. Enciso-Moreno, R. E. W. Hancock, and B. Rivas-Santiago, "LL-37 immunomodulatory activity during Mycobacterium tuberculosis infection in macrophages.," *Infect. Immun.*, vol. 83, no. 12, pp. 4495–503, Dec. 2015.
- [71] R. S. Rekha, S. S. V. J. Rao Muvva, M. Wan, R. Raqib, P. Bergman, S. Brighenti, G. H. Gudmundsson, and B. Agerberth, "Phenylbutyrate induces LL-37-dependent

- autophagy and intracellular killing of *Mycobacterium tuberculosis* in human macrophages.," *Autophagy*, vol. 11, no. 9, pp. 1688–99, 2015.
- [72] H. Chu, M. Pazgier, G. Jung, S.-P. Nuccio, P. A. Castillo, M. F. de Jong, M. G. Winter, S. E. Winter, J. Wehkamp, B. Shen, N. H. Salzman, M. A. Underwood, R. M. Tsois, G. M. Young, W. Lu, R. I. Lehrer, A. J. Bäuml, and C. L. Bevins, "Human α -defensin 6 promotes mucosal innate immunity through self-assembled peptide nanonets.," *Science*, vol. 337, no. 6093, pp. 477–81, Jul. 2012.
- [73] M. Faurschou, "Prodefensins are matrix proteins of specific granules in human neutrophils," *J. Leukoc. Biol.*, vol. 78, no. 3, pp. 785–793, May 2005.
- [74] J. J. Oppenheim, A. Biragyn, L. W. Kwak, and D. Yang, "Roles of antimicrobial peptides such as defensins in innate and adaptive immunity.," *Ann. Rheum. Dis.*, vol. 62 Suppl 2, p. ii17-21, Nov. 2003.
- [75] V. Driss, F. Legrand, E. Hermann, S. Loiseau, Y. Guerardel, L. Kremer, E. Adam, G. Woerly, D. Dombrowicz, and M. Capron, "TLR2-dependent eosinophil interactions with mycobacteria: role of alpha-defensins.," *Blood*, vol. 113, no. 14, pp. 3235–44, Apr. 2009.
- [76] M. Jacobsen, D. Reipsilber, A. Gutschmidt, A. Neher, K. Feldmann, H. J. Mollenkopf, A. Ziegler, and S. H. E. Kaufmann, "Candidate biomarkers for discrimination between infection and disease caused by *Mycobacterium tuberculosis*," *J. Mol. Med.*, vol. 85, no. 6, pp. 613–621, Feb. 2007.
- [77] B. H. Tan, C. Meinken, M. Bastian, H. Bruns, A. Legaspi, M. T. Ochoa, S. R. Krutzik, B. R. Bloom, T. Ganz, R. L. Modlin, and S. Stenger, "Macrophages acquire neutrophil granules for antimicrobial activity against intracellular pathogens.," *J. Immunol.*, vol. 177, no. 3, pp. 1864–71, Aug. 2006.
- [78] H. Taute, M. J. Bester, A. W. H. Neitz, and A. R. M. Gaspar, "Investigation into the mechanism of action of the antimicrobial peptides Os and Os-C derived from a tick defensin.," *Peptides*, vol. 71, pp. 179–87, Sep. 2015.
- [79] B. Rivas-Santiago, S. K. Schwander, C. Sarabia, G. Diamond, M. E. Klein-Patel, R. Hernandez-Pando, J. J. Ellner, and E. Sada, "Human β -defensin 2 is expressed and associated with *Mycobacterium tuberculosis* during infection of human alveolar epithelial cells.," *Infect. Immun.*, vol. 73, no. 8, pp. 4505–11, Aug. 2005.
- [80] K. O. Kisich, L. Heifets, M. Higgins, and G. Diamond, "Antimycobacterial agent based on mRNA encoding human beta-defensin 2 enables primary macrophages to restrict growth of *Mycobacterium tuberculosis*.," *Infect. Immun.*, vol. 69, no. 4, pp. 2692–9, Apr. 2001.
- [81] S. Sharma, I. Verma, and G. K. Khuller, "Therapeutic Potential of Human Neutrophil Peptide 1 against Experimental Tuberculosis," *Antimicrob. Agents Chemother.*, vol.

- 45, no. 2, pp. 639–640, Feb. 2001.
- [82] A. Kalita, I. Verma, and G. K. Khuller, “Role of human neutrophil peptide-1 as a possible adjunct to antituberculosis chemotherapy.,” *J. Infect. Dis.*, vol. 190, no. 8, pp. 1476–80, Oct. 2004.
- [83] C. E. Rivas-Santiago, B. Rivas-Santiago, D. A. León, J. Castañeda-Delgado, and R. Hernández Pando, “Induction of β -defensins by l-isoleucine as novel immunotherapy in experimental murine tuberculosis.,” *Clin. Exp. Immunol.*, vol. 164, no. 1, pp. 80–9, Apr. 2011.
- [84] A. Krause, S. Neitz, H. J. Mägert, A. Schulz, W. G. Forssmann, P. Schulz-Knappe, and K. Adermann, “LEAP-1, a novel highly disulfide-bonded human peptide, exhibits antimicrobial activity.,” *FEBS Lett.*, vol. 480, no. 2–3, pp. 147–50, Sep. 2000.
- [85] C. H. Park, E. V. Valore, A. J. Waring, and T. Ganz, “Hepcidin, a urinary antimicrobial peptide synthesized in the liver.,” *J. Biol. Chem.*, vol. 276, no. 11, pp. 7806–10, Mar. 2001.
- [86] A. H. Laftah, B. Ramesh, R. J. Simpson, N. Solanky, S. Bahram, K. Schümann, E. S. Debnam, and S. K. S. Srail, “Effect of hepcidin on intestinal iron absorption in mice.,” *Blood*, vol. 103, no. 10, pp. 3940–4, May 2004.
- [87] S. Yamaji, “Inhibition of iron transport across human intestinal epithelial cells by hepcidin,” *Blood*, vol. 104, no. 7, pp. 2178–2180, Oct. 2004.
- [88] E. Nemeth and T. Ganz, “The Role of Hepcidin in Iron Metabolism,” *Acta Haematol.*, vol. 122, no. 2–3, pp. 78–86, Jan. 2009.
- [89] T. Ganz, “Hepcidin--a peptide hormone at the interface of innate immunity and iron metabolism.,” *Curr. Top. Microbiol. Immunol.*, vol. 306, pp. 183–98, Jan. 2006.
- [90] F. B. Sow, G. R. Alvarez, R. P. Gross, A. R. Satoskar, L. S. Schlesinger, B. S. Zwillig, and W. P. Lafuse, “Role of STAT1, NF- κ B, and C/EBP β in the macrophage transcriptional regulation of hepcidin by mycobacterial infection and IFN- γ ,” *J. Leukoc. Biol.*, vol. 86, no. 5, pp. 1247–1258, Aug. 2009.
- [91] T. Ganz, “Hepcidin, a key regulator of iron metabolism and mediator of anemia of inflammation.,” *Blood*, vol. 102, no. 3, pp. 783–8, Aug. 2003.
- [92] C. D. Morris, A. R. Bird, and H. Nell, “The haematological and biochemical changes in severe pulmonary tuberculosis.,” *Q. J. Med.*, vol. 73, no. 272, pp. 1151–9, Dec. 1989.
- [93] F. B. Sow, W. C. Florence, A. R. Satoskar, L. S. Schlesinger, B. S. Zwillig, and W. P. Lafuse, “Expression and localization of hepcidin in macrophages: a role in host defense against tuberculosis,” *J. Leukoc. Biol.*, vol. 82, no. 4, pp. 934–945, Aug. 2007.
- [94] F. B. Sow, S. Nandakumar, V. Velu, K. L. Kellar, L. S. Schlesinger, R. R. Amara, W. P. Lafuse, T. M. Shinnick, and S. B. Sable, “Mycobacterium tuberculosis components

- stimulate production of the antimicrobial peptide hepcidin.," *Tuberculosis (Edinb)*., vol. 91, no. 4, pp. 314–21, Jul. 2011.
- [95] M. Javaheri-Kermani, T. Farazmandfar, A. Ajami, and Y. Yazdani, "Impact of hepcidin antimicrobial peptide on iron overload in tuberculosis patients.," *Scand. J. Infect. Dis.*, vol. 46, no. 10, pp. 693–6, Oct. 2014.
- [96] P. F. Levay and M. Viljoen, "Lactoferrin: a general review.," *Haematologica*, vol. 80, no. 3, pp. 252–67, Jan. .
- [97] J. L. Gifford, H. N. Hunter, and H. J. Vogel, "Lactoferricin: a lactoferrin-derived peptide with antimicrobial, antiviral, antitumor and immunological properties.," *Cell. Mol. Life Sci.*, vol. 62, no. 22, pp. 2588–98, Nov. 2005.
- [98] T. Isamida, T. Tanaka, Y. Omata, K. Yamauchi, K. Shimazaki, and A. Saito, "Protective effect of lactoferricin against *Toxoplasma gondii* infection in mice.," *J. Vet. Med. Sci.*, vol. 60, no. 2, pp. 241–4, Feb. 1998.
- [99] R. R. Arnold, J. E. Russell, W. J. Champion, M. Brewer, and J. J. Gauthier, "Bactericidal activity of human lactoferrin: differentiation from the stasis of iron deprivation.," *Infect. Immun.*, vol. 35, no. 3, pp. 792–9, Mar. 1982.
- [100] J. Qiu, D. R. Hendrixson, E. N. Baker, T. F. Murphy, J. W. St Geme, and A. G. Plaut, "Human milk lactoferrin inactivates two putative colonization factors expressed by *Haemophilus influenzae*." *Proc. Natl. Acad. Sci. U. S. A.*, vol. 95, no. 21, pp. 12641–6, Oct. 1998.
- [101] J. Kanwar, N. Anand, R. Kanwar, M. Dubey, R. Sehgal, A. Verma, and R. K. Vahishta, "Effect of lactoferrin protein on red blood cells and macrophages: mechanism of parasite–host interaction," *Drug Des. Devel. Ther.*, vol. 9, p. 3821, Jul. 2015.
- [102] K. J. Welsh, S.-A. Hwang, S. Boyd, M. L. Kruzel, R. L. Hunter, and J. K. Actor, "Influence of oral lactoferrin on *Mycobacterium tuberculosis* induced immunopathology," *Tuberculosis*, vol. 91, pp. S105–S113, Dec. 2011.
- [103] S.-A. Hwang, K. M. Wilk, Y. A. Bangale, M. L. Kruzel, and J. K. Actor, "Lactoferrin modulation of IL-12 and IL-10 response from activated murine leukocytes," *Med. Microbiol. Immunol.*, vol. 196, no. 3, pp. 171–180, Mar. 2007.
- [104] S.-A. Hwang, R. Arora, M. L. Kruzel, and J. K. Actor, "Lactoferrin enhances efficacy of the BCG vaccine: comparison between two inbred mice strains (C57BL/6 and BALB/c)," *Tuberculosis*, vol. 89, pp. S49–S54, Dec. 2009.
- [105] S.-A. Hwang, M. L. Kruzel, and J. K. Actor, "CHO expressed recombinant human lactoferrin as an adjuvant for BCG," *Int. J. Immunopathol. Pharmacol.*, vol. 28, no. 4, pp. 452–468, Aug. 2015.
- [106] R. E. Thom, M. J. Elmore, A. Williams, S. C. Andrews, F. Drobniewski, P. D. Marsh, and J. A. Tree, "The expression of ferritin, lactoferrin, transferrin receptor and solute

- carrier family 11A1 in the host response to BCG-vaccination and Mycobacterium tuberculosis challenge.," *Vaccine*, vol. 30, no. 21, pp. 3159–68, May 2012.
- [107] P. Jena, S. Mohanty, T. Mohanty, S. Kallert, M. Morgelin, T. Lindstrøm, N. Borregaard, S. Stenger, A. Sonawane, and O. E. Sørensen, "Azurophil granule proteins constitute the major mycobactericidal proteins in human neutrophils and enhance the killing of mycobacteria in macrophages.," *PLoS One*, vol. 7, no. 12, p. e50345, Jan. 2012.
- [108] W. M. Shafer, L. E. Martin, and J. K. Spitznagel, "Cationic antimicrobial proteins isolated from human neutrophil granulocytes in the presence of diisopropyl fluorophosphate.," *Infect. Immun.*, vol. 45, no. 1, pp. 29–35, Jul. 1984.
- [109] H. A. Pereira, J. K. Spitznagel, E. F. Winton, W. M. Shafer, L. E. Martin, G. S. Guzman, J. Pohl, R. W. Scott, M. N. Marra, and J. M. Kinkade, "The ontogeny of a 57-Kd cationic antimicrobial protein of human polymorphonuclear leukocytes: localization to a novel granule population.," *Blood*, vol. 76, no. 4, pp. 825–34, Aug. 1990.
- [110] J. E. Gabay, R. W. Scott, D. Campanelli, J. Griffith, C. Wilde, M. N. Marra, M. Seeger, and C. F. Nathan, "Antibiotic proteins of human polymorphonuclear leukocytes.," *Proc. Natl. Acad. Sci. U. S. A.*, vol. 86, no. 14, pp. 5610–4, Jul. 1989.
- [111] O. Chertov, H. Ueda, L. L. Xu, K. Tani, W. J. Murphy, J. M. Wang, O. M. Howard, T. J. Sayers, and J. J. Oppenheim, "Identification of human neutrophil-derived cathepsin G and azurocidin/CAP37 as chemoattractants for mononuclear cells and neutrophils.," *J. Exp. Med.*, vol. 186, no. 5, pp. 739–47, Aug. 1997.
- [112] O. Soehnlein, A. Zernecke, E. E. Eriksson, A. G. Rothfuchs, C. T. Pham, H. Herwald, K. Bidzhekov, M. E. Rottenberg, C. Weber, and L. Lindbom, "Neutrophil secretion products pave the way for inflammatory monocytes," *Blood*, vol. 112, no. 4, pp. 1461–1471, May 2008.
- [113] H. Tapper, A. Karlsson, M. Mörgelin, H. Flodgaard, and H. Herwald, "Secretion of heparin-binding protein from human neutrophils is determined by its localization in azurophilic granules and secretory vesicles.," *Blood*, vol. 99, no. 5, pp. 1785–93, Mar. 2002.
- [114] O. Soehnlein, X. Xie, H. Ulbrich, E. Kenne, P. Rotzius, H. Flodgaard, E. E. Eriksson, and L. Lindbom, "Neutrophil-derived heparin-binding protein (HBP/CAP37) deposited on endothelium enhances monocyte arrest under flow conditions.," *J. Immunol.*, vol. 174, no. 10, pp. 6399–405, May 2005.
- [115] M. Heinzelmann, M. A. Mercer-Jones, H. Flodgaard, and F. N. Miller, "Heparin-binding protein (CAP37) is internalized in monocytes and increases LPS-induced monocyte activation.," *J. Immunol.*, vol. 160, no. 11, pp. 5530–6, Jun. 1998.
- [116] O. Soehnlein, Y. Kai-Larsen, R. Frithiof, O. E. Sorensen, E. Kenne, K. Scharffetter-

- Kochanek, E. E. Eriksson, H. Herwald, B. Agerberth, and L. Lindbom, "Neutrophil primary granule proteins HBP and HNP1-3 boost bacterial phagocytosis by human and murine macrophages.," *J. Clin. Invest.*, vol. 118, no. 10, pp. 3491–502, Oct. 2008.
- [117] W. M. Shafer, L. E. Martin, and J. K. Spitznagel, "Late intraphagosomal hydrogen ion concentration favors the in vitro antimicrobial capacity of a 37-kilodalton cationic granule protein of human neutrophil granulocytes.," *Infect. Immun.*, vol. 53, no. 3, pp. 651–5, Sep. 1986.
- [118] J. . 1. Bieth, "Elastases: catalytic and biological properties," *Regul. matrix Accumulation, mecham, R., ed. (Academic Press. New York, pp. 217–320, 1986.*
- [119] A. Belaouaj, K. S. Kim, and S. D. Shapiro, "Degradation of outer membrane protein A in Escherichia coli killing by neutrophil elastase.," *Science*, vol. 289, no. 5482, pp. 1185–8, Aug. 2000.
- [120] F. L. Ribeiro-Gomes, M. C. A. Moniz-de-Souza, M. S. Alexandre-Moreira, W. B. Dias, M. F. Lopes, M. P. Nunes, G. Lungarella, and G. A. DosReis, "Neutrophils activate macrophages for intracellular killing of Leishmania major through recruitment of TLR4 by neutrophil elastase.," *J. Immunol.*, vol. 179, no. 6, pp. 3988–94, Sep. 2007.
- [121] C. T. N. Pham, "Neutrophil serine proteases: specific regulators of inflammation.," *Nat. Rev. Immunol.*, vol. 6, no. 7, pp. 541–50, Jul. 2006.
- [122] V. Brinkmann, U. Reichard, C. Goosmann, B. Fauler, Y. Uhlemann, D. S. Weiss, Y. Weinrauch, and A. Zychlinsky, "Neutrophil extracellular traps kill bacteria.," *Science*, vol. 303, no. 5663, pp. 1532–5, Mar. 2004.
- [123] A. Belaouaj, R. McCarthy, M. Baumann, Z. Gao, T. J. Ley, S. N. Abraham, and S. D. Shapiro, "Mice lacking neutrophil elastase reveal impaired host defense against gram negative bacterial sepsis.," *Nat. Med.*, vol. 4, no. 5, pp. 615–8, May 1998.
- [124] K. Steinwede, R. Maus, J. Bohling, S. Voedisch, A. Braun, M. Ochs, A. Schmiedl, F. Länger, F. Gauthier, J. Roes, T. Welte, F. C. Bange, M. Niederweis, F. Bühling, and U. A. Maus, "Cathepsin G and neutrophil elastase contribute to lung-protective immunity against mycobacterial infections in mice.," *J. Immunol.*, vol. 188, no. 9, pp. 4476–87, May 2012.
- [125] E. Boix, V. A. Salazar, M. Torrent, D. Pulido, M. V. Nogués, and M. Moussaoui, "Structural determinants of the eosinophil cationic protein antimicrobial activity," *Biol. Chem.*, vol. 393, no. 8, pp. 801–815, 2012.
- [126] E. Boix and M. V. Nogués, "Mammalian antimicrobial proteins and peptides: overview on the RNase A superfamily members involved in innate host defence.," *Mol. Biosyst.*, vol. 3, no. 5, pp. 317–35, May 2007.
- [127] H. F. Rosenberg, "RNase A ribonucleases and host defense: an evolving story.," *J. Leukoc. Biol.*, vol. 83, no. 5, pp. 1079–87, May 2008.

- [128] E. Pizzo and G. D'Alessio, "The success of the RNase scaffold in the advance of biosciences and in evolution.," *Gene*, vol. 406, no. 1–2, pp. 8–12, Dec. 2007.
- [129] P. Venge, J. Byström, M. Carlson, L. Håkansson, M. Karawaczyk, C. Peterson, L. Sevéus, and A. Trulsson, "Eosinophil cationic protein (ECP): molecular and biological properties and the use of ECP as a marker of eosinophil activation in disease.," *Clin. Exp. Allergy*, vol. 29, no. 9, pp. 1172–86, Oct. 1999.
- [130] J. Bystrom, K. Amin, and D. Bishop-Bailey, "Analysing the eosinophil cationic protein-- a clue to the function of the eosinophil granulocyte.," *Respir. Res.*, vol. 12, p. 10, Jan. 2011.
- [131] J. Monteseirín, A. Vega, P. Chacón, M. J. Camacho, R. El Bekay, J. A. Asturias, A. Martínez, P. Guardia, R. Pérez-Cano, and J. Conde, "Neutrophils as a novel source of eosinophil cationic protein in IgE-mediated processes.," *J. Immunol.*, vol. 179, no. 4, pp. 2634–41, Aug. 2007.
- [132] Y.-S. Liu, P.-W. Tsai, Y. Wang, T. Fan, C.-H. Hsieh, M. Chang, T.-W. Pai, C.-F. Huang, C.-Y. Lan, and H.-T. Chang, "Chemoattraction of macrophages by secretory molecules derived from cells expressing the signal peptide of eosinophil cationic protein," *BMC Syst. Biol.*, vol. 6, no. 1, p. 105, Jan. 2012.
- [133] V. K. Vijayan, A. M. Reetha, M. S. Jawahar, K. Sankaran, and R. Prabhakar, "Pulmonary eosinophilia in pulmonary tuberculosis.," *Chest*, vol. 101, no. 6, pp. 1708–9, Jun. 1992.
- [134] P. Akuthota, J. J. Xenakis, and P. F. Weller, "Eosinophils: offenders or general bystanders in allergic airway disease and pulmonary immunity?," *J. Innate Immun.*, vol. 3, no. 2, pp. 113–9, Jan. 2011.
- [135] H. Kita, "Eosinophils: multifaceted biological properties and roles in health and disease," *Immunol. Rev.*, vol. 242, no. 1, pp. 161–177, Jul. 2011.
- [136] H. Saiga, Y. Shimada, and K. Takeda, "Innate Immune Effectors in Mycobacterial Infection," *Clin. Dev. Immunol.*, vol. 2011, pp. 1–8, Jan. 2011.
- [137] O. Soehnlein, "Direct and alternative antimicrobial mechanisms of neutrophil-derived granule proteins," *J. Mol. Med.*, vol. 87, no. 12, pp. 1157–1164, Jul. 2009.
- [138] V. Borelli, F. Vita, S. Shankar, M. R. Soranzo, E. Banfi, G. Scialino, C. Brochetta, and G. Zabucchi, "Human eosinophil peroxidase induces surface alteration, killing, and lysis of *Mycobacterium tuberculosis*," *Infect. Immun.*, vol. 71, no. 2, pp. 605–13, Feb. 2003.
- [139] V. Driss, E. Hermann, F. Legrand, S. Loiseau, M. Delbeke, L. Kremer, Y. Guerardel, D. Dombrowicz, and M. Capron, "CR3-dependent negative regulation of human eosinophils by *Mycobacterium bovis* BCG lipoarabinomannan," *Immunol. Lett.*, vol. 143, no. 2, pp. 202–207, Apr. 2012.

- [140] J. Harder and J.-M. Schroder, "RNase 7, a novel innate immune defense antimicrobial protein of healthy human skin.," *J. Biol. Chem.*, vol. 277, no. 48, pp. 46779–84, Nov. 2002.
- [141] J. Zhang, K. D. Dyer, and H. F. Rosenberg, "Human RNase 7: a new cationic ribonuclease of the RNase A superfamily.," *Nucleic Acids Res.*, vol. 31, no. 2, pp. 602–7, Jan. 2003.
- [142] J. D. Spencer, A. L. Schwaderer, J. D. Dirosario, K. M. McHugh, G. McGillivray, S. S. Justice, A. R. Carpenter, P. B. Baker, J. Harder, and D. S. Hains, "Ribonuclease 7 is a potent antimicrobial peptide within the human urinary tract.," *Kidney Int.*, vol. 80, no. 2, pp. 174–80, Jul. 2011.
- [143] B. Becknell, T. E. Eichler, S. Beceiro, B. Li, R. S. Easterling, A. R. Carpenter, C. L. James, K. M. McHugh, D. S. Hains, S. Partida-Sanchez, and J. D. Spencer, "Ribonucleases 6 and 7 have antimicrobial function in the human and murine urinary tract.," *Kidney Int.*, vol. 87, no. 1, pp. 151–61, Jan. 2015.
- [144] D. Pulido, M. Torrent, D. Andreu, M. V. Nogués, and E. Boix, "Two human host defense ribonucleases against mycobacteria, the eosinophil cationic protein (RNase 3) and RNase 7.," *Antimicrob. Agents Chemother.*, vol. 57, no. 8, pp. 3797–805, Aug. 2013.
- [145] Arranz-Trullén J; Pulido D; Bhakta S and Boix E, "Unveiling the mode of action of human antimicrobial RNases against Mycobacterium tuberculosis using a surrogate macrophage infected model," *Manuscr. Prep.*
- [146] Z. Jiang, M. P. Higgins, J. Whitehurst, K. O. Kisich, M. I. Voskuil, and R. S. Hodges, "Anti-tuberculosis activity of α -helical antimicrobial peptides: de novo designed L- and D-enantiomers versus L- and D-LL-37.," *Protein Pept. Lett.*, vol. 18, no. 3, pp. 241–52, Mar. 2011.
- [147] B. M. Peters, M. E. Shirliff, and M. A. Jabra-Rizk, "Antimicrobial peptides: primeval molecules or future drugs?," *PLoS Pathog.*, vol. 6, no. 10, p. e1001067, Jan. 2010.
- [148] M. Abedinzadeh, M. Gaeini, and S. Sardari, "Natural antimicrobial peptides against Mycobacterium tuberculosis.," *J. Antimicrob. Chemother.*, vol. 70, no. 5, pp. 1285–9, May 2015.
- [149] Y. Lan, J. T. Lam, G. K. H. Siu, W. C. Yam, A. J. Mason, and J. K. W. Lam, "Cationic amphipathic D-enantiomeric antimicrobial peptides with in vitro and ex vivo activity against drug-resistant Mycobacterium tuberculosis," *Tuberculosis*, vol. 94, no. 6, pp. 678–689, Dec. 2014.
- [150] L. S. Vermeer, Y. Lan, V. Abbate, E. Ruh, T. T. Bui, L. J. Wilkinson, T. Kanno, E. Jumagulova, J. Kozłowska, J. Patel, C. A. McIntyre, W. C. Yam, G. Siu, R. A. Atkinson, J. K. W. Lam, S. S. Bansal, A. F. Drake, G. H. Mitchell, and A. J. Mason,

- “Conformational Flexibility Determines Selectivity and Antibacterial, Antiplasmodial, and Anticancer Potency of Cationic α -Helical Peptides,” *J. Biol. Chem.*, vol. 287, no. 41, pp. 34120–34133, Oct. 2012.
- [151] S.-T. Yang, J. Y. Lee, H.-J. Kim, Y.-J. Eu, S. Y. Shin, K.-S. Hahm, and J. Il Kim, “Contribution of a central proline in model amphipathic alpha-helical peptides to self-association, interaction with phospholipids, and antimicrobial mode of action.,” *FEBS J.*, vol. 273, no. 17, pp. 4040–54, Sep. 2006.
- [152] J. S. Khara, Y. Wang, X.-Y. Ke, S. Liu, S. M. Newton, P. R. Langford, Y. Y. Yang, and P. L. R. Ee, “Anti-mycobacterial activities of synthetic cationic α -helical peptides and their synergism with rifampicin.,” *Biomaterials*, vol. 35, no. 6, pp. 2032–8, Feb. 2014.
- [153] P. C. L. Kwok, A. Grabarek, M. Y. T. Chow, Y. Lan, J. C. W. Li, L. Casettari, A. J. Mason, and J. K. W. Lam, “Inhalable spray-dried formulation of D-LAK antimicrobial peptides targeting tuberculosis.,” *Int. J. Pharm.*, vol. 491, no. 1–2, pp. 367–74, Aug. 2015.
- [154] Y. Y. Llamas-González, C. Pedroza-Roldán, M. B. Cortés-Serna, A. L. Márquez-Aguirre, F. J. Gálvez-Gastélum, and M. A. Flores-Valdez, “The synthetic cathelicidin HHC-10 inhibits *Mycobacterium bovis* BCG in vitro and in C57BL/6 mice.,” *Microb. Drug Resist.*, vol. 19, no. 2, pp. 124–9, Apr. 2013.
- [155] M. Torrent, D. Pulido, J. Valle, M. V. Nogués, D. Andreu, and E. Boix, “Ribonucleases as a host-defence family: evidence of evolutionarily conserved antimicrobial activity at the N-terminus.,” *Biochem. J.*, vol. 456, no. 1, pp. 99–108, 2013.
- [156] M. Torrent, D. Pulido, B. G. De La Torre, M. F. García-Mayoral, M. V. Nogués, M. Bruix, D. Andreu, and E. Boix, “Refining the eosinophil cationic protein antibacterial pharmacophore by rational structure minimization,” *J. Med. Chem.*, vol. 54, no. 14, pp. 5237–5244, 2011.
- [157] M. F. García-Mayoral, M. Moussaoui, B. G. de la Torre, D. Andreu, E. Boix, M. V. Nogués, M. Rico, D. V Laurents, and M. Bruix, “NMR structural determinants of eosinophil cationic protein binding to membrane and heparin mimetics.,” *Biophys. J.*, vol. 98, no. 11, pp. 2702–11, Jun. 2010.
- [158] M. Torrent, D. Pulido, M. V. Nogués, and E. Boix, “Exploring New Biological Functions of Amyloids: Bacteria Cell Agglutination Mediated by Host Protein Aggregation,” *PLoS Pathog.*, vol. 8, no. 11, 2012.
- [159] E. Bąbolewska and E. Brzezińska-Błaszczyk, “Human-derived cathelicidin LL-37 directly activates mast cells to proinflammatory mediator synthesis and migratory response.,” *Cell. Immunol.*, vol. 293, no. 2, pp. 67–73, Feb. 2015.
- [160] S. A. Iacob and D. G. Iacob, “Antibacterial function of the human cathelicidin-18 peptide (LL-37) between theory and practice.,” *Protein Pept. Lett.*, vol. 21, no. 12, pp.

- 1247–56, Jan. 2014.
- [161] A. Neumann, E. T. M. Berends, A. Nerlich, E. M. Molhoek, R. L. Gallo, T. Meerloo, V. Nizet, H. Y. Naim, and M. von Kückritz-Blickwede, “The antimicrobial peptide LL-37 facilitates the formation of neutrophil extracellular traps.,” *Biochem. J.*, vol. 464, no. 1, pp. 3–11, Nov. 2014.
- [162] M. N. Becker, G. Diamond, M. W. Verghese, and S. H. Randell, “CD14-dependent lipopolysaccharide-induced beta-defensin-2 expression in human tracheobronchial epithelium.,” *J. Biol. Chem.*, vol. 275, no. 38, pp. 29731–6, Sep. 2000.
- [163] T. Ganz, “Hepcidin and its role in regulating systemic iron metabolism.,” *Hematology Am. Soc. Hematol. Educ. Program*, pp. 29–35, 507, Jan. 2006.
- [164] M. C. Modrzakowski and J. K. Spitznagel, “Bactericidal activity of fractionated granule contents from human polymorphonuclear leukocytes: antagonism of granule cationic proteins by lipopolysaccharide.,” *Infect. Immun.*, vol. 25, no. 2, pp. 597–602, Aug. 1979.
- [165] D. Campanelli, P. A. Detmers, C. F. Nathan, and J. E. Gabay, “Azurocidin and a homologous serine protease from neutrophils. Differential antimicrobial and proteolytic properties.,” *J. Clin. Invest.*, vol. 85, no. 3, pp. 904–15, Mar. 1990.
- [166] R. P. Almeida, A. Vanet, V. Witko-Sarsat, M. Melchior, D. McCabe, and J. E. Gabay, “Azurocidin, a Natural Antibiotic from Human Neutrophils: Expression, Antimicrobial Activity, and Secretion,” *Protein Expr. Purif.*, vol. 7, no. 4, pp. 355–366, Jun. 1996.
- [167] E. Boix, M. Torrent, D. Sánchez, and M. V. Nogués, “The antipathogen activities of eosinophil cationic protein.,” *Curr. Pharm. Biotechnol.*, vol. 9, no. 3, pp. 141–52, Jun. 2008.
- [168] A. Malik and J. K. Batra, “Antimicrobial activity of human eosinophil granule proteins: involvement in host defence against pathogens,” *Crit. Rev. Microbiol.*, vol. 38, no. 2, pp. 168–181, May 2012.
- [169] R. E. Hancock, “Cationic peptides: effectors in innate immunity and novel antimicrobials.,” *Lancet. Infect. Dis.*, vol. 1, no. 3, pp. 156–64, Oct. 2001.
- [170] A. L. Hilchie, K. Wuerth, and R. E. W. Hancock, “Immune modulation by multifaceted cationic host defense (antimicrobial) peptides.,” *Nat. Chem. Biol.*, vol. 9, no. 12, pp. 761–8, Dec. 2013.
- [171] A. Padhi, M. Sengupta, S. Sengupta, K. H. Roehm, and A. Sonawane, “Antimicrobial peptides and proteins in mycobacterial therapy: current status and future prospects.,” *Tuberculosis (Edinb.)*, vol. 94, no. 4, pp. 363–73, Jul. 2014.
- [172] P. H. Mygind, R. L. Fischer, K. M. Schnorr, M. T. Hansen, C. P. Sönksen, S. Ludvigsen, D. Raventós, S. Buskov, B. Christensen, L. De Maria, O. Taboureau, D. Yaver, S. G. Elvig-Jørgensen, M. V Sørensen, B. E. Christensen, S. Kjaerulff, N.

- Frimodt-Moller, R. I. Lehrer, M. Zasloff, and H.-H. Kristensen, "Plectasin is a peptide antibiotic with therapeutic potential from a saprophytic fungus.," *Nature*, vol. 437, no. 7061, pp. 975–80, Oct. 2005.
- [173] K. Hilpert, R. Volkmer-Engert, T. Walter, and R. E. W. Hancock, "High-throughput generation of small antibacterial peptides with improved activity.," *Nat. Biotechnol.*, vol. 23, no. 8, pp. 1008–12, Aug. 2005.
- [174] Y. Chen, C. T. Mant, S. W. Farmer, R. E. W. Hancock, M. L. Vasil, and R. S. Hodges, "Rational design of alpha-helical antimicrobial peptides with enhanced activities and specificity/therapeutic index.," *J. Biol. Chem.*, vol. 280, no. 13, pp. 12316–29, Apr. 2005.
- [175] I. Gryllos, H. J. Tran-Winkler, M.-F. Cheng, H. Chung, R. Bolcome, W. Lu, R. I. Lehrer, and M. R. Wessels, "Induction of group A Streptococcus virulence by a human antimicrobial peptide," *Proc. Natl. Acad. Sci.*, vol. 105, no. 43, pp. 16755–16760, Oct. 2008.
- [176] D. Avrahami and Y. Shai, "Conjugation of a magainin analogue with lipophilic acids controls hydrophobicity, solution assembly, and cell selectivity.," *Biochemistry*, vol. 41, no. 7, pp. 2254–63, Feb. 2002.
- [177] I. S. Radzishovsky, S. Rotem, D. Bourdetsky, S. Navon-Venezia, Y. Carmeli, and A. Mor, "Improved antimicrobial peptides based on acyl-lysine oligomers.," *Nat. Biotechnol.*, vol. 25, no. 6, pp. 657–9, Jun. 2007.
- [178] R. Gupta, M. Singh, and D. O'Hagan, "Poly(lactide-co-glycolide) microparticles for the development of single-dose controlled-release vaccines.," *Adv. Drug Deliv. Rev.*, vol. 32, no. 3, pp. 225–246, Jul. 1998.
- [179] B. Gupta, T. S. Levchenko, and V. P. Torchilin, "Intracellular delivery of large molecules and small particles by cell-penetrating proteins and peptides.," *Adv. Drug Deliv. Rev.*, vol. 57, no. 4, pp. 637–51, Feb. 2005.
- [180] M. J. Goldman, G. M. Anderson, E. D. Stolzenberg, U. P. Kari, M. Zasloff, and J. M. Wilson, "Human beta-defensin-1 is a salt-sensitive antibiotic in lung that is inactivated in cystic fibrosis.," *Cell*, vol. 88, no. 4, pp. 553–60, Feb. 1997.
- [181] D. M. E. Bowdish, D. J. Davidson, Y. E. Lau, K. Lee, M. G. Scott, and R. E. W. Hancock, "Impact of LL-37 on anti-infective immunity.," *J. Leukoc. Biol.*, vol. 77, no. 4, pp. 451–9, Apr. 2005.
- [182] I. . 14. Hamley, "Peptide fibrillization," *Angw. Chem. Int. Ed. Eng*, vol. 46, pp. 8182–8147, 2007.
- [183] S. Sim, Y. Kim, T. Kim, S. Lim, and M. Lee, "Directional assembly of α -helical peptides induced by cyclization.," *J. Am. Chem. Soc.*, vol. 134, no. 50, pp. 20270–2, Dec. 2012.

- [184] P. T. Liu, S. Stenger, H. Li, L. Wenzel, B. H. Tan, S. R. Krutzik, M. T. Ochoa, J. Schaubert, K. Wu, C. Meinken, D. L. Kamen, M. Wagner, R. Bals, A. Steinmeyer, U. Zügel, R. L. Gallo, D. Eisenberg, M. Hewison, B. W. Hollis, J. S. Adams, B. R. Bloom, and R. L. Modlin, "Toll-like receptor triggering of a vitamin D-mediated human antimicrobial response.," *Science*, vol. 311, no. 5768, pp. 1770–3, Mar. 2006.
- [185] Transparency Market Research, "Peptide Therapeutics Market: Global Industry Analysis, Size, Share, Growth, Trends and Forecast 2012-2018," *Transpar. Mark. Res.*, 2012.
- [186] K. Fosgerau and T. Hoffmann, "Peptide therapeutics: Current status and future directions," *Drug Discov. Today*, vol. 20, no. 1, pp. 122–8, Oct. 2014.

PAPER VI

Unveiling the mode of action of human antimicrobial RNases against *Mycobacterium tuberculosis* using a surrogate macrophage infected model

Arranz-Trullén J^{1,2}; Lu Lu¹, Pulido D^{1,3}; Bhakta S^{2*} and Boix E^{1*}

¹Department of Biochemistry and Molecular Biology, Faculty of Biosciences, UAB, Cerdanyola del Vallès, Spain

²Mycobacteria Research Laboratory, Department of Biological Sciences, ISMB, Birkbeck, University of London, London, UK

³Present address: Imperial College London, South Kensington Campus London, London SW7 2AZ, United Kingdom.

*corresponding authors: Ester Boix: Ester.Boix@uab.cat; Sanjib Bhakta: s.bhakta@bbk.ac.uk

Keywords: antimicrobial peptides, RNases, innate immunity, tuberculosis,

Abbreviations: AMPs, antimicrobial peptides; TB, tuberculosis; WHO, world health organisation; Mtb, *Mycobacterium tuberculosis* bacilli; MDR-TB, multidrug-resistant tuberculosis; XDR-TB, extensively drug-resistant tuberculosis; HTS, high-throughput screening

Abstract

Mycobacteria are the causative agent of serious health problems worldwide, such as tuberculosis (TB), which is still difficult to cure in many developing countries. The emergence of multi-drug resistant TB strains and inherent incompatibilities with current anti-HIV treatments has worsened the clinical scenario, demanding the development of novel antimycobacterial agents. *Mycobacterium tuberculosis* (Mtb) is a successful human pathogen able to develop survival strategies to evade the immune system and dwell for an undefined period inside one of the most inhospitable innate cell types, the macrophage. Together with other innate immune mechanisms, antimicrobial peptides (AMPs) have a key prominent role in the host self-defence weapons targeting Mtb.

Human RNases (hRNases) are small cationic proteins secreted by innate cells upon infection and displaying a variety of antimicrobial properties. Among the wide range of reported antipathogen activities, recombinant hRNases 3 and 7 were previously proven effective in vitro against mycobacteria. Moreover, mycobacterial infection stimulates the expression and secretion of hRNase 3. In order to further investigate the effectiveness of these antimicrobial proteins against mycobacteria we have applied a surrogate method for screening antimicrobial peptides against *M. tuberculosis* within a host cell environment. *Mycobacterium aurum* was selected as fast-growing non-pathogenic species that can dwell inside cultured macrophage cells. The present results support the optimized model application for screening novel antimycobacterial peptides and show that hRNases 3, 6 and 7 were able to internalize into the infected macrophages without producing any cytotoxicity, being effective at a low micromolar concentration against intracellular resident mycobacteria. In addition, we explored the RNases mechanism of action by comparing the protein N-terminal derived peptides and active site mutants' action. Results indicated that the RNases antimycobacterial activity is mostly retained at the N-terminal domain. However, comparison of performance of the wild type RNases and respective active site mutants in the macrophage infected ex vivo model suggests that the enzymatic activity is also contributing to the eradication of intracellular mycobacteria.

Introduction

Tuberculosis (TB) is a serious and elderly infectious disease that is currently close to reach one of the highest and deadliest index worldwide. According to the World Health Organisation (WHO), TB has produced 1.5 million TB deaths, almost 9 million new cases have been detected in 2014 and around a third of the world population is hosting *Mycobacterium tuberculosis* in its latent form ¹. In recent years we have undoubtedly witnessed a general decline in the TB incidence rate as well as in the absolute number of registered cases of tuberculosis. Nonetheless, the emergence of a growing number of new cases of multi-drug resistant TB (MDR-TB) and even more troubling extensively drug-resistant TB (XDR-TB) cases have put forward the eradication of tuberculosis, both in developed and undeveloped countries, as one of the major challenges to overcome in the twenty-first century ¹. Furthermore, this situation has been particularly aggravated by HIV coinfection and ineffective chemotherapy treatments. Moreover, host immune responses against *M. tuberculosis* bacilli (Mtb) involve high immune machinery complexity and are not clearly understood yet. Hence, enlargement of novel and effective therapies to battle mycobacteria are immediately required ². *Mycobacterium tuberculosis*, the causative agent of tuberculosis, is an intracellular pathogen able to survive under stressful conditions and indefinitely inside primary host immune cells, preferably residing into human alveolar macrophages ³. Several studies have recently shown that features such as its high infectivity, slow growth and complex physiological structure make *mycobacterium tuberculosis* a major challenge to be faced, since the specific mechanisms that reinforce the high virulence of Mtb still remain partially unknown ^{4,5,6}. Notwithstanding the antimicrobial activity of macrophages, *Mycobacterium tuberculosis* has been able to establish a series of strategies to handle the host immune machinery, interfere with and slow down the phagosomal maturation, counteract mycobactericidal molecules and ultimately survive in a rough intracellular macrophage environment ^{4,7,8}. There by, the search for new anti-TB agents able to penetrate the host immune cells and eradicate the pathogen intracellularly without causing damage to the host, is now an almost indispensable alternative.

A mycobacterial infection denouement largely depends on the readiness of the host immune system to counter the pathogen. During infection a large assortment of antimicrobial protein and peptides (AMPs) are released by host immune cells to the bloodstream and nearby tissues to the infected areas ⁹. At the same time, neutrophil and eosinophil granules, loaded with lytic enzymes and antimicrobial molecules, can be acquired by macrophages to counter bacterial invasion ^{10,11,12}. Because AMPs exert a potent bactericidal effect against a wide range of human pathogens and the likelihood of microbial resistance is very low due to their diversity in terms of mechanism of action and targets, they are emerging as a new generation of natural antibiotics and its administration in combination with or without other drugs is showing new approaches with very promising results.

Our research group is currently working on the anti-pathogenic mechanism of action of a family of proteins involved, among many other functions, in host defence. The RNase A superfamily encompasses eight functional members in humans, known as the "canonical RNases"¹³. Interestingly, some family members have been found secreted by key effector innate cells, preserving AMPs well-characterized antimicrobial features and taking part in numerous immunity processes against a wide variety of human pathogens such as mycobacteria ^{10,14}. Human RNases (hRNases) 3, 6 and 7 are small highly cationic proteins secreted by host defence system cells with demonstrated antimicrobial activity against a variety of microbes ^{15,16,17,18,19}. Particularly, Torrent *et al.* carried out a preliminary characterization of the RNases derived peptides, revealing that the

antimicrobial mechanism of action is mostly retained at the N-Terminal region of the protein²⁰. Furthermore, it has been recently shown that RNase 3 and 7 are potentially active *in vitro* against mycobacteria²¹. Another specific feature reported for these antimicrobial proteins, is the capacity to agglutinate both Gram-negative bacteria and mycobacteria^{21,22}. The usual practice for the screening of actively dividing microbe inhibitors is usually performed under *in vitro* conditions due to high costs and low effectiveness of *in vivo* assays. However, many of the *in vitro* tests currently used are not adapted to the high-throughput screening (HTS) systems, which improve the identification of new compounds rapidly²³. In this study we have adapted the previous integrated surrogate model and the spot culture growth inhibition (SPOTi) assay for screening inhibitors against *M. tuberculosis*²⁴ to the analysis of proteins and peptides. In order to check the effectiveness of antimicrobial RNases, their derived N-terminal peptides and validate this screening system we have used the non-pathogenic and fast growing *Mycobacterium aurum* and RAW 264.7 macrophages as surrogates for *M. tuberculosis* and primary immune cells respectively. In this work we have shown for the first time that RNases are able to eradicate mycobacteria within the host's primary immune cells.

Materials and Methods

Protein expression and purification

Recombinant hRNase 3 and hRNase 7 were expressed in *E. coli* BL21 (DE3) using the pET11c plasmid vector as previously described²⁵. Human RNase 6 was obtained from DNA 2.0 (Menlo Park, CA, USA). RNase 6 gene was subsequently cloned into pET11c vectors. Active site mutations into the hRNases genes were introduced using the Quick change™ site-directed mutagenesis kit (Santa Clara, CA, USA) following the manufacturer's procedure. *E. coli* BL21(DE3) (Novagen, Madison, WI, USA) competent cells were transformed with the pET11c/RNase3, 6 and RNase7 plasmids. For high yield expression, bacteria were grown in TB, containing 400 µg/mL ampicillin. Recombinant RNase6 was expressed in *E. coli* BL21(DE3) (Novagen, Madison, WI, USA) cells after induction with 1 mM IPTG (St. Louis, MO, USA), added when the culture showed an OD600 of 0.6. The protein was then refolded by a rapid 100-fold dilution into 0.1 M Tris-HCl, pH 7.5, containing 0.5 M L-arginine, and GSSG (St. Louis, MO, USA) was added to obtain a GSH/GSSG ratio of 4. Dilution in the refolding buffer was adjusted to obtain a final protein concentration of 30–150 µg/mL. The protein was incubated in refolding buffer for 48–72 h at 4°C. The folded protein was then concentrated, dialyzed against 0.015 M Tris-HCl, pH 7, and purified by cation exchange chromatography on a Resource S column equilibrated with the same buffer. Further purification was achieved by a second reverse phase chromatography on a Vydac C4 column (Grace-Alltech, Bannockburn, IL, USA). The homogeneity of the purified proteins was checked by 15% SDS-PAGE and Coomassie Blue staining, MALDI-TOF and N-terminal sequencing. Taken from¹⁹.

Peptide synthesis

Solid-phase peptide synthesis was done by Fmoc-based chemistry on Fmoc-Rink-amide (MBHA) resin (0.1 mmol) in a model 433 synthesizer (Applied Biosystems) running FastMoc protocols. Peptides were isolated by precipitation with ice-cold diethyl ether and separated by centrifugation (3000 g for 20 min at 4°C), dissolved in 0.1 M acetic acid, and freeze-dried. Analytical reversed-phase HPLC was performed on a Luna C18 column (4.6 mm×50 mm, 3 µm; Phenomenex). Linear 5–60% gradients of solvent B (0.036% TFA in ACN) into solvent A (0.045% TFA in water) were used for elution at a flow rate of 1 ml/min and with UV detection at 220 nm. MALDI-TOF mass spectra were recorded in the

reflector or linear mode in a Voyager DE-STR workstation (Applied biosystems) using an α -hydroxycinnamic acid matrix. Fractions of adequate (>90%) HPLC homogeneity and with the expected mass were pooled, freeze-dried and used in subsequent experiments. Taken from ²⁰.

Growth and maintenance of mycobacterial species

Biosafety level 2 mycobacterial species *M. aurum* (NC 10437) was purchased from the UK National Collection of Type Cultures (NCTC). Cells cultures of *M. aurum*, *M. smegmatis* mc2155 (ATCC 700084) and *M. bovis* BCG Pasteur (ATCC 35734) were grown in Middlebrook (MB) 7H9 medium (BD Biosciences) enriched with 10% (v/v) albumin/dextrose/catalase (ADC; BD Biosciences) containing 0.05% Tween 80 and 0.05% Glycerol 50% for liquid growth at 35°C and 150rpm (for BCG, 37°C 2rpm(rolling)), and in MB7H10 (BD Biosciences) with 10% (v/v) oleic acid/albumin/dextrose/catalase (OADC; BD Biosciences) for solid agar growth at 35°C. Stock cultures of log-phase cells were maintained in glycerol (25% final concentration of glycerol) at -80°C.

High throughput extracellular SPOTi assay

Antimicrobial activity was calculated as the 100% minimum inhibitory concentration (MIC₁₀₀), defined as the lowest protein/peptide concentration that completely inhibits microbial growth. The MIC of each protein and peptide [RNase 3, RNase 6 RNase 7, RN1(1-45), RN2(1-45), RN3(1-45), RN4(1-45), RN5(1-45), RN6(1-45), RN7(1-45) and RN8(1-45)] was determined from two independent experiments performed in triplicate for each concentration. Log-phase cultures of *M. smegmatis* mc2155, *M. aurum* and *M. bovis* BCG (Optical Density (OD)₆₀₀≈1) were first checked for quality control using cold Ziehl–Neelsen (ZN) staining (also called ‘acid fast staining’; TB-colour staining kit, BDH/Merck) according to the manufacturer’s protocol. The cultures were then diluted to give approximately 2.5x10⁵ CFU/ml. Bacterial suspension was incubated with proteins or peptides serially diluted from 50 to 0.1 μ M at 37°C for 4-6 hr in phosphate-buffered saline (PBS). Samples were plated onto 2 mL of B7H10/OADC in each well of a 24-well Costar plate (Appleton Woods) and cell growth at 35°C was recorded after 2 days for *M. smegmatis*, 4-5 days for *M. aurum* and 14 days for *M. bovis* BCG.

Minimum agglutination activity (MAC) assay

Mycobacterial cells were grown at 35°C to an OD₆₀₀ of 1.0; cells were then diluted to an OD₆₀₀ of 0.1, centrifuged at 5,000 xg for 2 min, and resuspended either in 1X PBS or M7H9/ADC media containing 0.05% Tween 80 and 0.05% Glycerol 50%. An aliquot of 100 μ l of the mycobacterial suspension was treated with increasing protein or peptide concentrations (from 0.01 to 20 μ M) and incubated at 35°C for 1 h. The aggregation behaviour was observed by visual inspection with a stereomicroscope at 50x, and the agglutinating activity is expressed as the minimum agglutinating concentration of the sample tested, as previously described ¹⁶.

Growth and maintenance of mouse macrophage cell line (RAW 264.7)

RAW 264.7 cells (NCTC #91062702) were maintained in 25 or 75 cm² tissue culture flasks (BD Biosciences) containing RPMI-1640 complete medium [RPMI-1640 medium supplemented with 2 mM L-glutamine and 10% heat-inactivated fetal bovine serum (37°C, humidified 5% CO₂)], and passaged twice before the assay. Before passage, cells were washed twice with 1X PBS to remove unattached cells. Adhered cells were detached using a lidocaine/EDTA mixture (10 mM lidocaine HCl, 10 mM EDTA in 1X PBS) at room temperature for 10 min followed by hitting the side of the flask against the palm of the hand, and then diluting with an equal volume of fresh medium. Cells were

then centrifuged at 1200 rpm for 5 min and resuspended in fresh medium. The number of viable cells was counted using a Trypan Blue assay. Stock cultures of the cells were maintained at -80°C by adding actively growing cells to an equal volume of Bambanker™ Cell Freezing Media (Anachem).

Cell toxicity assay using RAW 264.7 macrophages and THP1 human cell line

The assay was performed in 96-well cell culture flat-bottom plates (Costar; Appleton Woods) in triplicate. Proteins or peptides were serially diluted from 50 to 0.1 μM (100 μl) in each well. To each well, 100 μl of diluted macrophage cells (5×10^5 cells/mL) was added. After 48 h of incubation, cells were washed twice with 1X PBS, and fresh RPMI-1640 complete medium was added. Plates were then treated with 30 μl of a freshly prepared 0.01% resazurin solution and incubated overnight at 37°C. The following day the change in colour was observed and the fluorescence intensity was measured (λ_{em} 560 nm, λ_{ex} 590 nm, FLUOstar OPTIMA microplate reader; BMG LABTECH GmbH). The 50% growth inhibitory concentration (GIC_{50}) was determined.

Infection of *M. aurum* in RAW 264.7 macrophages

A macrophage cell suspension was adjusted to 1×10^6 cells/mL, and 1 mL was added onto circular coverslips (Appleton Wood) of 6-well cell culture flat-bottom plates with another 4 ml of fresh RPMI-1640 complete medium containing 0.05% Tween 80 and 0.05% Glycerol 50%. After 15 min of incubation, 1×10^7 cells of mid-log phase *M. aurum* cells harvested in RPMI-1640 complete medium were added to each well at moi 10:1 and were incubated at 37°C²⁴. 2h post-infection, and at different times (24, 48 and 72 h); coverslips were washed thrice with RPMI-1640 medium and assessed by ZN staining using a TB-colour staining kit. Co-infection was optimized by counting bacteria per macrophage cell under a bright field microscope (Zeiss) with coverslips mounted onto slides. Acid fast-stained phagocytosed mycobacteria images were captured at X1000 magnification.

Survival assay of *M. aurum* in RAW 264.7 macrophages

For the survival assay, 5×10^4 macrophages cells were infected with 5×10^5 mycobacteria cells of *M. aurum* following the previous optimized infection protocol in 96-well plates²⁴. Then macrophages were lysed at different times (0, 24, 48, 72 h) in distilled water at room temperature for 10-15 min followed by scrubbing using a syringe plunger or pipet tip. The lysed cells were spread onto plates containing MB7H10 OADC agar, and then incubated at 37°C to determine the colony forming units (CFUs).

Development of a 24-well plate SPOTi assay with infected RAW 264.7 macrophages

For the killing assay, macrophages (5×10^4 cells per well) were infected with *M. aurum* at 10:1 moi for 1.5 h at 37°C in a 96-well plate as described²⁴. The culture was washed with RPMI-1640 thrice and incubated with different sub- GIC_{50} concentration of the proteins and peptides (from 20 to 0.1 μM) in RPMI-1640 complete medium. Inhibitors were incubated for different times (4 24, 48, 72 h). Cells were then washed twice with RPMI-1640 and lysed in 50 μl of distilled water at room temperature for 10 min. Then, 15 μl was spotted onto wells of a 24-well plate containing MB7H10/OADC/agar and incubated at 37°C for 4-5 days to determine intracellular survival. Antimicrobial activity was expressed as the MIC_{100} , defined as the lowest protein concentration that completely inhibits the intracellular mycobacterial growth.

Fluorescent labelling of RNases

hRNase 3, hRNase 6 and hRNase7 were labelled with Alexa Fluor 488 Labelling kit (Molecular Probes, Invitrogen, Carlsbad, CA), following the manufacturer's instruction as previously described¹⁷. To 0.5 mL of 2 mg/mL protein solution in phosphate saline buffer (PBS), 50 μ L of 1 mol/L sodium bicarbonate, pH 8.3, was added. The protein was incubated for 1 h at room temperature with the reactive dye, with tiring, and the labelled protein was separated from the free dye by PD-10 desalting column (Merck Millipore).

Intracellular tracking of RNases into RAW 264.7 macrophages using confocal microscopy

Labelled protein distribution in cell cultures was followed by confocal microscopy. About 2.5×10^5 RAW cells were harvested in 3 cm diameter microscopy plates (Novagen) 2-3 hours before the assay. Macrophages were washed with RPMI and labelled with Hoechst 33342 and CellMask Deep Red Plasma membrane Stain (Thermo Fisher Scientific, C10046) at 0.5 μ g/mL for 5-10 min before observation in Leica TCS SP5 AOBS equipped with a PL APO 63 \times 1.4-0.6 CS oil immersion objective (Leica Microsystems, Mannheim, Germany). Several minutes later, Alexa Fluor labelled proteins were added at 2 μ M to the cultures and time lapse was recorded at intervals of 30 sec for 30 min. Fluorochromes were excited by 405 nm (Hoechst 33342), 649nm (CellMask Deep Red) and 488 nm (Alexa Fluor 488). Emissions were collected with a HyD detector.

Western-blot analysis

Expression of the autophagy marker LC3 was followed by western blot. Total protein of the cell lysate was extracted from RAW 264.7 cells (after different time-point incubation with proteins) in confluent 6-well plates after 1 \times wash with PBS by using TRI Reagent[®](Sigma-Aldrich) kit as described by the manufacturer. Total protein pool was isolated from the phenol-ethanol supernatant layer. The protein concentration was determined with the Quick Start Bradford Protein Assay (BIO-RAD) according to the manufacturer's instructions. Equal amounts of protein (15-20 μ g) for each sample were mixed with 6 \times loading buffer and heated at 95 $^{\circ}$ C for 5 min, separated on a 15% SDS-PAGE gel and then transferred to a Immobilon-FL PDVF membrane (Millipore, IPFL07810). After transfer, presence of proteins and equal loading of lysates was confirmed using Ponceau S (Sigma, P3504) and membranes were blocked at 1 h in 3-5% BSA in TBS-tween. The primary antibodies include anti LC3B (Sigma, L7543) and anti GAPDH (abcam, ab9483), both produced in rabbit. Secondary antibody used was anti-rabbit HRP. Supersignal[®] West Pico Chemiluminescent Substrate (ThermoScientific) was used for the detection of HRP. Bands were detected using an Odyssey fluorescence analyzer (Licor). Densitometry analysis was performed using Quantity One software.

Cellular RNA degradation analysis

Mycobacteria infected macrophages were harvested in 6-well plates and treated with the proteins at 2 μ M final concentration for 4, 24, 48 and 72 h. After incubation, cells were washed, detached from the flasks and sedimented in sterile tubes. Total RNA was extracted from cellular pellets, using TRI Reagent[®](Sigma-Aldrich) kit as described by manufacturer. Samples were analysed in a high sensitivity nucleic acid microfluidic chip using an Experion[™] Automated Electrophoresis Station (Bio-Rad, Madrid, Spain). Both eukaryote and prokaryote total RNA high sensitivity assays were run for each sample. Eukaryotic/prokaryotic cellular rRNA populations were quantified by virtual gel densitometry.

Results

Selection of mycobacterial species for in vitro and ex vivo studies

First, a comparison of the growth curves of three mycobacterial species was performed. Based on cell morphology, generation time, antibiotic susceptibility and intracellular survival ability, we compared *M. smegmatis* mc²155, *M. aurum* and *M. bovis* BCG in order to establish a bacteriological model for this study. The mycobacterial species were first observed for their morphology using cold ZN staining. *M. aurum* showed a similar pattern to *M. bovis* BCG, while *M. smegmatis* mc²155 cells were more elongated (acid fast-stained cells at mid-log phase; Figure S1ABC). The mycobacterial species were also studied for their physiological properties by plotting their growth curves (OD₆₀₀ against time). As *M. aurum* is a scotochromogenic specie, a spectrum analysis was performed to exclude possible interference by chromogenic substrate at 600 nm. The growths of mycobacterial species were observed at active growth rate. Although *M. smegmatis* mc²155 showed the fastest growth, comparative growth curves showed that *M. aurum* also take less time to enter the log phase compared with *M. bovis* BCG (Figure S1D). For *M. aurum*, log-phase cells were collected after 36 h, SPOTi assays were performed after 5 days and colonies were obtained on plates after 8 days; for *M. bovis* BCG the corresponding values were 3-4 days, 14 days and 28 days (Table S1).

Growth Inhibition and Agglutination of mycobacterial species in vitro by RNases

First, the effectivity of the antimicrobial hRNases 3, 6 and 7, the three main hRNases described to display antimicrobial properties^{26,27,19}, together with their active site mutants (H15A) and N-terminus peptides was tested against mycobacteria at the extracellular level. In addition, the hRNase-derived peptides were designed taking as a reference the 1–45 segment in hRNase 3, based on previous work in our laboratory that defined the protein minimal domain retaining full antimicrobial properties^{20,15}. Here, the N-terminal peptides, comprising equivalent structural regions of the human canonical RNases N-termini (residues 1–45 of hRNases) were selected for synthesis. In all cases, the peptides included the first two α -helices as well as the first β -strand from the parental protein. Recombinant hRNases together with their N-terminal derived peptides were obtained as described in materials and methods and based in our previous studies^{15,28,20}. A solid agar-based SPOTi assay was performed in a 24-well plate format (Figure S2). The MICs were determined for complete inhibition by adding up to 50 μ M final concentration of proteins and peptides to cell cultures of *M. bovis* BCG, *M. smegmatis* mc²155 and *M. aurum* (figure S2). Similar results were obtained for the three species, with slightly better effectivity for *M. aurum*. Extracellular MIC results were determined for complete inhibition and are summarized in tables 2 and 3. hRNases 3, 6 and 7 as well as their respective active-site mutants were found extracellularly effective against the three mycobacterial species, with similar values below 20 μ M. On the other hand, screening of the eight N-terminal derived peptides indicated that only the ones corresponding to antimicrobial active parental proteins (hRNases 3, 6 and 7) showed significant growth inhibition, halving the MIC values in the case of RN3(1-45). Following, considering that cell agglutination ability contributes to the antimicrobial mechanism of action of some of the previously studied hRNases¹⁹, we checked the protein/peptide ability to aggregate mycobacteria as previously described¹⁶. The agglutinating activity was evaluated as the minimum agglutinating concentration of the sample tested for the three assayed mycobacterial species. We found that, both hRNase 3 and hRNase 6 were able to

agglutinate *M. smegmatis* mc²155 and *M. aurum* as well as *M. bovis* BCG in a range between 1 and 5 μ M while hRNase 7 showed no significant agglutinating capacity at the maximum tested concentration (figure S3). No significant changes were observed when comparing each antimicrobial hRNase with its respective active site mutant at the extracellular level (table 2). This scenario is in agreement with previous studies where it has been demonstrated that the enzymatic activity of hRNases is independent of its antimicrobial properties²⁹.

Study of the RNases action on an ex vivo infection model

To screen the hRNases and derived peptides activity, a macrophage infected model was selected in order to check their effectivity in eradicating resistant mycobacterial forms, such as macrophage resident mycobacteria.

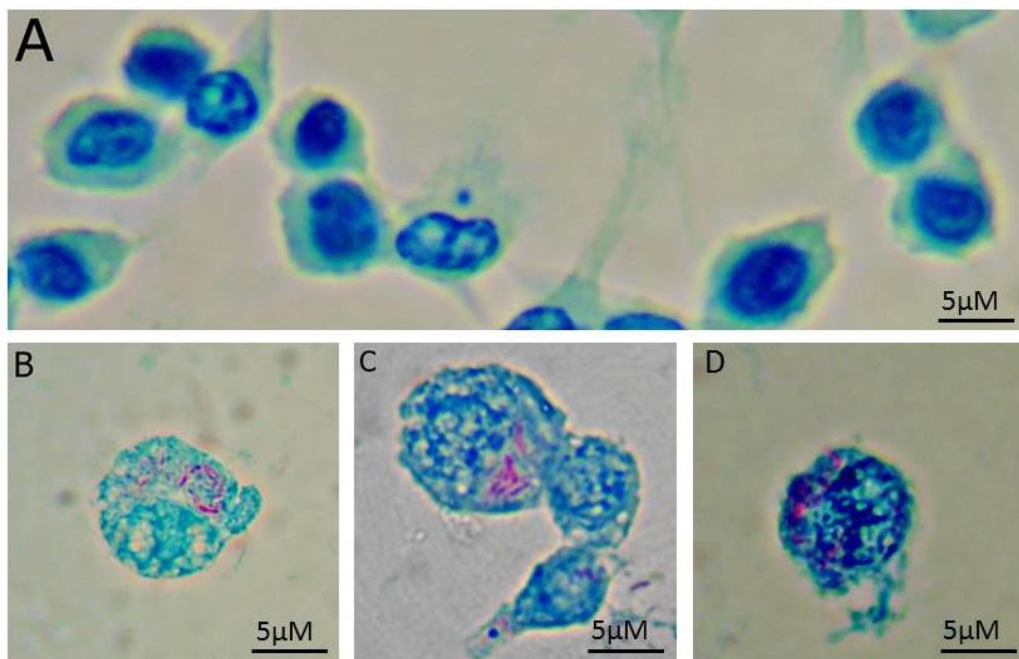


Figure 1. *M. aurum* phagocytosis by RAW 264.7 macrophages. A) Non-infected macrophages. B, C, D) Three images were selected of *M. aurum* infected macrophages 2h post-infection at similar conditions assessed by ZN staining. Co-infection was optimized by counting bacteria per macrophage cell under a bright field microscope.

RAW 264.7 for an ex vivo macrophage infected model

First, monolayers of the murine RAW 264.7 cell line were cultured, spread uniformly, let to adhere well and start to differentiate into active macrophages within 15 min (figure S4). The 90% viability of macrophage cells was determined by using a Trypan Blue assay. Additionally, we also studied their viability and cell morphology directly through the inverted microscope (figure S4 and collected samples, which were fixed and stained with malaquite green (figure 1). Before infection, macrophages in logarithmic growth phase were used for testing the cytotoxicity of the proteins and peptides against RAW 264.7 macrophage cells before testing the proteins and peptides for intracellular inhibition (figure S5). All AMPs were found to be non-toxic to RAW 264 below 25 μ M, as determined by GIC₅₀ values. (see Table 2 and Figure S5).

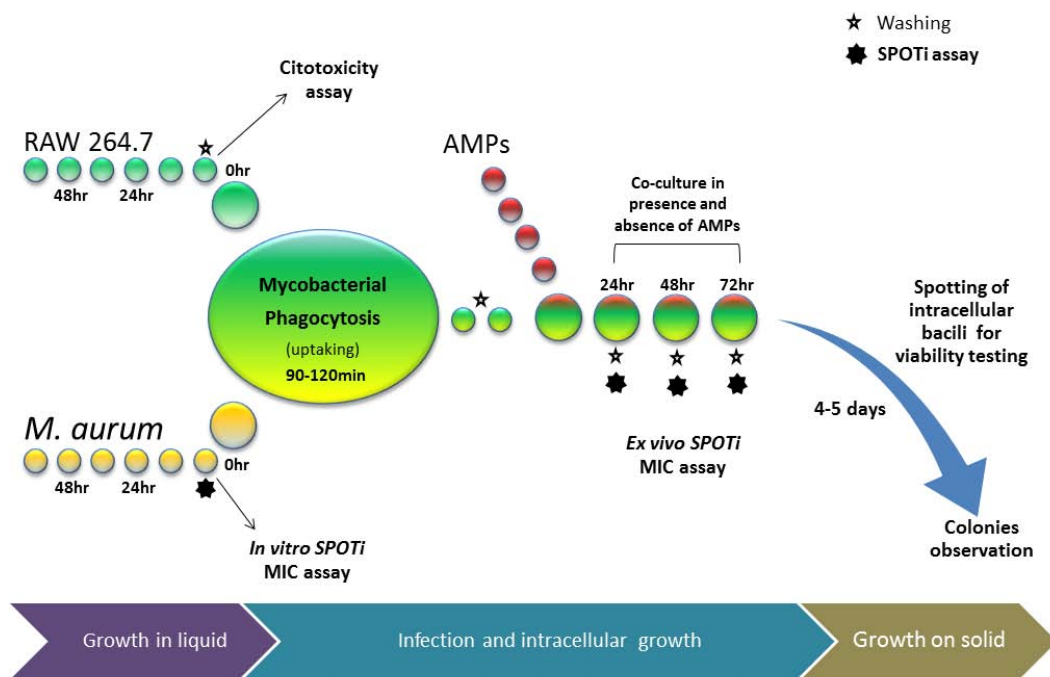


Figure 2. Schematic representation of the surrogate macrophage infected model for the screening of hRNases and N-terminal peptides.

Uptake and infection of mycobacterial species into RAW 264.7 macrophages

Next, the mycobacteria uptake assay was performed following the optimized protocol by *Gupta et al*²⁴. Previous studies supported the selection of *M. aurum* as a fast-growing mycobacterial model organism for drug screening. An aliquot of *M. aurum* culture was used for screening against extracellular bacilli by performing a SPOTi assay, and the rest of the culture was used to further check the uptake assay. Uptake of *M. aurum* was assessed using ZN staining of infected (Fig. 1B, C, D) and non-infected (Fig. 1A) macrophages. Staining results showed the presence of engulfed pink (carbol fuchsin-stained) *M. aurum* inside blue (malaquite-green-stained) macrophage cells. Phagocytosis was observed between 90 and 120 min (moi 10:1)(figure 1B,C,D). At the same time, we performed a cellular infection monitoring, RAW 264.7 cells growth at different time intervals (24, 48 and 72 h) in the presence and absence of *M. aurum* (figure S6).

Killing of M. aurum within RAW 264.7 macrophages

Following, the outline of the developed infected macrophage model as illustrated in Figure 2, was adapted and validated to test the antimicrobial hRNases action. Intracellular growth inhibition of *M. aurum* was observed at different time intervals in the presence and absence of the proteins and peptides using the SPOTi assay (Figure 3). Intracellular survival was evaluated by cfu counting in the absence or presence of a subinhibitory concentration of protein. *M. aurum* was able to survive intracellularly and entered into logarithmic growth phase in 48 h, with a 10-fold increase in bacilli in the following 24 h (Figure 4). Significant inhibition by AMPs was observed after 48 h. Therefore, a 48-72 hr AMP-incubation time point was chosen for our model. CFU assay using the infected macrophage model showed high significant and progressive reduction in *M. aurum* cells when incubated with hRNases compared with those non-treated from 48 hr onwards (Figure 4). On the other hand, no reduction was shown in the number of macrophage cells. The murine macrophage/*M. aurum* high-throughput screening model was optimized with the following

parameters: 10:1 moi uptake, 90 min infection, and 24-72hr AMP incubation. Intracellular MICs for all the proteins and peptides phagocytosed by *M. aurum* were calculated (tables 2 and 3). It is noteworthy that proteins and N-terminal peptides exhibited an overall improvement when tested against host macrophage intracellular mycobacteria respect to the extracellular mycobacteria culture. We observed a significant improvement of the MIC values at the intracellular level compared to the extracellular ones (Tables 2 and 3). Thus, a positive effect at the intracellular environment effect for the hRNases and peptides should be considered. Figure 5 displays a broad comparison of the mycobactericidal effect of hRNases 3, 6, 7 and their respective active site mutants using the macrophage infected model during 72 hr. In agreement with previous results, significant inhibition was exhibited by RNases and their active-site mutants from 48 hr onwards (see statistics in Table S3). Interestingly, when we compare the effectiveness of RNase 3 and its active site mutant, we noticed a significant decrease of mycobacterial growth inhibition in the case of hRNase3-H15A (Fig. 5, Fig. 3-Fig. S7D, Table S3). With the aim of further study this effect, it was decided to choose hRNase 3 as a model (figure 4), whose values compared with its active-site mutant showed to be previously significant (figure 5). This trend seems to be also reproduced by hRNases 6 and 7 respective H15A mutants, although no statistically significant differences were observed (Fig. 5, Fig. S7B and S7E, Fig. S7C and S7F, Table S3). All mutants showed more higher MICs compared with their parental proteins, which, suggests that the RNase activity could be directly involved in the total eradication of the mycobacteria, preventing their recovery (Table2, figures 4 and 5).

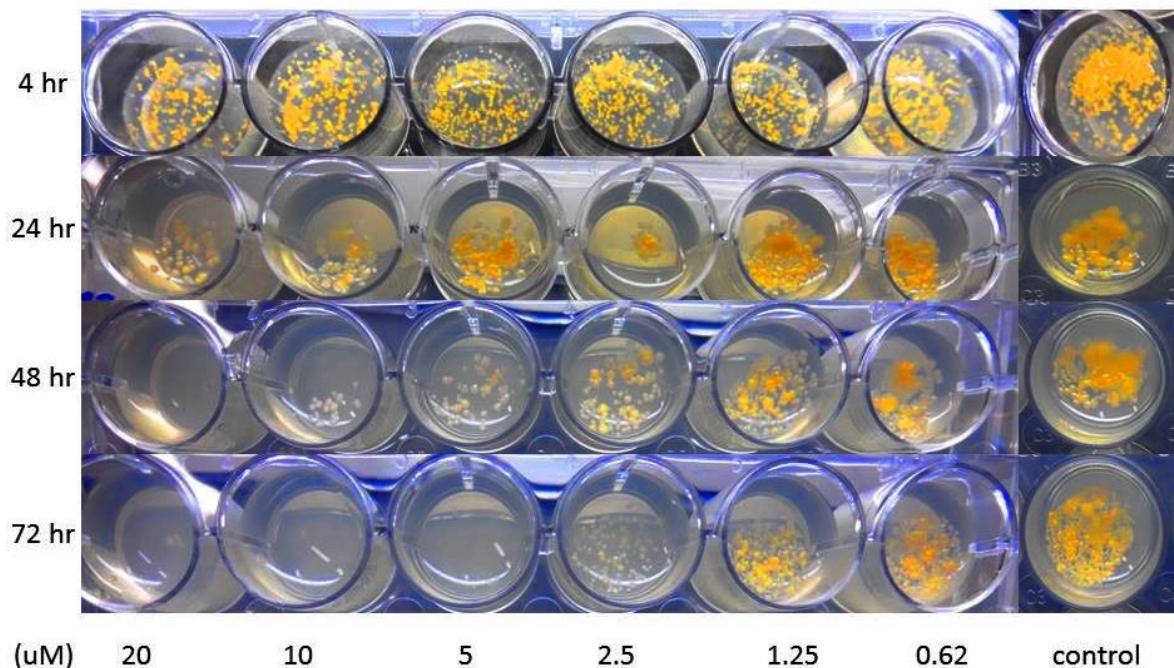


Figure 3. Growth inhibition of *M. aurum* inside RAW 264.7 cells at different time intervals for different concentrations of RNase 3. Macrophages were infected with *M. aurum* at 10:1 moi for 1.5 h at 37°C. The culture was washed with RPMI-1640 thrice and incubated with different sub-GIC₅₀ concentration of the proteins and peptides in RPMI-1640 complete medium. Inhibitors were incubated for different times. Macrophages were then washed twice with RPMI-1640 and lysed. Then, an aliquot was spotted onto wells of a 24-well plate containing MB7H10/OADC/agar and incubated at 37°C for 4-5 days to determine intracellular survival.

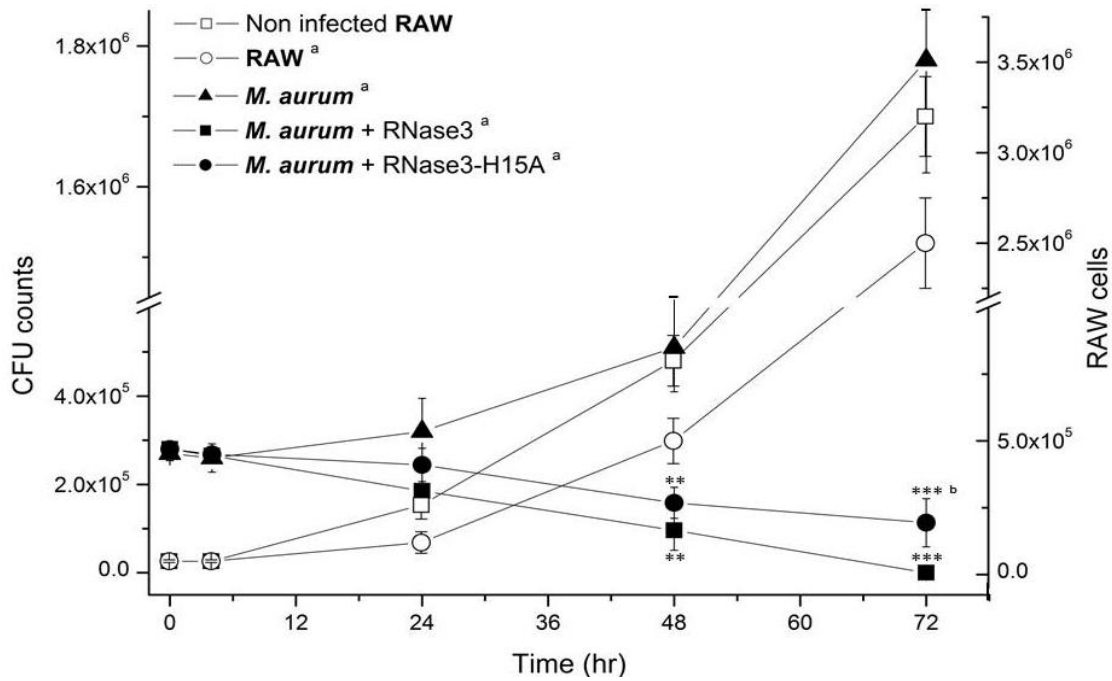


Figure 4. Intracellular survival of *M. aurum* in infected RAW 264.7 macrophages after treatment with RNases. Macrophages were infected following materials and methods conditions. Afterwards the cells were treated with RNase 3 and its active-site mutant at 5 μ M final concentration for 4, 24, 48 and 72 hours. Intracellular bacterial viability was determined based on the number of colony forming units (CFUs). Results are shown from 3 independent experiments performed in triplicate. SEM interval is indicated. ^a Cell/CFU counting using the macrophage infected model. The P value were calculated using as reference negative control (*M. aurum*) (*corresponds to $P < 0.05$, ** to $P < 0.01$ and *** to $P < 0.001$). ^b The calculated P value using as reference active-site mutant activity at 72 hr was considered to be statistically significant ($P < 0.05$).

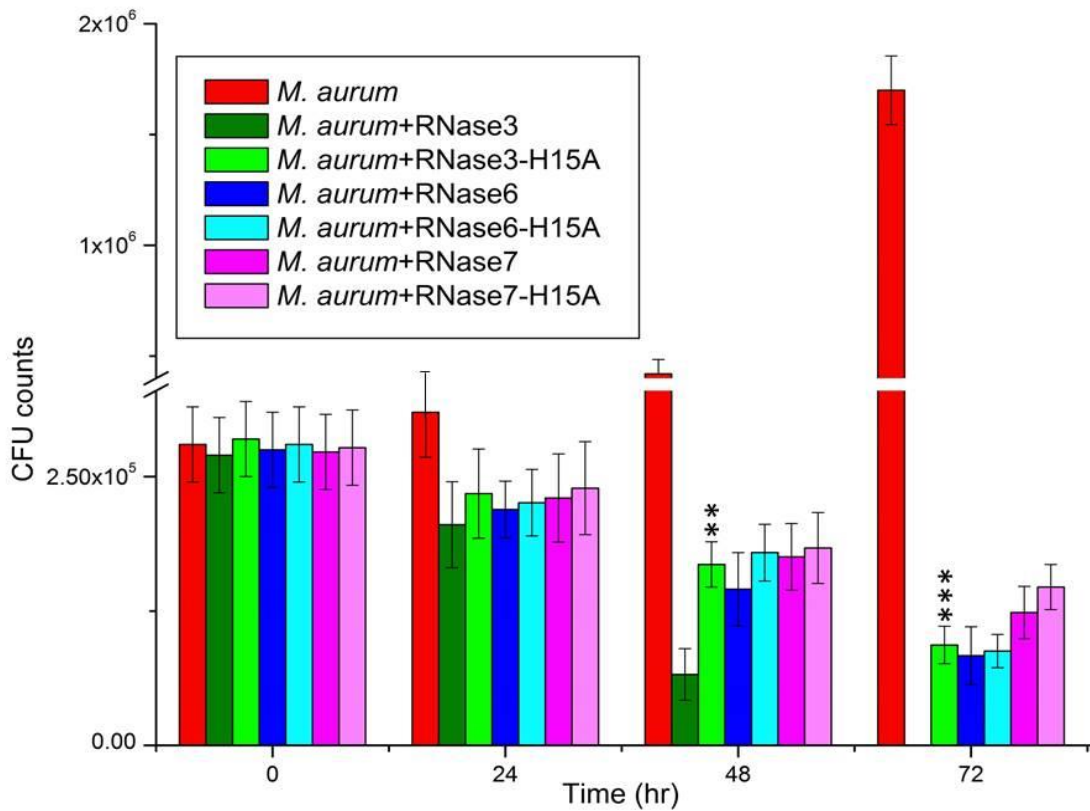


Figure 5. Antimycobacterial activity comparison of RNases 3, 6, 7 and their respective active-site mutants against *M. aurum* using the surrogate macrophage infected model. Assays were performed using 5 μ M of protein final concentration. Survival rate of *M. aurum* is depicted in the figure as the CFUs counting after 5 days incubation time at 37°C. SEM interval is indicated. The P value were calculated for each parental protein and active-site mutant pair (*corresponds to $P < 0.05$, ** to $P < 0.01$ and *** to $P < 0.001$).

Internalization of RNases into RAW 264.7 macrophages

Intracellular MIC values improvement encouraged us to confirm the internalization of proteins within the infected macrophages preceding the subsequent mycobacteria killing. Protein internalization was evaluated by confocal microscopy in the presence of a subinhibitory concentration of human ribonucleases 3, 6 and 7. The fluorescent marker Alexa Fluor-488 was chosen to label and track the protein location. In addition, macrophages cell membranes and nuclei were stained with Deep red and Hoechst respectively. As observed in figure 6, human RNases 3, 6 and 7 are able to internalize inside the macrophages through a vesicle-mediated mechanism and be recruited into larger compartments, which might correspond to phagosomes. Analysis of the profiles of selected regions of interest confirmed the protein location at the cellular vesicles compartment (Figure 7). Additionally, time lapse assays allowed us to study the kinetics of protein internalization in order to characterize the internalization process. Results showed that it is a fast process, where most of the protein enters into the macrophage within the first 30 minutes. Examples of internalization fluorescence profiles of hRNases 3, 6 and 7 are also shown at 0, 5 and 30 min in Figure S8.

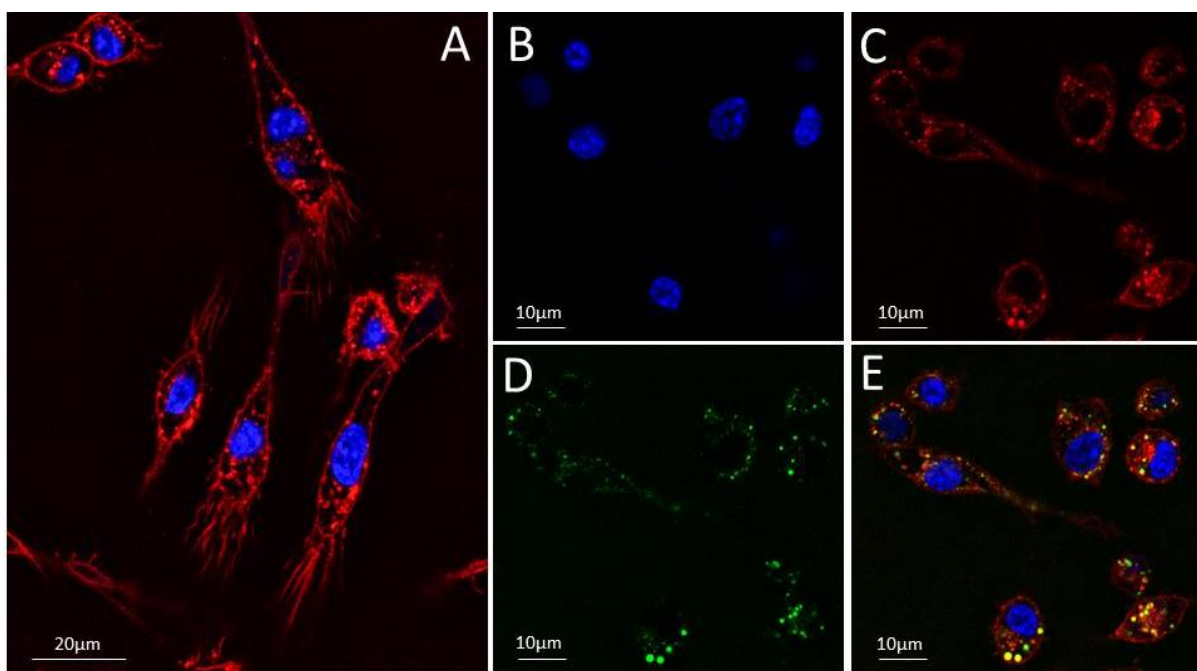


Figure 6. Confocal microscopy tracking of RNase 3 in macrophage cultures. (A) RAW 264.7 macrophages cells were stained with Hoechst (blue) and Deep Red to visualize the nuclei (B) and membrane (red) (C) respectively. Alexa Fluor 488 was used to label and track the protein location (D). (E) 30 min post-treatment with RNase 3 . Protein tracking assays were performed during 45 min approximately, using $\sim 2.5 \times 10^5$ cells/mL and adding 2 μ M of labelled protein final concentration. The images were taken using a Leica TCS SP5 AOBS microscope (see Materials and methods section for more details).

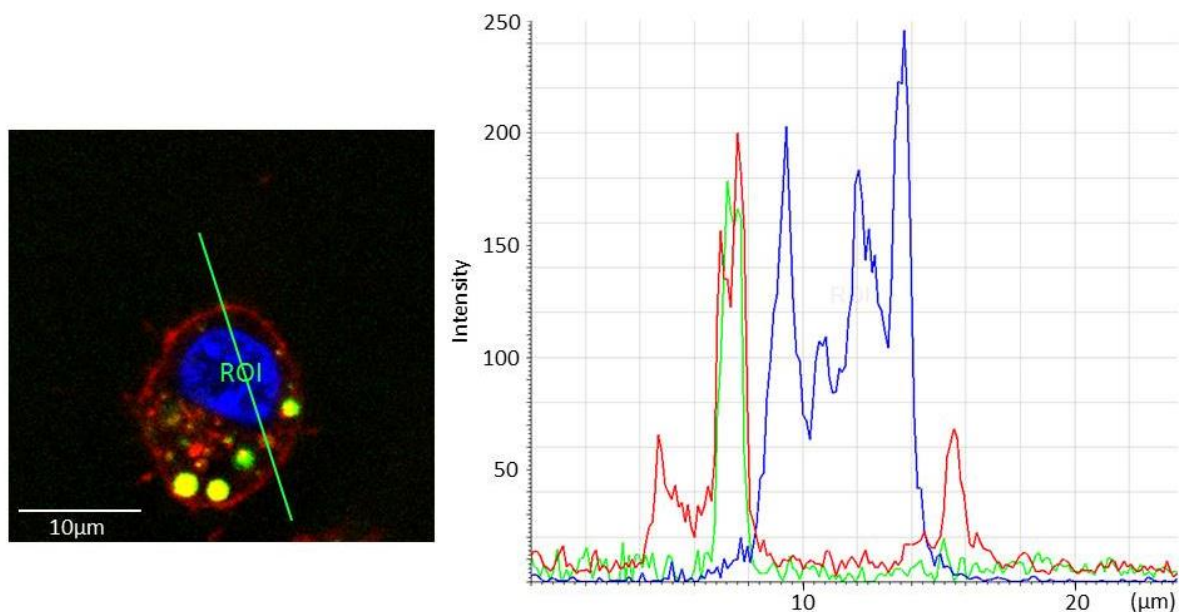


Figure 7. Confocal microscopy analysis of RAW 264.7 cell culture ($\sim 2.5 \times 10^5$ cells/mL) incubated with $2 \mu\text{M}$ of hRNase 3 labelled with Alexa Fluor 488 (green). Cells were stained following the assay incubation conditions detailed in the experimental procedures section. After protein addition, the evolution of the fluorescence signals was analysed by confocal microscopy. A total of 20 cells were analysed by regions of interest (ROIs) using Leica TCS software. The images were taken using a Leica TCS SP5 AOBS microscope.

Cellular RNA degradation assay

Previous work in our laboratory indicated that the main bacteria killing action of RNase 3 and 7 involves the mycobacterial cell wall binding and membrane lysis²¹. However, recent studies on the RNases action on *Candida albicans* cultures revealed the contribution of the protein enzymatic activity³⁰. The present data suggest that the RNase catalytic activity might complement the first bacteria wall disruption. Although equivalent MIC values for the wild type proteins and their respective site-active mutants were obtained at the extracellular level, significant differences are appreciated at the intracellular level (Table 2), supporting that the mechanism of action of RNases involve more than a mere action at the membrane. Therefore, we envisaged the analysis of the potential RNase activity on the mycobacteria RNA. Total cellular RNA from the infected macrophages was extracted from both treated and untreated cultures and analyzed by capillary electrophoresis. To estimate the relative activity on mycobacteria RNA, the corresponding time course of the decrease in rRNA subunits 16s and 23s was evaluated by densitometry as a function of time. The results confirmed a progressive reduction in mycobacteria cellular RNA degradation in the case of the wild type hRNase 3 while no significant reduction was detected for its active site mutant (figure 9). This effect was also observed for hRNase 7 and its active-site mutant (Table S2C). It is interesting to note that differences in the rate of RNA degradation are more pronounced at long period intervals. A progressive decrease of the rRNA is observed as a function of time in the presence of the wild type RNases. This reduction is not observed in the case of the control and mutant active-site samples (Figure 8, Table S2B). On the other hand, the macrophage rRNA levels were stable in all cases (Table S2).

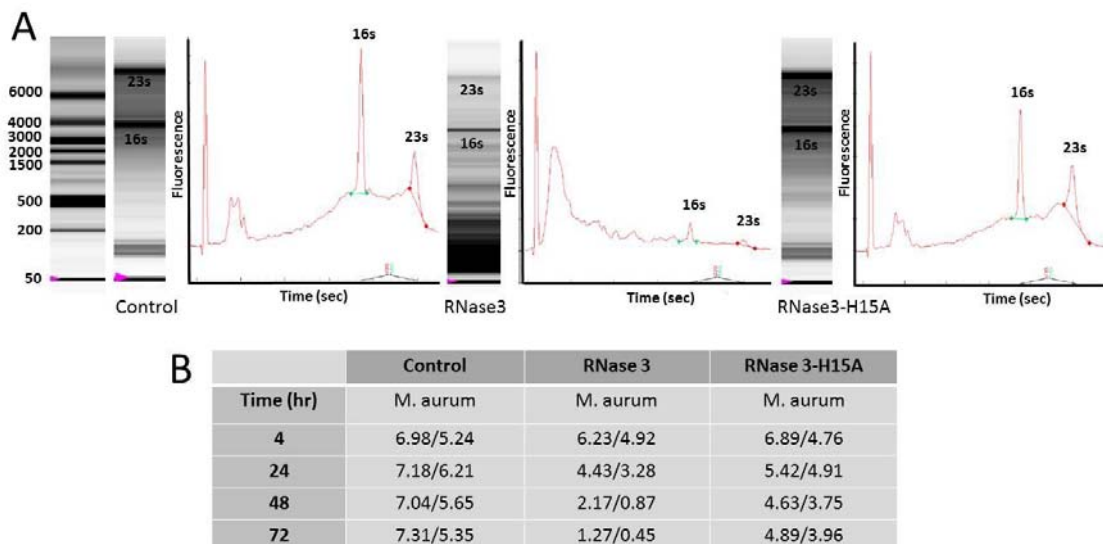


Figure 8. Intracellular effect of RNase 3 and its active-site mutant (RNase3-H15A) on *Mycobacterium aurum* cellular RNA. *Mycobacteria* infected macrophages were treated with 2 μ M of each protein and incubated at different time intervals. Following, total RNA was extracted as described in Experimental Procedures. (A) Samples were analyzed by an Experion automated capillary electrophoresis equipment and RNA was visualized with the Experion software. Control lane corresponds to cellular RNA from untreated infected macrophages. Middle and right lanes correspond to cellular RNA from treated macrophages with RNase3 and RNase3-H15A respectively after 72hr of incubation. B) Peak areas corresponding to 16/23s (prokaryotic) subunits of rRNA of non-treated (control) and treated cells with RNase3 and its active-site mutant are shown for each incubation time. Data represent mean \pm SD, n=3.

The autophagy-related protein LC3-II is upregulated during macrophage infection and exposure to RNases

Assuming autophagy as an essential process in the control of intracellular *M. aurum* growth and considering the ability of members of the RNase A family and others RNases to induce autophagy^{31,32,33,34} we decided to explore if the RNases antimycobacterial action was also mediated by this process. Therefore, we analysed the expression of the LC3b autophagy marker, which plays an important role in the autophagosome formation. First, in order to study the effect of *M. aurum* infection on RAW macrophages, we monitored the LC3b expression by immunoblotting. We observed an increase in the LC3b-II fraction in detriment of LC3-I on infected macrophages, suggesting an increment in basal autophagy. Next, we investigated whether the expression and processing of LC3 is modified by RNase treatment. A slight increase was observed in both the expression and processing of LC3 in RNase3 treated infected macrophages. The increase in lipidated LC3-II correlates with the autophagosome formation, as an indicator of the induction of the autophagic condition. Results are shown in Figure 10.

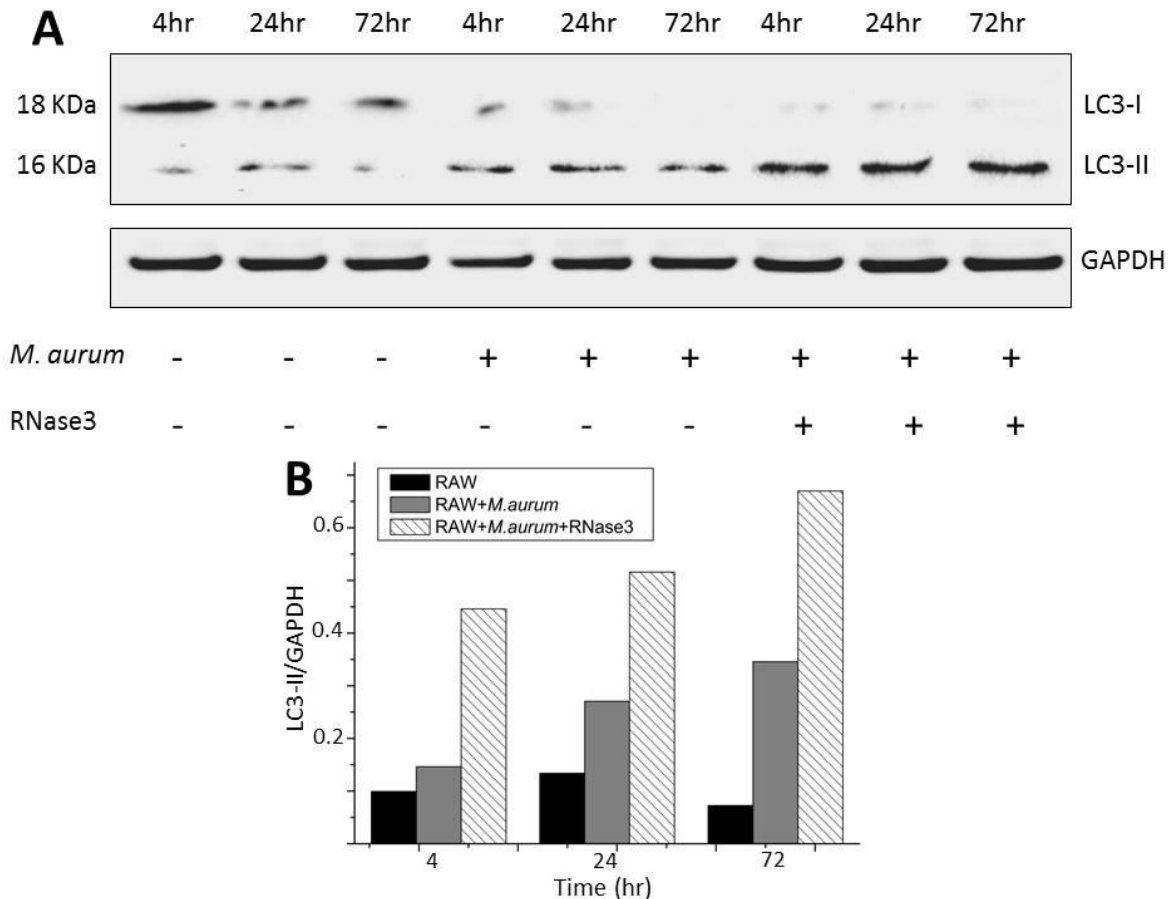


Figure 10. RNase 3 induced autophagy in RAW macrophages, upregulated the expression and activated the processing of LC3. Mice macrophages were infected with the non-virulent strain of *Mycobacterium aurum* and treated with hRNase3 for 4, 24 and 72hr. A) Immunoblot of LC3-processing in RAW macrophages at 4, 24 and 72 h of hRNase3 treatment. Equal amounts of protein (15-20 μ g) for each sample were mixed with 6 \times loading buffer and heated at 95 $^{\circ}$ C for 5 min, separated on a 15% SDS-PAGE gel and then transferred to a Immobilon-FL PDVF membrane. Non-infected control cellular sample is included as RAW. B) Densitometry analysis of LC3-II/GAPDH levels. Data represent mean \pm SD, n=2.

Table 2. Extra and intracellular Minimum Inhibitory Concentration (MIC), Minimum Agglutination Concentration (MAC) for mycobacteria and Growth Inhibitory Concentration (GIC₅₀) for macrophages treated with RNase 3, RNase 6, RNase 7 and their respective active centre mutants (RNase 3-H15A, RNase 6-H15A, RNase 7-H15A).

Protein	MIC ₁₀₀ (μ M)			MAC (μ M)			GIC ₅₀	
	Extracellular		Intracellular	<i>M. aurum</i>	<i>M. smegmatis</i>	<i>M. bovis</i> BCG		
	<i>M. aurum</i>	<i>M. smegmatis</i>	<i>M. aurum</i> [†]					
R3	18.75 \pm 0.05	9.37 \pm 0.05	18.75 \pm 0.05	5 \pm 0.05	2.34 \pm 0.5	1.17 \pm 0.3	4.68 \pm 1	>25
R3-H15A	18.75 \pm 0.05	18.75 \pm 0.05	18.75 \pm 0.05	> 10	4.68 \pm 0.5	4.68 \pm 1.0	4.68 \pm 1	>25
R6	18.75 \pm 0.05	18.75 \pm 0.05	18.75 \pm 0.05	10 \pm 0.05	4.68 \pm 1.0	2.34 \pm 0.5	4.68 \pm 1	>25
R6-H15A	18.75 \pm 0.05	18.75 \pm 0.05	37.50 \pm 0.05	> 10	4.68 \pm 1.0	2.34 \pm 0.5	4.68 \pm 1	>25
R7	18.75 \pm 0.05	18.75 \pm 0.05	18.75 \pm 0.05	10 \pm 0.05	>10	>10	>25	>25
R7-H15A	18.75 \pm 0.05	18.75 \pm 0.05	18.75 \pm 0.05	> 10	>10	>10	>25	>25

* Results are an average of three independent repeated experiments. Mean average values \pm SEM are indicated.

[†] MIC₁₀₀ results were obtained using the intracellular SPOTi assay

Table 3. Extra and intracellular Minimum Inhibitory Concentration (MIC) for mycobacteria and Growth Inhibitory Concentration (GIC₅₀) for macrophages treated with RNase derived N-Terminal peptides.

Protein/Peptide	MIC ₁₀₀ (μM)			GIC ₅₀ (μM)	
	Extracellular			Intracellular	
	<i>M. aurum</i>	<i>M. smegmatis</i>	<i>M. bovis</i> BCG	<i>M. aurum</i> [†]	RAW 264.7
RN1	>50	>50	>50	>20	>50
RN2	>50	>50	>50	>20	25-50
RN3	9.37 ± 0.05	9.37 ± 0.05	18.75 ± 0.05	5 ± 0.05	25-50
RN4	>50	18.75 ± 0.05	37.5 ± 0.05	>20	>50
RN5	>50	>50	>50	>20	>50
RN6	18.75 ± 0.05	37.5 ± 0.05	18.75 ± 0.05	10 ± 0.05	25-50
RN7	18.75 ± 0.05	18.75 ± 0.05	18.75 ± 0.05	10 ± 0.05	25-50
RN8	>50	>50	>50	>20	>50

*Summary of MIC₁₀₀ and GIC₅₀ of RNase derived N-terminal peptides. Results are an average of three independent repeated experiments. Mean average values ± SEM are indicated.

[†] MIC₁₀₀ results were obtained using the intracellular SPOTi assay

Discussion

Previous studies have demonstrated that macrophages act as a protecting niche for latent mycobacteria and this scenario could be the trigger for the reactivation of TB^{35,36}. Autophagy, free radicals generation and production of antimicrobial peptides are some of the main innate defence mechanisms used by host cells to eradicate intracellular mycobacteria³⁶. Both processes are significant and relevant for a consistent innate host response. However, the manner in which the host defence system acts against intracellular dwelling mycobacteria is poorly understood. Hence, the development of new drug screening platforms for tracking anti-TB agents in a scenario similar to the host cell environment was required. Gupta and Bhakta²⁴ established an integrated high-throughput assay for testing agents for in-cell growth inhibition of mycobacteria. The use of the non-pathogenic, fast-growing, biosafety level 2 *M. aurum* and the fast-growing, skill-engulfing RAW 264.7 cells provide a notable advantage to this method, offering an economic, low-hazardous and rapid surrogate macrophage infected model for primary drug screening. Improved knowledge of the mechanism of action of physiologically active AMPs against mycobacteria would facilitate the development of new anti-tuberculosis therapies. The antimicrobial RNase 3, 6 and 7 have been widely found effective against a full-scale spectrum of microbes^{29,37,18}. Particularly, some studies have revealed an increase in both eosinophil population as in the expression of hRNase 3 during mycobacteria infections^{10,38}. Moreover, it has been shown that hRNase 3 and hRNase 7 as well as their N-terminal derived peptides were potent antimycobacterial agents, being active in a low micromolar range²¹. These promising results together with the novel surrogate macrophage infected model approach encouraged us to further explore the RNase mechanism of action in an innate host cell environment. Considering the three more active human antimicrobial RNases (3, 6 and 7), the present results highlight that these RNases, as well as their derivative peptides, display a high antimicrobial activity showing MIC values at a sub micro molar range for all the tested mycobacterial species (Tables 2 and 3). Proteins and peptides showed a similar extracellular mycobactericidal activity against *M. aurum*, *M. smegmatis* mc²155 and *M. bovis* BCG, with slightly better MIC values for hRNase 3 (Table 2). Therefore, the present results on mycobacteria species corroborate the previous reports on the RNases bactericidal action^{26,19,39}. On the other hand, although previous studies using bacterial species^{29,19} indicated no correlation between the catalytic

and antimicrobial activities, a recent study has shown that the antimicrobial RNases can act following a dual mechanism, using both lytic and enzymatic activities against an eukaryotic pathogen⁴⁰. Supported by all this background, we decided to study further the mechanism of action of these host defence proteins against mycobacteria by evaluating the performance of mutant variants devoided of enzymatic activity. It is important to remark that previous studies demonstrated the absence of structural changes when replacing the active site H15 by alanine in hRNase 3^{40,41}. In any case, no significant differences were observed in the calculated MIC values when the wild type and single point mutants were assessed at the extracellular level. Following, the agglutination properties of the proteins were analysed, observing that hRNases 3 and 6 were active but no agglutination ability against the three mycobacterial species was observed for hRNase 7. Although the three proteins adopt the same 3D overall fold, they share a low sequence identity (~ 40%). Previous results from our group attributed the agglutination properties to the presence of a specific hydrophobic patch¹⁹. Differences at the N-terminus aggregation prone region could explain the absence of protein cell agglutination activity in the case of RNase 7. Comparison of 3D structures and the aggregation propensity profiles of hRNases show a lower agglutinating tendency in case of hRNase 7 (Figure S9B and C). These results are in agreement with previous studies where RNases 3 and 7 and their respective N-terminus peptides were tested against *Mycobacterium vaccae*²¹. Previous work indicated that the main mycobactericidal mechanism for these proteins occurs at the membrane level²¹. We should consider that hRNases 3, 6 and 7 present the usual properties of cationic AMPs, a high proportion of hydrophobic residues that would favour the pathogen cell wall interaction and a positive net charge which would facilitates the binding to the negatively charged microbial envelopes²⁹. After checking that the RNases were non-toxic to macrophages at a concentration more than 10 fold the calculated MIC values, we decided to evaluate their activity on an ex vivo model. Following, we verify the ability of the RNases to inhibit the mycobacterial growth intracellularly by applying an adapted SPOTi assay (Figs. 3 and 4). Intracellular MIC values and CFU counting assay supported the ability of RNases and their derived peptides to kill *M. aurum* within RAW macrophages. Moreover, all proteins and peptides which were found extracellularly effective against *M. aurum* improved intracellularly their effectivity range (Tables 2 and 3). In addition, the potential contribution of the proteins enzymatic activity was also considered. It is noteworthy to remark here the significant differences on the mycobacteria inhibitory growth activity between the wild-type RNases and their respective active site mutants (H15A) at the macrophage intracellular level, both assessed by the MIC value determination and viable cells counting. A decrease in the active site mutants mycobactericidal ability is observed at long incubation times when working at sublethal concentrations (Table 2, Fig. 4 and 5). Although previous studies have reported that the antimicrobial and catalytic activities of RNases were apparently unrelated^{42,43}, RNases were recently proposed as multifaceted proteins, combining enzymatic and microbicidal action, together with other assigned immunomodulatory properties^{44,40}. In fact, our group has recently described a dual mode of action of RNases against *Candida albicans* that involves both membranolytic and enzymatic mechanisms in their antimicrobial action⁴⁰. In addition, analogous examples of multifunctional antimicrobial proteins, combining both extra and intracellular targets with an assortment of immunomodulatory effects, have been described in the literature^{45,46,47}. Interestingly, assay conditions (i.e. the tested AMP working concentrations and assessed incubation times) are essential for the observation of phenomena such as immunomodulation or intracellular targeting^{48,46}. In tune with these facts, we analysed the intracellular effect of hRNases 3, 6, 7 and their active-site mutants on *M. aurum* cellular RNA. For this purpose, total cellular RNA was purified from infected

macrophages and analysed by capillary electrophoresis. The respective bands corresponding to eukaryote and prokaryote rRNA were quantified. Interestingly, reduction of the 16 and 23s rRNA peak area was observed for the wild-type hRNases but no overall significant reduction for the respective active-site mutants was detected, supporting the catalytic activity of RNases as a complementary process to kill the mycobacteria inside the macrophages (Fig. 8, Table S2). To note, in the case of the hRNase6-H15A mutant some RNA degradation activity was observed. As it has been recently reported by our research group, 3D structural resolution and molecular modelling predictions have highlighted in hRNase 6 a multisubsite arrangement for substrate binding and the contribution of a novel secondary catalytic site that would favour the cleavage of RNA substrates⁴⁹. This could be in accordance with the decrease in RNA levels in samples treated with the hRNase 6-H15A mutant, respect to the other mutants values (Table S2). In order to further characterize the mechanism of action of RNases in the surrogate macrophage infected model and further explain the observed results, we assayed the ability of the RNases to internalize within the macrophages. Protein labelling using the alexa 488 fluorophore and confocal microscopy were applied in order to visualize and track the hRNases location. Confocal micrographs revealed a fast protein uptake (< 30 min) and a prominent ratio of protein internalization in RAW macrophages after incubation with a subinhibitory concentration (Fig. 6, S8). Equivalent internalization rates were registered for hRNase 3, 6 and 7 active-site mutants (results not shown). In addition, examination of fluorescence intensity profiles of different region of interest showed the protein vesicle-storage inside the macrophages (Fig 7 and S8). As mentioned before, upon detection of invading mycobacteria, macrophages launch the innate host response, activating the production of cytokines and triggering antimicrobial mechanisms, such as autophagy induction⁵⁰. In this process, members of the LC3 family protein, in which LC3b is the preponderant form, display an important role. The different degrees of LC3 maturation can be measured by immunoblotting and two isoforms of LC3 can be detected: LC3-I, which is normally found at cytoplasmic level and LC3-II, an autophagy marker, which is generated from LC3-I after several cleavage and lipid modification steps^{51,52,53}. Here, the monitoring of LC3 processing through immunoblotting of protein extracts of infected macrophages treated with the RNases allowed us to visualize the LC3 processing (fig. 10). While non-infected macrophages showed a LC3-I upregulation, infected macrophages showed the opposite scenario, with a high expression of LC3-II in detriment of LC3-I. Furthermore, infected macrophages which have been treated with RNase revealed even a greater presence of LC3-II (Figure 10). Considering all these facts, we could hypothesize that mycobacteria infection promotes macrophages autophagosome induction and these phenomena can be enhanced by the antimicrobial RNase treatment, which could facilitate an easier and faster removal of the intracellular mycobacteria. Similar examples of intracellular antimicrobial mechanism of action are available in the literature. Walch *et al.* reported that granulysin is actively internalized via lipid rafts by *Listeria innocua*-challenged dendritic cells into early endosomes and then transferred to phagosomes with the subsequent microbial lysis⁵⁴. Interestingly, T lymphocytes have been found to kill intracellular *M. tuberculosis* through granulysin-dependent mechanism of action⁵⁵. In addition, it has been found that granulysin is in charge of the mycobactericidal activity of NK cells or lymphocytes^{56,57}. Similar results were shown for *Mycobacterium leprae*, which can also dwell into phagosomes of host cells⁵⁸. In a similar manner, RNases are secreted by different innate cell types and are responsible of several processes involved in the host defense^{29,19,30}. Present results show a clear internalization of RNases and subsequent reduction of intracellular mycobacterial population, which, we presume would take place at the phagosomal compartment. We can hypothesize that RNases are also inducing an autophagy process

in infected macrophages. Indeed, other RNase A superfamily members have recently been reported to display antitumoral properties via an autophagy pathway^{31,32}. On the other hand, another key requirement for efficient AMPs is to achieve a high intracellular life time within the macrophages. Supporting that, RNases, as secretory proteins, offer a high stability and resistance in a hostile environment, such as the extracellular or phagosomal environment. Indeed, both hRNase A and hRNase 3 are examples of proteins with an unusual high stability^{59,60}. Further work is in progress to characterize in detail the putative autophagy process induced by RNases treatment and track the RNases traffic inside the infected macrophages. Notwithstanding, the present results have disclosed a multifaceted role for hRNases as effective AMPs against microbial resistant forms, as macrophage intracellular dwelling mycobacteria. In conclusion, our data highlight an underlying role of human antimicrobial RNases and their N-terminal derived peptides as effective molecules during mycobacterial infection, able to reduce the mycobacteria growth and facilitate the clearance of macrophage dwelling mycobacteria through a multi-faceted mechanism of action. Future work is in progress to extent the therapeutic potentiality of RNases to develop alternative antibiotics to target microbial resistant forms.

Acknowledgments

The authors wish to thank the Laboratori d'Anàlisi i Fotodocumentació (UAB), where spectrofluorescence assays were performed. Experimental work was supported by the *Ministerio de Economía y Competitividad* (Grants BFU2012-38695 and SAF2015-66007P to EB) co-financed by FEDER funds and *Generalitat de Catalunya* (Grant 2014-SGR-728). JAT was a recipient of a predoctoral fellowship (Personal Investigador en Formación, Universitat Autònoma de Barcelona). Authors thank Javier Valle and David Andreu, Dpt. Of Experimental and Health Sciences, Pompeu Fabra University, Spain for the synthesis of the peptides.

References

1. Zumla, A. *et al.* The WHO 2014 global tuberculosis report--further to go. *Lancet. Glob. Heal.* **3**, e10-2 (2015).
2. Pai, M. & Schito, M. Tuberculosis diagnostics in 2015: landscape, priorities, needs, and prospects. *J. Infect. Dis.* **211 Suppl**, S21-8 (2015).
3. Maitra, A. *et al.* Tackling tuberculosis: Insights from an international TB Summit in London. *Virulence* **6**, 561–572 (2015).
4. Gupta, A., Kaul, A., Tsolaki, A. G., Kishore, U. & Bhakta, S. Mycobacterium tuberculosis: immune evasion, latency and reactivation. *Immunobiology* **217**, 363–74 (2012).
5. Maitra, A. & Bhakta, S. Mycobacterium tuberculosis ... Can we beat it? Report from a Euroscicon Conference 2013. *Virulence* **4**, 499–503 (2014).
6. Siegrist, M. S. & Bertozzi, C. R. Mycobacterial lipid logic. *Cell Host Microbe* **15**, 1–2 (2014).
7. Pieters, J. Mycobacterium tuberculosis and the macrophage: maintaining a balance. *Cell Host Microbe* **3**, 399–407 (2008).
8. Welin, A., Raffetseder, J., Eklund, D., Stendahl, O. & Lerm, M. Importance of Phagosomal Functionality for Growth Restriction of *Mycobacterium tuberculosis* in Primary Human Macrophages. *J. Innate Immun.* **3**, 508–518 (2011).
9. Saiga, H., Shimada, Y. & Takeda, K. Innate Immune Effectors in Mycobacterial

- Infection. *Clin. Dev. Immunol.* **2011**, 1–8 (2011).
10. Driss, V. *et al.* TLR2-dependent eosinophil interactions with mycobacteria: role of alpha-defensins. *Blood* **113**, 3235–44 (2009).
 11. Soehnlein, O. Direct and alternative antimicrobial mechanisms of neutrophil-derived granule proteins. *J. Mol. Med.* **87**, 1157–1164 (2009).
 12. Lasco, T. M. *et al.* Rapid accumulation of eosinophils in lung lesions in guinea pigs infected with *Mycobacterium tuberculosis*. *Infect. Immun.* **72**, 1147–9 (2004).
 13. Sorrentino, S. The eight human ‘canonical’ ribonucleases: molecular diversity, catalytic properties, and special biological actions of the enzyme proteins. *FEBS Lett.* **584**, 2194–200 (2010).
 14. Akuthota, P., Xenakis, J. J. & Weller, P. F. Eosinophils: offenders or general bystanders in allergic airway disease and pulmonary immunity? *J. Innate Immun.* **3**, 113–9 (2011).
 15. Torrent, M., de la Torre, B. G., Nogués, V. M., Andreu, D. & Boix, E. Bactericidal and membrane disruption activities of the eosinophil cationic protein are largely retained in an N-terminal fragment. *Biochem. J.* **421**, 425–434 (2009).
 16. Pulido, D. *et al.* Antimicrobial action and cell agglutination by the eosinophil cationic protein are modulated by the cell wall lipopolysaccharide structure. *Antimicrob. Agents Chemother.* **56**, 2378–2385 (2012).
 17. Torrent, M. *et al.* Comparison of human RNase 3 and RNase 7 bactericidal action at the Gram-negative and Gram-positive bacterial cell wall. *FEBS J.* **277**, 1713–1725 (2010).
 18. Becknell, B. *et al.* Ribonucleases 6 and 7 have antimicrobial function in the human and murine urinary tract. *Kidney Int.* **87**, 151–61 (2015).
 19. Pulido, D. *et al.* Insights into the antimicrobial mechanism of action of human RNase6: Structural determinants for bacterial cell agglutination and membrane permeation. *Int. J. Mol. Sci.* **17**, 552 (2016).
 20. Torrent, M. *et al.* Ribonucleases as a host-defence family: evidence of evolutionarily conserved antimicrobial activity at the N-terminus. *Biochem. J.* **456**, 99–108 (2013).
 21. Pulido, D., Torrent, M., Andreu, D., Nogués, M. V. & Boix, E. Two human host defense ribonucleases against mycobacteria, the eosinophil cationic protein (RNase 3) and RNase 7. *Antimicrob. Agents Chemother.* **57**, 3797–805 (2013).
 22. Torrent, M., Nogués, V. M. & Boix, E. A theoretical approach to spot active regions in antimicrobial proteins. *BMC Bioinformatics* **10**, 373 (2009).
 23. Gruppo, V. *et al.* Rapid microbiologic and pharmacologic evaluation of experimental compounds against *Mycobacterium tuberculosis*. *Antimicrob. Agents Chemother.* **50**, 1245–50 (2006).
 24. Gupta, A. & Bhakta, S. An integrated surrogate model for screening of drugs against mycobacterium tuberculosis. *J. Antimicrob. Chemother.* **67**, 1380–1391 (2012).
 25. Torrent, M. *et al.* Comparison of the membrane interaction mechanism of two antimicrobial RNases: RNase 3/ECP and RNase 7. *Biochim. Biophys. Acta - Biomembr.* **1788**, 1116–1125 (2009).
 26. Boix, E. *et al.* Structural determinants of the eosinophil cationic protein antimicrobial activity. *Biol. Chem.* **393**, 801–815 (2012).
 27. Harder, J. & Schroder, J.-M. RNase 7, a novel innate immune defense antimicrobial protein of healthy human skin. *J. Biol. Chem.* **277**, 46779–84 (2002).
 28. Sánchez, D. *et al.* Mapping the eosinophil cationic protein antimicrobial activity by chemical and enzymatic cleavage. *Biochimie* **93**, 331–8 (2011).

29. Boix, E. *et al.* Structural determinants of the eosinophil cationic protein antimicrobial activity. *Biol. Chem.* **393**, 801–15 (2012).
30. Salazar, V. A. *et al.* Exploring the mechanisms of action of human secretory RNase 3 and RNase 7 against *Candida albicans*. *Microbiologyopen* (2016). doi:10.1002/mbo3.373
31. Fiorini C, Gotte G, Donnarumma F, Picone D, D. M. Bovine seminal ribonuclease triggers Beclin1-mediated autophagic cell death in pancreatic cancer cells. - PubMed - NCBI. *Biochim Biophys Acta* **1843**, 976–84 (2014).
32. Fiorini C, Cordani M, Gotte G, Picone D, D. M. Onconase induces autophagy sensitizing pancreatic cancer cells to gemcitabine and activates Akt/mTOR pathway in a ROS-dependent manner. - PubMed - NCBI. *Biochim Biophys Acta* **1853**, 549–60 (2015).
33. Siddiqui, M. A. & Malathi, K. RNase L induces autophagy via c-Jun N-terminal kinase and double-stranded RNA-dependent protein kinase signaling pathways. *J. Biol. Chem.* **287**, 43651–64 (2012).
34. Chakrabarti, A., Ghosh, P. K., Banerjee, S., Gaughan, C. & Silverman, R. H. RNase L triggers autophagy in response to viral infections. *J. Virol.* **86**, 11311–21 (2012).
35. Bao, Z. *et al.* A potential target gene for the host-directed therapy of mycobacterial infection in murine macrophages. *Int. J. Mol. Med.* (2016). doi:10.3892/ijmm.2016.2675
36. Bloom, B. R. & Modlin, R. L. Mechanisms of Defense against Intracellular Pathogens Mediated by Human Macrophages. *Microbiol. Spectr.* **4**, (2016).
37. Spencer, J. D. *et al.* Ribonuclease 7 is a potent antimicrobial peptide within the human urinary tract. *Kidney Int.* **80**, 174–80 (2011).
38. Driss, V. *et al.* CR3-dependent negative regulation of human eosinophils by *Mycobacterium bovis* BCG lipoarabinomannan. *Immunol. Lett.* **143**, 202–207 (2012).
39. Harder, J. & Schroder, J.-M. RNase 7, a novel innate immune defense antimicrobial protein of healthy human skin. *J. Biol. Chem.* **277**, 46779–84 (2002).
40. Salazar, V. A. *et al.* Exploring the mechanisms of action of human secretory RNase 3 and RNase 7 against *Candida albicans*. *Microbiologyopen* 1–16 (2016). doi:10.1002/mbo3.373
41. García-Mayoral, M. F. *et al.* NMR structural determinants of eosinophil cationic protein binding to membrane and heparin mimetics. *Biophys. J.* **98**, 2702–11 (2010).
42. Huang, Y.-C. *et al.* The flexible and clustered lysine residues of human ribonuclease 7 are critical for membrane permeability and antimicrobial activity. *J. Biol. Chem.* **282**, 4626–33 (2007).
43. Boix, E. & Nogués, M. V. Mammalian antimicrobial proteins and peptides: overview on the RNase A superfamily members involved in innate host defence. *Mol. Biosyst.* **3**, 317–35 (2007).
44. Gupta, S. K., Haigh, B. J., Griffin, F. J. & Wheeler, T. T. The mammalian secreted RNases: mechanisms of action in host defence. *Innate Immun.* **19**, 86–97 (2013).
45. Hancock, R. E. W. & Sahl, H.-G. Antimicrobial and host-defense peptides as new anti-infective therapeutic strategies. *Nat. Biotechnol.* **24**, 1551–7 (2006).
46. Haney, E. F. & Hancock, R. E. W. Peptide design for antimicrobial and immunomodulatory applications. *Biopolymers* **100**, 572–83 (2013).
47. Nicolas, P. Multifunctional host defense peptides: intracellular-targeting antimicrobial peptides. *FEBS J.* **276**, 6483–96 (2009).

48. Holm T1, Netzereab S, Hansen M, Langel U, H. M. Uptake of cell-penetrating peptides in yeasts. *FEBS Lett* **579**, 5217–22 (2005).
49. Prats-Ejarque, G. *et al.* The first crystal structure of human RNase6 reveals a novel substrate binding and cleavage site arrangement. *Biochem. J.* (2016). doi:10.1042/BCJ20160245
50. Wang, J. *et al.* MicroRNA-155 promotes autophagy to eliminate intracellular mycobacteria by targeting Rheb. *PLoS Pathog.* **9**, e1003697 (2013).
51. Kabeya, Y. *et al.* LC3, GABARAP and GATE16 localize to autophagosomal membrane depending on form-II formation. *J. Cell Sci.* **117**, 2805–12 (2004).
52. Heintze, J., Costa, J. R., Weber, M. & Ketteler, R. Ribose 5-phosphate isomerase inhibits LC3 processing and basal autophagy. *Cell. Signal.* **28**, 1380–1388 (2016).
53. Sultana Rekha, R. *et al.* Phenylbutyrate induces LL-37-dependent autophagy and intracellular killing of mycobacterium tuberculosis in human macrophages. *Autophagy* **11**, 1688–1699 (2015).
54. Walch, M. *et al.* Uptake of granulysin via lipid rafts leads to lysis of intracellular *Listeria innocua*. *J. Immunol.* **174**, 4220–7 (2005).
55. Dieli, F. *et al.* Granulysin-dependent killing of intracellular and extracellular *Mycobacterium tuberculosis* by Vgamma9/Vdelta2 T lymphocytes. *J. Infect. Dis.* **184**, 1082–5 (2001).
56. Gansert, J. L. *et al.* Human NKT cells express granulysin and exhibit antimycobacterial activity. *J. Immunol.* **170**, 3154–61 (2003).
57. Stenger, S. *et al.* An antimicrobial activity of cytolytic T cells mediated by granulysin. *Science* **282**, 121–5 (1998).
58. Ochoa, M. T. *et al.* T-cell release of granulysin contributes to host defense in leprosy. *Nat. Med.* **7**, 174–9 (2001).
59. Ribo, M. *et al.* Thermal unfolding of eosinophil cationic protein / ribonuclease 3 : A nonreversible process. *Protein Sci.* **15**, 2816–2827 (2006).
60. Raines RT. Ribonuclease A. *Chem Rev* **98**, 1045–1066 (1998).

4. GENERAL DISCUSSION

4. General discussion and future outlook

4.1 Unveiling the antimicrobial mechanism of action of RNase 6

Human RNase 6 is a small cationic protein belonging to the vertebrate-specific RNase A family. The fact that distantly related members within the family displayed antimicrobial properties suggested that the family arose with a role in host defence^{174,175}. The family comprises in humans eight members. Recent studies indicated that RNase 6 is secreted by diverse type of innate cells upon infection^{218,193}. Due its high degree of production in neutrophils and monocytes as well as its induced expression by bacterial infections, an anti-pathogenic function by RNase 6 is proposed^{193,219}. In this chapter we have thoroughly investigated the mode of action of that antimicrobial protein and its derived N-terminal peptide. Results have been compared with one of the most extensively studied proteins within the family, the RNase 3, specifically secreted by eosinophils by infection and inflammation²⁰⁹. RNase 6 characterization highlights a high and fast antimicrobial activity, with a predilection for the cell membrane as the main bactericidal target, as have also been described for RNase 3^{204,205,220}. Previous studies identified the main structural determinants for antimicrobial activity of representative human RNases^{221,205,103}. Interestingly it was possible to demonstrate that the key region that provides the bactericidal activity lies at the amino acid N-terminal sequence¹²³. Supported by all these data, we decided to carry out the characterization of the RNase 6 N-terminal region, which showed to retain most of the bactericidal activity of the parental protein and hardly displayed any cytotoxicity against mammalian cells. Similarly to RNase 3, the RNase 6 meets the main characteristics of the antimicrobial peptides (AMPs), exhibiting a remarkable cationicity with an important ratio of hydrophobic residues, which would facilitate interaction with bacterial cell wall and bacterial membrane destabilization. These features are mostly retained at the protein N-terminus. Results using phospholipid liposomes as a membrane model confirmed that RNase 6, as well as its derived N-terminal peptide, was able to interact with the negatively charged membranes and efficiently destabilize the lipid bilayers. Moreover, RNase 6 also displays a high LPS binding activity that could mediate the observed agglutination activity towards Gram-negative bacterial cells. Indeed, previous work from our research group analyzed the RNase 3 bacterial agglutination activity, which correlated with the protein LPS binding and was suggested to promote bacterial clearance at the infection focus^{189,217}. In this chapter we have observed that RNase 6 and its derived N-terminal peptide are also able to aggregate both large unilamellar vesicles and Gram-negative bacteria in a micro molar range. Electron microscopy analysis have not only demonstrated this agglutination ability but also achieved to corroborate the bacterial cell damage in the presence of these antimicrobial molecules. Finally, site-directed mutagenesis was used to generate two mutants of two key hydrophobic residues (W1A and I13A) in the protein prone aggregation region. The results confirmed these two residues as key amino acids in the aggregation patch since the bacterial agglutination and antimicrobial activities were significantly reduced¹⁹⁵. Thus, we consider that the discovery of all these new data could contribute to

set the basis for the generation of new antibacterial agents based on the characterized AMPs. Future work would require the verification of their therapeutic effectiveness.

4.2 Crystal structure of human RNase 6: Structure- functional insights into its nucleotide binding mode

The analysis of the first reported crystal structure of RNase 6 has provided the structural basis for the understanding of the protein catalytical and biological properties. The protein displays the overall kidney shaped globular fold characteristic of the canonical RNase A family members. In particular, the crystal structure obtained at 1.72 Å resolution in complex with sulphate anions has allowed not only the recognition of the main phosphate binding site (His15, His122 and Lys38), conserved in all the family members, but also other secondary binding sites showing abundance of cationic residues. Furthermore, the presence of an abundant proportion of cationic residues exposed at the protein surface could mediate the displayed antimicrobial mechanism. Interestingly, one of the achievements of this work was to demonstrate the existence of a novel additional catalytic site, corresponding to His36/His39 residues. The characterization of the enzyme polynucleotide cleavage pattern, the percentage of remnant catalytic activity shown by the RNase 6-H15A mutant and the detection of a close by Lys residue which fits in the required active site geometry corroborated the hypothesis. Nevertheless, this additional active site behaved as a weaker catalyst, even though the atomic distances between histidines are similar to those of the main active site. Chromatography profiles of substrate degradation showed preference of RNase 6 for the cleavage of polymeric RNA strands through a predominant endonucleolytic activity. Complementarily, molecular modelling studies of RNase 6 in complex with polynucleotides revealed new binding sites that could reinforce the enhanced catalysis of polynucleotide substrates thanks to a better anchor of the protein through a multisubsite arrangement binding via cationic surface clusters and the potential contribution of the secondary catalytic site. Although the resolution of the first three-dimensional structure of RNase 6 facilitated the understanding of its structure-function relationship, more studies are in progress to fully comprehend its enzymatic and biological properties.

4.3 Exploring the mechanism of action of human secretory RNases and their N-terminal derived peptides against *Candida albicans*

Although fungal infections do not pose a lethal threat, the impact that these diseases cause on human health is often disregarded. The incidence of fungal infections has increased during recent years, largely due to advances in modern medicine which have contributed to increase the population of immune- and clinically-compromised patients; hence, these

infections represent a serious public health threat²²². As an alternative for fastest-growing drug development, exploring and repurposing the mode of action of our own immune defence system is a coherent and encouraging initiative/stratagem. Particularly, human antimicrobial RNases, being proteins that play a key role in host defence and having been proven effective against pathogenic fungi, constitute an appropriate standard for the development of new therapies based on proteins and antimicrobial peptides^{196,201}. Little is known about the mode of action of antimicrobial peptides (AMPs) against yeast species. In this chapter we have assessed the fungicidal activity of two of the main human antimicrobial RNases, the eosinophil cationic protein (ECP or RNase 3) and the skin-derived RNase 7, which are directly involved in host defence^{223,209}. hRNase 3 is specifically expressed in the secondary granules of eosinophils during infection processes and exhibits a high antimicrobial activity against a wide range of human pathogens²⁰⁹ and hRNase7 is an antimicrobial protein secreted by a variety of epithelial tissues, especially the skin, displaying a protective barrier against various pathogens^{224,225}. Complementarily, to corroborate and verify that the antimicrobial activity of human RNases is retained at its N-terminal region¹²³, we have performed a comparison between the eight N-termini peptides corresponding to each of the RNase A family members. *Candida albicans*, of rapid growth and ease of handling, was the eukaryote model chosen. The highest fungicidal activities were achieved by RNase 3, 7 and their derived N-terminal peptides followed by the RNase 6 N-terminal peptide, all of them with minimum fungicidal activity concentrations on the low micromolar range. A similar pattern was also reproduced when assessing the cell wall damage. One of the great advances of this work has been to reveal a novel and dual mode of action of RNase 3 and 7 against *Candida albicans*. Both proteins have not only exercised a destabilizing role at the cell wall level but have also been able to internalize within the yeast cells, and display their enzymatic action. Our results corroborate the potential multifaceted character of human RNases as also reported for other antimicrobial proteins in the literature, that are capable to exert both mechanical and enzymatic activities as well as immunomodulatory functions^{226,3}. It is important to note that the distinct AMPs properties depend largely on the working concentrations. While damage at microbial cell wall level is favoured by high concentrations, intracellular action and development of immunomodulatory functions can be observed at sub lethal conditions²²⁷. Results confirm that RNase 3 and 7 are internalized into *C. albicans* cells and contribute through their catalytic activity to the cell death. In order to verify the contribution of the intracellular enzymatic activity, active site mutants from both proteins were tested. Both H15A variants showed similar cell binding, membrane destabilization and cell internalisation properties. However, their fungicidal activity and ability to degrade intracellular RNA was significantly reduced. We have simultaneously studied the contribution of the protein cell binding process by analyzing the RNase 3-W35A mutant. Previous work indicated that W35 in RNase 3 is a key residue in the protein interactions with membrane and cell wall components. Our findings highlight the importance of this residue for cell disruption and internalization of the protein. In conclusion, we have found for the first time a dual mechanism of action for

human RNases. On the one hand, we have reported that RNases 3, 7 and their N-terminal peptides are effective against *C. albicans* at a low micromolar concentration. In particular, the RN3, 6 and 7(1-45) peptides, showing the higher antimicrobial and agglutinating properties, represent a breakthrough in the design of novel antifungal therapies. On the other hand, non-specific RNA degradation is proposed as an additional mechanism by which RNases could also promote the decrease of pathogen viability. Further studies are envisaged in other fungal species with a more clinical perspective and towards a better understanding of the features required for the RNases mechanism of action.

4.4 Tackling mycobacteria, a global threat: disclosing the mycobactericidal mechanism of action of hRNases through a macrophage infected model.

The battle against mycobacteria has steadily found a space in the present times but a co-ordinated performance from scientists to clinics is required. Tuberculosis (TB) and mycobacterial infections emerge as a grave issue to the world and it is not only a mere scientific challenge but also a socio-economic encumbrance. Growing occurrence of *Mycobacterium tuberculosis* strains with multidrug resistance (MDR) and extensively drug-resistance (XDR) is a novel and dramatic component of this critic scenario, which has been recognized by WHO as a “global emergency”. Nowadays, the human vaccine BCG is the most widely administered all over the world, but its protective efficacy is still controversial, since it does not protect against the predominant pulmonary form of the disease in adults. All these facts, together with the ability of mycobacteria to evolve and dwell inside the human macrophages for an undefined period of time, make completely necessary to develop new antimicrobial strategies. Lot of studies available in the literature have evidenced the potential therapeutic roles of antimicrobial peptides and proteins (AMPs) in a large variety of human diseases. Moreover, these biological molecules participate in diverse cell physiological processes and act as signalling mediators in the host defence system. Human antimicrobial RNases are considered part of the host defence system and have important roles in many biological processes related to innate immune response^{58,228}. Previous studies have shown hRNases 3, 6 and 7 to be the most effective members within the ribonuclease A family^{209,193}. Moreover, it has been shown that their antimicrobial properties have been evolutionary conserved at the N-terminus¹²³. Interestingly, hRnase 3 antimicrobial abilities were found not dependent on the enzymatic activity of the protein^{188,186}. However, a recent study has shown a dual antimicrobial mechanism of action that involves the ribonuclease activity²²⁹. Taken into consideration the reported contribution of hRnase 3 in vivo to mycobacterial growth inhibition²³⁰ and the recent confirmation that recombinant hRNases 3 and 7 displayed an effective mycobactericidal action a low micromolar range²²⁰, we decided to investigate further the role of hRNases during mycobacterial infection. hRNases 3, 6 and 7, together with their active-site mutants as well as their N-terminal derived peptides were tested against *Mycobacterium* not only *in*

vitro but also *ex vivo* through an integrated surrogate model. Non-pathogenic and fast growing *Mycobacterium aurum* and RAW 264.7 macrophages were used as surrogates for *M. tuberculosis* and primary immune cells respectively. Results confirmed that hRNases, active-site mutants and their respective N-terminal peptides were able to eradicate *Mycobacterium* extracellularly in a low micromolar range. It is worth noting the improvement in the ability to inhibit actively dividing mycobacteria of all proteins and peptides using the higher throughput intracellular SPOTi assay. Although it is well-known that the mechanism of action of hRNases is mainly deployed on the cell wall, the ability to clump pathogens is also considered as an important part of the mycobactericidal mechanism¹⁰³. Discrepancies in terms of the minimum agglutinating values demonstrated the high capacity of hRNases 3 and 6 to agglutinate mycobacteria, while the lack of this property was shown in case of hRNase 7. Differences in the aggregation prone region due to the presence of specific hydrophobic patches between these hRNases were reported¹⁹⁵, which could explain this scenario. Therefore, it would be possible to suggest that hRNases may trigger an agglutinating process in order to contribute the mycobacterial clearance within the macrophage. On the other hand, contrasting results between active-site mutants and their respective parental proteins at the intracellular level made us suspect a likely involvement of the enzymatic activity of these proteins in their antimicrobial mechanism, as it has been recently described²²⁹. Mycobacteria total cellular RNA from infected macrophages treated with proteins was analysed. Significant reduction in rRNA purified from infected and treated macrophages was shown compared with controls. Furthermore, no significant reduction was detected for active-site mutants, supporting ribonuclease activity as a complementary mode of action to eradicate mycobacteria inside macrophages. In addition, results also confirmed the ability of hRNases to internalize within the macrophages, corroborating their capacity to exhibit the antimycobactericidal mechanism within host cells. Complementary, we have analysed the expression of LC3 protein, an autophagy induction marker. Results suggested that mycobacteria infection promotes autophagosome formation within macrophages and this process could be favoured by hRNase treatment, facilitating an easier removal of macrophage dwelling mycobacteria. In conclusion, although further work is in progress to complete this study, the present results help to highlight the multi-faceted mode of action of hRNases against macrophage resident mycobacteria, validate the SPOTi method as a convenient intracellular-screening platform and place hRNases as potential templates to develop novel therapeutic anti tuberculosis agents.

5. CONCLUSIONS

5. Conclusions

Paper I:

- First time characterization of the bactericidal properties of human RNase 6
- Antimicrobial mechanism of action encompasses two steps: a first interaction with the negatively charged bacterial envelopes, followed by a combination of membrane destabilization and bacterial agglutination
- The N-terminal domain of the protein was proven to retain the antimicrobial properties of the whole protein
- The results presents hRNase 6 as a useful template for the development of new antimicrobial agents

Paper II:

- The hRNase 6 first crystal structure provide the opportunity to explore its structure-function relationship
- The combination of structural analysis together with molecular modelling and kinetic characterization identified the key regions contributing to the substrate specificity and catalytic properties
- The results highlighted a multisubsite arrangement on RNase 6 structure for substrate binding and the contribution of a secondary catalytic site that facilitates the cleavage of polynucleotide substrates

Paper III:

- hRNase 3 and hRNase 7 showed a low antimicrobial effective doses against *Candida albicans*
- Both RNases were able to combine membrane lytic and enzymatic RNase activity in a dual mechanism
- The nonspecific RNA degradation was suggested as an additional effective mechanism of targeting pathogen viability
- RNases provide an optimal system for the design of both nonantigenic nanodelivery tools and novel applied therapies to eradicate fungal pathogens

Paper IV:


- The N-terminal peptides 3, 6 and 7 showed a high candidacidal effectiveness and were selected as the best templates for the development of novel antifungal agents
- The results correlated well with those obtained from previous studies in bacteria, suggesting the N-termini conservation in hRNases

Paper V:

- The functional and structural properties of AMPs are analyzed effective against mycobacteria
- hRNases fulfill the same properties and therefore can be included as potential AMPs in anti-TB drug design TB
- AMPs expressed by our organism innate cells are a good model for the design of alternative antibiotics to facilitate mycobacterial eradication of resistant forms, residents inside the host cells

Paper VI:

- The results present an underlying role of human antimicrobial RNases and their N-terminal derived peptides as effective molecules during mycobacterial infection
- hRNases 3, 6 and 7 showed high mycobacterial growth inhibition and the effective removal of macrophage dwelling mycobacteria through a multi-faceted mechanism of action

 hRNases and their derived peptides highlight its potential as bactericidal, candidacidal and antimycobacterial templates for drug development

6. REFERENCES

6. References

1. Padhi A, Sengupta M, Sengupta S, Roehm KH, Sonawane A. Antimicrobial peptides and proteins in mycobacterial therapy: current status and future prospects. *Tuberculosis (Edinb)*. 2014;94(4):363-373. doi:10.1016/j.tube.2014.03.011.
2. Kaspar AA, Reichert JM. Future directions for peptide therapeutics development. *Drug Discov Today*. 2013;18(17-18):807-817. doi:10.1016/j.drudis.2013.05.011.
3. Smith VJ, Dyrzynda EA. Antimicrobial proteins: From old proteins, new tricks. *Mol Immunol*. 2015;68(2 Pt B):383-398. doi:10.1016/j.molimm.2015.08.009.
4. Bulet P, Stöcklin R, Menin L. Anti-microbial peptides: from invertebrates to vertebrates. *Immunol Rev*. 2004;198:169-184. <http://www.ncbi.nlm.nih.gov/pubmed/15199962>. Accessed March 4, 2016.
5. Wang G, Li X, Wang Z. APD2: the updated antimicrobial peptide database and its application in peptide design. *Nucleic Acids Res*. 2009;37(Database issue):D933-7. doi:10.1093/nar/gkn823.
6. Dutta P, Das S. Mammalian Antimicrobial Peptides: Promising Therapeutic Targets Against Infection and Chronic Inflammation. *Curr Top Med Chem*. 2016;16(1):99-129. <http://www.ncbi.nlm.nih.gov/pubmed/26139111>. Accessed February 19, 2016.
7. Zaiou M. Multifunctional antimicrobial peptides: therapeutic targets in several human diseases. *J Mol Med (Berl)*. 2007;85(4):317-329. doi:10.1007/s00109-006-0143-4.
8. Hiemstra PS, Amatngalim GD, van der Does AM, Taube C. Antimicrobial peptides and innate lung defenses: Role in infectious and non-infectious lung diseases and therapeutic applications. *Chest*. October 2015. doi:10.1378/chest.15-1353.
9. Wang G. Database-Guided Discovery of Potent Peptides to Combat HIV-1 or Superbugs. *Pharmaceuticals (Basel)*. 2013;6(6):728-758. doi:10.3390/ph6060728.
10. Mylonakis E, Podsiadlowski L, Muhammed M, Vilcinskas A. Diversity, evolution and medical applications of insect antimicrobial peptides. *Philos Trans R Soc Lond B Biol Sci*. 2016;371(1695). doi:10.1098/rstb.2015.0290.
11. Barber MF, Kronenberg Z, Yandell M, Elde NC. Antimicrobial Functions of Lactoferrin Promote Genetic Conflicts in Ancient Primates and Modern Humans. *PLoS Genet*. 2016;12(5):e1006063. doi:10.1371/journal.pgen.1006063.
12. Wang, G.; Li, X.; Zasloff M. *A Database View of Natural Antimicrobial Peptides: Nomenclature, Classification and Amino Acid Sequence Analysis*. In *Antimicrobial Peptides: Discovery, Design and Novel Therapeutic Strategies*; Wang, G., Ed.; CABI: Wallingford, England, 2010; Pp. 1-21.; 2010.
13. Wang Z. APD: the Antimicrobial Peptide Database. *Nucleic Acids Res*. 2004;32(90001):590D-592. doi:10.1093/nar/gkh025.
14. Hancock REW, Sahl H-G. Antimicrobial and host-defense peptides as new anti-

- infective therapeutic strategies. *Nat Biotechnol.* 2006;24(12):1551-1557. doi:10.1038/nbt1267.
15. Wang G. Improved methods for classification, prediction, and design of antimicrobial peptides. *Methods Mol Biol.* 2015;1268:43-66. doi:10.1007/978-1-4939-2285-7_3.
 16. Wiesner J, Vilcinskas A. Antimicrobial peptides: the ancient arm of the human immune system. *Virulence.* 1(5):440-464. doi:10.4161/viru.1.5.12983.
 17. Zanetti M. The role of cathelicidins in the innate host defenses of mammals. *Curr Issues Mol Biol.* 2005;7(2):179-196. <http://www.ncbi.nlm.nih.gov/pubmed/16053249>. Accessed January 8, 2016.
 18. Lehrer RI, Ganz T. Cathelicidins: a family of endogenous antimicrobial peptides. *Curr Opin Hematol.* 2002;9(1):18-22. <http://www.ncbi.nlm.nih.gov/pubmed/11753073>. Accessed January 8, 2016.
 19. Bandurska K, Berdowska A, Barczyńska-Felusiak R, Krupa P. Unique features of human cathelicidin LL-37. *Biofactors.* 2015;41(5):289-300. doi:10.1002/biof.1225.
 20. Kai-Larsen Y, Agerberth B. The role of the multifunctional peptide LL-37 in host defense. *Front Biosci.* 2008;13:3760-3767. <http://www.ncbi.nlm.nih.gov/pubmed/18508470>. Accessed January 8, 2016.
 21. Steiner H, Hultmark D, Engström A, Bennich H, Boman HG. Sequence and specificity of two antibacterial proteins involved in insect immunity. *Nature.* 1981;292(5820):246-248. <http://www.ncbi.nlm.nih.gov/pubmed/7019715>. Accessed January 19, 2016.
 22. Bulet P, Stöcklin R. Insect antimicrobial peptides: structures, properties and gene regulation. *Protein Pept Lett.* 2005;12(1):3-11. <http://www.ncbi.nlm.nih.gov/pubmed/15638797>. Accessed March 18, 2016.
 23. Boman HG. Innate immunity and the normal microflora. *Immunol Rev.* 2000;173:5-16. <http://www.ncbi.nlm.nih.gov/pubmed/10719663>. Accessed March 18, 2016.
 24. Baek M-H, Kamiya M, Kushibiki T, et al. Lipopolysaccharide-bound structure of the antimicrobial peptide cecropin P1 determined by nuclear magnetic resonance spectroscopy. *J Pept Sci.* March 2016. doi:10.1002/psc.2865.
 25. Burian M, Schitteck B. The secrets of dermcidin action. *Int J Med Microbiol.* 2015;305(2):283-286. doi:10.1016/j.ijmm.2014.12.012.
 26. Rieg S, Seeber S, Steffen H, et al. Generation of multiple stable dermcidin-derived antimicrobial peptides in sweat of different body sites. *J Invest Dermatol.* 2006;126(2):354-365. doi:10.1038/sj.jid.5700041.
 27. Paulmann M, Arnold T, Linke D, et al. Structure-activity analysis of the dermcidin-derived peptide DCD-1L, an anionic antimicrobial peptide present in human sweat. *J Biol Chem.* 2012;287(11):8434-8443. doi:10.1074/jbc.M111.332270.
 28. Schitteck B. The multiple facets of dermcidin in cell survival and host defense. *J Innate*

- Immun.* 2012;4(4):349-360. doi:10.1159/000336844.
29. Zasloff M. Magainins, a class of antimicrobial peptides from *Xenopus* skin: isolation, characterization of two active forms, and partial cDNA sequence of a precursor. *Proc Natl Acad Sci U S A.* 1987;84(15):5449-5453. <http://www.pubmedcentral.nih.gov/articlerender.fcgi?artid=298875&tool=pmcentrez&rendertype=abstract>. Accessed March 2, 2016.
 30. Sai KP, Reddy PN, Babu M. Investigations on wound healing by using amphibian skin. *Indian J Exp Biol.* 1995;33(9):673-676. <http://www.ncbi.nlm.nih.gov/pubmed/8557310>. Accessed March 18, 2016.
 31. Clara A, Manjramkar DD, Reddy VK. Preclinical evaluation of magainin-A as a contraceptive antimicrobial agent. *Fertil Steril.* 2004;81(5):1357-1365. doi:10.1016/j.fertnstert.2003.09.073.
 32. Marquette A, Salnikov ES, Glattard E, Aisenbrey C, Bechinger B. Magainin 2-PGLa Interactions in Membranes - Two Peptides that Exhibit Synergistic Enhancement of Antimicrobial Activity. *Curr Top Med Chem.* 2016;16(1):65-75. <http://www.ncbi.nlm.nih.gov/pubmed/26139118>. Accessed March 18, 2016.
 33. Mor A, Nicolas P. Isolation and structure of novel defensive peptides from frog skin. *Eur J Biochem.* 1994;219(1-2):145-154. <http://www.ncbi.nlm.nih.gov/pubmed/8306981>. Accessed March 18, 2016.
 34. Mor A, Hani K, Nicolas P. The vertebrate peptide antibiotics dermaseptins have overlapping structural features but target specific microorganisms. *J Biol Chem.* 1994;269(50):31635-31641. <http://www.ncbi.nlm.nih.gov/pubmed/7989335>. Accessed March 18, 2016.
 35. Navon-Venezia S, Feder R, Gaidukov L, Carmeli Y, Mor A. Antibacterial properties of dermaseptin S4 derivatives with in vivo activity. *Antimicrob Agents Chemother.* 2002;46(3):689-694. <http://www.pubmedcentral.nih.gov/articlerender.fcgi?artid=127478&tool=pmcentrez&rendertype=abstract>. Accessed March 18, 2016.
 36. Lequin O, Ladram A, Chabbert L, et al. Dermaseptin S9, an alpha-helical antimicrobial peptide with a hydrophobic core and cationic termini. *Biochemistry.* 2006;45(2):468-480. doi:10.1021/bi051711i.
 37. Fox MA, Thwaite JE, Ulaeto DO, Atkins TP, Atkins HS. Design and characterization of novel hybrid antimicrobial peptides based on cecropin A, LL-37 and magainin II. *Peptides.* 2012;33(2):197-205. doi:10.1016/j.peptides.2012.01.013.
 38. Cotton S, Donnelly S, Robinson MW, Dalton JP, Thivierge K. Defense peptides secreted by helminth pathogens: antimicrobial and/or immunomodulator molecules? *Front Immunol.* 2012;3:269. doi:10.3389/fimmu.2012.00269.
 39. Richardson JS, Richardson DC. Natural beta-sheet proteins use negative design to avoid edge-to-edge aggregation. *Proc Natl Acad Sci U S A.* 2002;99(5):2754-2759. doi:10.1073/pnas.052706099.

40. Van Wetering S, Mannesse-Lazeroms SP, Van Sterkenburg MA, Daha MR, Dijkman JH, Hiemstra PS. Effect of defensins on interleukin-8 synthesis in airway epithelial cells. *Am J Physiol*. 1997;272(5 Pt 1):L888-96. <http://www.ncbi.nlm.nih.gov/pubmed/9176253>. Accessed January 8, 2016.
41. Prohászka Z, Német K, Csermely P, Hudecz F, Mező G, Füst G. Defensins purified from human granulocytes bind C1q and activate the classical complement pathway like the transmembrane glycoprotein gp41 of HIV-1. *Mol Immunol*. 1997;34(11):809-816. <http://www.ncbi.nlm.nih.gov/pubmed/9444979>. Accessed January 8, 2016.
42. Chu H, Pazgier M, Jung G, et al. Human α -defensin 6 promotes mucosal innate immunity through self-assembled peptide nanonets. *Science*. 2012;337(6093):477-481. doi:10.1126/science.1218831.
43. White SH, Wimley WC, Selsted ME. Structure, function, and membrane integration of defensins. *Curr Opin Struct Biol*. 1995;5(4):521-527. <http://www.ncbi.nlm.nih.gov/pubmed/8528769>. Accessed March 21, 2016.
44. Daly NL, Chen Y-K, Rosengren KJ, et al. Retrocyclin-2: structural analysis of a potent anti-HIV theta-defensin. *Biochemistry*. 2007;46(35):9920-9928. doi:10.1021/bi700720e.
45. Levay PF, Viljoen M. Lactoferrin: a general review. *Haematologica*. 80(3):252-267. <http://www.ncbi.nlm.nih.gov/pubmed/7672721>. Accessed November 7, 2015.
46. Gifford JL, Hunter HN, Vogel HJ. Lactoferricin: a lactoferrin-derived peptide with antimicrobial, antiviral, antitumor and immunological properties. *Cell Mol Life Sci*. 2005;62(22):2588-2598. doi:10.1007/s00018-005-5373-z.
47. Krause A, Neitz S, Mägert HJ, et al. LEAP-1, a novel highly disulfide-bonded human peptide, exhibits antimicrobial activity. *FEBS Lett*. 2000;480(2-3):147-150. <http://www.ncbi.nlm.nih.gov/pubmed/11034317>. Accessed January 8, 2016.
48. Park CH, Valore E V, Waring AJ, Ganz T. Hecpudin, a urinary antimicrobial peptide synthesized in the liver. *J Biol Chem*. 2001;276(11):7806-7810. doi:10.1074/jbc.M008922200.
49. Fázio MA, Oliveira VX, Bulet P, Miranda MTM, Daffre S, Miranda A. Structure-activity relationship studies of gomesin: importance of the disulfide bridges for conformation, bioactivities, and serum stability. *Biopolymers*. 2006;84(2):205-218. doi:10.1002/bip.20396.
50. Tamamura H, Murakami T, Horiuchi S, et al. Synthesis of protegrin-related peptides and their antibacterial and anti-human immunodeficiency virus activity. *Chem Pharm Bull (Tokyo)*. 1995;43(5):853-858. <http://www.ncbi.nlm.nih.gov/pubmed/7553971>. Accessed March 21, 2016.
51. Nakamura T, Furunaka H, Miyata T, et al. Tachyplesin, a class of antimicrobial peptide from the hemocytes of the horseshoe crab (*Tachyplesus tridentatus*). Isolation and chemical structure. *J Biol Chem*. 1988;263(32):16709-16713. <http://www.ncbi.nlm.nih.gov/pubmed/3141410>. Accessed March 21, 2016.

52. Lehrer RI, Lichtenstein AK, Ganz T. Defensins: antimicrobial and cytotoxic peptides of mammalian cells. *Annu Rev Immunol.* 1993;11:105-128. doi:10.1146/annurev.iy.11.040193.000541.
53. Ganz T. Hepcidin and its role in regulating systemic iron metabolism. *Hematology Am Soc Hematol Educ Program.* January 2006:29-35, 507. doi:10.1182/asheducation-2006.1.29.
54. Zhang Z-T, Zhu S-Y. Drosomycin, an essential component of antifungal defence in *Drosophila*. *Insect Mol Biol.* 2009;18(5):549-556. doi:10.1111/j.1365-2583.2009.00907.x.
55. Cohen L, Moran Y, Sharon A, Segal D, Gordon D, Gurevitz M. Drosomycin, an innate immunity peptide of *Drosophila melanogaster*, interacts with the fly voltage-gated sodium channel. *J Biol Chem.* 2009;284(35):23558-23563. doi:10.1074/jbc.M109.023358.
56. Lamberty M, Caille A, Landon C, et al. Solution structures of the antifungal heliomicin and a selected variant with both antibacterial and antifungal activities. *Biochemistry.* 2001;40(40):11995-12003. <http://www.ncbi.nlm.nih.gov/pubmed/11580275>. Accessed March 21, 2016.
57. Krijgsveld J, Zaat SA, Meeldijk J, et al. Thrombocidins, microbicidal proteins from human blood platelets, are C-terminal deletion products of CXC chemokines. *J Biol Chem.* 2000;275(27):20374-20381. <http://www.ncbi.nlm.nih.gov/pubmed/10877842>. Accessed March 21, 2016.
58. Boix E, Nogués MV. Mammalian antimicrobial proteins and peptides: overview on the RNase A superfamily members involved in innate host defence. *Mol Biosyst.* 2007;3(5):317-335. doi:10.1039/b617527a.
59. Lawyer C, Pai S, Watabe M, et al. Antimicrobial activity of a 13 amino acid tryptophan-rich peptide derived from a putative porcine precursor protein of a novel family of antibacterial peptides. *FEBS Lett.* 1996;390(1):95-98. <http://www.ncbi.nlm.nih.gov/pubmed/8706838>. Accessed March 21, 2016.
60. Selsted ME, Novotny MJ, Morris WL, Tang YQ, Smith W, Cullor JS. Indolicidin, a novel bactericidal tridecapeptide amide from neutrophils. *J Biol Chem.* 1992;267(7):4292-4295. <http://www.ncbi.nlm.nih.gov/pubmed/1537821>. Accessed March 21, 2016.
61. Cociancich S, Dupont A, Hegy G, et al. Novel inducible antibacterial peptides from a hemipteran insect, the sap-sucking bug *Pyrrhocoris apterus*. *Biochem J.* 1994;300 (Pt 2):567-575. <http://www.pubmedcentral.nih.gov/articlerender.fcgi?artid=1138199&tool=pmcentrez&rendertype=abstract>. Accessed March 21, 2016.
62. Bulet P, Dimarcq JL, Hetru C, et al. A novel inducible antibacterial peptide of *Drosophila* carries an O-glycosylated substitution. *J Biol Chem.* 1993;268(20):14893-14897. <http://www.ncbi.nlm.nih.gov/pubmed/8325867>. Accessed March 21, 2016.
63. Rogers LA. THE INHIBITING EFFECT OF STREPTOCOCCUS LACTIS ON LACTOBACILLUS

- BULGARICUS. *J Bacteriol.* 1928;16(5):321-325.
<http://www.pubmedcentral.nih.gov/articlerender.fcgi?artid=375033&tool=pmcentrez&rendertype=abstract>. Accessed January 21, 2016.
64. Oppenheim FG, Xu T, McMillian FM, et al. Histatins, a novel family of histidine-rich proteins in human parotid secretion. Isolation, characterization, primary structure, and fungistatic effects on *Candida albicans*. *J Biol Chem.* 1988;263(16):7472-7477.
<http://www.ncbi.nlm.nih.gov/pubmed/3286634>. Accessed March 21, 2016.
65. Baltzer SA, Brown MH. Antimicrobial peptides: promising alternatives to conventional antibiotics. *J Mol Microbiol Biotechnol.* 2011;20(4):228-235. doi:10.1159/000331009.
66. Shin D-M, Jo E-K. Antimicrobial Peptides in Innate Immunity against Mycobacteria. *Immune Netw.* 2011;11(5):245. doi:10.4110/in.2011.11.5.245.
67. Isamida T, Tanaka T, Omata Y, Yamauchi K, Shimazaki K, Saito A. Protective effect of lactoferricin against *Toxoplasma gondii* infection in mice. *J Vet Med Sci.* 1998;60(2):241-244. <http://www.ncbi.nlm.nih.gov/pubmed/9524950>. Accessed January 8, 2016.
68. Shafer WM, Martin LE, Spitznagel JK. Cationic antimicrobial proteins isolated from human neutrophil granulocytes in the presence of diisopropyl fluorophosphate. *Infect Immun.* 1984;45(1):29-35.
<http://www.pubmedcentral.nih.gov/articlerender.fcgi?artid=263254&tool=pmcentrez&rendertype=abstract>. Accessed January 8, 2016.
69. Pereira HA, Spitznagel JK, Winton EF, et al. The ontogeny of a 57-Kd cationic antimicrobial protein of human polymorphonuclear leukocytes: localization to a novel granule population. *Blood.* 1990;76(4):825-834.
<http://www.ncbi.nlm.nih.gov/pubmed/2200540>. Accessed January 8, 2016.
70. Gabay JE, Scott RW, Campanelli D, et al. Antibiotic proteins of human polymorphonuclear leukocytes. *Proc Natl Acad Sci U S A.* 1989;86(14):5610-5614.
<http://www.pubmedcentral.nih.gov/articlerender.fcgi?artid=297672&tool=pmcentrez&rendertype=abstract>. Accessed January 8, 2016.
71. Chertov O, Ueda H, Xu LL, et al. Identification of human neutrophil-derived cathepsin G and azurocidin/CAP37 as chemoattractants for mononuclear cells and neutrophils. *J Exp Med.* 1997;186(5):739-747.
<http://www.pubmedcentral.nih.gov/articlerender.fcgi?artid=2199011&tool=pmcentrez&rendertype=abstract>. Accessed January 8, 2016.
72. Soehnlein O, Zerneck A, Eriksson EE, et al. Neutrophil secretion products pave the way for inflammatory monocytes. *Blood.* 2008;112(4):1461-1471. doi:10.1182/blood-2008-02-139634.
73. 1. Bieth J. Elastases: catalytic and biological properties. *Regul matrix Accumulation, mecham, R, ed (Academic Press New York.* 1986:217-320.
74. Belaaouaj A, Kim KS, Shapiro SD. Degradation of outer membrane protein A in *Escherichia coli* killing by neutrophil elastase. *Science.* 2000;289(5482):1185-1188.

- <http://www.ncbi.nlm.nih.gov/pubmed/10947984>. Accessed January 8, 2016.
75. Ribeiro-Gomes FL, Moniz-de-Souza MCA, Alexandre-Moreira MS, et al. Neutrophils activate macrophages for intracellular killing of *Leishmania major* through recruitment of TLR4 by neutrophil elastase. *J Immunol.* 2007;179(6):3988-3994. <http://www.ncbi.nlm.nih.gov/pubmed/17785837>. Accessed January 8, 2016.
 76. Epand RM, Shai Y, Segrest JP, Anantharamaiah GM. Mechanisms for the modulation of membrane bilayer properties by amphipathic helical peptides. *Biopolymers.* 1995;37(5):319-338. doi:10.1002/bip.360370504.
 77. Jahnsen RD, Frimodt-Møller N, Franzyk H. Antimicrobial activity of peptidomimetics against multidrug-resistant *Escherichia coli*: a comparative study of different backbones. *J Med Chem.* 2012;55(16):7253-7261. doi:10.1021/jm300820a.
 78. Epand RM, Vogel HJ. Diversity of antimicrobial peptides and their mechanisms of action. *Biochim Biophys Acta.* 1999;1462(1-2):11-28. <http://www.ncbi.nlm.nih.gov/pubmed/10590300>. Accessed March 22, 2016.
 79. Pace CN, Scholtz JM. A helix propensity scale based on experimental studies of peptides and proteins. *Biophys J.* 1998;75(1):422-427. <http://www.pubmedcentral.nih.gov/articlerender.fcgi?artid=1299714&tool=pmcentrez&rendertype=abstract>. Accessed March 22, 2016.
 80. Eisenberg D. Three-dimensional structure of membrane and surface proteins. *Annu Rev Biochem.* 1984:595-623.
 81. Watson JL, Gillies ER. Amphipathic beta-strand mimics as potential membrane disruptive antibiotics. *J Org Chem.* 2009;74(16):5953-5960. doi:10.1021/jo900933r.
 82. Wieprecht T, Dathe M, Krause E, et al. Modulation of membrane activity of amphipathic, antibacterial peptides by slight modifications of the hydrophobic moment. *FEBS Lett.* 1997;417(1):135-140. <http://www.ncbi.nlm.nih.gov/pubmed/9395091>. Accessed March 22, 2016.
 83. Fernández-Vidal M, Jayasinghe S, Ladokhin AS, White SH. Folding amphipathic helices into membranes: amphiphilicity trumps hydrophobicity. *J Mol Biol.* 2007;370(3):459-470. doi:10.1016/j.jmb.2007.05.016.
 84. Thaker HD, Cankaya A, Scott RW, Tew GN. Role of Amphiphilicity in the Design of Synthetic Mimics of Antimicrobial Peptides with Gram-negative Activity. *ACS Med Chem Lett.* 2013;4(5):481-485. doi:10.1021/ml300307b.
 85. Uematsu N, Matsuzaki K. Polar angle as a determinant of amphipathic alpha-helix-lipid interactions: a model peptide study. *Biophys J.* 2000;79(4):2075-2083. doi:10.1016/S0006-3495(00)76455-1.
 86. Lee T-H, Hall KN, Aguilar M-I. Antimicrobial Peptide Structure and Mechanism of Action: A Focus on the Role of Membrane Structure. *Curr Top Med Chem.* 2016;16(1):25-39. <http://www.ncbi.nlm.nih.gov/pubmed/26139112>. Accessed March 31, 2016.

87. Kondejewski LH, Jelokhani-Niaraki M, Farmer SW, et al. Dissociation of antimicrobial and hemolytic activities in cyclic peptide diastereomers by systematic alterations in amphipathicity. *J Biol Chem.* 1999;274(19):13181-13192. <http://www.ncbi.nlm.nih.gov/pubmed/10224074>. Accessed March 22, 2016.
88. Scheinpflug K, Nikolenko H, Komarov I V, Rautenbach M, Dathe M. What Goes around Comes around-A Comparative Study of the Influence of Chemical Modifications on the Antimicrobial Properties of Small Cyclic Peptides. *Pharmaceuticals (Basel).* 2013;6(9):1130-1144. doi:10.3390/ph6091130.
89. Scheinpflug K, Krylova O, Nikolenko H, Thurm C, Dathe M. Evidence for a novel mechanism of antimicrobial action of a cyclic R-,W-rich hexapeptide. *PLoS One.* 2015;10(4):e0125056. doi:10.1371/journal.pone.0125056.
90. Trabi M, Craik DJ. Circular proteins--no end in sight. *Trends Biochem Sci.* 2002;27(3):132-138. <http://www.ncbi.nlm.nih.gov/pubmed/11893510>. Accessed March 22, 2016.
91. Yin LM, Edwards MA, Li J, Yip CM, Deber CM. Roles of hydrophobicity and charge distribution of cationic antimicrobial peptides in peptide-membrane interactions. *J Biol Chem.* 2012;287(10):7738-7745. doi:10.1074/jbc.M111.303602.
92. Horovitz A, Serrano L, Avron B, Bycroft M, Fersht AR. Strength and co-operativity of contributions of surface salt bridges to protein stability. *J Mol Biol.* 1990;216(4):1031-1044. doi:10.1016/S0022-2836(99)80018-7.
93. Kumar S, Nussinov R. Close-range electrostatic interactions in proteins. *Chembiochem.* 2002;3(7):604-617. doi:10.1002/1439-7633(20020703)3:7<604::AID-CBIC604>3.0.CO;2-X.
94. Rajabi M, de Leeuw E, Pazgier M, Li J, Lubkowski J, Lu W. The conserved salt bridge in human alpha-defensin 5 is required for its precursor processing and proteolytic stability. *J Biol Chem.* 2008;283(31):21509-21518. doi:10.1074/jbc.M801851200.
95. Hunter HN, Demcoe AR, Jenssen H, Gutteberg TJ, Vogel HJ. Human lactoferricin is partially folded in aqueous solution and is better stabilized in a membrane mimetic solvent. *Antimicrob Agents Chemother.* 2005;49(8):3387-3395. doi:10.1128/AAC.49.8.3387-3395.2005.
96. Dathe M, Nikolenko H, Meyer J, Beyermann M, Bienert M. Optimization of the antimicrobial activity of magainin peptides by modification of charge. *FEBS Lett.* 2001;501(2-3):146-150. <http://www.ncbi.nlm.nih.gov/pubmed/11470274>. Accessed March 11, 2016.
97. de Leeuw E, Rajabi M, Zou G, Pazgier M, Lu W. Selective arginines are important for the antibacterial activity and host cell interaction of human alpha-defensin 5. *FEBS Lett.* 2009;583(15):2507-2512. doi:10.1016/j.febslet.2009.06.051.
98. Vogel HJ, Schibli DJ, Jing W, Lohmeier-Vogel EM, Epanand RF, Epanand RM. Towards a structure-function analysis of bovine lactoferricin and related tryptophan- and arginine-containing peptides. *Biochem Cell Biol.* 2002;80(1):49-63.

- <http://www.ncbi.nlm.nih.gov/pubmed/11908643>. Accessed March 29, 2016.
99. Shepherd CM, Vogel HJ, Tieleman DP. Interactions of the designed antimicrobial peptide MB21 and truncated dermaseptin S3 with lipid bilayers: molecular-dynamics simulations. *Biochem J*. 2003;370(Pt 1):233-243. doi:10.1042/BJ20021255.
 100. Aliste MP, MacCallum JL, Tieleman DP. Molecular dynamics simulations of pentapeptides at interfaces: salt bridge and cation- π interactions. *Biochemistry*. 2003;42(30):8976-8987. doi:10.1021/bi027001j.
 101. Torrent M, Cuyás E, Carreras E, et al. Topography studies on the membrane interaction mechanism of the eosinophil cationic protein. *Biochemistry*. 2007;46(3):720-733. doi:10.1021/bi061190e.
 102. Carreras E, Boix E, Navarro S, Rosenberg HF, Cuchillo CM, Nogués MV. Surface-exposed amino acids of eosinophil cationic protein play a critical role in the inhibition of mammalian cell proliferation. *Mol Cell Biochem*. 2005;272(1-2):1-7. <http://www.ncbi.nlm.nih.gov/pubmed/16010966>. Accessed March 29, 2016.
 103. Pulido D, Moussaoui M, Nogués MV, Torrent M, Boix E. Towards the rational design of antimicrobial proteins: single point mutations can switch on bactericidal and agglutinating activities on the RNase A superfamily lineage. *FEBS J*. 2013;280(22):5841-5852. doi:10.1111/febs.12506.
 104. Deslouches B, Phadke SM, Lazarevic V, et al. De novo generation of cationic antimicrobial peptides: influence of length and tryptophan substitution on antimicrobial activity. *Antimicrob Agents Chemother*. 2005;49(1):316-322. doi:10.1128/AAC.49.1.316-322.2005.
 105. Cabiaux V, Agerberth B, Johansson J, Homblé F, Goormaghtigh E, Ruyschaert JM. Secondary structure and membrane interaction of PR-39, a Pro+Arg-rich antibacterial peptide. *Eur J Biochem*. 1994;224(3):1019-1027. <http://www.ncbi.nlm.nih.gov/pubmed/7925399>. Accessed March 29, 2016.
 106. Scocchi M, Tossi A, Gennaro R. Proline-rich antimicrobial peptides: converging to a non-lytic mechanism of action. *Cell Mol Life Sci*. 2011;68(13):2317-2330. doi:10.1007/s00018-011-0721-7.
 107. Fernández-Carneado J, Kogan MJ, Castel S, Giralt E. Potential peptide carriers: amphipathic proline-rich peptides derived from the N-terminal domain of gamma-zein. *Angew Chem Int Ed Engl*. 2004;43(14):1811-1814. doi:10.1002/anie.200352540.
 108. Cassone M, Vogiatzi P, La Montagna R, et al. Scope and limitations of the designer proline-rich antibacterial peptide dimer, A3-APO, alone or in synergy with conventional antibiotics. *Peptides*. 2008;29(11):1878-1886. doi:10.1016/j.peptides.2008.07.016.
 109. Zhao B-C, Lin H-C, Yang D, Ye X, Li Z-G. Disulfide Bridges in Defensins. *Curr Top Med Chem*. 2015;16(2):206-219. <http://www.ncbi.nlm.nih.gov/pubmed/26126908>. Accessed March 30, 2016.

110. Mandal M, Nagaraj R. Antibacterial activities and conformations of synthetic alpha-defensin HNP-1 and analogs with one, two and three disulfide bridges. *J Pept Res.* 2002;59(3):95-104. <http://www.ncbi.nlm.nih.gov/pubmed/11985703>. Accessed March 30, 2016.
111. Varkey J, Nagaraj R. Antibacterial activity of human neutrophil defensin HNP-1 analogs without cysteines. *Antimicrob Agents Chemother.* 2005;49(11):4561-4566. doi:10.1128/AAC.49.11.4561-4566.2005.
112. Powers JP, Rozek A HR. Structure-activity relationships for the beta-hairpin cationic antimicrobial peptide polyphemusin I. *Biochim Biophys Acta.* 2004;1698(2):239-250.
113. Zhao C, Liu L LR. Identification of a new member of the protegrin family by cDNA cloning. *FEBS Lett.* 1994;346(2-3):285-288.
114. Mangoni ME, Aumelas A, Charnet P, Roumestand C, Chiche L, Despaux E, Grassy G, Calas B CA. Change in membrane permeability induced by protegrin 1: implication of disulphide bridges for pore formation. *FEBS Lett.* 1996;383(1-2):93-98.
115. Gutschmann T. Interaction between antimicrobial peptides and mycobacteria. *Biochim Biophys Acta.* 2016;1858(5):1034-1043.
116. Malmsten M. Interactions of Antimicrobial Peptides with Bacterial Membranes and Membrane Components. *Curr Top Med Chem.* 2016;16(1):16-24.
117. Wan Z, Lu S, Zhao D, Ding Y, Chen P. Arginine-Rich Ionic Complementary Peptides as Potential Drug Carriers: Impact of Peptide Sequence on Size, Shape and Cell Specificity. *Nanomedicine.* March 2016. doi:10.1016/j.nano.2016.01.008.
118. Gopal R, Park S-C, Ha K-J, et al. Effect of Leucine and Lysine substitution on the antimicrobial activity and evaluation of the mechanism of the HPA3NT3 analog peptide. *J Pept Sci.* 2009;15(9):589-594. doi:10.1002/psc.1155.
119. Mitchell DJ, Kim DT, Steinman L, Fathman CG, Rothbard JB. Polyarginine enters cells more efficiently than other polycationic homopolymers. *J Pept Res.* 2000;56(5):318-325. <http://www.ncbi.nlm.nih.gov/pubmed/11095185>. Accessed March 30, 2016.
120. Kawaguchi Y, Takeuchi T, Kuwata K, et al. Syndecan-4 Is a Receptor for Clathrin-mediated Endocytosis of Arginine-rich Cell-penetrating Peptides. *Bioconjug Chem.* March 2016. doi:10.1021/acs.bioconjchem.6b00082.
121. Morita S, Tagai C, Shiraishi T, Miyaji K, Iwamuro S. Differential mode of antimicrobial actions of arginine-rich and lysine-rich histones against Gram-positive *Staphylococcus aureus*. *Peptides.* 2013;48:75-82. doi:10.1016/j.peptides.2013.07.025.
122. Tagai C, Morita S, Shiraishi T, Miyaji K, Iwamuro S. Antimicrobial properties of arginine- and lysine-rich histones and involvement of bacterial outer membrane protease T in their differential mode of actions. *Peptides.* 2011;32(10):2003-2009. doi:10.1016/j.peptides.2011.09.005.
123. Torrent M, Pulido D, Valle J, Nogués MV, Andreu D, Boix E. Ribonucleases as a host-

- defence family: evidence of evolutionarily conserved antimicrobial activity at the N-terminus. *Biochem J.* 2013;456(1):99-108. doi:10.1042/BJ20130123.
124. Oren Z, Shai Y. Selective lysis of bacteria but not mammalian cells by diastereomers of melittin: structure-function study. *Biochemistry.* 1997;36(7):1826-1835. doi:10.1021/bi962507l.
125. Gonçalves S, Abade J, Teixeira A, Santos NC. Lipid composition is a determinant for human defensin HNP1 selectivity. *Biopolymers.* 2012;98(4):313-321. <http://www.ncbi.nlm.nih.gov/pubmed/23193595>. Accessed March 31, 2016.
126. Ilić N, Novković M, Guida F, et al. Selective antimicrobial activity and mode of action of adeptantins, glycine-rich peptide antibiotics based on anuran antimicrobial peptide sequences. *Biochim Biophys Acta.* 2013;1828(3):1004-1012. doi:10.1016/j.bbamem.2012.11.017.
127. Mavri J, Vogel HJ. Ion pair formation of phosphorylated amino acids and lysine and arginine side chains: a theoretical study. *Proteins.* 1996;24(4):495-501. doi:10.1002/(SICI)1097-0134(199604)24:4<495::AID-PROT8>3.0.CO;2-D.
128. Dathe M, Wieprecht T. Structural features of helical antimicrobial peptides: their potential to modulate activity on model membranes and biological cells. *Biochim Biophys Acta.* 1999;1462(1-2):71-87. <http://www.ncbi.nlm.nih.gov/pubmed/10590303>. Accessed March 31, 2016.
129. Huang HW. Molecular mechanism of antimicrobial peptides: the origin of cooperativity. *Biochim Biophys Acta.* 2006;1758(9):1292-1302. doi:10.1016/j.bbamem.2006.02.001.
130. Holthuis JCM, Menon AK. Lipid landscapes and pipelines in membrane homeostasis. *Nature.* 2014;510(7503):48-57. doi:10.1038/nature13474.
131. Bobone S, Gerelli Y, De Zotti M, et al. Membrane thickness and the mechanism of action of the short peptaibol trichogin GA IV. *Biochim Biophys Acta.* 2013;1828(3):1013-1024. doi:10.1016/j.bbamem.2012.11.033.
132. Kourie JI, Shorthouse AA. Properties of cytotoxic peptide-formed ion channels. *Am J Physiol Cell Physiol.* 2000;278(6):C1063-87. <http://www.ncbi.nlm.nih.gov/pubmed/10837335>. Accessed April 1, 2016.
133. Bessin Y, Saint N, Marri L, Marchini D, Molle G. Antibacterial activity and pore-forming properties of ceratotoxins: a mechanism of action based on the barrel stave model. *Biochim Biophys Acta.* 2004;1667(2):148-156. doi:10.1016/j.bbamem.2004.09.011.
134. Wang KF, Nagarajan R, Camesano TA. Antimicrobial peptide alamethicin insertion into lipid bilayer: a QCM-D exploration. *Colloids Surf B Biointerfaces.* 2014;116:472-481. doi:10.1016/j.colsurfb.2014.01.036.
135. Cantor RS. Size distribution of barrel-stave aggregates of membrane peptides: influence of the bilayer lateral pressure profile. *Biophys J.* 2002;82(5):2520-2525. doi:10.1016/S0006-3495(02)75595-1.

136. Sengupta D, Leontiadou H, Mark AE, Marrink S-J. Toroidal pores formed by antimicrobial peptides show significant disorder. *Biochim Biophys Acta*. 2008;1778(10):2308-2317. doi:10.1016/j.bbamem.2008.06.007.
137. Yang L, Harroun TA, Weiss TM, Ding L, Huang HW. Barrel-stave model or toroidal model? A case study on melittin pores. *Biophys J*. 2001;81(3):1475-1485. doi:10.1016/S0006-3495(01)75802-X.
138. Bolintineanu D, Hazrati E, Davis HT, Lehrer RI, Kaznessis YN. Antimicrobial mechanism of pore-forming protegrin peptides: 100 pores to kill E. coli. *Peptides*. 2010;31(1):1-8. doi:10.1016/j.peptides.2009.11.010.
139. Shai Y, Oren Z. From "carpet" mechanism to de-novo designed diastereomeric cell-selective antimicrobial peptides. *Peptides*. 2001;22(10):1629-1641. <http://www.ncbi.nlm.nih.gov/pubmed/11587791>. Accessed April 8, 2016.
140. Shai Y. Mechanism of the binding, insertion and destabilization of phospholipid bilayer membranes by alpha-helical antimicrobial and cell non-selective membrane-lytic peptides. *Biochim Biophys Acta*. 1999;1462(1-2):55-70. <http://www.ncbi.nlm.nih.gov/pubmed/10590302>. Accessed April 8, 2016.
141. Sharma S, Verma I, Khuller GK. Biochemical interaction of human neutrophil peptide-1 with Mycobacterium tuberculosis H37Ra. *Arch Microbiol*. 1999;171(5):338-342. <http://www.ncbi.nlm.nih.gov/pubmed/10382264>. Accessed February 5, 2016.
142. Senior AE, Nadanaciva S, Weber J. The molecular mechanism of ATP synthesis by F1F0-ATP synthase. *Biochim Biophys Acta*. 2002;1553(3):188-211. <http://www.ncbi.nlm.nih.gov/pubmed/11997128>. Accessed February 5, 2016.
143. Santos P, Gordillo A, Osses L, Salazar LM, Soto CY. Effect of antimicrobial peptides on ATPase activity and proton pumping in plasma membrane vesicles obtained from mycobacteria. *Peptides*. 2012;36(1):121-128. doi:10.1016/j.peptides.2012.04.018.
144. Park CB, Kim HS, Kim SC. Mechanism of action of the antimicrobial peptide buforin II: buforin II kills microorganisms by penetrating the cell membrane and inhibiting cellular functions. *Biochem Biophys Res Commun*. 1998;244(1):253-257. doi:10.1006/bbrc.1998.8159.
145. Ghosh A, Kar RK, Jana J, et al. Indolicidin targets duplex DNA: structural and mechanistic insight through a combination of spectroscopy and microscopy. *ChemMedChem*. 2014;9(9):2052-2058. doi:10.1002/cmdc.201402215.
146. Sharma A, Pohane AA, runrao, Bansal S, Bajaj A, Jain V, Srivastava A. Cell penetrating synthetic antimicrobial peptides (SAMPs) exhibiting potent and selective killing of mycobacterium by targeting its DNA. *Chemistry*. 2015;21(9):3540-3545. doi:10.1002/chem.201404650.
147. Hansen AM, Bonke G, Larsen CJ, Yavari N, Nielsen PE, Franzyk H. Antibacterial peptide nucleic acid - antimicrobial peptide (PNA-AMP) conjugates: Antisense targeting of fatty acid biosynthesis. *Bioconjug Chem*. 2016. doi:10.1021/acs.bioconjchem.6b00013.

148. Rietschel ET, Brade H, Holst O, et al. Bacterial endotoxin: Chemical constitution, biological recognition, host response, and immunological detoxification. *Curr Top Microbiol Immunol*. 1996;216:39-81. <http://www.ncbi.nlm.nih.gov/pubmed/8791735>. Accessed April 12, 2016.
149. Martin L, van Meegern A, Doemming S, Schuerholz T. Antimicrobial Peptides in Human Sepsis. *Front Immunol*. 2015;6:404. doi:10.3389/fimmu.2015.00404.
150. Scott MG, Vreugdenhil AC, Buurman WA, Hancock RE, Gold MR. Cutting edge: cationic antimicrobial peptides block the binding of lipopolysaccharide (LPS) to LPS binding protein. *J Immunol*. 2000;164(2):549-553. <http://www.ncbi.nlm.nih.gov/pubmed/10623792>. Accessed April 12, 2016.
151. Scott MG, Davidson DJ, Gold MR, Bowdish D, Hancock REW. The human antimicrobial peptide LL-37 is a multifunctional modulator of innate immune responses. *J Immunol*. 2002;169(7):3883-3891. <http://www.ncbi.nlm.nih.gov/pubmed/12244186>. Accessed April 12, 2016.
152. Brandenburg K, Heinbockel L, Correa W, Lohner K. Peptides with dual mode of action: Killing bacteria and preventing endotoxin-induced sepsis. *Biochim Biophys Acta - Biomembr*. 2016;1-9. doi:10.1016/j.bbamem.2016.01.011.
153. Territo MC, Ganz T, Selsted ME, Lehrer R. Monocyte-chemotactic activity of defensins from human neutrophils. *J Clin Invest*. 1989;84(6):2017-2020. doi:10.1172/JCI114394.
154. Scott MG, Dullaghan E, Mookherjee N, et al. An anti-infective peptide that selectively modulates the innate immune response. *Nat Biotechnol*. 2007;25(4):465-472. doi:10.1038/nbt1288.
155. Yang D, Chen Q, Chertov O, Oppenheim JJ. Human neutrophil defensins selectively chemoattract naive T and immature dendritic cells. *J Leukoc Biol*. 2000;68(1):9-14. <http://www.ncbi.nlm.nih.gov/pubmed/10914484>. Accessed April 12, 2016.
156. Yang D, Chertov O, Oppenheim JJ. Participation of mammalian defensins and cathelicidins in anti-microbial immunity: receptors and activities of human defensins and cathelicidin (LL-37). *J Leukoc Biol*. 2001;69(5):691-697. <http://www.ncbi.nlm.nih.gov/pubmed/11358975>. Accessed April 12, 2016.
157. Zuyderduyn S, Ninaber DK, Hiemstra PS, Rabe KF. The antimicrobial peptide LL-37 enhances IL-8 release by human airway smooth muscle cells. *J Allergy Clin Immunol*. 2006;117(6):1328-1335. doi:10.1016/j.jaci.2006.03.022.
158. Tjabringa GS, Aarbiou J, Ninaber DK, et al. The antimicrobial peptide LL-37 activates innate immunity at the airway epithelial surface by transactivation of the epidermal growth factor receptor. *J Immunol*. 2003;171(12):6690-6696. <http://www.ncbi.nlm.nih.gov/pubmed/14662872>. Accessed April 12, 2016.
159. Carretero M, Escámez MJ, García M, et al. In vitro and in vivo wound healing-promoting activities of human cathelicidin LL-37. *J Invest Dermatol*. 2008;128(1):223-236. doi:10.1038/sj.jid.5701043.

160. Tarnawski A, Szabo IL, Husain SS, Soreghan B. Regeneration of gastric mucosa during ulcer healing is triggered by growth factors and signal transduction pathways. *J Physiol Paris*. 95(1-6):337-344. <http://www.ncbi.nlm.nih.gov/pubmed/11595458>. Accessed April 12, 2016.
161. Tokumaru S, Sayama K, Shirakata Y, et al. Induction of keratinocyte migration via transactivation of the epidermal growth factor receptor by the antimicrobial peptide LL-37. *J Immunol*. 2005;175(7):4662-4668. <http://www.ncbi.nlm.nih.gov/pubmed/16177113>. Accessed April 12, 2016.
162. Aarbiou J, Verhoosel RM, Van Wetering S, et al. Neutrophil defensins enhance lung epithelial wound closure and mucin gene expression in vitro. *Am J Respir Cell Mol Biol*. 2004;30(2):193-201. doi:10.1165/rcmb.2002-0267OC.
163. Lillard JW, Boyaka PN, Chertov O, Oppenheim JJ, McGhee JR. Mechanisms for induction of acquired host immunity by neutrophil peptide defensins. *Proc Natl Acad Sci U S A*. 1999;96(2):651-656. <http://www.ncbi.nlm.nih.gov/pubmed/9892688>. Accessed April 12, 2016.
164. Tani K, Murphy WJ, Chertov O, et al. Defensins act as potent adjuvants that promote cellular and humoral immune responses in mice to a lymphoma idiotype and carrier antigens. *Int Immunol*. 2000;12(5):691-700. <http://www.ncbi.nlm.nih.gov/pubmed/10784615>. Accessed April 12, 2016.
165. Funderburg N, Lederman MM, Feng Z, et al. Human α -defensin-3 activates professional antigen-presenting cells via Toll-like receptors 1 and 2. *Proc Natl Acad Sci U S A*. 2007;104(47):18631-18635. doi:10.1073/pnas.0702130104.
166. Biragyn A, Surenhu M, Yang D, et al. Mediators of innate immunity that target immature, but not mature, dendritic cells induce antitumor immunity when genetically fused with nonimmunogenic tumor antigens. *J Immunol*. 2001;167(11):6644-6653. <http://www.ncbi.nlm.nih.gov/pubmed/11714836>. Accessed April 12, 2016.
167. van Wetering S, Sterk PJ, Rabe KF, Hiemstra PS. Defensins: key players or bystanders in infection, injury, and repair in the lung? *J Allergy Clin Immunol*. 1999;104(6):1131-1138. <http://www.ncbi.nlm.nih.gov/pubmed/10588992>. Accessed April 12, 2016.
168. Davidson DJ, Currie AJ, Reid GSD, et al. The cationic antimicrobial peptide LL-37 modulates dendritic cell differentiation and dendritic cell-induced T cell polarization. *J Immunol*. 2004;172(2):1146-1156. <http://www.ncbi.nlm.nih.gov/pubmed/14707090>. Accessed April 12, 2016.
169. Shin D-M, Jo E-K. Antimicrobial Peptides in Innate Immunity against Mycobacteria. *Immune Netw*. 2011;11(5):245-252. doi:10.4110/in.2011.11.5.245.
170. FINDLAY D, HERRIES DG, MATHIAS AP, RABIN BR, ROSS CA. The active site and mechanism of action of bovine pancreatic ribonuclease. *Nature*. 1961;190:781-784. <http://www.ncbi.nlm.nih.gov/pubmed/13699542>. Accessed April 14, 2016.
171. Cuchillo CM, Nogués MV, Raines RT. Bovine pancreatic ribonuclease: fifty years of the

- first enzymatic reaction mechanism. *Biochemistry*. 2011;50(37):7835-7841. doi:10.1021/bi201075b.
172. Sorrentino S. The eight human “canonical” ribonucleases: molecular diversity, catalytic properties, and special biological actions of the enzyme proteins. *FEBS Lett*. 2010;584(11):2194-2200. doi:10.1016/j.febslet.2010.04.018.
173. Cho S, Zhang J. Zebrafish ribonucleases are bactericidal: implications for the origin of the vertebrate RNase A superfamily. *Mol Biol Evol*. 2007;24(5):1259-1268. doi:10.1093/molbev/msm047.
174. Pizzo E, D’Alessio G. The success of the RNase scaffold in the advance of biosciences and in evolution. *Gene*. 2007;406(1-2):8-12. doi:10.1016/j.gene.2007.05.006.
175. Rosenberg HF. RNase A ribonucleases and host defense: an evolving story. *J Leukoc Biol*. 2008;83(5):1079-1087. doi:10.1189/jlb.1107725.
176. Boix E, Salazar VA, Torrent M, Pulido D, Nogués MV, Moussaoui M. Structural determinants of the eosinophil cationic protein antimicrobial activity. *Biol Chem*. 2012;393(8):801-815. doi:10.1515/hsz-2012-0160.
177. Hogan SP, Rosenberg HF, Moqbel R, et al. Eosinophils: biological properties and role in health and disease. *Clin Exp Allergy*. 2008;38(5):709-750. doi:10.1111/j.1365-2222.2008.02958.x.
178. Rosenberg HF, Dyer KD, Foster PS. Eosinophils: changing perspectives in health and disease. *Nat Rev Immunol*. 2013;13(1):9-22. doi:10.1038/nri3341.
179. Lee JJ, Dimina D, Macias MP, et al. Defining a link with asthma in mice congenitally deficient in eosinophils. *Science*. 2004;305(5691):1773-1776. doi:10.1126/science.1099472.
180. Acharya KR, Ackerman SJ. Eosinophil granule proteins: form and function. *J Biol Chem*. 2014;289(25):17406-17415. doi:10.1074/jbc.R113.546218.
181. Rosenberg HF, Ackerman SJ, Tenen DG. Human eosinophil cationic protein. Molecular cloning of a cytotoxin and helminthotoxin with ribonuclease activity. *J Exp Med*. 1989;170(1):163-176. <http://www.ncbi.nlm.nih.gov/pubmed/2473157>. Accessed April 29, 2016.
182. Boix E, Leonidas DD, Nikolovski Z, Nogués M V, Cuchillo CM, Acharya KR. Crystal structure of eosinophil cationic protein at 2.4 Å resolution. *Biochemistry*. 1999;38(51):16794-16801. <http://www.ncbi.nlm.nih.gov/pubmed/10606511>. Accessed April 29, 2016.
183. Lehrer RI, Szklarek D, Barton A, Ganz T, Hamann KJ, Gleich GJ. Antibacterial properties of eosinophil major basic protein and eosinophil cationic protein. *J Immunol*. 1989;142(12):4428-4434. <http://www.ncbi.nlm.nih.gov/pubmed/2656865>. Accessed April 29, 2016.
184. Malik A, Batra JK. Antimicrobial activity of human eosinophil granule proteins:

- involvement in host defence against pathogens. *Crit Rev Microbiol*. 2012;38(2):168-181. doi:10.3109/1040841X.2011.645519.
185. Maeda T, Kitazoe M, Tada H, et al. Growth inhibition of mammalian cells by eosinophil cationic protein. *Eur J Biochem*. 2002;269(1):307-316. <http://www.ncbi.nlm.nih.gov/pubmed/11784325>. Accessed April 29, 2016.
186. Rosenberg HF. Recombinant human eosinophil cationic protein. Ribonuclease activity is not essential for cytotoxicity. *J Biol Chem*. 1995;270(14):7876-7881. <http://www.ncbi.nlm.nih.gov/pubmed/7713881>. Accessed April 29, 2016.
187. Venge P, Byström J. Eosinophil cationic protein (ECP). *Int J Biochem Cell Biol*. 1998;30(4):433-437. <http://www.ncbi.nlm.nih.gov/pubmed/9675876>. Accessed April 29, 2016.
188. Carreras E, Boix E, Rosenberg HF, Cuchillo CM, Nogués MV. Both aromatic and cationic residues contribute to the membrane-lytic and bactericidal activity of eosinophil cationic protein. *Biochemistry*. 2003;42(22):6636-6644. doi:10.1021/bi0273011.
189. Torrent M, Pulido D, Nogués MV, Boix E. Exploring New Biological Functions of Amyloids: Bacteria Cell Agglutination Mediated by Host Protein Aggregation. *PLoS Pathog*. 2012;8(11). doi:10.1371/journal.ppat.1003005.
190. Rosenberg HF, Dyer KD. Molecular cloning and characterization of a novel human ribonuclease (RNase k6): increasing diversity in the enlarging ribonuclease gene family. *Nucleic Acids Res*. 1996;24(18):3507-3513. <http://www.ncbi.nlm.nih.gov/pubmed/8836175>. Accessed April 15, 2016.
191. Deming MS, Dyer KD, Bankier AT, Piper MB, Dear PH, Rosenberg HF. Ribonuclease k6: chromosomal mapping and divergent rates of evolution within the RNase A gene superfamily. *Genome Res*. 1998;8(6):599-607. <http://www.ncbi.nlm.nih.gov/pubmed/9647635>. Accessed September 1, 2015.
192. Dyer KD, Rosenberg HF, Zhang J. Isolation, characterization, and evolutionary divergence of mouse RNase 6: evidence for unusual evolution in rodents. *J Mol Evol*. 2004;59(5):657-665. doi:10.1007/s00239-004-2657-0.
193. Becknell B, Eichler TE, Beceiro S, et al. Ribonucleases 6 and 7 have antimicrobial function in the human and murine urinary tract. *Kidney Int*. 2015;87(1):151-161. doi:10.1038/ki.2014.268.
194. Prats-Ejarque G, Arranz-Trullen J, Blanco JA, et al. The first crystal structure of human RNase6 reveals a novel substrate binding and cleavage site arrangement. *Biochem J*. 2016;(2016). doi:10.1042/BCJ20160245.
195. Pulido D, Arranz-Trullén J, Prats-Ejarque G, et al. Insights into the Antimicrobial Mechanism of Action of Human RNase6: Structural Determinants for Bacterial Cell Agglutination and Membrane Permeation. *Int J Mol Sci*. 2016;17(4):552. doi:10.3390/ijms17040552.

196. Harder J, Schroder J-M. RNase 7, a novel innate immune defense antimicrobial protein of healthy human skin. *J Biol Chem*. 2002;277(48):46779-46784. doi:10.1074/jbc.M207587200.
197. Köten B, Simanski M, Gläser R, Podschun R, Schröder J-M, Harder J. RNase 7 contributes to the cutaneous defense against *Enterococcus faecium*. *PLoS One*. 2009;4(7):e6424. doi:10.1371/journal.pone.0006424.
198. Fritz P, Beck-Jendroschek V, Brasch J. Inhibition of dermatophytes by the antimicrobial peptides human β -defensin-2, ribonuclease 7 and psoriasin. *Med Mycol*. 2012;50(6):579-584. doi:10.3109/13693786.2012.660203.
199. Zhang J, Dyer KD, Rosenberg HF. Human RNase 7: a new cationic ribonuclease of the RNase A superfamily. *Nucleic Acids Res*. 2003;31(2):602-607. <http://www.ncbi.nlm.nih.gov/pubmed/12527768>. Accessed May 2, 2016.
200. Zhang J, Dyer KD, Rosenberg HF. Human RNase 7: a new cationic ribonuclease of the RNase A superfamily. *Nucleic Acids Res*. 2003;31(2):602-607. <http://www.ncbi.nlm.nih.gov/pubmed/12527768>. Accessed April 25, 2016.
201. Huang Y-C, Lin Y-M, Chang T-W, et al. The flexible and clustered lysine residues of human ribonuclease 7 are critical for membrane permeability and antimicrobial activity. *J Biol Chem*. 2007;282(7):4626-4633. doi:10.1074/jbc.M607321200.
202. Wang H, Schwaderer AL, Kline J, Spencer JD, Kline D, Hains DS. Contribution of structural domains to the activity of ribonuclease 7 against uropathogenic bacteria. *Antimicrob Agents Chemother*. 2013;57(2):766-774. doi:10.1128/AAC.01378-12.
203. Boix E, Torrent M, Sánchez D, Nogués MV. The antipathogen activities of eosinophil cationic protein. *Curr Pharm Biotechnol*. 2008;9(3):141-152. <http://www.ncbi.nlm.nih.gov/pubmed/18673279>. Accessed September 2, 2015.
204. Torrent M, Sánchez D, Buzón V, Nogués MV, Cladera J, Boix E. Comparison of the membrane interaction mechanism of two antimicrobial RNases: RNase 3/ECP and RNase 7. *Biochim Biophys Acta - Biomembr*. 2009;1788(5):1116-1125. doi:10.1016/j.bbamem.2009.01.013.
205. Torrent M, Badia M, Moussaoui M, Sanchez D, Nogués MV, Boix E. Comparison of human RNase 3 and RNase 7 bactericidal action at the Gram-negative and Gram-positive bacterial cell wall. *FEBS J*. 2010;277(7):1713-1725. doi:10.1111/j.1742-4658.2010.07595.x.
206. Boix E, Pulido D, Moussaoui M, Nogués MV, Russi S. The sulfate-binding site structure of the human eosinophil cationic protein as revealed by a new crystal form. *J Struct Biol*. 2012;179(1):1-9. doi:10.1016/j.jsb.2012.04.023.
207. Ashkenazy H, Erez E, Martz E, Pupko T, Ben-Tal N. ConSurf 2010: calculating evolutionary conservation in sequence and structure of proteins and nucleic acids. *Nucleic Acids Res*. 2010;38(Web Server issue):W529-33. doi:10.1093/nar/gkq399.
208. Gudmundsson GH, Agerberth B. Neutrophil antibacterial peptides, multifunctional

- effector molecules in the mammalian immune system. *J Immunol Methods*. 1999;232(1-2):45-54. <http://www.ncbi.nlm.nih.gov/pubmed/10618508>. Accessed May 4, 2016.
209. Boix E, Salazar VA, Torrent M, Pulido D, Nogués MV, Moussaoui M. Structural determinants of the eosinophil cationic protein antimicrobial activity. *Biol Chem*. 2012;393(8):801-815. doi:10.1515/hsz-2012-0160.
210. Giancola C, Ercole C, Fotticchia I, et al. Structure-cytotoxicity relationships in bovine seminal ribonuclease: new insights from heat and chemical denaturation studies on variants. *FEBS J*. 2011;278(1):111-122. doi:10.1111/j.1742-4658.2010.07937.x.
211. Sánchez D, Moussaoui M, Carreras E, Torrent M, Nogués V, Boix E. Mapping the eosinophil cationic protein antimicrobial activity by chemical and enzymatic cleavage. *Biochimie*. 2011;93(2):331-338. doi:10.1016/j.biochi.2010.10.005.
212. Schroeder BO, Wu Z, Nuding S, et al. Reduction of disulphide bonds unmasks potent antimicrobial activity of human β -defensin 1. *Nature*. 2011;469(7330):419-423. doi:10.1038/nature09674.
213. Burton MF, Steel PG. The chemistry and biology of LL-37. *Nat Prod Rep*. 2009;26(12):1572-1584. doi:10.1039/b912533g.
214. Nibbering PH, Ravensbergen E, Welling MM, et al. Human lactoferrin and peptides derived from its N terminus are highly effective against infections with antibiotic-resistant bacteria. *Infect Immun*. 2001;69(3):1469-1476. doi:10.1128/IAI.69.3.1469-1476.2001.
215. Zanfardino A, Pizzo E, Di Maro A, Varcamonti M, D'Alessio G. The bactericidal action on *Escherichia coli* of ZF-RNase-3 is triggered by the suicidal action of the bacterium OmpT protease. *FEBS J*. 2010;277(8):1921-1928. doi:10.1111/j.1742-4658.2010.07614.x.
216. Torrent M, de la Torre BG, Nogués VM, Andreu D, Boix E. Bactericidal and membrane disruption activities of the eosinophil cationic protein are largely retained in an N-terminal fragment. *Biochem J*. 2009;421(3):425-434. doi:10.1042/BJ20082330.
217. Torrent M, Odorizzi F, Nogués MV, Boix E. Eosinophil cationic protein aggregation: identification of an N-terminus amyloid prone region. *Biomacromolecules*. 2010;11(8):1983-1990. doi:10.1021/bm100334u.
218. Goo SM, Cho S. The expansion and functional diversification of the mammalian ribonuclease a superfamily epitomizes the efficiency of multigene families at generating biological novelty. *Genome Biol Evol*. 2013;5(11):2124-2140. doi:10.1093/gbe/evt161.
219. Rosenberg HF, Dyer KD. Molecular cloning and characterization of a novel human ribonuclease (RNase k6): increasing diversity in the enlarging ribonuclease gene family. *Nucleic Acids Res*. 1996;24(18):3507-3513. <http://www.pubmedcentral.nih.gov/articlerender.fcgi?artid=146131&tool=pmcentre&rendertype=abstract>. Accessed September 1, 2015.

-
220. Pulido D, Torrent M, Andreu D, Nogués MV, Boix E. Two human host defense ribonucleases against mycobacteria, the eosinophil cationic protein (RNase 3) and RNase 7. *Antimicrob Agents Chemother*. 2013;57(8):3797-3805. doi:10.1128/AAC.00428-13.
221. Torrent M, Navarro S, Moussaoui M, Nogués MV, Boix E. Eosinophil cationic protein high-affinity binding to bacteria-wall lipopolysaccharides and peptidoglycans. *Biochemistry*. 2008;47(11):3544-3555. doi:10.1021/bi702065b.
222. Brown GD, Denning DW, Gow NAR, Levitz SM, Netea MG, White TC. Hidden killers: human fungal infections. *Sci Transl Med*. 2012;4(165):165rv13. doi:10.1126/scitranslmed.3004404.
223. Harder J, Schroder J-M. RNase 7, a novel innate immune defense antimicrobial protein of healthy human skin. *J Biol Chem*. 2002;277(48):46779-46784. doi:10.1074/jbc.M207587200.
224. Spencer JD, Schwaderer AL, Dirosario JD, et al. Ribonuclease 7 is a potent antimicrobial peptide within the human urinary tract. *Kidney Int*. 2011;80(2):174-180. doi:10.1038/ki.2011.109.
225. Simanski M, Köten B, Schröder J-M, Gläser R, Harder J. Antimicrobial RNases in cutaneous defense. *J Innate Immun*. 2012;4(3):241-247. doi:10.1159/000335029.
226. Gupta SK, Haigh BJ, Griffin FJ, Wheeler TT. The mammalian secreted RNases: mechanisms of action in host defence. *Innate Immun*. 2013;19(1):86-97. doi:10.1177/1753425912446955.
227. Haney EF, Hancock REW. Peptide design for antimicrobial and immunomodulatory applications. *Biopolymers*. 2013;100(6):572-583. doi:10.1002/bip.22250.
228. Rosenberg HF. RNase A ribonucleases and host defense: an evolving story. *J Leukoc Biol*. 2008;83(5):1079-1087. doi:10.1189/jlb.1107725.
229. Salazar VA, Arranz-Trullén J, Navarro S, et al. Exploring the mechanisms of action of human secretory RNase 3 and RNase 7 against *Candida albicans*. *Microbiologyopen*. June 2016. doi:10.1002/mbo3.373.
230. Driss V, Legrand F, Hermann E, et al. TLR2-dependent eosinophil interactions with mycobacteria: role of alpha-defensins. *Blood*. 2009;113(14):3235-3244. doi:10.1182/blood-2008-07-166595.

7. ANNEXES

Supplementary Materials: Insights into the Antimicrobial Mechanism of Action of Human RNase6: Structural Determinants for Bacterial Cell Agglutination and Membrane Permeation

David Pulido, Javier Arranz-Trullén, Guillem Prats-Ejarque, Diego Velázquez, Marc Torrent, Mohammed Moussaoui and Ester Boix

Table S1. Comparison of the proteins and peptide antimicrobial activities determined by the *BacTiter-Glo* bacterial viability assay.

Protein/Peptide	ED ₅₀ (μM) ^a	
	<i>E. coli</i>	<i>S. aureus</i>
RNase3	0.4 ± 0.1	0.9 ± 0.2
RNase6	1.1 ± 0.2	1.8 ± 0.5
RN6(1–45)	2.1 ± 0.5	2.2 ± 0.1

^a Fifty percent effective dose concentrations (ED₅₀) were calculated by fitting the data to a dose-response curve. Values are given as mean ± SEM.

Table S2. Minimal inhibitory concentration (MIC) of RNase3, RNase6 and RN6(1–45).

Protein/Peptide	MIC ₁₀₀ (μM) ^a					
	<i>E. coli</i>	<i>P. aeruginosa</i>	<i>A. baumannii</i>	<i>S. aureus</i>	<i>M. luteus</i>	<i>E. faecium</i>
RNase3	0.31	0.15	0.31	0.31	0.62	1.25
RNase6	0.62	0.62	0.62	1.25	1.25	1.25
RN6(1–45)	1.25	0.62	0.93	2.5	1.25	1.25

^a The 100% Minimal inhibitory concentration (MIC₁₀₀) was calculated as described in Materials and Methods. All values are averaged from two replicates of two independent experiments.

Table S3. Comparison of RNase6 and RNase6-H15A mutant antimicrobial activity.

Protein/Peptide	MBC ₁₀₀ (μM) ^a	
	<i>E. coli</i>	<i>S. aureus</i>
RNase6	0.92 ± 0.05	1.87 ± 0.56
RNase6-H15A	0.92 ± 0.14	1.87 ± 0.20

^a The 100% Minimal bactericidal concentration (MBC₁₀₀) was calculated as described in Materials and Methods. MBC₁₀₀ values were calculated by CFU counting on plated Petri dishes. All values are averaged from three replicates of two independent experiments. Values are given as mean ± SEM.

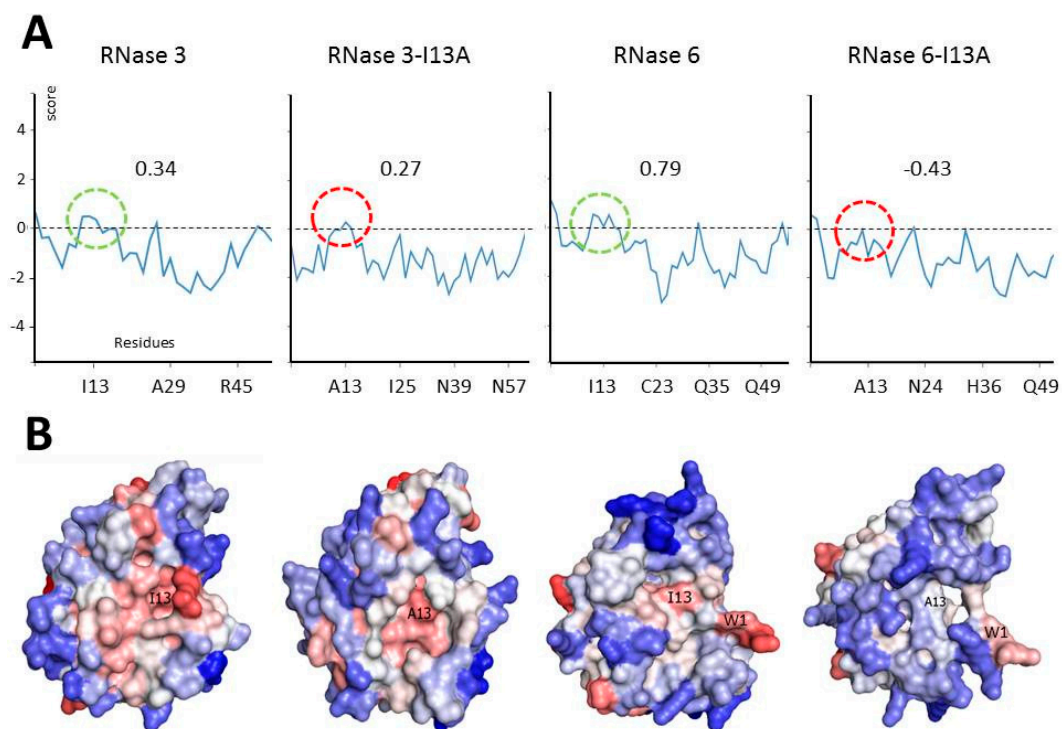


Figure S1. Aggregation propensity prediction of RNase3 (A); RNase6 (B) and their I13A respective mutants. The 3D structure of RNase3 and RNase6 were built using the protein data bank (PDB) ID:4A2O [35] and PDB ID:4X09 [34] respectively. (A) The aggregation profile of the polypeptide chain is represented as a line plot using the calculated A3D score values. Residues with positive scores in the analyzed structure, therefore predicted as aggregation-prone, are indicated at the top profiles. A3D score values for residue 13 are depicted in each profile, green circles show the aggregation propensity for wild type proteins and red circles highlight the decrease of the aggregation propensity in mutants; (B) Protein structure is coloured according to the A3D score of the residues. Areas with high-predicted aggregation propensity are labelled using a red gradient and areas with high-predicted solubility are labelled with a blue gradient. White areas are not predicted to influence aggregation (A3D score \approx 0).

Title: The first crystal structure of human RNase 6 reveals a novel substrate binding and cleavage site arrangement. Authors: Prats-Ejarque¹ G, Arranz-Trullén¹ J; Blanco¹ JA; Pulido^{1,2} D; Nogués¹ MV; Moussaoui¹ M; and Boix¹ E[¶].

¹ Department of Biochemistry and Molecular Biology, Faculty of Biosciences, Universitat Autònoma de Barcelona, E-08193 Cerdanyola del Vallès, Spain

² Present address: Imperial College London, South Kensington Campus London, London SW7 2AZ, United Kingdom

[¶]Author to whom correspondence should be addressed; E-Mail ester.boix@uab.cat; Tel.: +34-93-581-2565; Fax: +34-93-581-1264

Supplementary Material content:

Table S1: RNase 6 secondary structure elements.

Table S2: Intermolecular packing interactions between symmetry related molecules in the RNase 6 crystal.

Table S3: Atomic interactions between sulphate anions, glycerol and RNase 6 residues.

Table S4. Relative catalytic activity efficiency of RNase 6 in relation to RNase A.

Table S5: Proposed RNase 6 residues involved in base and phosphate substrate subsite.

Table S6. Estimated pK_a values for selected His residues in RNase 6 and RNase A structures.

Figure S1. Electron density map for S1-S4 sulfate anions.

Figure S2. Comparison of RNases activities by a zymogram assay using a poly(C) containing SDS-PAGE gel.

Figure S3. Structural superposition of RNase 6 and other representative RNase A family members.

Figure S4. Comparison of poly(C) cleavage patterns by RNase 6-H15A and RNase 7-H15A.

Structure validation report for RNase 6 crystal structure (PDB ID: 4X09).

Table S1: RNase 6 secondary structure elements.

<i>loop residues</i>		<i>helix residues</i>		<i>strand residues</i>	
L1	W1 – T6	α 1	K7 – H15	β 1	Q40 – L44
L2	I16 – Q22	α 2	C23 – T34	β 2	S59 – I60
L3	Q35 – H39	α 3	F48 – D56	β 3	C69 – Q71
L4	H45 – S47			β 4	V76 – S85
L5	L57 – L58			β 5	R92 – K100
L6	V61 – N68			β 6	F102 – D107
L7	S72 – P75			β 7	V119 – I126
L8	G86 – C91				
L9	P108– L118				

Table S2: Intermolecular packing interactions between symmetry related molecules in the RNase 6 crystal. Only hydrogen bond interactions are included, taking a cut-off of 3.4 Å as a reference, as calculated by the *PDBePISA* server [1].

<i>symmetry operation</i>	<i>crystal molecule interacting atom</i>	<i>symmetry related molecule interacting atom</i>	<i>distance (Å)</i>
x-1, y, z	Arg82 Nη1	Ser112 O	3.24
	Arg82 Nη2	Asp113 Oδ1	3.22
	Ile126 N	Pro115 O	3.06
	Lys63 Nζ	Tyr116 O	2.84
	Lys63 Nζ	Pro115 O	3.13
	Gln98 Oε1	Tyr116 Oη	2.43
	Gly86 N	Met0 O	2.97
x, y-1, z	Gln71 Oε1	Gln35 Oε1	3.40
	Gln71 Nε2	Tyr88 Oη	2.99
x-1/2, -y-1/2, -z	Tyr99 N	Ser19 Oγ	2.92
	Ser19 Oγ	Gln49 Nε2	2.67
-x, y-1/2, -z-1/2	Arg65 Nη2	Leu5 O	2.53

Table S3: Atomic interactions between sulphate anions, glycerol and RNase 6 residues. Potential hydrogen bond distances have been considered using a cut-off distance of 3.4 Å.

<i>ligand interaction site and atom</i>		<i>interacting protein atom</i>	<i>distance (Å)</i>
S1	O1	HOH60	2.59
		HOH99	3.12
		HOH124	3.34
	O2	His122 Nδ1	2.66
		HOH42	3.02
		HOH81	2.70
	O3	Gln14 Nε2	3.22
		His15 Nε2	3.35
		<i>HOH109</i>	2.54
	O4	Leu123 N	2.79
		His15 Nε2	2.92
		HOH42	3.12
S2	O1	His67 N	3.21
		HOH70	3.11
		HOH98	2.67
		HOH118	3.32
	O2	HOH48	2.22
		HOH98	2.75
	O3	His67 N	3.20
		Arg66 Nε	2.64
		HOH98	2.62
S3	O1	<i>Arg92 Nε</i>	3.25
		<i>Arg92 Nη2</i>	3.05
		HOH82	3.02
	O2	<i>Arg92 Nε</i>	3.03
		HOH35	3.11
		<i>HOH56</i>	3.39
		<i>HOH72</i>	2.70
	O3	<i>HOH56</i>	3.26
		O4	Arg25 Nη1
			HOH52
S4	O1	His36 Nδ2	2.54
		B/HOH92	3.26
		<i>HOH54</i>	2.84
		<i>Arg66 Nη2</i>	3.39
	O2	HOH107	2.70
		O3	His39 Nε2
	B/HOH92		2.20
	O4	A/HOH92	3.15
		B/HOH92	3.21
	GOL	O1	Ser 59 N
<i>HOH108</i>			2.16
O2		A/Ser59 Oy	2.83
		HOH101	3.05
O3		HOH36	3.29
		<i>Gln110 Oε1</i>	3.16

Table S4. Relative catalytic activity efficiency of RNase 6 in relation to RNase A.

	UpA	UpG	CpA	C>p	Poly(C)	Poly(U)	Poly(U):Poly(A)
RNase A	100	100	100	100	100	100	100
RNase 6	0.13	ND	0.02	0.07	0.41	3.25	26
RNase 3	0.01	ND	0.007	0.05	0.48	2.29	ND

Data are expressed in relative percentage values(%).

ND: Not detected at the assayed concentrations.

Table S5: Proposed RNase 6 residues involved in base and phosphate substrate subsite. Binding sites are labelled as defined for RNase A, where B₁ and p₁ are located at the main active site. Residues at hydrogen bond or van der Waals distances identified in the protein -heptanucleotide complex predicted by molecular dynamics are included.

Protein subsite	Protein residue
p ₋₃ /p ₋₂	His36, His39, Lys87
B ₋₂	His36
p ₋₁	Arg82
p ₀	Lys63
B ₁	Thr42, Gln40
p ₁	His15, Gln14, Lys38, His122
B ₂	Asn64, Asn68, Arg66, His122
p ₂	Lys7, Trp10

Table S6. Estimated pK_a values for selected His residues in RNase 6 and RNase A structures. Values were calculated using *ROSIE* (<http://rosie.rosettacommons.org/> [2]).

	Residue	pK_a^a
RNase 6 ^b	His15	5.3
	His122	6.6
	His36	6.5
	His39	6.3
	His67 ^e	6.1
RNase A ^c	His12	5.8
	His119	6.8
	His105 ^e	6.4
RNase A-K7H/R10H ^d	H7	6.8
	H10	6.7
	H12	5.8
	H119	6.4
	H105 ^e	6.5

^a Starting reference pK_a values for His side chain pK_a was 6.3.

^b Values calculated using RNase 6 crystal structure (PDB ID: 4X09).

^c Values calculated using RNase A crystal structure (PDB ID: 7RSA).

^d Values for RNase A-K7H/R10H crystal structure are taken from PDB ID:5ET4 (Blanco et al., unpublished results). Values are the average from the 4 protein chains at the asymmetric unit.

^e His67(RNase 6) and His105 (RNase A) were taken as reference controls as solvent exposed His residue not involved in Coulombic interactions with neighbouring residues.

Figure legends

Figure S1: A-D) Electron density map for S1 to S4 sulfate anions and their respective protein environment residues. Water molecules are depicted with red crosses. Sigma 2Fo-Fc and FoFc electron density maps contoured at 1.5 and 3 sigma levels are shown (colored in dark and light blue respectively). Fo-Fc electron density map was built in the absence of ligands. Sulfate nomenclature corresponds to Table S3 numbering.

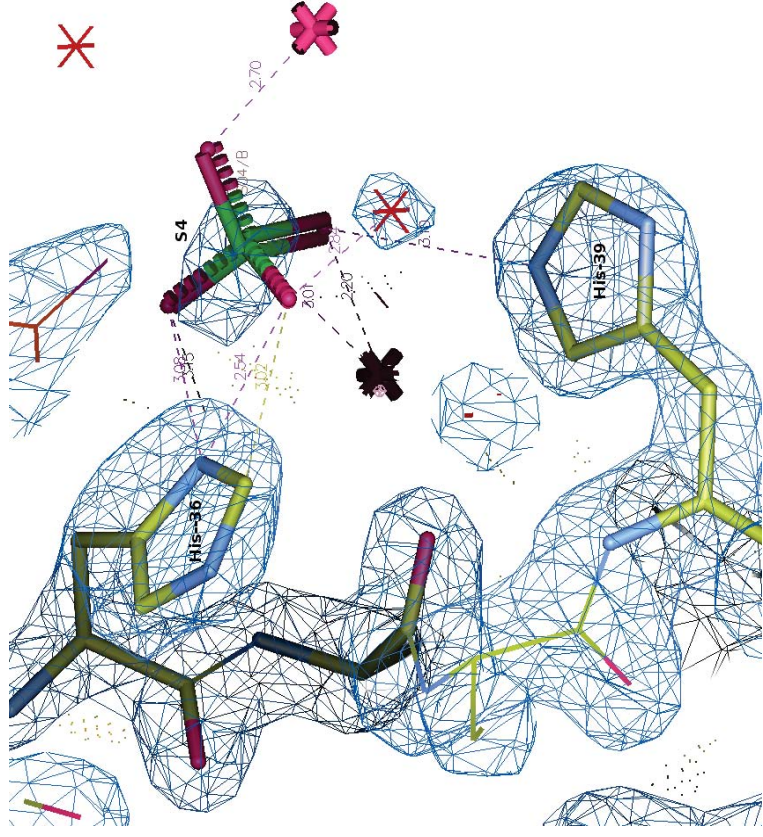
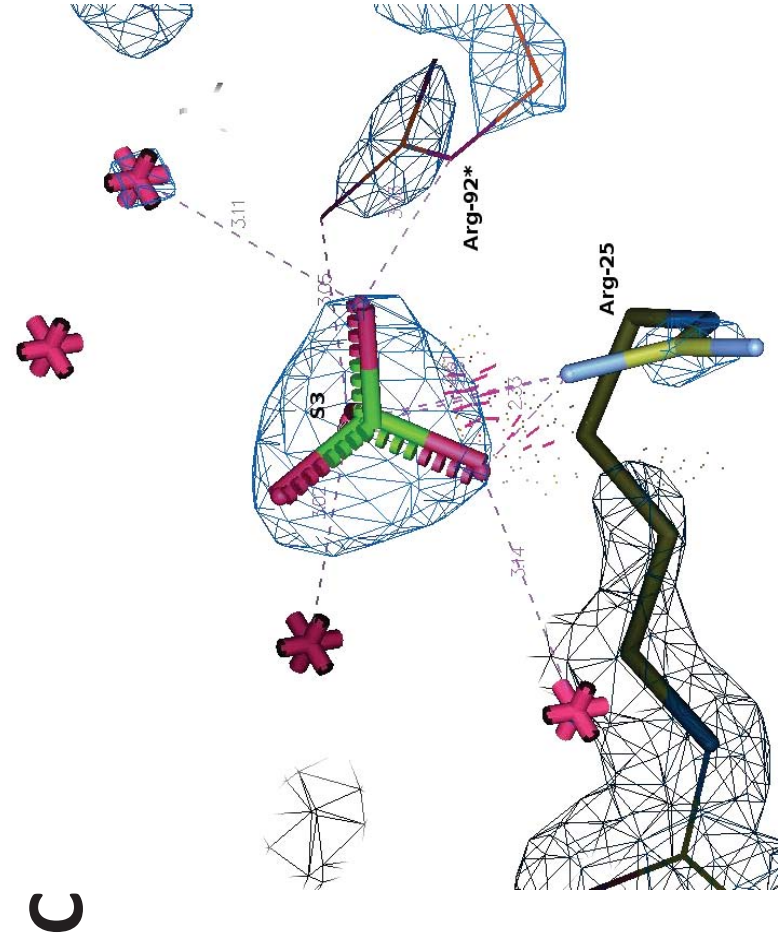
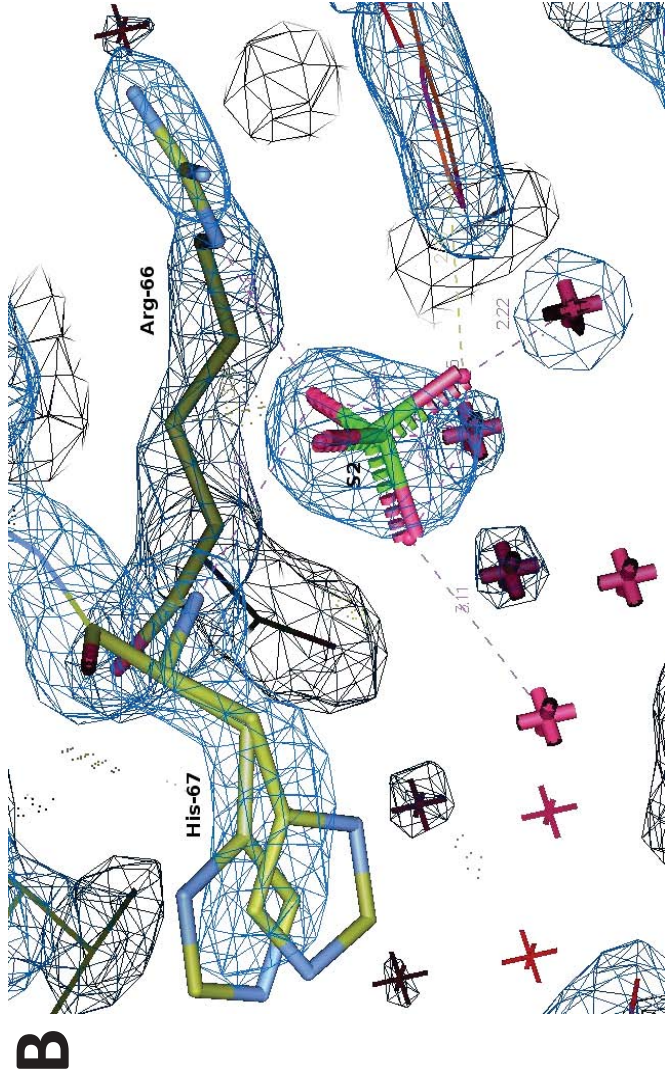
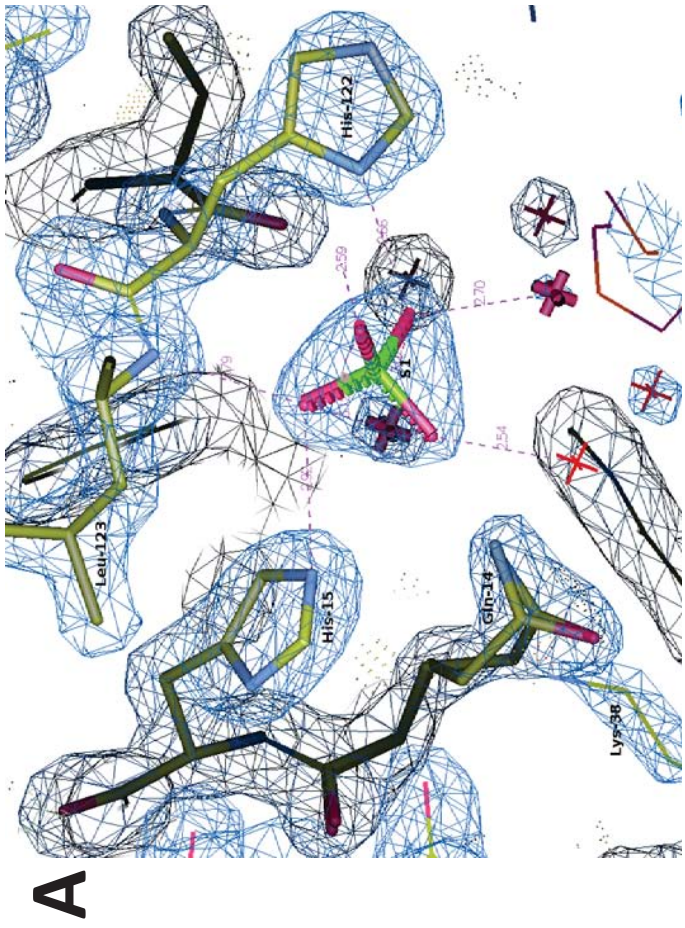
Figure S2. Catalytic activities were determined by the zymogram technique in 15% SDS-PAGE containing poly(C) as a substrate. **A.** (Lane 1) 750 pg of RNase A. (Lane 2) 120 ng of RNase 3. (Lane 3) 120 ng of RNase 6. (Lane 4) 120 ng of RNase 7. **B.** (Lane 1) 100 ng of RNase 6. (Lane 2) 100 ng of RNase 6 H15A-H36A. (Lane 3) 250 ng of RNase 6 H15A-H36A. (Lane 4) 500 ng of RNase 6 H15A-H36A. (Lane 5) 100 ng of RNase 6 H15A.

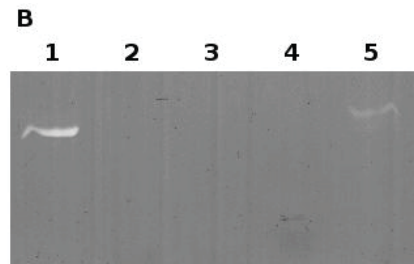
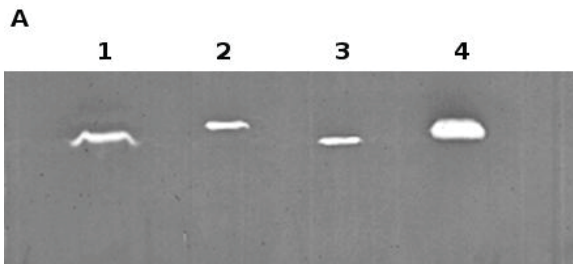
Figure S3. Structural superposition of RNase 6 and representative RNase A family structures (RNase A, RNase 1 and RNase 3). A) Overall structural superposition showing Loop L3. B) Amplification of L3 loop showing equivalent residues to His 36 and His 39 in RNase 6. RNase 6 is coloured in green, RNase A in blue, RNase 1 in magenta and RNase 3 in yellow. Picture was drawn with *PyMol 1.7.2* (Delano Scientific).

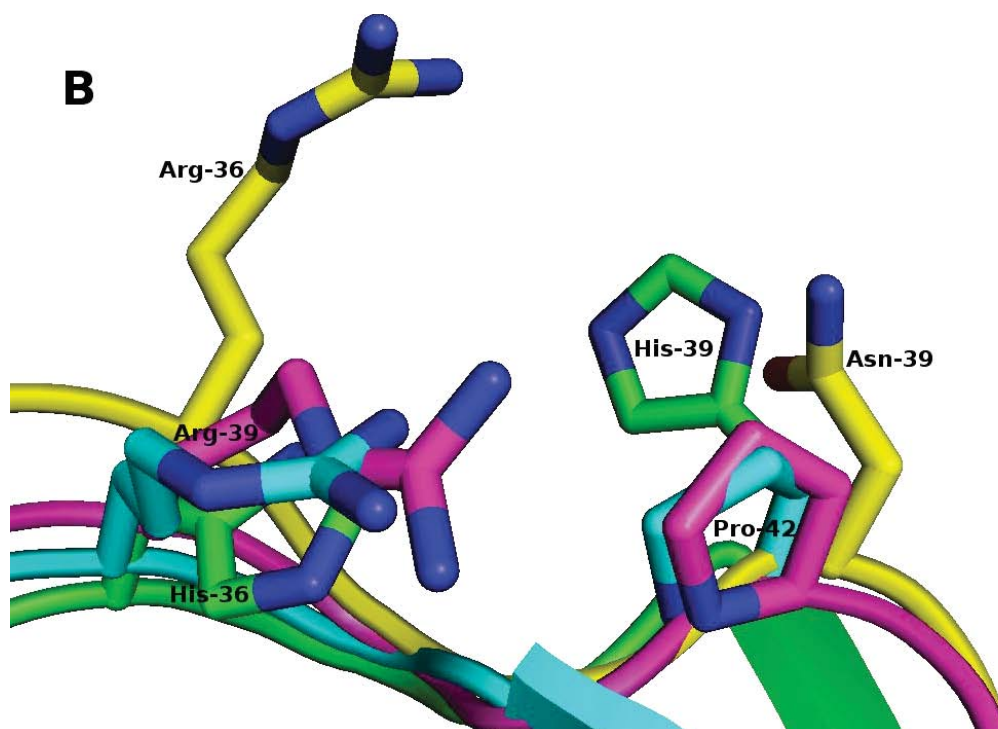
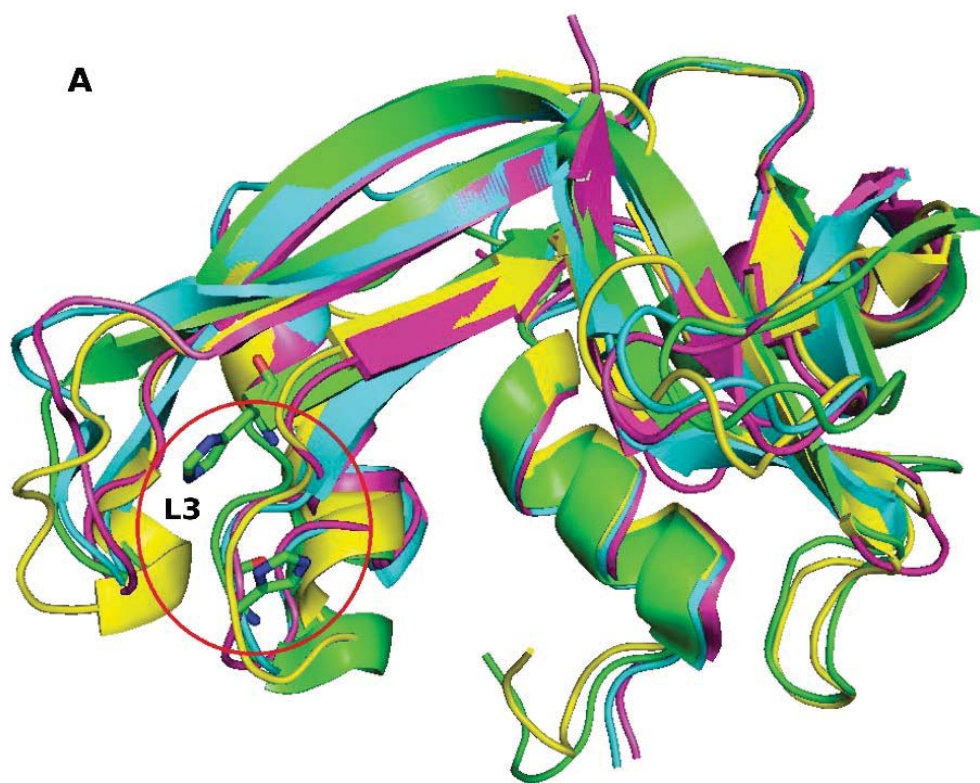
Figure S4. Poly(C) cleavage patterns by RNase 6-H15A and RNase 7-H15A. Both chromatograms correspond to the polynucleotide digestion products obtained after 30 min of incubation with 1.4 μ M of enzyme.

References

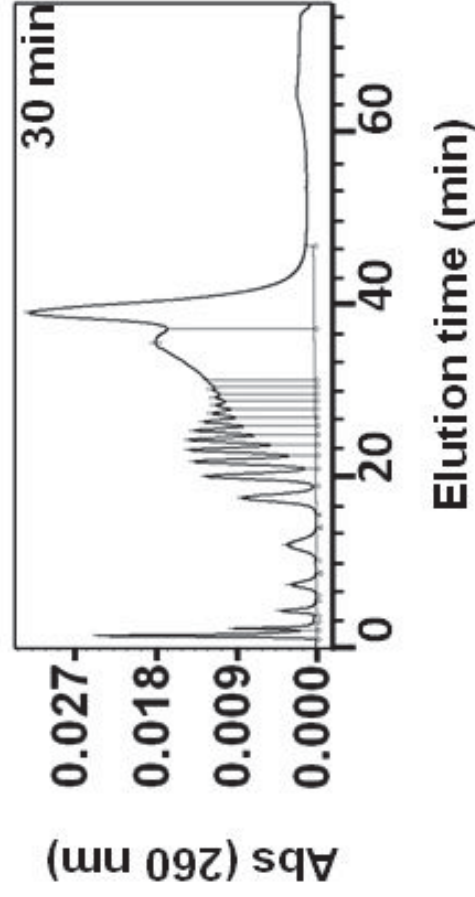
- 1 Krissinel, E. and Henrick, K. (2007) Inference of macromolecular assemblies from crystalline state. *J. Mol. Biol.*, England **372**, 774–797.
- 2 Kilambi, K. P. and Gray, J. J. (2012) Rapid calculation of protein pKa values using Rosetta. *Biophys. J.*, United States **103**, 587–595.



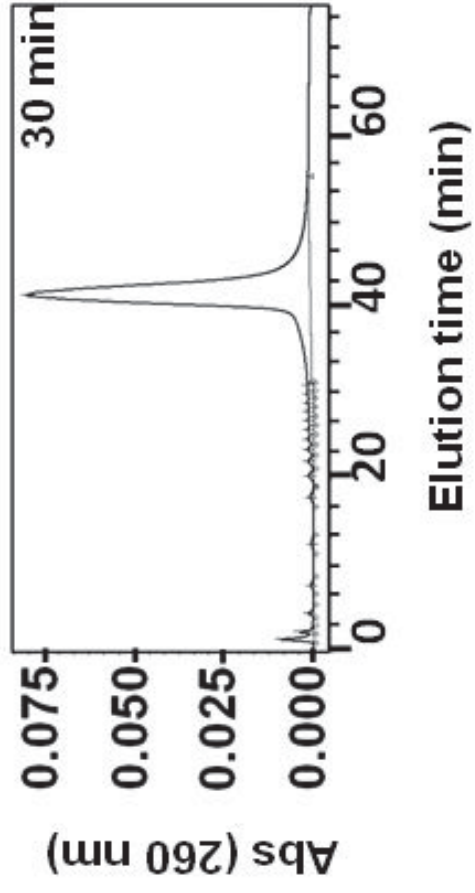




RNase 6-H15A



RNase 7-H15A



SUPPORTING INFORMATION:

Exploring the mechanisms of action of human secretory RNase 3 and RNase 7 against *Candida albicans*

Vivian A. Salazar¹; Javier Arranz-Trullen¹; Susanna Navarro^{1,2}; Jose A. Blanco¹; Daniel Sánchez¹; Mohammed Moussaoui¹; and Ester Boix¹

¹From the Department of Biochemistry and Molecular Biology, Faculty of Biosciences, Universitat Autònoma de Barcelona, E-08193 Cerdanyola del Vallès, Spain and ²Institut de Biotecnologia i Biomedicina, Universitat Autònoma de Barcelona, E-08193 Cerdanyola del Vallès, Spain. E-mail: Ester.Boix@uab.cat

List of supplementary material:

Table S1. Data collection, processing and structure refinement statistics of RNase 3-H15A crystal structure solving.

Table S2: Effect of NaCl and Ca²⁺ addition on the antifungal activity of RNase 3 and RNase 7.

Figure S1. Binding of RNase 3 and RNase 7 to *Candida* cells.

Figure S2: Effects of RNase 3, RNase 3-H15A and RNase 3-W35A on *C. albicans* visualized by confocal microscopy.

Figure S3: Kinetic profile of *C. albicans* cell survival incubated with RNase 3 and RNase 7.

Figure S4: Analysis of *C. albicans* cell culture incubated with wild-type and mutant RNases by FACS.

Figure S5. Kinetic profile of cellular ATP levels of *C. albicans* incubated with RNase 3 and RNase 3-H15A.

Table S1. Data collection, processing and structure refinement statistics of RNase 3-H15A crystal structure solving.

	RNase 3-H15A (PDB ID: 4OWZ)
<i>Data collection</i>	
Space group	P4 ₃ 22
Unit cell	
<i>a</i> , <i>b</i> , <i>c</i> (Å)	62.54 62.54 175.23
α, β, γ (°)	90.0 90.0 90.0
Resolution (Å)	1.47
Number of reflections (measured/unique)	775132/48793
R _{merge} ^{a, b} (%)	4.2 (44.7)
<i>I</i> / <i>σ_I</i> ^b	34.9 (6.8)
Completeness for range (%) ^b	100.0 (100.0)
Wilson B factor (Å ²) ^b	21.6
Matthews coefficient (Å ³ /Da) ^b	2.20
Solvent content (%)	43.59
<i>Refinement parameters</i>	
Resolution range (Å)	62.54 – 1.47
R _{cryst} ^c / R _{free} ^d (%)	20.02/22.25
Bond lengths (Å)	0.007
Bond angles (deg)	1.115
Number of protein atoms	2335
Number of water molecules	413
B-factors (Å ²)	
Protein atoms	
• All	23.05/26.22
• Main chain	20.63/23.39
• Side chain	25.03/28.70
Anion atoms	27.89
Water molecules	39.15

^a $R_{merge} = \frac{\sum_{hkl} \sum_{j=1}^N |I_{hkl} - I_{hkl}(j)|}{\sum_{hkl} \sum_{j=1}^N I_{hkl}(j)}$, where *N* is the redundancy of the data.

^b Outermost shell is 1.47-1.62

^c $R_{crystal} = \frac{\sum_h |F_o - F_c|}{\sum_h F_o}$, where *F_o* and *F_c* are the observed and calculated structure factor amplitudes of reflection *h*, respectively.

^d *R_{free}* is equal to *R_{cryst}* for a randomly selected 5% subset of reflections not used in the refinement.

Table S2: Effect of NaCl and Ca²⁺ addition on the antifungal activity of RNase 3 and RNase 7. The minimal fungicidal concentration (MFC₁₀₀) was determined on *Candida albicans* cultures diluted in Low ionic strength Phosphate Buffer (Low-PB: 10 mM sodium phosphate, pH 7.5); High ionic strength Phosphate Buffer (High-PB: 10 mM sodium phosphate, NaCl 0.15M, pH 7.5) and Sabouraud Broth (SB) by CFU counting on plated Petri dishes as described in the methodology.

Protein	MFC ₁₀₀ (μM)				
	Low-PB	High-PB	SB	SB + 150 mM NaCl	SB + 1 mM Ca ²⁺
RNase 7	2.5-5	2.5	2.5-5	5-10	20
RNase 3	2.5-5	2.5	2.5	10	>20

SUPPLEMENTAL FIGURES

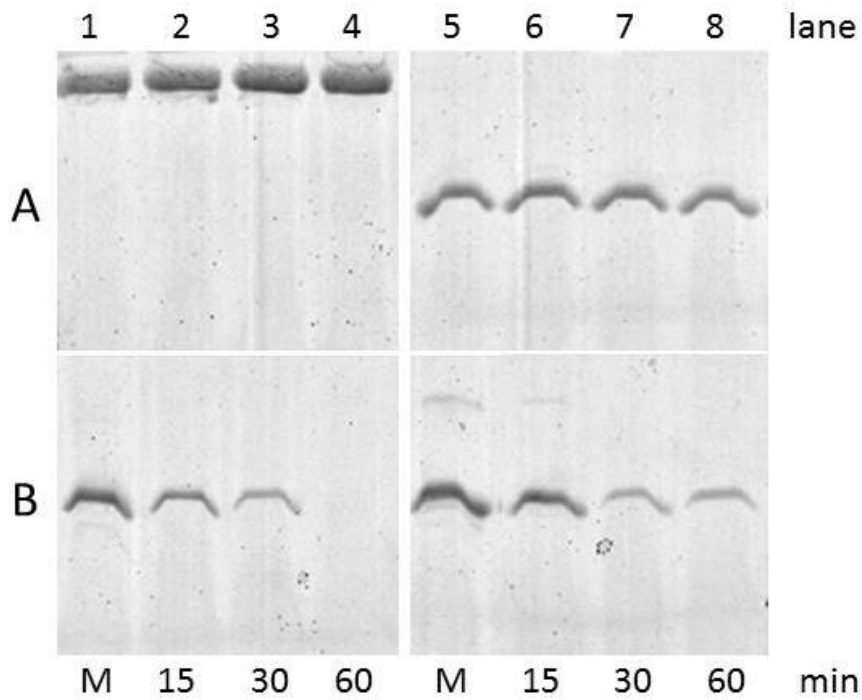


Figure S1. Binding of RNase 3 and RNase 7 to *Candida* cells. Lanes 1A-4A correspond to bovine serum albumin (BSA). Lanes 5A-8A correspond to RNase A. Lanes 1B-4B correspond to RNase 3. Lanes 5B-8B correspond to RNase 7. Lanes 1A, 5A, 1B and 5B correspond to reference proteins.

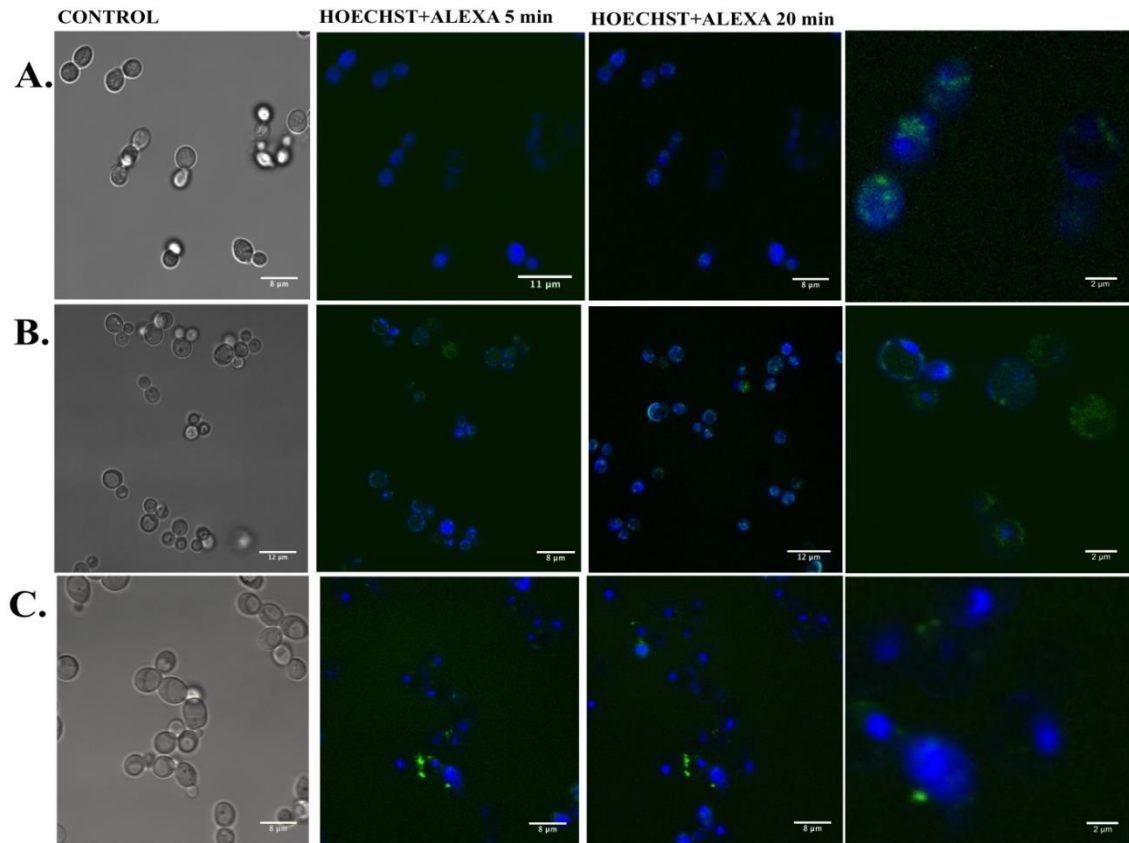


Figure S2: Effects of RNase 3, RNase 3-H15A and RNase 3-W35A (A-C) on *C. albicans* in mid-exponential growth phase ($\sim 3 \times 10^6$ cell/mL) visualized by confocal microscopy. The yeast morphology is showing in the left-hand side. The second and third panels show the merged Hoechst and Alexa Fluor 488– labeled protein after 5 and 20 min of incubation respectively. Last panel corresponds to a magnified window of the 20 min incubation condition. The protein final concentration was 3 μ M. *ImageJ* software was used for analysis. The magnification scale is indicated at the bottom of each micrograph. Images were taken using a Leica TCS SP5 AOBS microscope.

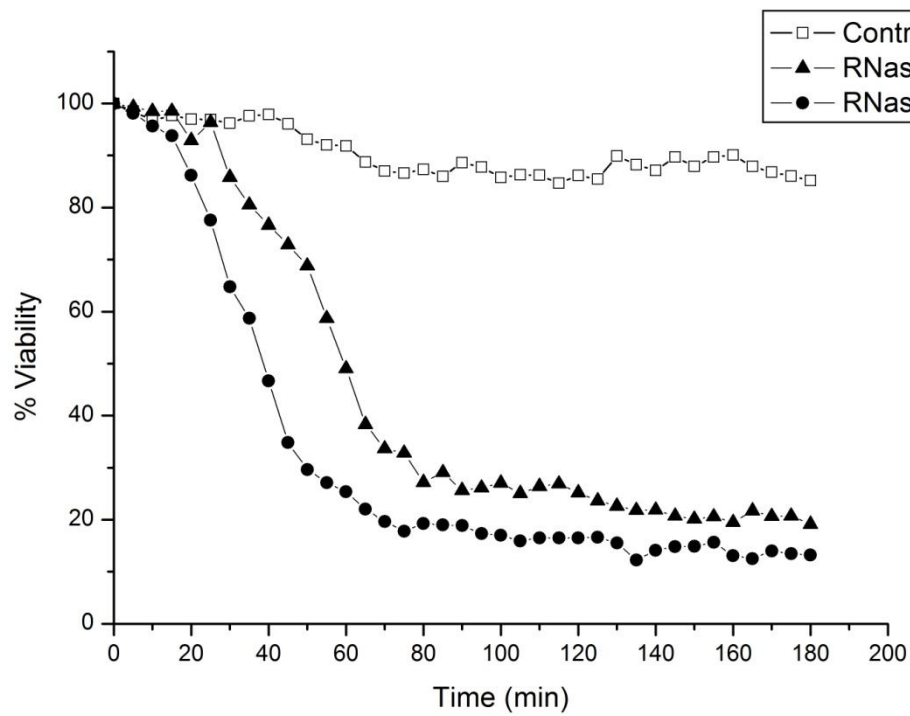


Figure S3: Kinetic profile of calculated *Candida albicans* cell survival after incubation of yeast cell culture ($\sim 2 \times 10^6$ cells/mL) with 1 μ M of RNase 3 and RNase 7 at 37°C. Viability percentage was evaluated using the Live/Dead[®] kit, where live and dead cells are stained with SYTO[®]9 and propidium iodide (PI) dyes respectively.

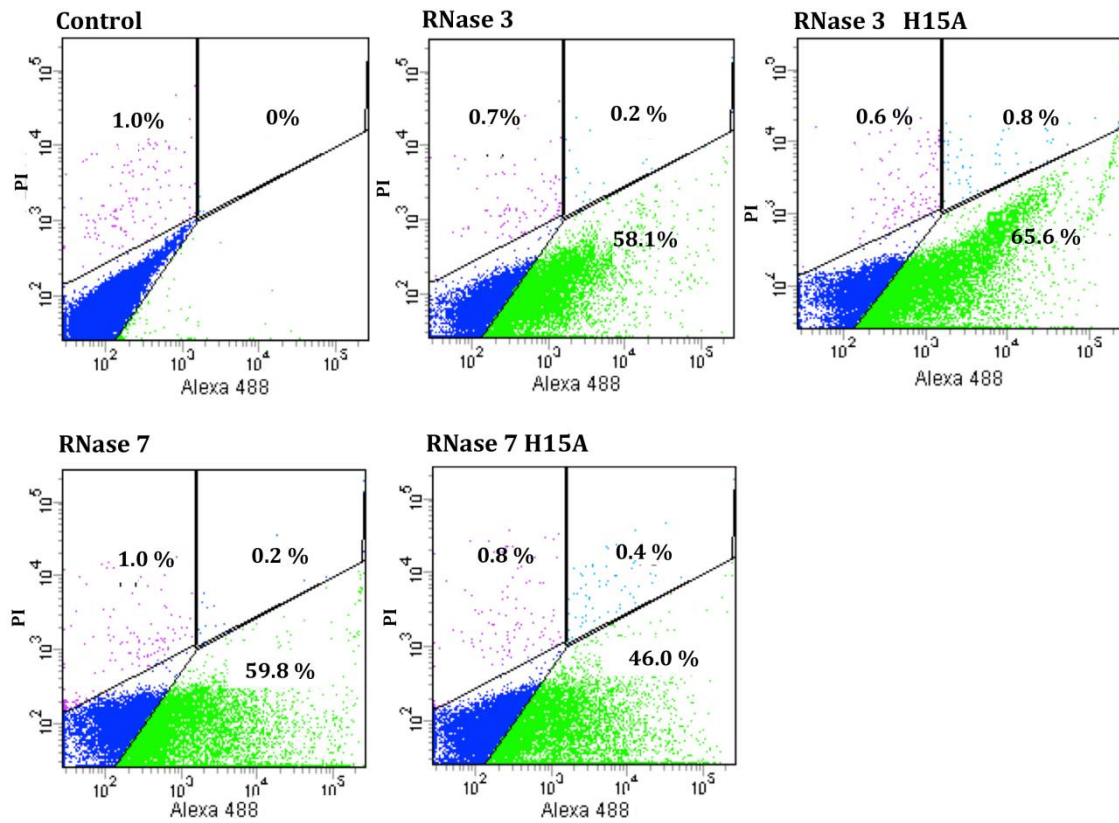


Figure S4: Analysis of *C. albicans* cell culture incubated with proteins by FACS. A total of 25000 *Candida* cells were gated by Forward scatter (FSC) / Side scatter (SSC). *C. albicans* cell cultures (1×10^6 cells/mL) were incubated with 3.5 μ M of RNase 3, RNase 7 and mutants during 45 min; the samples were analyzed using a FACSCalibur cytometer. Dot plot diagrams of Protein-Alexa Fluor 488/ PI show yeast population divided in four quadrants corresponding to: *Candida cells* (blue color), cells with colocalized protein (green color), dead cells (purple color) and dead cells with colocalized protein (light blue color). Control corresponds to untreated cells.

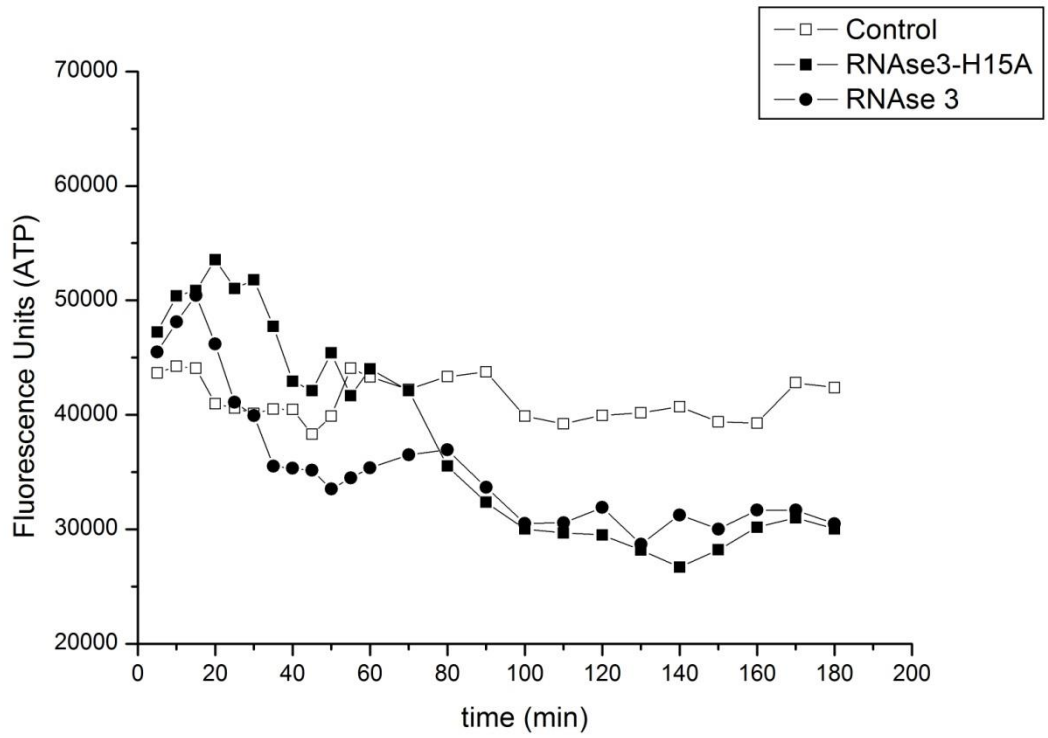


Figure S5. Kinetic profile of cellular ATP levels assessed by using the *Bac-Titer Glo*TM Assay. Yeast cell cultures grown up to $\sim 3 \times 10^6$ cells/mL were incubated with 1 μ M of RNase 3 and RNase 3-H15A at 37°C.

Supplementary materials: Unveiling the mode of action of human antimicrobial RNases against *Mycobacterium tuberculosis* using a surrogate macrophage infected model

Arranz-Trullén J^{1,2}; Lu Lu¹, Pulido D^{1,3}; Bhakta S^{2*} and Boix E^{1*}

Table S1. Comparative growth pattern of *M. smegmatis* mc²155, *M. aurum* and *M. bovis* BCG

Parameters	<i>M. smegmatis</i> mc ² 155	<i>M. aurum</i>	<i>M. bovis</i> BCG
Generation time (h)	2.7	9.6	20
Time to observe single colony (days)	3	8	28
Time to observe spot (days)	2	5	14
Level of bio-safety containment	1	2	2/3
Growth rate	fast	medium	slow

*Generation time was calculated according to $(t_2-t_1) \times \ln(2) / \ln(q_2/q_1)$ where t_2 is the final time, t_1 is the beginning of growth (end of lag phase), q_2 is the cell number at t_2 , and q_1 is the cell number at t_1 .

A Time (hr)	Control		RNase 3		RNase 3-H15A	
	<i>M. aurum</i>	RAW 264.7	<i>M. aurum</i>	RAW 264.7	<i>M. aurum</i>	RAW 264.7
4	6.98/5.24	6.67/6.88	6.23/4.92	7.39/5.20	5.89/4.76	8.34/7.53
24	7.18/6.21	6.72/5.39	5.43/3.28	5.43/3.21	5.42/4.91	9.41/5.52
48	7.04/5.65	6.50/4.84	2.17/0.87	6.69/4.16	4.63/3.75	5.74/4.67
72	7.31/5.35	8.37/6.79	1.27/0.45	6.80/3.64	4.89/3.96	6.95/6.43

B Time (hr)	Control		RNase 6		RNase 6-H15A	
	<i>M. aurum</i>	RAW 264.7	<i>M. aurum</i>	RAW 264.7	<i>M. aurum</i>	RAW 264.7
4	7.21/6.45	6.93/7.25	7.22/5.57	8.25/6.50	6.54/5.32	7.56/7.73
24	6.83/6.73	7.31/5.76	4.63/3.63	6.67/4.42	4.31/3.88	8.26/6.31
48	7.28/6.18	6.41/5.18	2.73/1.14	5.92/5.47	3.77*/2.52*	6.85/5.83
72	7.26/6.10	7.94/6.53	1.67/1.24	6.13/4.87	2.59**/2.13**	7.16/5.94

C Time (hr)	Control		RNase 7		RNase 7-H15A	
	<i>M. aurum</i>	RAW 264.7	<i>M. aurum</i>	RAW 264.7	<i>M. aurum</i>	RAW 264.7
4	6.44/6.61	7.51/6.38	6.76/5.41	7.83/6.42	6.35/5.92	7.92/7.44
24	6.57/6.75	7.36/6.14	5.26/4.05	6.33/5.64	5.81/5.74	7.74/6.35
48	7.12/5.33	6.65/5.02	3.12/2.32	6.54/5.61	5.56/4.89	6.16/4.42
72	6.84/6.21	7.74/6.53	1.84/1.38	5.47/5.07	4.78/5.15	6.59/6.13

Table S2. Effect of hRNases 3, 6, 7 and their respective active-site mutants on *M. aurum* cellular RNA. Micobacteria infected macrophages were treated with 2 μ M of each protein and incubated at different time intervals. Following, total RNA was extracted as described in Experimental Procedures. Samples were analyzed by an Experion automated electrophoresis station (prokaryote total RNA high sensitivity chip) and RNA was visualized with the Experion software. Left lane contains molecular mass markers, where reference base pairs are indicated. Control lanes correspond to cellular RNA from untreated infected macrophages. (table) Peak area corresponding to 18/28s (eukaryotic) and 16/23s (prokaryotic) subunits of rRNA of treated cells for wild-type and active-site mutant RNases are shown for each incubation time. Data represent mean \pm SD, n=3. The P value were calculated using as reference for each mutant the respective wild-type protein activity (*corresponds to $P < 0.05$ and ** to $P < 0.01$).

Table S3. Statistics of CFU assay (fig 4)

	m. aurum	Rnase 3	RNase 3-H15A	24 hr
RNase 3	NSS		^b NSS	
RNase 3-H15A	NSS	^b NSS		

	m. aurum	Rnase 3	RNase 3-H15A	48 hr
RNase 3	**		^b NSS	
RNase 3-H15A	**	^b NSS		

	m. aurum	Rnase 3	RNase 3-H15A	72 hr
RNase 3	***		^b *	
RNase 3-H15A	***	^b *		

The P value were calculated using as reference negative control (*M. aurum*) (*corresponds to $P < 0.05$, ** to $P < 0.01$ and *** to $P < 0.001$). ^b The calculated P value using as reference active-site mutant was considered to be statistically significant ($P < 0.05$).

Table S4. Statistics of CFU assay (fig 5)

A	M. aurum	RNase 3-H15A	RNase 6-H15A	RNase 7-H15A	RNase 3	RNase 6	RNase 7	0 hr
RNase 3	^a NSS	^b NSS	NSS	NSS		NSS	NSS	
RNase 6	^a NSS	NSS	^b NSS	NSS	NSS		NSS	
RNase 7	^a NSS	NSS	NSS	^b NSS	NSS	NSS		
RNase 3-H15A	NSS			NSS				
RNase 6-H15A	NSS	NSS		NSS				
RNase 7-H15A	NSS	NSS	NSS					

B	M. aurum	RNase 3-H15A	RNase 6-H15A	RNase 7-H15A	RNase 3	RNase 6	RNase 7	24 hr
RNase 3	^a **	^b NSS	NSS	NSS		NSS	NSS	
RNase 6	^a *	NSS	^b NSS	NSS	NSS		NSS	
RNase 7	^a NSS	NSS	NSS	^b NSS	NSS	NSS		
RNase 3-H15A	NSS		NSS	NSS				
RNase 6-H15A	NSS	NSS		NSS				
RNase 7-H15A	NSS	NSS	NSS					

C	M. aurum	RNase 3-H15A	RNase 6-H15A	RNase 7-H15A	RNase 3	RNase 6	RNase 7	48 hr
RNase 3	^a ***	^b **	**	**		*	**	
RNase 6	^a **	NSS	^b NSS	NSS	*		NSS	
RNase 7	^a **	NSS	NSS	^b NSS	**	NSS		
RNase 3-H15A	^a **		NSS	NSS				
RNase 6-H15A	^a **	NSS		NSS				
RNase 7-H15A	^a **	NSS	NSS					

D	M. aurum	RNase 3-H15A	RNase 6-H15A	RNase 7-H15A	RNase 3	RNase 6	RNase 7	72 hr
RNase 3	^a ***	^b ***	***	***		***	***	
RNase 6	^a ***		^b NSS		***		NSS	
RNase 7	^a ***	NSS	NSS	^b NSS	***	NSS		
RNase 3-H15A	^a ***		NSS	NSS				
RNase 6-H15A	^a ***	NSS		*				
RNase 7-H15A	^a ***	NSS	*					

^a The P value were calculated using as reference negative control (*M. aurum*) (*corresponds to $P < 0.05$, ** to $P < 0.01$ and *** to $P < 0.001$).

^b The P value were calculated using as reference each wild-type activity (*corresponds to $P < 0.05$, ** to $P < 0.01$ and *** to $P < 0.001$).

P value > 0.05 , this difference is considered to be not statistically significant (NSS)

P value < 0.05 , this difference is considered to be statistically significant (SS)

P value < 0.01 , this difference is considered to be very statistically significant (VSS)

P value < 0.001 , this difference is considered to be extremely statistically significant (ESS)

E	RNase 3 (0 hr)	RNase 3 (24 hr)	RNase 3 (48 hr)	RNase 3 (72 hr)
RNase 3 (0 hr)		NSS	***	***
RNase 3 (24 hr)	NSS		**	***
RNase 3 (48 hr)	***	**		*
RNase 3 (72hr)	***	***	*	

F	RNase 6 (0 hr)	RNase 6 (24 hr)	RNase 6 (48 hr)	RNase 6 (72 hr)
RNase 6 (0 hr)		NSS	*	**
RNase 6 (24 hr)	NSS		NSS	**
RNase 6 (48 hr)	*	NSS		NSS
RNase 6 (72hr)	**	**	NSS	

G	RNase 7 (0 hr)	RNase 7 (24 hr)	RNase 7 (48 hr)	RNase 7 (72 hr)
RNase 7 (0 hr)		NSS	NSS	**
RNase 7 (24 hr)	NSS		NSS	*
RNase 7 (48 hr)	NSS	NSS		NSS
RNase 7 (72hr)	**	*	NSS	

H	RNase 3-H(0 hr)	RNase 3-H (24 hr)	RNase 3-H (48 hr)	RNase 3-H (72 hr)
RNase 3-H (0 hr)		NSS	*	***
RNase 3-H (24 hr)	NSS		NSS	**
RNase 3-H(48 hr)	*	NSS		*
RNase 3-H (72hr)	***	**	*	

I	RNase 6-H (0hr)	RNase 6-H (24 hr)	RNase 6-H (48 hr)	RNase 6-H (72 hr)
RNase 6-H (0 hr)		NSS	*	***
RNase 6-H (24 hr)	NSS		NSS	***
RNase 6-H (48 hr)	*	NSS		*
RNase 6-H (72hr)	***	***	*	

J	RNase 7-H (0hr)	RNase 7-H (24 hr)	RNase 7-H (48 hr)	RNase 7-H (72 hr)
RNase 7-H (0 hr)		NSS	**	***
RNase 7-H (24 hr)	NSS		NSS	***
RNase 7-H (48 hr)	**	NSS		NSS
RNase 7-H (72hr)	***	***	NSS	

^c The *P* value were calculated using as reference wild-type or active-site mutant activity in other time-point incubation time (*corresponds to $P < 0.05$, ** to $P < 0.01$ and *** to $P < 0.001$).

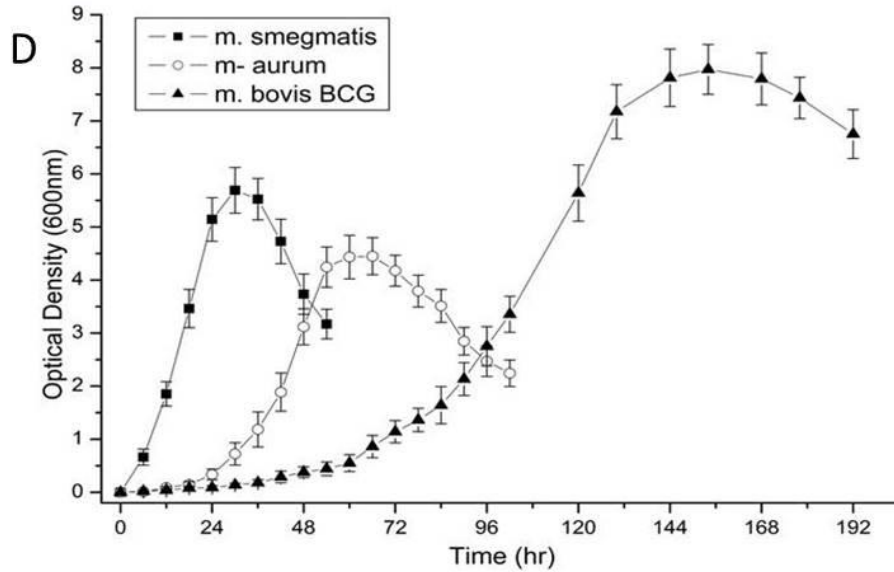
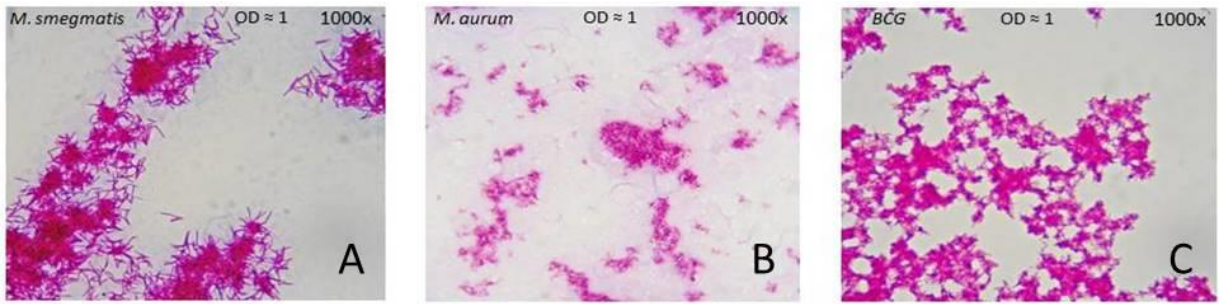


Figure S1. Comparative growth curves of *M. smegmatis* mc²155, *M. aurum* and *M. bovis* BCG. Each point represents the mean value of optical density from three independent experiments. The standard deviation of the mean for each is shown as an error bar. Microscopic observation of log phase (OD₆₀₀ ≈ 1.0) acid fast stained *M. smegmatis* mc²155 (cfu: 1×10⁹ cells/mL), *M. aurum* (cfu: 1×10⁹ cells/mL) and *M. bovis* BCG (CFU: ×10⁹ cells/mL).

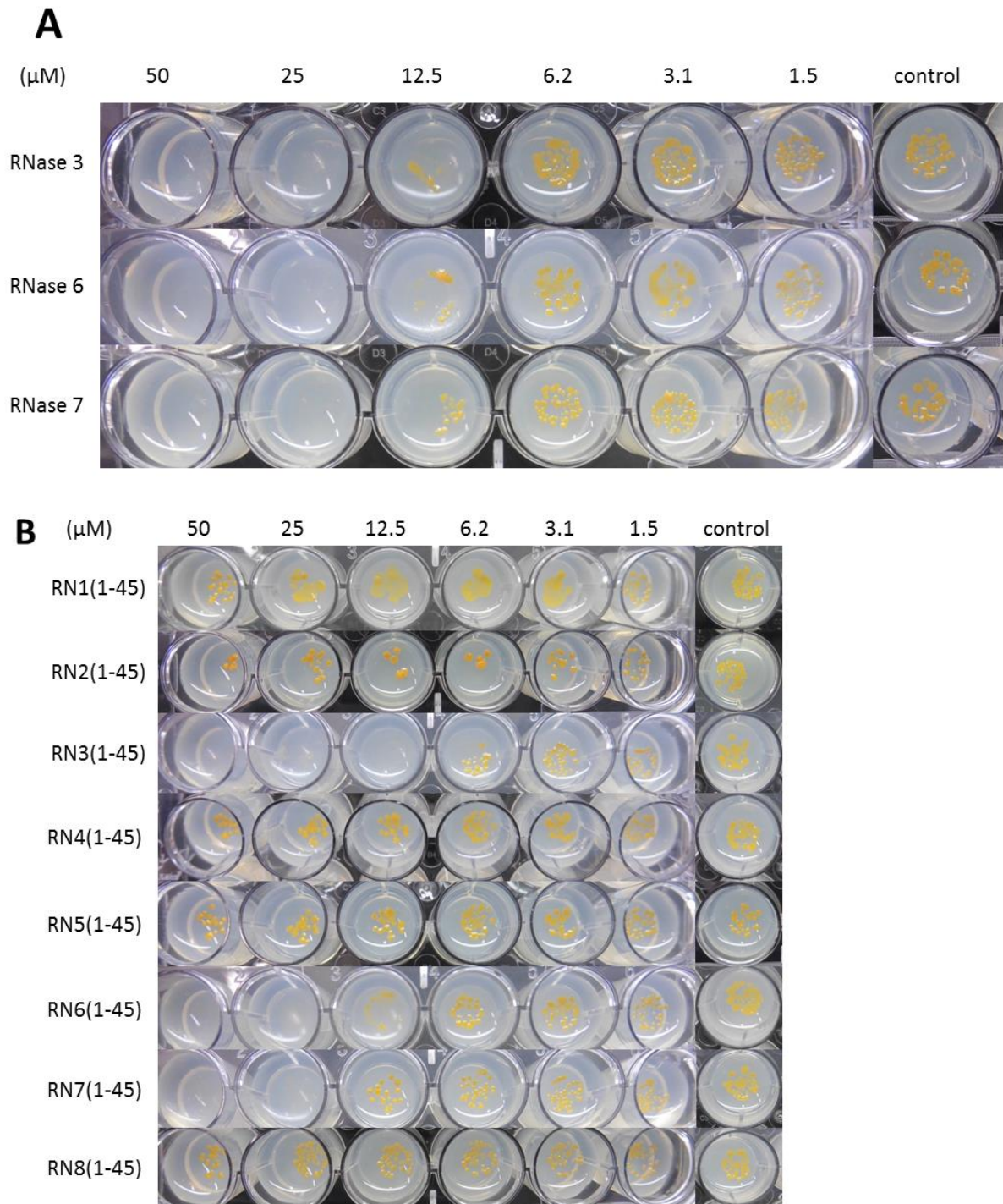


Figure S2. Extracellular susceptibility of *M. aurum* to anti-TB AMPs using the 24-well plate format SPOTi assay. The assay was performed with three biological replicates. A) RNase 3, RNase 6 and RNase 7 and control samples. B) RNase derived N-terminal peptides. See materials and methods section.

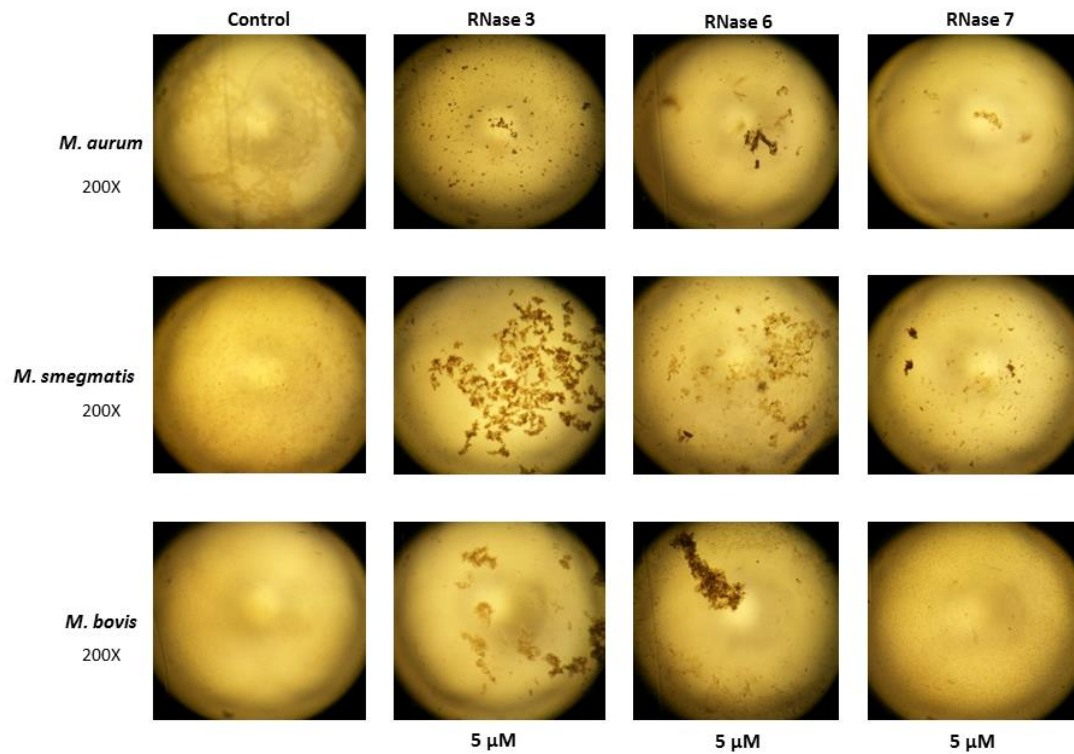


Figure S3. Minimal agglutination activity of RNase 3, RNase 6 and RNase 7. Mycobacterial cells were grown at 35°C to and then diluted to an OD600 of 0.1, centrifuged at 5,000 xg for 2 min, and resuspended either in 1X PBS or M7H9/ADC media containing 0.05% Tween 80 and 0.05% Glycerol 50%. An aliquot of 100 μ l of the mycobacterial suspension was treated with increasing protein or peptide concentrations (from 0.01 to 20 μ M) and incubated at 35°C for 1 h. The aggregation behaviour was observed by visual inspection with a stereomicroscope at 50x.

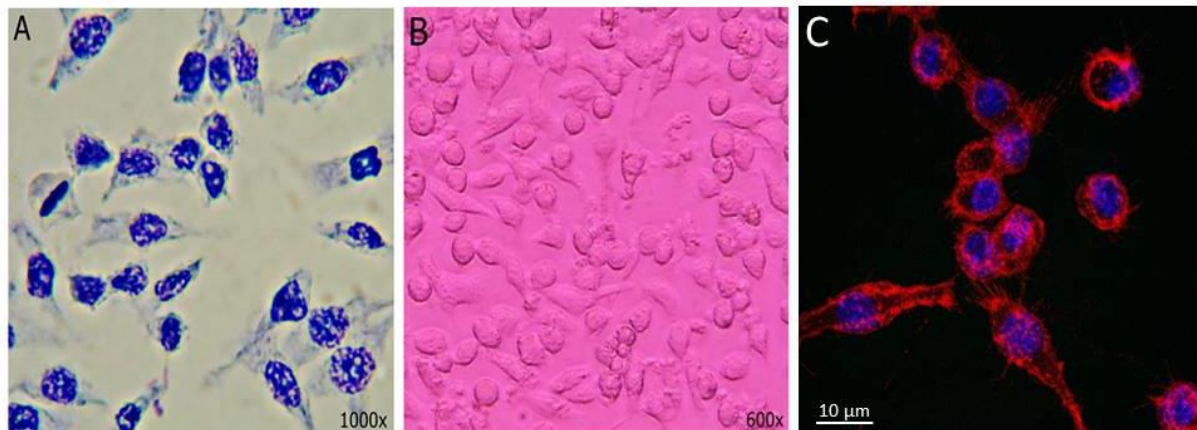


Figure S4. RAW 264. 7 Macrophages viability and cell morphology directly through the inverted microscope (B) and collected samples, which were fixed and stained with malaquite green (A). Additionally macrophages were stained with Hoescht 33342 and CellMask Deep Red Plasma membrane Stain (Thermo Fisher Scientific, C10046) at 0.5 μ g/mL for 5-10 min before observation (C).

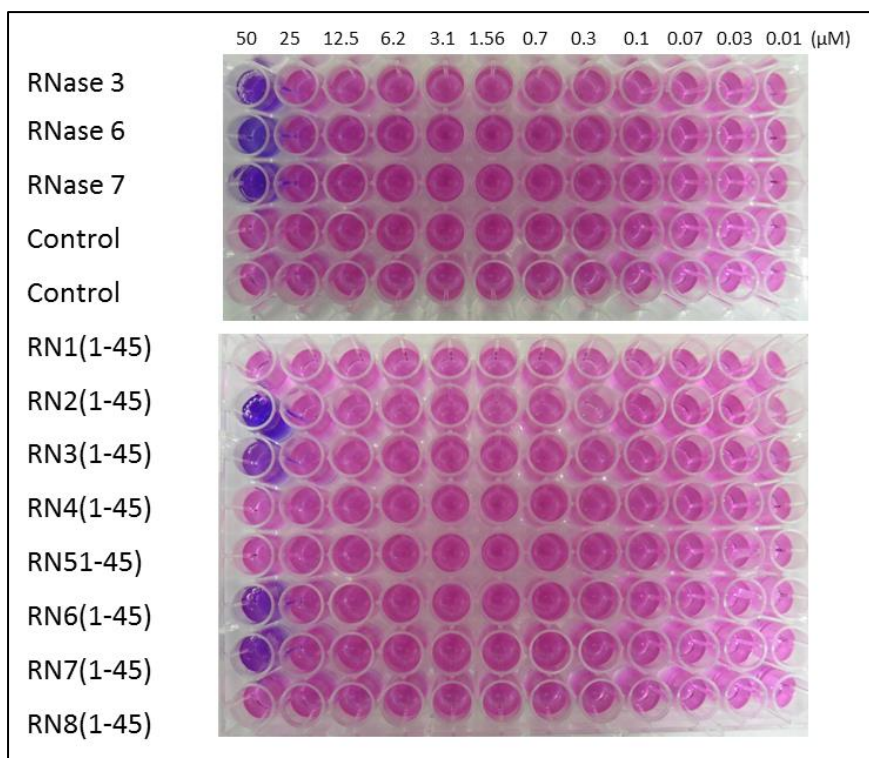


Figure S5. Toxicity of hRNases and its derived peptides against RAW 264.7. Proteins or peptides were serially diluted from 50 to 0.1 μM (100 μl) in each well. To each well, 100 μL of diluted macrophage cells (5×10⁵ cells/mL) was added. After 48 h of incubation, cells were washed twice with 1X PBS, and fresh RPMI-1640 complete medium was added. Plates were then treated with 30 μl of a freshly prepared 0.01% resazurin solution and incubated overnight at 37°C. The following day the change in colour was observed and the fluorescence intensity was measured.

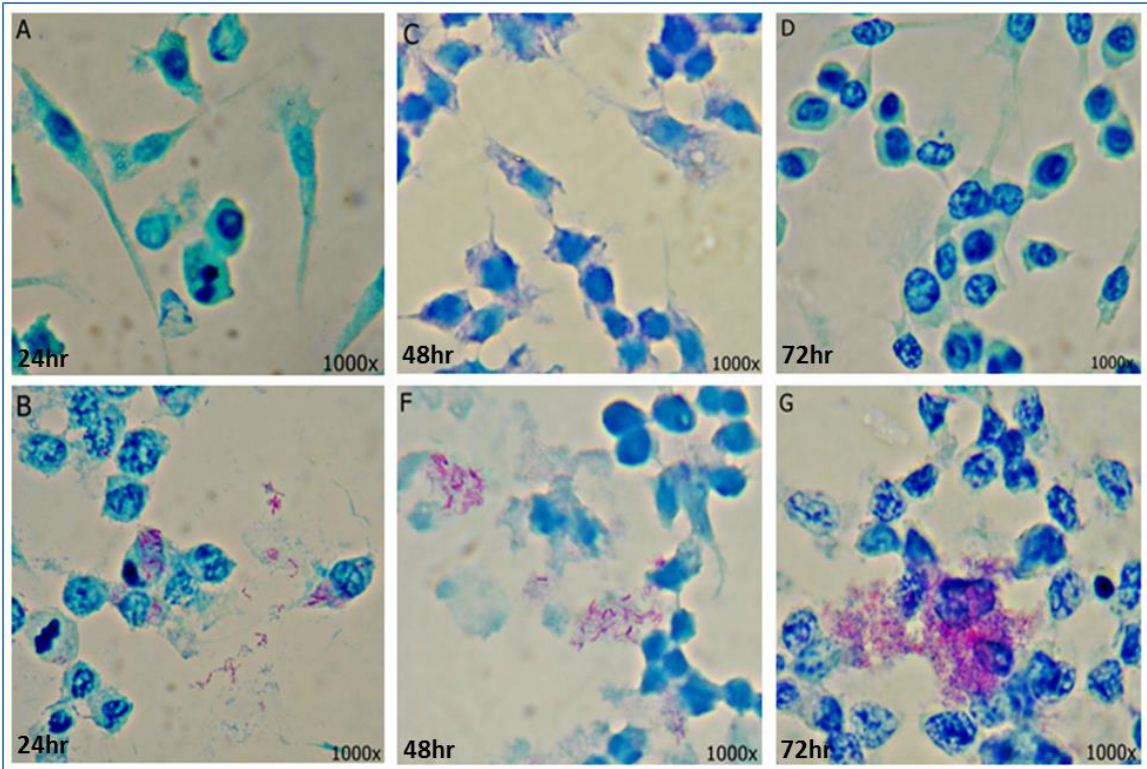
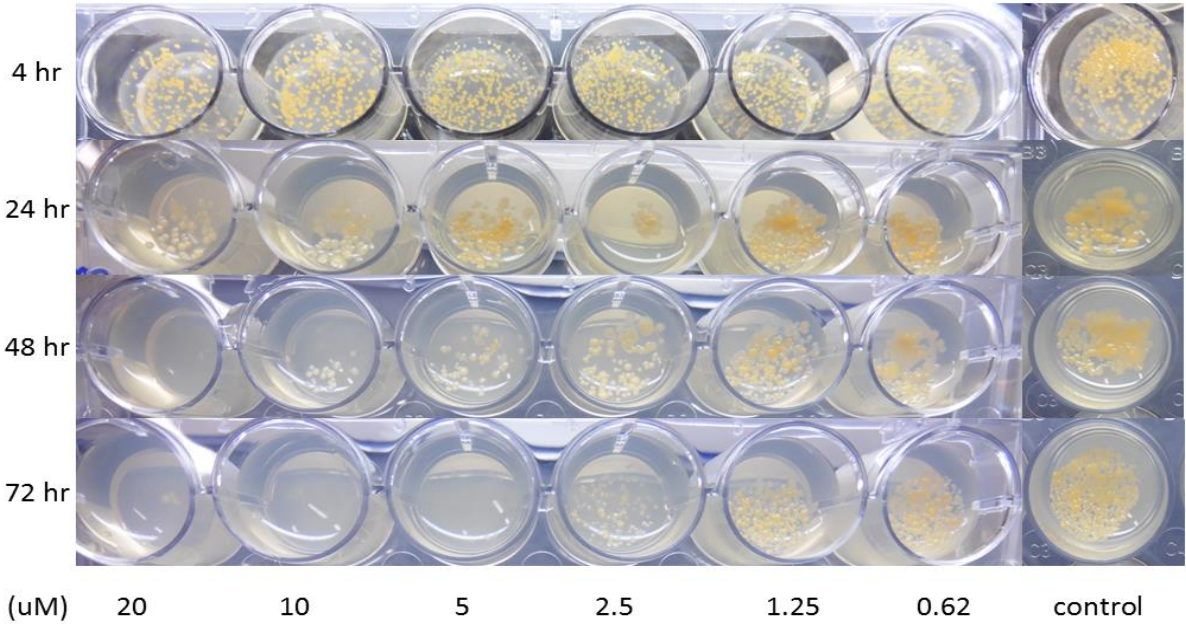
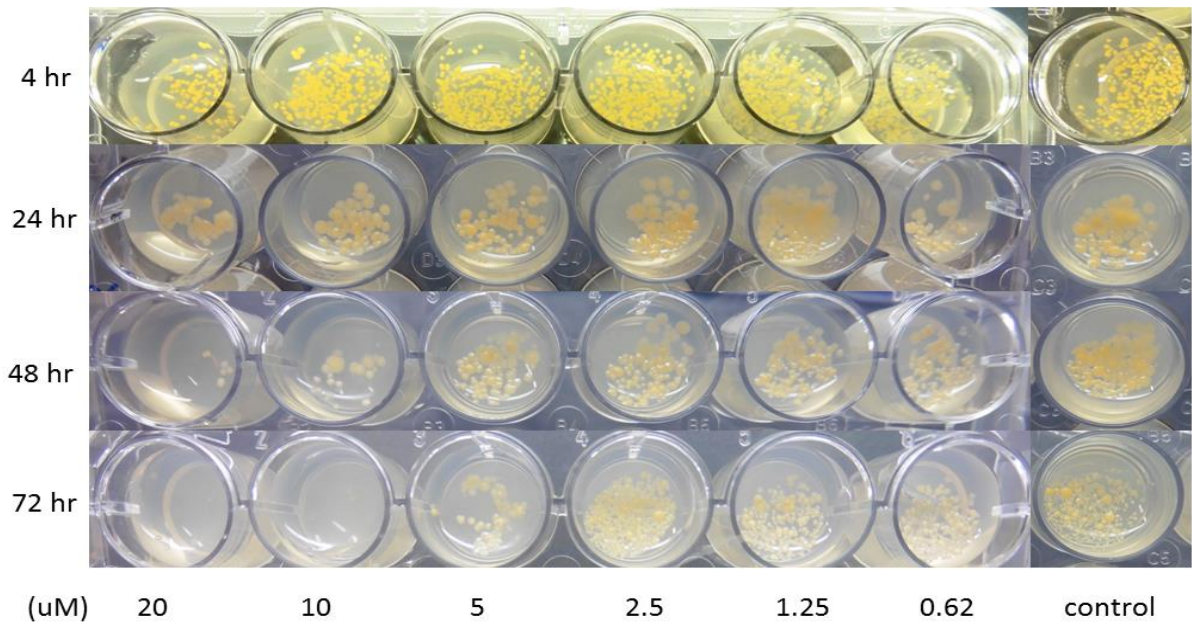


Figure S6. Macrophage growth monitoring in absence (A, C, D) and in presence (B, F, G) of *M. aurum*. Culture conditions described in materials and methods section.

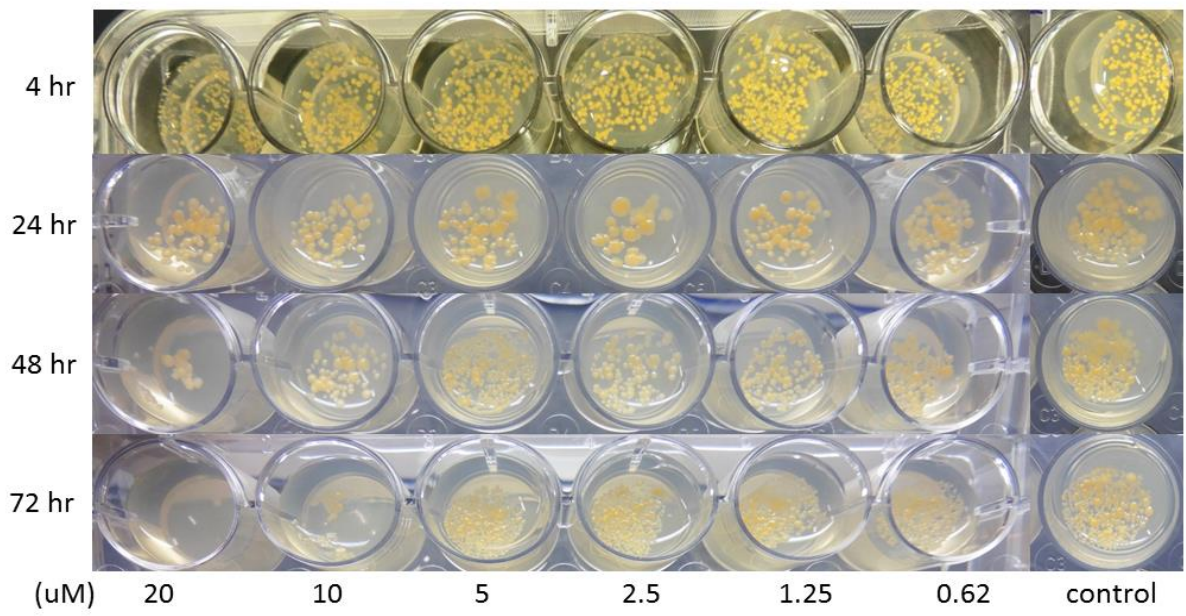
A



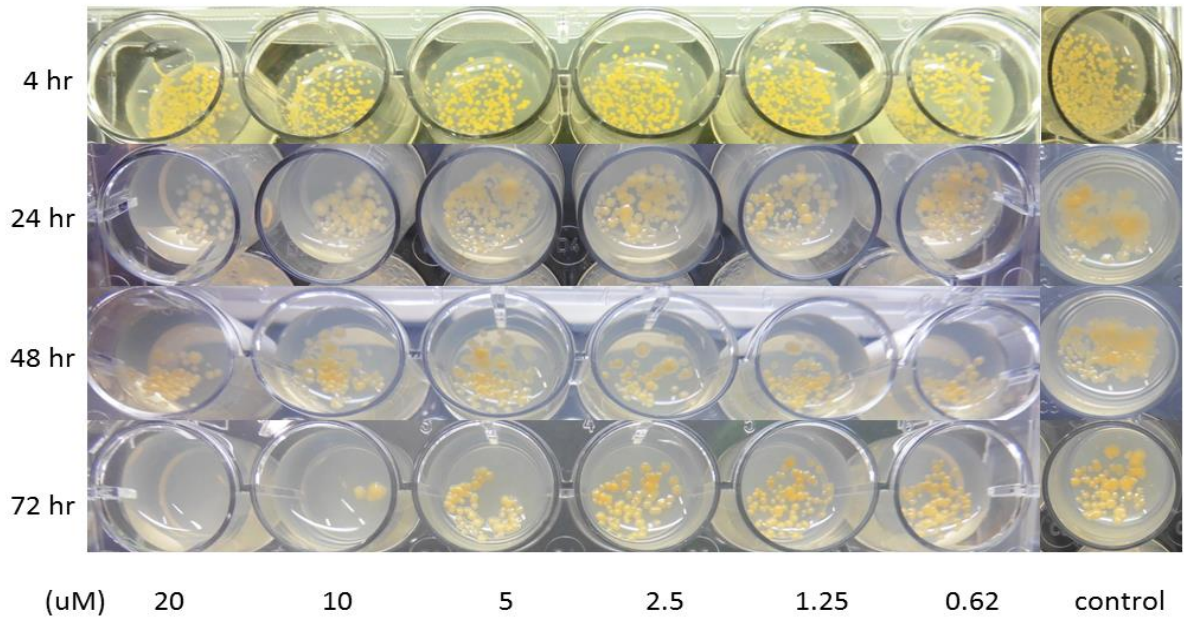
B



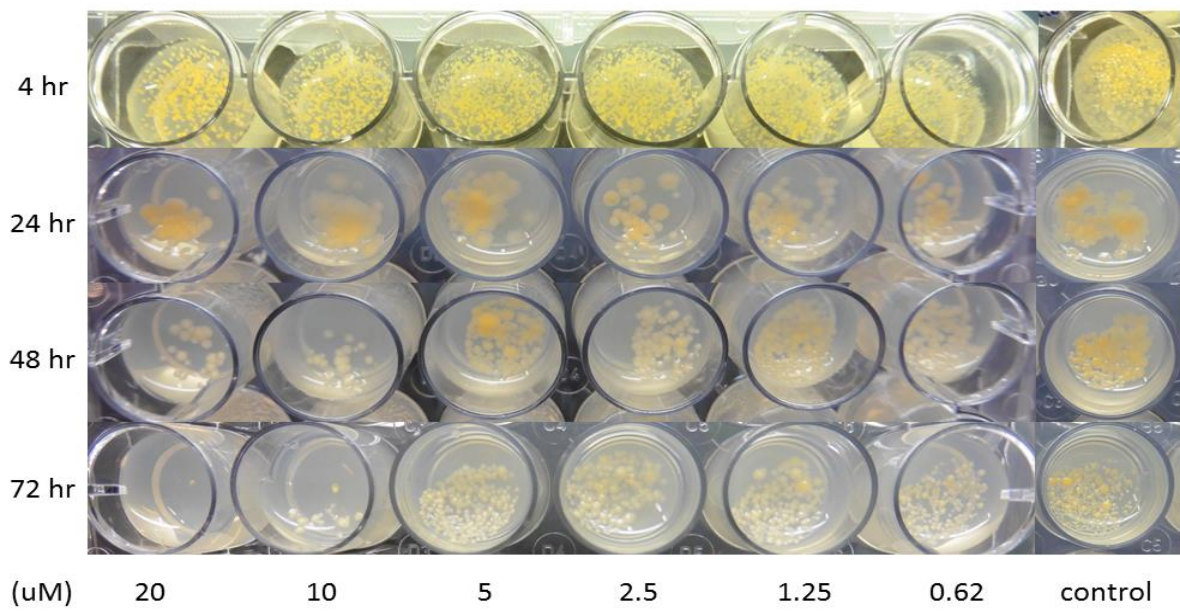
C

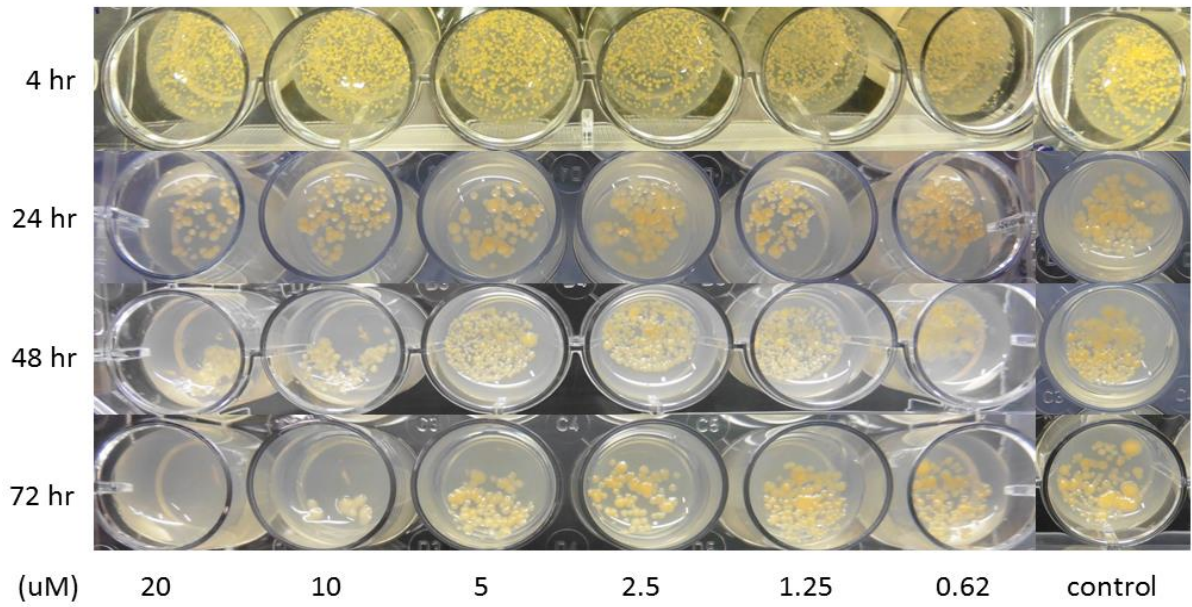
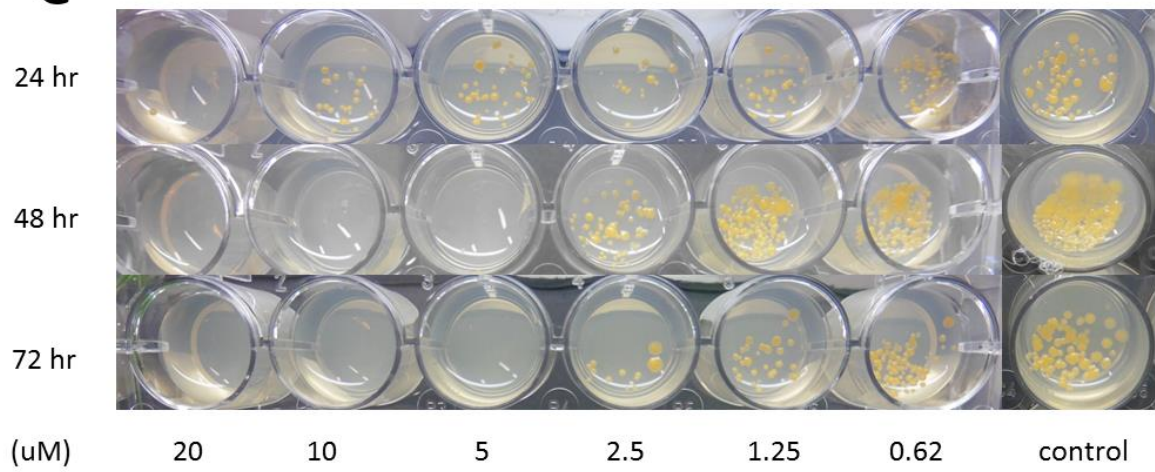
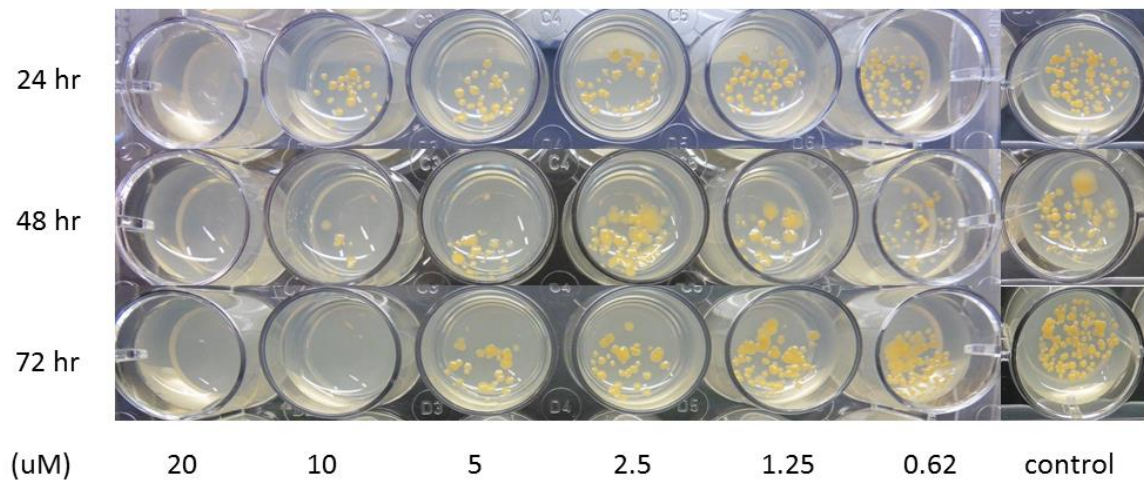


D



E



F**G****H**

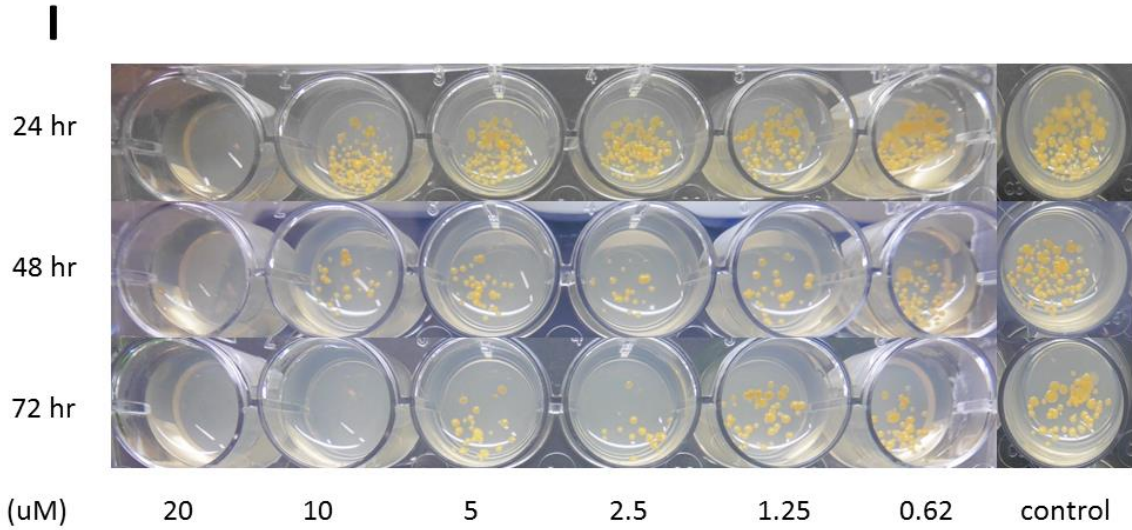
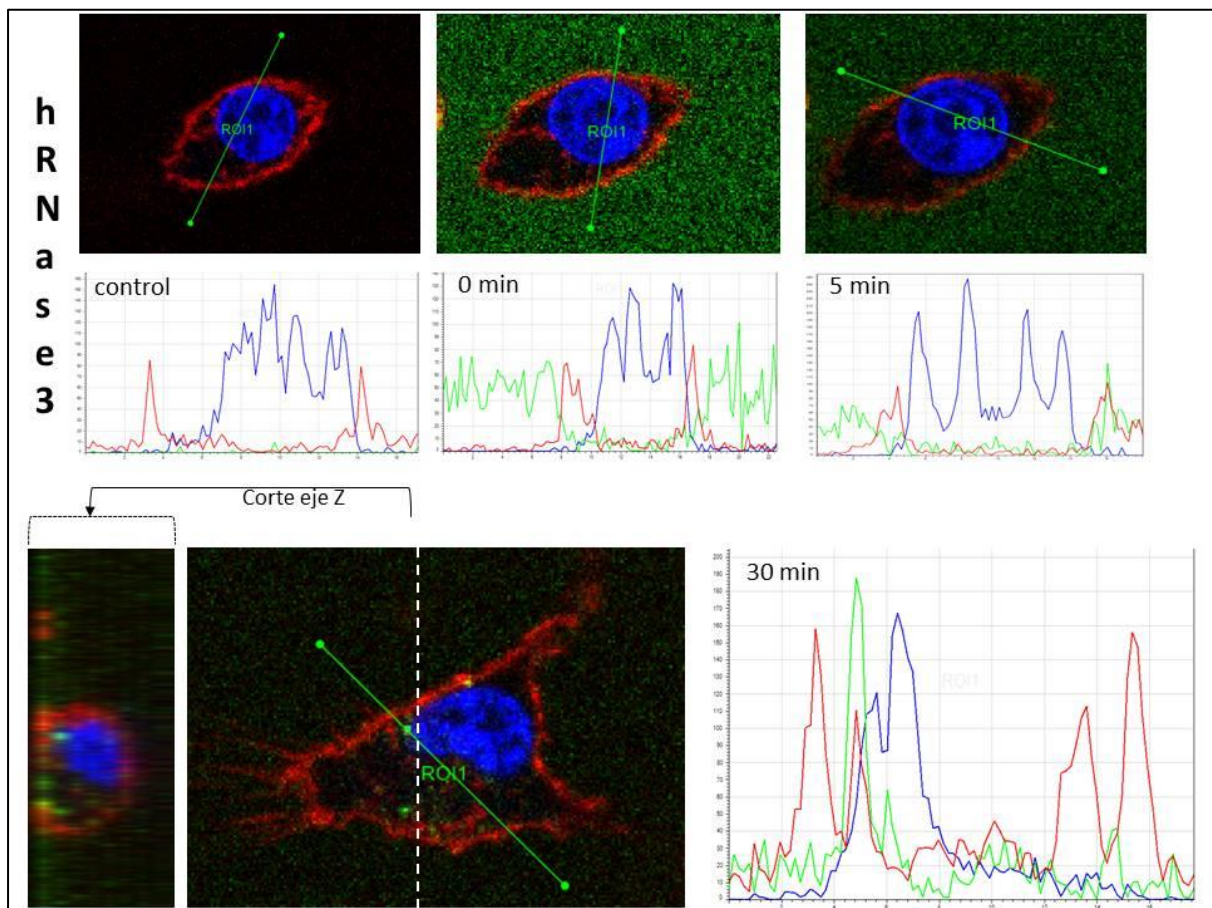
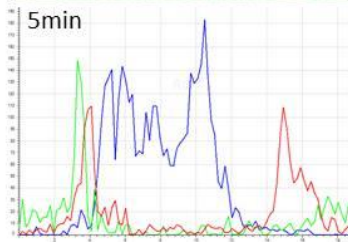
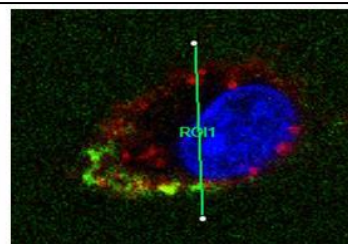
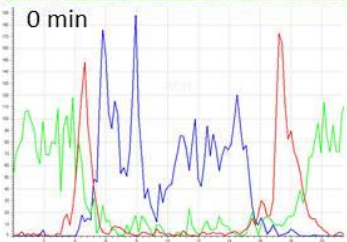
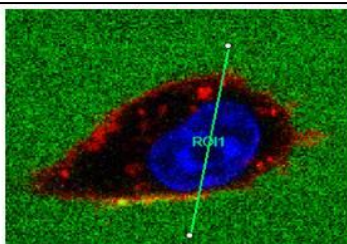
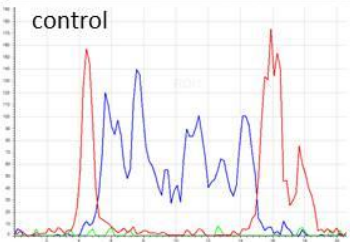
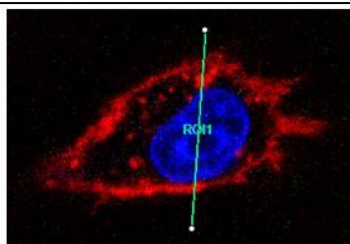


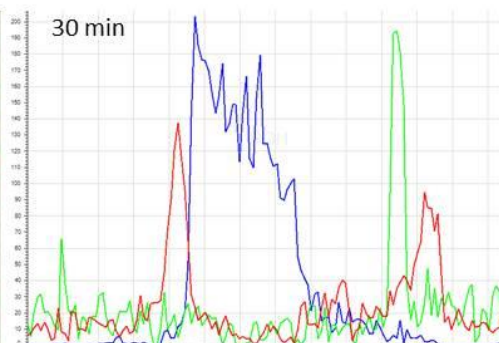
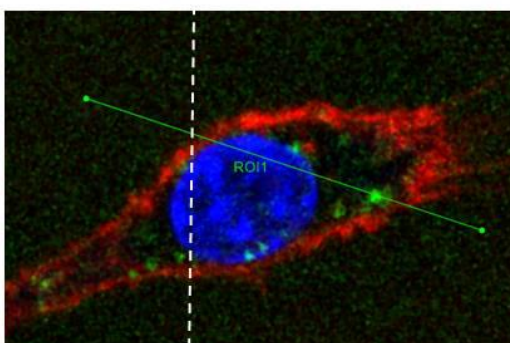
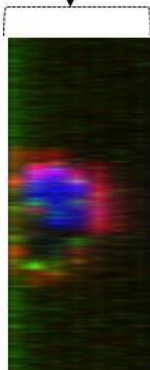
Figure S7. Growth inhibition of *M. aurum* inside RAW 264.7 cells at different time intervals for different concentrations of RNases. hRNase 3 (A), hRNase 6 (B), hRNase 7 (C), hRNase 3-H15A (D), hRNase 6-H15a (E), hRNase 7-H15A (F), RN3 (G), RN6 (H) and RN7 (I).



h
R
N
a
s
e
6



Z axis



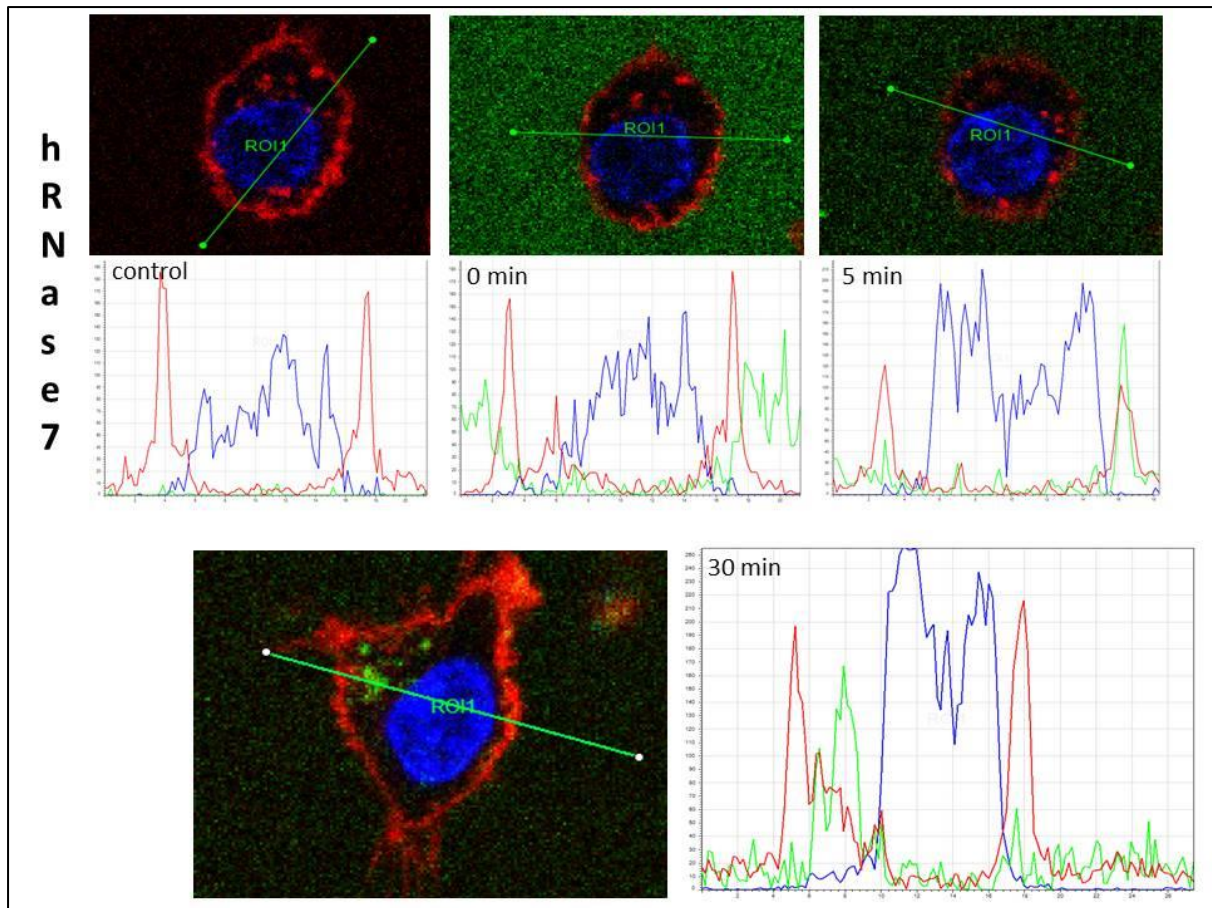


Figure S8. Confocal microscopy analysis of RAW 264.7 cell culture incubated with hRNases labelled with Alexa Fluor 488 (green). Cells were stained following the assay incubation conditions detailed in the experimental procedures section. After protein addition, the evolution of the fluorescence signals was analysed by confocal microscopy. A total of 20 cells were analysed by regions of interest (ROIs) using Leica TCS software. The images were taken using a Leica TCS SP5 AOBs microscope. Each panel detail the name of the hRNase assayed.

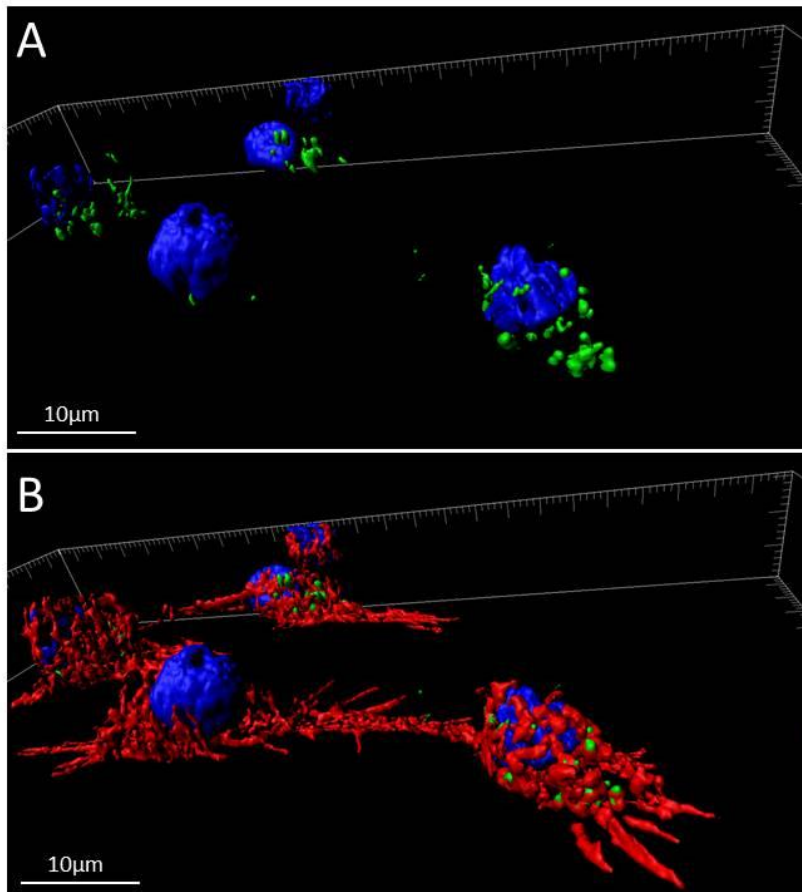
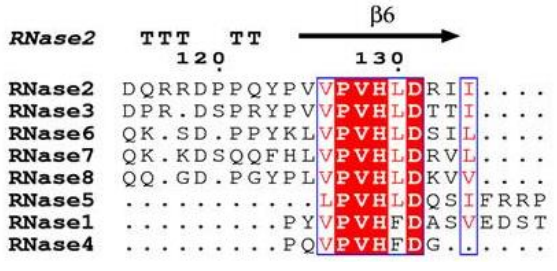
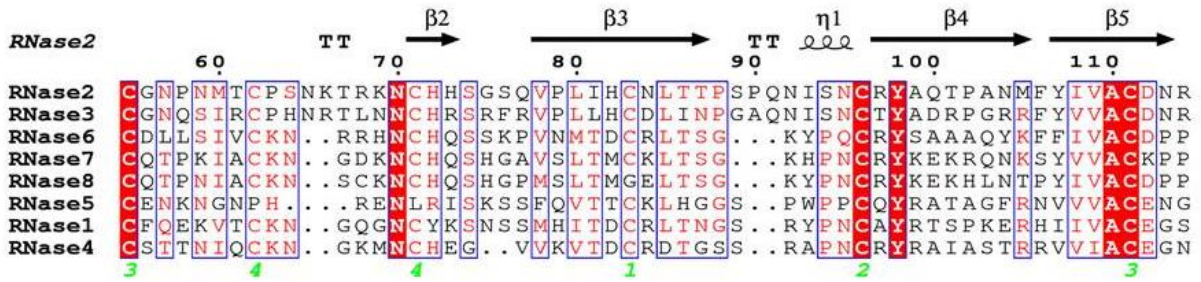
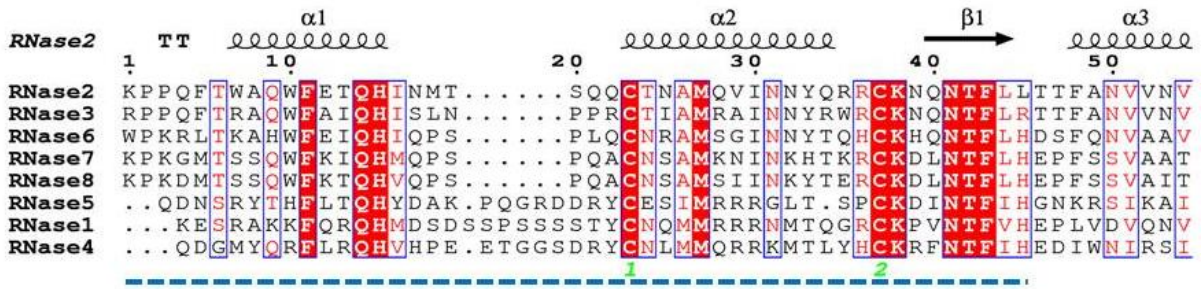
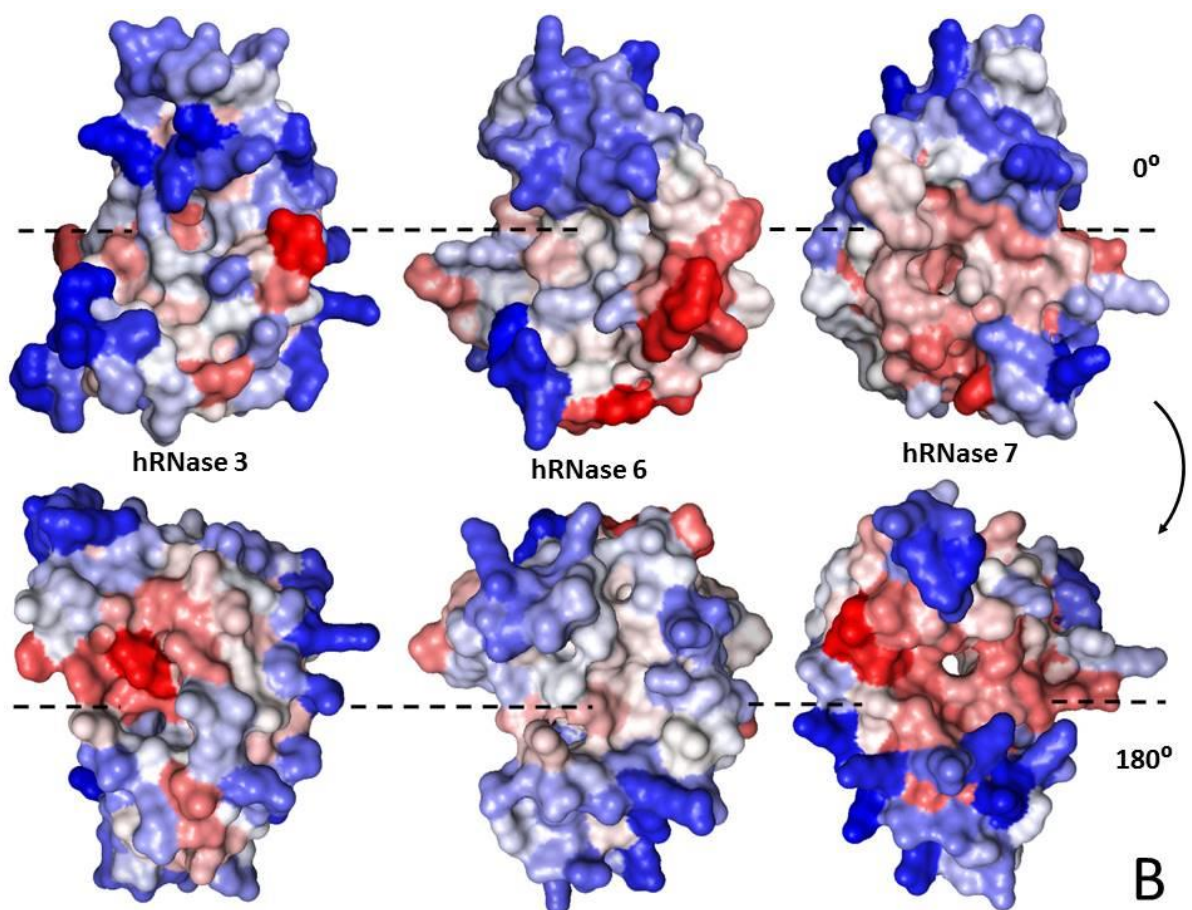


Figure S9. 3D reconstruction of RAW 264.7 macrophages post-treatment with hRNase 3. Confocal microscopy analysis of RAW 264.7 cell culture incubated with 2 μM of hRNase 3 labelled with Alexa Fluor 488 (green). Cells were stained following the assay incubation conditions detailed in the experimental procedures section. After protein addition, the evolution of the fluorescence signals was analysed by confocal microscopy. The images were taken using a Leica TCS SP5 AOBS microscope.



A



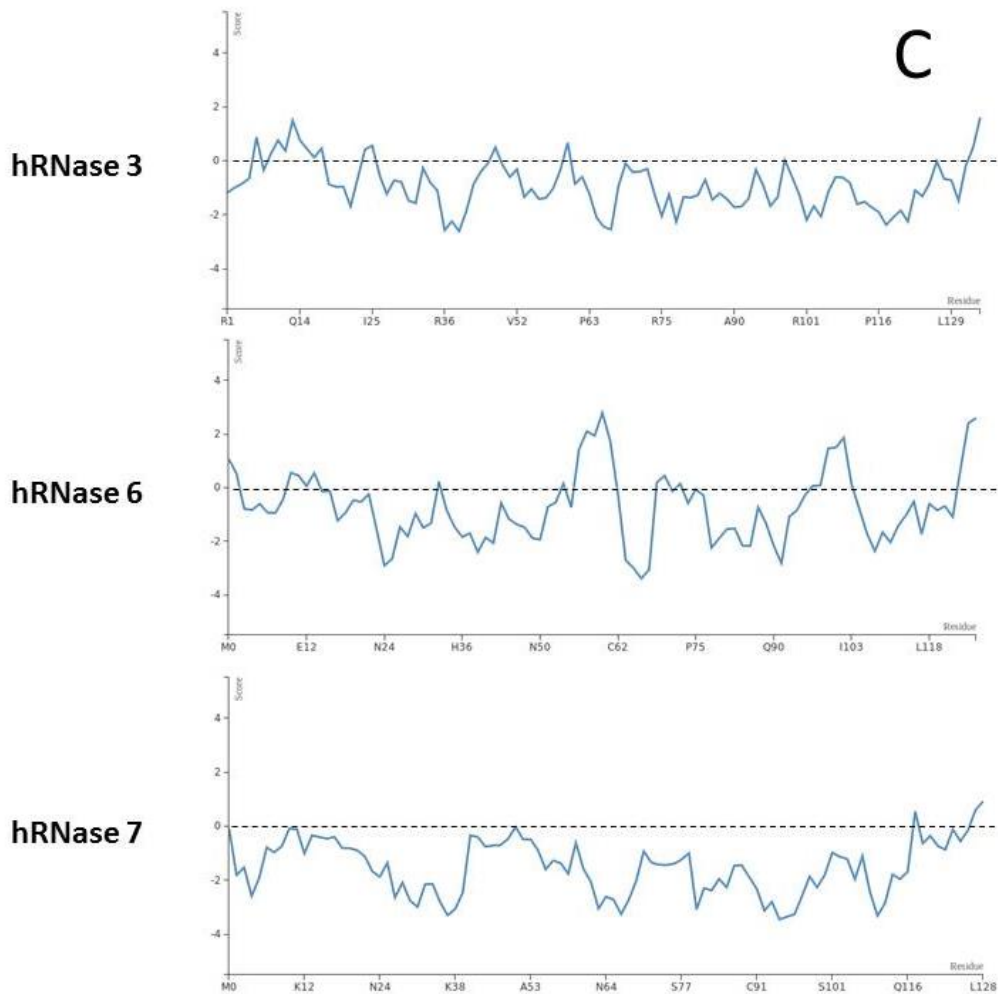


Figure S9. A) Alignment of the eight human canonical RNases (Sript3¹), the N-terminal domain is highlighted in blue. Sequence allocation was performed following the homology between hRNses. B) 3D structure of RNases (Aggrescan3D²). A3D exploits an experimentally derived intrinsic aggregation propensity scale for natural amino acids. This structure-based approach identifies aggregation patches (red coloured) focusing the prediction on protein surface. C) Aggregation profile propensity of hRNases 3, 6 and 7 based on A3D score for protein residues.

References

1. Robert, X. & Gouet, P. Deciphering key features in protein structures with the new ENDscript server. *Nucleic Acids Res.* **42**, W320-4 (2014).
2. Zambrano, R. *et al.* AGGRESKAN3D (A3D): server for prediction of aggregation properties of protein structures. *Nucleic Acids Res.* **43**, W306-13 (2015).

